Final Report

Low-Cost Regional Aircraft

Group 22 – Design a regional aircraft with the lowest possible operational cost

A. W. Abbenhuis	4367510	A. C. K. Loke	4458443
V. A. van der Arend	4271092	A. Piva	4374975
M. A. Heilig	4378679	P. A. M. Uijterwaal	4357809
G. W. H. Hoekman	4355725	R. Veldhuis	4138570
S. Kozlowska	4458575	M. P. van der Zwaard	4481410

Technische Universiteit Delft

TUDelft

This page is intentionally left blank.

Final Report

Low-Cost Regional Aircraft

Version 2.0

written by

Group 22

for the Design Synthesis Exercise

2017 / 2018 – Spring Edition

at the faculty of Aerospace Engineering.

Authors:	A. W. Abbenhuis	4367510
	V. A. van der Arend	4271092
	M. A. Heilig	4378679
	G. W. H. Hoekman	4355725
	S. Kozlowska	4458575
	A. C. K. Loke	4458443
	A. Piva	4374975
	P. A. M. Uijterwaal	4357809
	R. Veldhuis	4138570
	M. P. van der Zwaard	4481410

Date: July 3, 2018

Project duration: April 30, 2018 – July 6, 2018

Supervisor:	Asst. prof. ir. J. Sinke,	TU Delft (SI&C)
Coaches:	Ir. Y. Zhang,	TU Delft (Aero)
	Ir. H. Koornneef,	TU Delft (ATO)

TUDelft

Preface

The demand for air travel is ever increasing. Customers want to fly shorter distances more frequently, entailing an increase in the regional aircraft market. However, current regional aircraft are not up to the most recent standards. Technology has greatly advanced in recent years while safety and environmental standards have changed. Advances in lightweight materials, more efficient engines and other fields warrant an investigation into the design of a new regional aircraft. In order to make this aircraft attractive for airlines, focus must be placed on one of the most costly aspects: the operational costs. Designing this low cost regional aircraft is the subject of Group 22's Design Synthesis Exercise (DSE).

The DSE is the final assignment of the Aerospace Engineering bachelor curriculum. It is intended to demonstrate skill and knowledge acquired during the bachelor program and apply it to a specific and realistic problem. This problem is solved by a group of 10 students in a multidisciplinary setting. The Design Synthesis Exercise can be divided into four phases: a planning phase, a requirements phase, a concept phase and a final design phase. This report represents the conclusion of the final phase.

We would like to thank our principal tutor, asst. prof. ir. J. Sinke, and our coaches, ir. Y. Zhang and ir. H. Koornneef, for their continued support and assistance during our project. We also would like to thank the staff of the faculty of Aerospace Engineering, without whom several questions would not have been answered. Lastly, we would also like to thank the faculty of Aerospace Engineering for the use of their facilities during this project.

<div align="right">

Group 22
Delft, June 2018

</div>

A. W. Abbenhuis   *V. A. van der Arend*   *M. A. Heilig*   *G. W. H. Hoekman*   *S. Kozlowska*

A. C. K. Loke   *A. Piva*   *P. A. M. Uijterwaal*   *R. Veldhuis*   *M. P. van der Zwaard*

Contents

List of Abbreviations

$MW5$ MAMAWRAPS-V

AC   Alternating Current
ADIRU   Air Data Inertial Reference Unit
ADSEE   Aerospace Design and Systems Engineering Elements
AHM   Aircraft Health Monitoring
ann   Anneald
ANoPP   Aircraft Noise Prediction Program
APU   Auxiliary Power Unit
ATC   Air Traffic Control
ATM   Air Traffic Management
ATR   Aerei da Trasporto Regionale *or* Avions de Transport Régional
AVIC   Aviation Industry Corporation of China
AVL   Athena Vortex Lattice

BEP   Break-Even Point

C   Composite
c.g.   Centre of Gravity
CBS   Cost Breakdown Structure
CO_2 Carbon Dioxide
CRFP   Carbon Fibre Reinforced Polymer

DC   Direct Current
DOC   Direct Operating Costs

EASA   European Aviation Safety Agency
EBD   Electrical Block Diagram
EC   Earliest Completion
EFIS   Electronic Flight Instrument System
EICAS   Engine Indicators and Crew Alerting System
EIS   Entry Into Service
EPNdB   Effective Perceived Noise in Decibels
ERJ   Embraer Regional Jet
ES   Earliest Start

FAR   Federal Aviation Regulations
FMC   Flight Management System
FOD   Foreign Object Debris
FSS   Flight Service Station
FTK   Freight Tonne-Kilometre
FVC   Fibre Volume Content

GDP   Gross Domestic Product
GE   General Electric
GLARE   Glass Reinforced Aluminium

HLD   High-Lift Device
HM   High Modulus
HS   High Strength

IOC   Indirect Operating Costs
ISA   International Standard Atmosphere
ITTC   International Towing Tank Conference

KCAS	Knots Calibrated Air Speed
KEAS	Knots Equivalent Air Speed
KIAS	Knots Indicated Air Speed
KTAS	Knots True Air Speed

LC	Latest Completion
LS	Latest Start
LT	Longitudinal Transverse

M	Metal
MAC	Mean Aerodynamic Chord
MCC	Maintenance Control Centre
MFD	Multi-Function Display
MIT	Massachusetts Institute of Technology
MLDT	Mean Logistic Delay Time
MLW	Maximum Landing Weight
MMT	Mean Maintenance Time
MTBF	Mean Time Between Failures
MTBMA	Mean Time Between Maintenance Actions
Mth	Months
MTOW	Maximum Take-Off Weight
MTTR	Mean Time To Repair
MZFW	Maximum Zero Fuel Weight

NASA	National Aeronautics and Space Administration
NF	Natural-Fibre
NFC	Natural-Fibre Composite
NO_x	Mono-Nitrogen Oxide

O&L	Operations and Logistics
OCC	Operations Control Centre
OEI	One Engine Inoperative
OEW	Operational Empty Weight
OL	Operational Life-Time
OPS	Operations

PEEK	Polyether Ether Ktone
PEI	Polyehylenimine
PERT	Program Evaluation and Review Technique
PFD	Primary Flight Display
PW	Pratt & Whitney

RAT	Ram Air Turbine
ROC	Rate of Climb
RoI	Return on Investment
RPK	Revenue Passenger-Kilometre

SF	Synthetic Fibre

TAT	Turnaround Time
TPR	Thermoplastic Resin
TSFC	Thrust-Specific Fuel Consumption
TSR	Thermoset Resin

V&V	Verification and Validation
VLM	Vortex-Lattice Methods

List of Symbols

Symbol	Description	Unit
$\dot{m}_{\text{fuel}}$	Fuel mass flow	kg/s
η_{prop}	Propeller efficiency	-
η_c	Plasticity reduction factor for compression	-
η_s	Plasticity reduction factor for shear	-
γ	Climb angle	deg
λ	Taper ratio	-
λ_h	Horizontal tail taper ratio	-
λ_v	Vertical tail taper ratio	-
$\Lambda_{0.25h}$	Horizontal tail quarter chord sweep	deg
$\Lambda_{0.25v}$	Vertical tail quarter chord sweep	deg
$\Lambda_{c/4}$	Quarter chord sweep angle	deg
μ_r	Dynamic friction coefficient	-
ν	Poisson's ratio	-
ρ	Density	kg/m^3
ρ_0	Air density at sea level	kg/m^3
σ_{hoop}	Circumferential stress	MPa
σ_{max}	Maximum stress	MPa
σ_{min}	Minimum stress	MPa
σ_{ult}	Ultimate stress	MPa
σ_y	Yield stress	MPa
$\sigma_{\text{compressive}_{\text{yield}}}$	Yielding compressive stress	MPa
$\sigma_{\text{max}_{\text{all}}}$	Allowable maximum stress	MPa
$\sigma_{\text{min}_{\text{all}}}$	Allowable minimum stress	MPa
$\sigma_{\text{tensile}_{\text{yield}}}$	Yielding tensile stress	MPa
σ_a	Axial stress	MPa
σ_{cc}	Crippling stress	MPa
σ_{n+1}	Direct stress of following boom	MPa
σ_{n-1}	Direct stress of previous boom	MPa
σ_n	Boom direct stress	MPa
$\sigma_{r_{\text{max}}}$	Maximum radial stress	MPa
σ_z	Stress in z-direction	MPa
τ_{max}	Maximum shear stress	MPa
τ_{torsion}	Shear stress due to torsion	MPa
$\tau_{\text{max}_{\text{all}}}$	Allowable maximum shear stress	MPa
τ_{xy}	Shear stress in y direction	MPa
τ_{yz}	Shear stress in z direction	MPa
τ_{zx}	Shear stress in x direction	MPa

α	Angle of attack	deg
α_0	Zero-lift angle of attack	deg
δ_e	Elevator deflection	deg
μ_{br}	Dynamic friction coefficient for braking	-
A	Aspect ratio	-
a	Speed of sound	m/s
a_{br}	Deceleration during braking	m/s^2
A_{stringer}	Stringer area	mm^2
A_h	Horizontal tail aspect ratio	-
A_i	Inherent availability	-
A_o	Operational availability	-
A_v	Vertical tail aspect ratio	-
A_0	Operational availability	-
$A_{D/W}$	Coefficient wheel diameter/width	-
A_{en}	Enclosed area	mm^2
A_i	Inherent availability	-
b	Wing span	m
$b/2_h$	Horizontal tail semi-span	m
b_{eff}	Effective stringer width	mm
b_{frame}	Frame pitch	cm
b_{stringer}	Stringer pitch	cm
b_v	Vertical tail span	m
$B_{D/W}$	Coefficient wheel diameter/width	-
$b_{n,n+1}$	Distance with following boom	mm
$b_{n,n-1}$	Distance with previous boom	mm
B_n	Boom area	mm^2
b_n	Segment width	mm
c_{MAC}	Chord length at MAC location	m
c_r	Chord length at root	m
c_t	Chord length at tip	m
C_v	Vertical tail volume coefficient	-
C_{δ_a}	Effect of aileron deflection on aircraft forces & moments	-
C_{δ_e}	Effect of elevator deflection on aircraft forces & moments	-
C_{δ_r}	Effect of rudder deflection on aircraft forces & moments	-
C_{D_0}	Zero-lift drag coefficient	-
$C_{D_{\mathrm{opt}}}$	Optimal drag coefficient	-
$C_{D_{\mathrm{max,\ TO}}}$	Maximum drag coefficient at take-off	-

C_{L_α}	Lift gradient with respect to angle of attack	-
C_{l_α}	Rolling moment gradient with respect to angle of attack	-
C_{l_β}	Rolling moment gradient with respect to sideslip angle	-
$C_{L_{\text{max, land}}}$	Maximum lift coefficient at landing	-
$C_{L_{\text{max}}}$	Maximum lift coefficient	-
$C_{L_{\text{opt}}}$	Optimal lift coefficient	-
C_{L_h}	Lift coefficient of horizontal tail	-
$C_{L_{\alpha_h}}$	Tail lift gradient	-
$C_{L_{\alpha_{a-h}}}$	Lift gradient of main wing	-
C_L	Lift force coefficient	-
C_l	Rolling moment gradient	-
C_{m_α}	Pitching moment gradient with respect to angle of attack	-
C_{m_h}	Pitching moment gradient due to tail lift	-
$C_{m_{ac}}$	Pitching moment around the aerodynamic centre	-
C_m	Pitching moment gradient	-
C_{n_α}	Yawing moment gradient with respect to angle of attack	-
C_{n_β}	Yawing moment gradient with respect to sideslip angle	-
C_{n_v}	Yawing moment coefficient due to vertical tail force	-
C_n	Yawing moment gradient	-
c_{rh}	Horizontal tail root chord	m
c_{rv}	Vertical tail root chord	m
c_{th}	Horizontal tail tip chord	m
c_{tv}	Vertical tail tip chord	m
C_X	Longitudinal force gradient	-
C_{Y_α}	Side force gradient with respect to angle of attack	-
C_{Y_β}	Side force gradient with respect to sideslip angle	-
C_{Y_v}	Vertical tail force coefficient	-
C_Y	Side force gradient	-
D	Aerodynamic drag	N
D_{seg}	Aerodynamic drag per segment	N
E	Young's modulus	GPa
e	Oswald efficiency factor	-
$F_{c,cr}$	Critical skin buckling stress due to compression	MPa
$F_{s,cr}$	Critical skin buckling stress due to shear	MPa
F_{ccn}	Crippling stress per segment	MPa
F_{st}	Allowable stringer stress	MPa
G	Shear modulus	GPa
g	Gravitational acceleration	m/s^2

G_{OEI}	Specific climb gradient with one engine inoperative	deg
H	Height of the centre of gravity of the fuselage	m
h	Cruise altitude	km
h_{scr}	Screen height	m
I_{xx}	Moment of inertia around the x-axis	mm^4
I_{xy}	Product moment of inertia	mm^4
I_{yy}	Moment of inertia around the y-axis	mm^4
K_c	Flat plate buckling constant for compression	-
K_e	Compression buckling constant	-
K_s	Flat plate buckling constant for shear	-
L	Lift	N
L	Rib spacing	m
L_{avg}	Average lift	N
l_h	Horizontal tail arm	m
l_v	Vertical tail distance	m
M_{cr}	Cruise Mach number	m/s
M_{ff}	Fuel fraction	-
$M_{\text{ff}_{\text{trapped}}}$	Trapped fuel fraction	-
M_x	Bending moment around x-axis	Nm
M_y	Bending moment around y-axis	Nm
n_{frames}	Frames number	-
n_{load}	Load factor	-
n_{safety}	Safety factor	-
$n_{\text{stringers}}$	Number of stringers	-
P_{crit}	Critical buckling load	N
P_{shp}	Power	hp
P_a	Available power	W
P_r	Required power	W
p_0	Outside pressure	Pa
p_i	Inner pressure	Pa
q_b	Open section shear flow	N/mm
$q_{s,0}$	Shear flow of closed section	N/mm
q_s	Shear flow	N/mm
R	Turn radius	m
r	Fuselage radius	m
r_0	Outside radius	m
r_i	Inner radius	m
S	Total wing area	m^2

s_{ground}	Roll distance	m
S_h	Horizontal tail surface	m^2
S_v	Vertical tail area	m^2
S_{wf}	Wetted wing area covered by flaps	m^2
S_x	Shear force in x-direction	N
S_y	Shear force in y-direction	N
T	Thrust	N
T	Torque	Nm
T_{req}	Required thrust	N
T_{segment}	Thrust per segment	N
t_{skin}	Skin thickness	mm
t_n	Segment thickness	mm
V	Cruise speed	m/s
V_1	Take-off decision speed	m/s
V_{avg}	Average speed	m/s
V_{EAS}	Equivalent airspeed	m/s
V_{LOF}	Lift-off speed	m/s
V_{stall}	Stall velocity	m/s
V_{TAS}	True airspeed	m/s
V_{bl}	Block speed	km/hr
V_{vt}	Velocity of the vertical tail	m/s
W_{begin}	Weight at the beginning of phase	N
W_{end}	Weight at the end of phase	N
W_{FG}	Fuselage group weight	N
W_{payload}	Payload weight	N
W_{WG}	Wing group weight	N
W_f	Fuel weight	N
x_{airborn}	Airborne distance	m
$x_{\text{c.g.}}$	Position of the centre of gravity	m
x_{climb}	Climb distance	m
X_{crit}	Critical location	m
X_{LEMAC}	Distance from the nose to the leading edge of the MAC	m
X_{OE}	Aircraft operational empty weight centre of gravity location	m
x_{trans}	Transition distance	m
X_{WG}	Wing c.g. location	m
x_n	Distance from boom to centroid in x-direction	mm
x_w	Position of the main wing with respect to the aircraft nose	m
y_n	Distance from boom to centroid in y-direction	mm

List of Figures

List of Tables

1

Executive Overview

1.1. Project Description
In order to provide a complete overview of the project, first, the project description must be stated. This can be subdivided into the Mission Need Statement, the Project Objective and the initial project requirements.

Mission Need Statement   The Mission Need statement is as given below:

> *Transport 50 to 75 passengers with the lowest possible operational costs over a distance of 1500 to 2500 km with an aircraft from regional airports with a paved runway length of 1500 m.*

Project Objective Statement   The Project Objective Statement is as follows:

> *Develop a regional aircraft for the transportation of 50 to 75 passengers over a range of 1500 to 2500 km maximum with the key design goal of lowest possible operational costs in 11 weeks with 10 TU Delft BSc. Aerospace Engineering students. The aircraft at least must be able to operate from regional airports with tarmac runways of only 1500 m, be optimised for sustainability and comply with latest safety and environmental regulations. The design of the aircraft shall implement current and near future technologies and be feasible for production to start in five years.*

Project Requirements   The project has several initial requirements, which can be found below. These requirements, together with other requirements following from the market and requirement analysis were assessed during the design phase and the result can be found in the compliance matrix in Appendix E.

- Lowest possible operational costs as the key criterion.
- Range between 1500 to 2500 km.
- Passenger capacity ranging from 50 to 75 in economy class.
- Ability to fly from regional airports with limited handling facilities.
- Take-off distance of less than 1500 m on tarmac.
- Optimisation for sustainability.
- Compliance with safety and environmental regulations.

1.2. Organisation
The team consist of 10 members who are all BSc. students at the faculty of Aerospace Engineering. The team is organised in a way that each member has both a managerial and technical role. The organisation can be found in Figure 1.1. The roles were divided at the beginning of the project. After five weeks into the project, the roles were evaluated within the team. At the start of the detailed design phase in week six, the evaluation was done once more. After careful consideration, it was decided that everybody would keep their role for the remaining weeks.

1.3. Market Analysis
The aviation market is steadily growing. In 2012, the annual growth rate was 5% and it is expected to increase in the future. The aviation market represented 5 trillion revenue passenger-kilometres (RPK) in that year and is expected to grow to 20 trillion in the next 20 years. This opens up a lot of possibilities in the regional aircraft market.
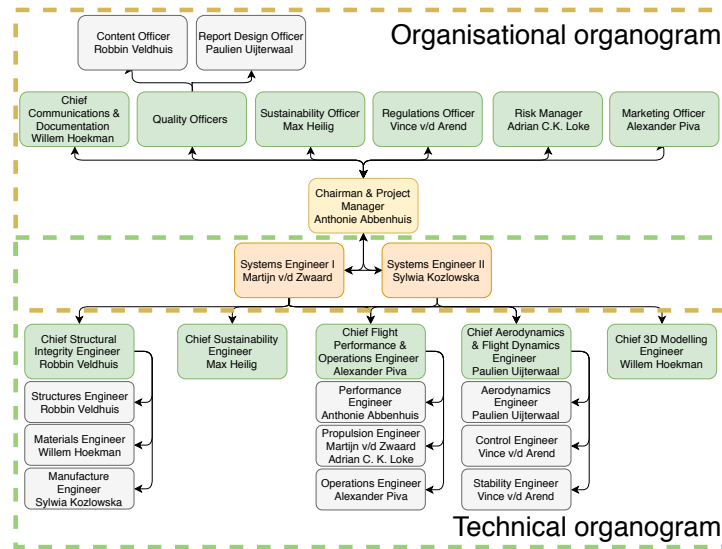
Figure 1.1: *Organisation of team 22.*

The largest growth for the regional market is expected to be in the Asia-Pacific region, especially in China, whereas the most aircraft will be sold in the Asia-Pacific and North American region. As the market will expand in the regions stated above, the amount of airports in those regions will increase as well.

As a new competitor in the market, it is essential to determine the expected market share. Based on the market share of competitors, the $MW5$ project will take up to 10% of the market, translating into 600 aircraft at a predicted unit selling price of 41 million USD.

In Figure 1.2 the range capability of the $MW5$ is given from two different airports, Minneapolis in Figure 1.2a and Paris in Figure 1.2b. The ranges of the CRJ700 and the MRJ70 are provided for the purpose of comparison.

(a) *Range capability from Minneapolis.*

(b) *Range capability from Paris.*
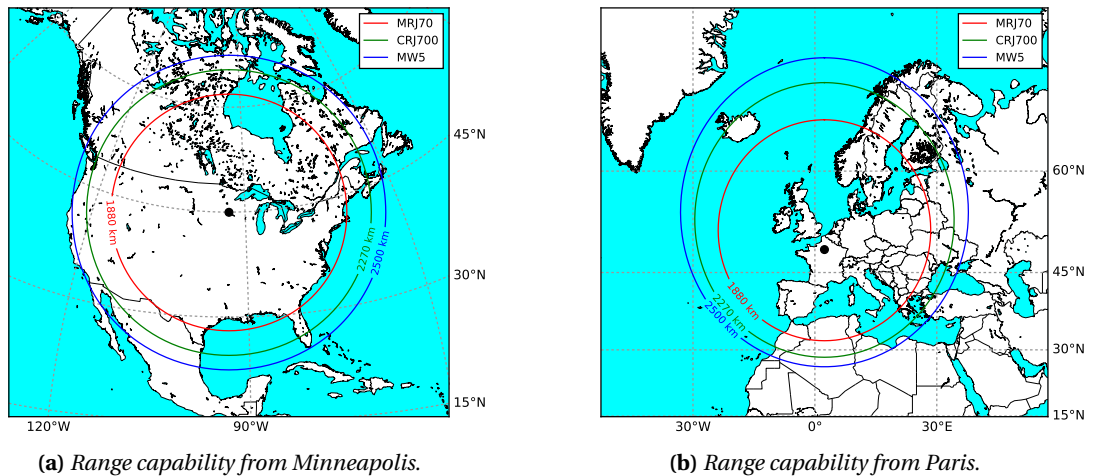
Figure 1.2: *Range capability of the $MW5$.*

1.4. Detailed Design

Previously, a design option tree was used to generate options which were then traded off to determine a final concept. This concept entered the detailed design phase of the project. Several aspects were used to evaluate and optimise the performance of the aircraft. These are flight performance, aerodynamics, flight dynamics and structures and materials. The final design drawings can be found in Figure 1.3. The aircraft has a low wing configuration, T-tail and two efficient high-bypass ratio rear-mounted engines.

Figure 1.3: *Isometric view of the final design.*

The aircraft is designed for 76 passengers in an economy class seating arrangement. Different seating arrangements are offered to give versatility to the aircraft. The differences can be found in the table below. The aircraft has a default seating arrangement of 2 + 2, but other arrangements are available upon request by the customer.

Table 1.1: *Differences between different configurations.*

Class	Seat pitch [cm]	Seat width [cm]	Recline [deg]	Rows	Passengers
Economy	78.7	43.2	3	19	76
Economy+	94.0	43.2	5	16	64
Mixed	78.7/94.0	43.2	3/5	18	72

Flight Performance   To comply with requirements as set by the customer, a flight performance analysis is performed. From this, multiple important aspects are analysed such as the take-off distance, the range, the fuel burn and a proper engine selection. After an initial analysis, it is found that the balanced field length is the driving design requirement for the engine. From this, it followed that an engine of at least 53.5 kN was necessary to comply with a take-off length of 1500 m. The selected engine will be a 'scaled-down' version of the P&W1215G, called the P&W1200G, and can be seen in Figure 1.4.
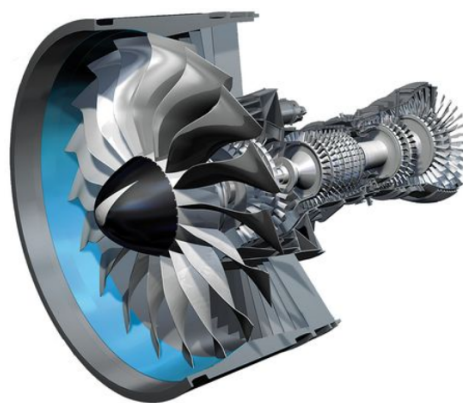
Figure 1.4: *The selected engine; a scaled-down version of the P&W1215G.*

With the selected engine, it was determined that the required runway length for take-off is 1490 m. From further analysis, it is found that the fuel burn during a flight is approximately 4810 kg if 76 passengers were transported over a range of 2500 km and that it would take a little under 3.5 hours. Furthermore, some typical flight parameters are analysed to determine the performance. These parameters were the maximum rate of

climb, the turning performance, the landing performance, the payload-range diagram and the flight enve-
lope. Also, recommendations are given to optimise the fuel burn.

Aerodynamics   In order to optimise the aerodynamics of the aircraft, several different procedures are fol-
lowed. First, using the program AVL and Vortex-Lattice theory, the 2D main wing is optimised. This planform
is optimised for minimum drag using an iteration of 5 parameters (the aspect ratio, two taper ratios and two
sweep angles). The results of this optimisation can be found below.

Table 1.2: *Starting values based on statistics compared to end values after optimisation.*

	A	λ_1	λ_2	Λ_1	Λ_2	D
Before optimisation	10.0	0.80	0.40	10 deg	25 deg	3.9 kN
After optimisation	10.5	0.68	0.44	12 deg	25 deg	3.2 kN

Next, the airfoil is selected. Since the design cruise Mach number is 0.78, the focus is placed on supercritical
airfoils. The wing requires two different airfoils; one at the root and one at the tip. The airfoils at the interme-
diate points and the kink are determined using interpolation. The results are that the Whitcomb supercritical
airfoil is used at the root and kink location, while the NASA SC21010 airfoil is used at the tip.

Subsequently, the different tail surfaces are sized and an appropriate airfoil is selected. Using statistical
data and relationships, the stabiliser surfaces are determined. Each stabiliser has two airfoils, one at the root
and one at the tip. For the horizontal stabiliser, the NACA 0010 airfoil is selected at the root and the NACA
0009 airfoil for the tip. The vertical stabiliser has a NACA 0011 airfoil on both the root and the tip. Figures of
the airfoils can be found below.

(a) *Whitcomb, root and kink airfoil.*

(b) *NASA SC21010, tip airfoil.*

Figure 1.5: *Airfoils used for the main wing.*

(a) *NACA 0011, vertical stabiliser.*

(b) *NACA 0010, root airfoil and
horizontal stabilser.*

(c) *NACA 0009, tip airfoil and
horizontal stabilser.*

Figure 1.6: *Airfoils used for vertical and horizontal stabiliser.*

Flight Dynamics   In order to check the stability of the aircraft, first, the control surfaces are sized. This is
done using an iterative method starting from previous results. A loading diagram and scissor plot are con-
structed to determine the final size of the tail.

Next, the control surfaces are sized. The ailerons are sized using historical guidelines. To reduce adverse
yaw caused by aileron deflection, differential aileron control is chosen. Next, using data from XFLR5, the ele-
vator is sized. It is assumed that the elevator spans the entire horizontal stabiliser, making sure the contribu-
tion to the moment coefficient is sufficient. Finally, using XFLR5 as well, the rudder is sized to accommodate
changes in sideslip angle. It was concluded that a rudder spanning from 10 to 90 % of the chord is sufficient
to meet the requirements.

Subsequently, the high lift devices are sized. The high lift devices make sure the aircraft is able to produce
the increase in lift coefficient required for take-off and landing. The main location of high lift devices is at the
leading and trailing edges of the main wing. On the leading edge, slats are added. For the trailing edge, several
options are evaluated. By looking at the required increase in lift, the complexity of the system and several
other parameters, a trade-off produced the final flap type. Slotted flaps proved sufficient for the design and
are therefore chosen.

The second part of the Flight Dynamics assessment consists of the stability of the aircraft. First, the equations of motion are determined which are then used to assess the stability of the aircraft in several different modes. From the eigenmotion analysis, displayed in Table 1.3, it can be seen that the symmetrical eigenmotions have a negative real part, meaning that the oscillations are damped. For the asymmetrical eigenmotions the real part of the eigenvalue is only negative for the aperiodic and Dutch roll. The eigenvalues for the symmetric and asymmetric case can be found in Table 1.3.

Table 1.3: *Eigenvalues and corresponding characteristics of the eigenmotions.*

Motion	Eigenvalues	Damping	Period [s]	Half amplitude [s]
Symmetrical	$-0.2937 + 0.5696i$	0.4583	11.031	2.3599
	$-0.0045 + 0.1839i$	0.0242	34.157	155.4851
Asymmetrical	-1.7868	1.0000	N/A	0.3879
	$-0.0879 + 1.2631i$	0.0694	4.9742	7.8892
	0.0146	1.0000	N/A	-47.4753

Structures and Materials   In order to determine the proper material, the focus is placed on the two most prominent structural elements. These are the fuselage and the wings. An initial material trade-off followed by a second more in-depth trade-off resulted in the choice of Al-Li 8090-T851 as the main material. The benefits mostly come from the low-density and relatively low increase in material cost compared to other materials while maintaining good producibility and maintainability. Several additional considerations are also made with respect to smaller aircraft components. For these components, different materials were chosen. It was determined that the control surfaces would be made from composites because of their light weight.

The loading diagrams for the aircraft are generated and, in combination with the flight envelope, used to determine the critical load cases for the structures mentioned above. For both the fuselage and the wing, the appropriate stringers are chosen. This resulted in Z-stringers for the fuselage and a combination of Z- and hat-stringers for the wing.

Next, stress analysis using the von Mises stress criterion is used to calculate the required thicknesses of the different elements. For the fuselage sizing, crippling, buckling and shear are taken into account. For the wing, bending and torsion are assessed. It is shown that both sections are able to carry the required loads.

1.5. Production Plan

Now that the materials have been determined the material properties can be used to plan the production of the aircraft. Key aspects to be taken into account during this process are the batch size, shape, desired surface finish and cost.

For each of the large material groups, metals and composites, the appropriate manufacturing processes are determined using the criteria stated above. They are determined using several different trade-offs. For Z-stringers, bending was the best option. Ribs are best produced using rubber forming and ailerons will be produced using the infusion process.

Next to the different manufacturing techniques, the manufacturing sequence is determined. The components will be assembled from least complex to most complex. To reduce the risk of delays, it is desirable to have equally sized work stations. The preliminary manufacturing sequence can be found in Figure 1.7.

1.6. Operations & Logistics

Because reduction of operational cost is the most important goal for this design, the operations and logistics are studied extensively to optimise turnaround time and the scheduling of maintenance. For the ground operations a PERT model is used to determine the critical path, which is the most time consuming, during the time the $MW5$ is on the ground. After that, a closer look at embarking, fuelling and push back was done to optimise the operations. Finally, a Gantt chart is provided which determines that the time on the ground can be as little as 27.5 minutes. The Gantt chart can be found in Figure 9.4 where all the different actions that have to be performed while the aircraft is on the ground are listed. For maintenance different strategies were considered in terms of maintenance and a maintenance planning logistic is made where every check (A, B, C or D) is considered.
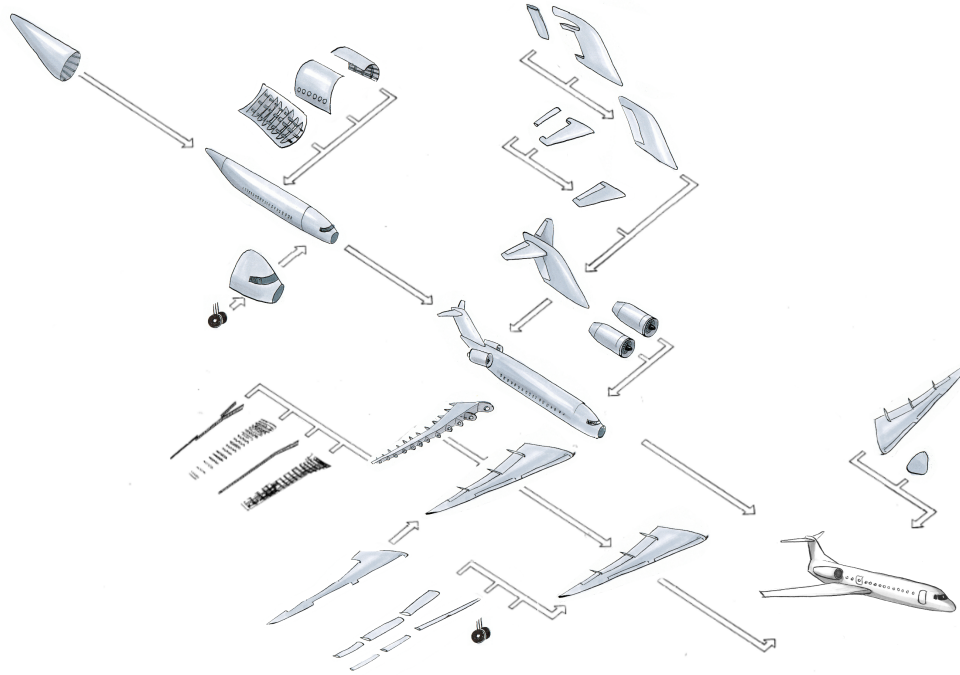
Figure 1.7: *Manufacturing Sequence.*

1.7. Finance

A financial analysis is performed to investigate the costs and profits for both airlines as well as the manufacturer of the aircraft. For the total program cost, different costs are found. The development cost for the $MW5$ is estimated to be 1 billion USD or 1.6 million USD per aircraft. Production cost is estimated to be 30.4 million USD per aircraft. A unit aircraft price is determined to be 38.6 million USD including a 20% profit margin.

As operating cost is an important factor for the airliner, those costs are analysed as well. A distinction is made between direct operating costs and indirect operating costs. The direct operating costs consist of flying, maintenance, depreciation and some other minor parts. It is found that for an operator the $MW5$ will cost 2875 USD/block hour. Indirect operating cost mainly depends on the airline itself but is estimated to be 55% of the direct operating cost. A total cost reduction for airlines operating $MW5$ is around 8 to 11% compared to airlines operating current regional aircraft.

For the return on investment (RoI) and the break-even point again a distinction is made between manufacturer and operator. For the manufacturer the RoI is expected to be 19% and for the operator 12.2% with a competitive ticket price. The break-even point for the manufacturer is reached after 270 aircraft are sold. For the operator, the BEP is reached in the ninth year.

1.8. Future

The DSE project ends at the detailed design phase. However, the development of $MW5$ is not yet completed and many steps have to be made before release to the market. These future steps can be divided into three different phases: detailed design, development and operational lifetime of the aircraft. The first of these phase will take up about 1.5 years. This is followed by half a year of tool manufacture and facility set-up during the development phase. After this, the prototypes are produced, tested and the certification process is started. Once the aircraft receives its type certification, it is ready to entire service.

<div style="text-align: right; font-size: 4em;">2</div>

Market Analysis

The aviation market is a dynamic market which is constantly changing. While steadily growing, the composition of aircraft in use changes all the time. Throughout the years new markets rose as the demand for air travel increased. In this chapter, a market analysis is performed in order to get a feeling on the feasibility of introducing a new low-cost regional aircraft. In Section 2.1 the aviation market as a whole is described, followed by a more detailed analysis of the regional market in Section 2.2. Furthermore, the customer requirements followed by the competitors in the market are discussed. The market share and target unit price are then tackled. Finally, an overview of all the system requirements is presented.

2.1. Aviation Market

The growth of the aviation market is linked to the growth of the gross domestic product (GDP). Over the last 20 years, the GDP steadily increased with 2.8% per year and it can be seen that the world passenger air traffic, which is measured in revenue passenger-kilometre (RPK), has grown steeper with 5.0%. This is shown in Figure 2.1.
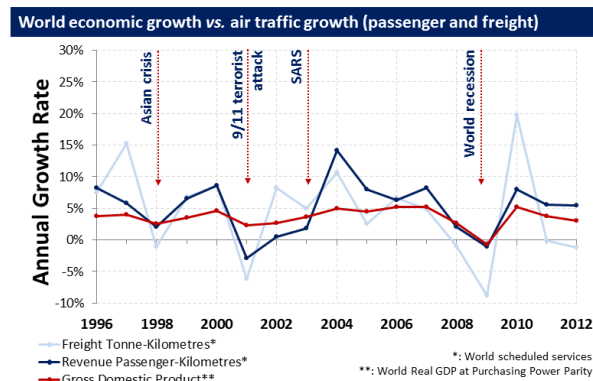
Figure 2.1: *Air traffic growth and world economic growth [67].*

Although the increase in the past 20 years has been steady, there were some crises which influenced the growth of the aviation market. In Figure 2.2 it can be seen that in the last 40 years some crises stagnated the growth of the market. However, historical trends express the capacity by the world aviation industry to always recover from these, which makes it a matter of *when* it will recover more than *if* it will [65, 67].

It can be further found in Figure 2.2 that the aviation market consisted of more than 5 trillion RPKs in 2012. According to different market outlooks [9, 14, 33, 66], it is expected that for the next 20 years the RPKs will increase to almost 20 trillion. The enormous growth in aviation offers opportunities to new manufacturers, as the estimated amount of aircraft demand will steadily increase.

Another trend in the aviation market is the development of more sustainable aircraft [47]. Some of the earlier experienced crises were related to oil dependencies. Due to the significant influence that an increase in oil price has on the airline profits, the demand for more sustainable aircraft is increasing. In addition, because of the positive effect on the environment, regulations are getting stricter and stricter on sustainability factors. This shift leads to more light-weight designs, more efficient engines and the use of electrical systems.
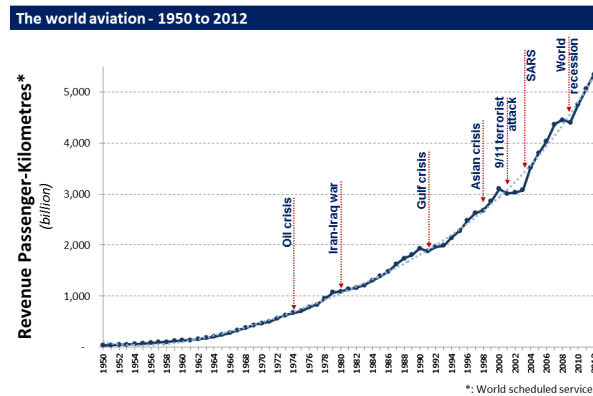
Figure 2.2: *Influence of world crises.*

2.2. Regional Market

The regional aircraft is an evolving and expanding market that is shaping modern aviation industry. In the past two decades, there has been an increasing demand for short distance flights to fulfil the interest in short holidays and city trips. The market rise can also be explained by the increased globalisation, where a great percentage of people live in other countries. In case of Europe, for example, these countries are close to each other. On the other hand, regions such as North America and China have a strong regional aircraft demand as people mostly live in relatively close cities, which is mostly due to business and labour opportunities.

The regional market will strongly expand worldwide, but each world region has a different increase. The region that is forecasted to expand the most is the Asia-Pacific one, with the steepest growth in China. The biggest markets in terms of sold regional aircraft are expected to be Asia-Pacific and North America.

The advantage of regional aircraft from the point of view of operators is their relatively low costs. In fact, operational costs are substantially lower than for bigger aircraft. Furthermore, these can operate at regional airports, which have limited equipment, opening up to a whole new market. The costs to operate on regional airports are much lower.

To fulfil the predicted demand, according to CAPA [10], a total amount of 1.1 trillion USD will be invested in the coming decades to build new airports. Many of these airport plans are intended for regional airports, especially in regions such as North America, Europe, South-East Asia and Latin America. In the case of China, bigger airports will be built but they are intended also for regional aircraft.

2.3. Customer Requirements & Needs

The customer requested the team a new regional aircraft design that aimed at low operational costs. Firstly, the mission need statement is formulated such that the goal of the design is clear to all stakeholders. The statement is formulated as follows:

> *Transport 50 to 75 passengers with the lowest possible operational costs over a distance of 1500 to 2500 km with an aircraft from regional airports with 1500 m tarmac runway maximum.*

Based on the mission need statement, the team formulated the customer requirements in order to fulfil the wishes of the customer regarding the new aircraft design. These requirements were initially stated, which means that they could have been subjected to change. In fact, it can be noticed in the list of requirements that Cus.5 is not present anymore. This was the outcome of analysed considerations throughout the design phase which led to change the take-off distance requirement from 1200 to 1500 m. The requirements are:

Cus.1:   The operational costs shall be lower compared to competitive aircraft.

Cus.2:   The range at maximum payload shall be more than 1500 km but less than 2500 km.

Cus.3:   The number of passengers shall be between 50 to 75 in an economy class setting.

Cus.4:   The aircraft shall be able to operate from regional airports.

Cus.6:   The design, operation, production and recycling shall be optimised for sustainability.

Cus.7:   The aircraft shall comply with the latest safety and environmental regulations.

Cus.8:   The take-off distance on tarmac shall be less than 1500 m.

2.4. Competition

An analysis of the competition is essential in order to understand the market requirements and opportunities. In fact, once these are identified, the design focus can be determined. Furthermore, through a competition analysis, it is possible to understand the potential share market that can be taken by the new aircraft design. This is crucial to determine a business plan.

There are three main aircraft manufacturers who are dominating the regional aircraft industry. As it can be seen from Figure 2.3, these are respectively Embraer, ATR and Bombardier. Two other manufacturers are also to be taken into account, which are Mitsubishi and AVIC, as they have not yet entered the market, but already have a market share due to outstanding orders [50]. All values shown in the figure are expected market shares for each company in 20 years.
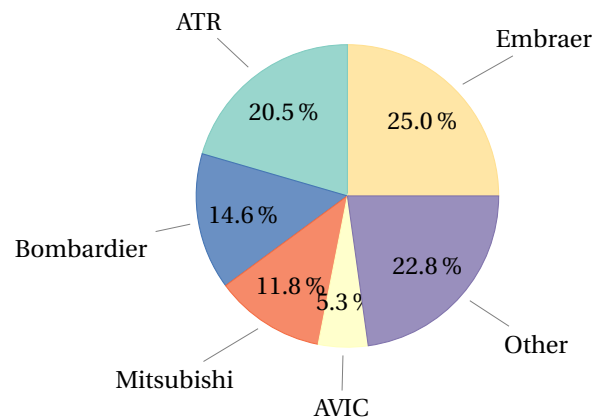
Figure 2.3: *Market share per manufacturer.*

Embraer is the market leader for the regional aircraft market. Their expected deliveries by 2036 is 2300 aircraft with a 70 to 90 passenger seating capacity [33], and their focus is mainly on North America and Asia-Pacific. Between their aircraft, the ERJ-170 ER is the one with the most similarities with respect to the design goal.

ATR is a slightly different aircraft manufacturer with respect to the others. Instead of turbofan engines, they use turboprop engines and focus more on a slightly lower passenger capacity. They expect to sell around 2000 aircraft in the next 20 years and they focus mostly on the upcoming Asia-Pacific region. Their ATR 72 is the most comparable aircraft and, because of such, it is regarded as a strong competitor.

Bombardier is the third biggest manufacturer. They have turbofan powered aircraft and expect to sell around the same amount of aircraft as the 2 other competitors, namely 2000, in the coming 20 years. Their focus is not only the Asia-Pacific region but also Europe. The CRJ700 is the aircraft which mostly relates to the requirements of the $MW5$.

The two other manufacturers, Mitsubishi and AVIC, are entering the market. Mitsubishi has concluded its test flights and expects to enter the market in 2020. They already have 288 [76] outstanding orders and 184 options. AVIC is producing the Comac ARJ21 and is already delivering aircraft. Of the 300 orders, they have delivered 5 aircraft [86].

Table 2.1: *Comparable aircraft from competitors.*

Name	ATR 72-500	Bombardier CRJ700 ER	Embraer ERJ-170 ER	Mitsubishi MRJ70	AVIC MA700
Passengers, max.	74	78	78	78	86
Range [km]	1455	2270	2760	1880	1500
MTOW [kg]	22,800	34,019	37,200	36,850	27,600
Engine	PW127F	CF34-8C5B1	CF34-8E	PW1215G	PW150C
Take-off field length [m]	1220	1516	1582	1450	1309

In Table 2.1 the comparable aircraft can be found from the different manufacturers. This gives an idea of how some of the parameters, such as MTOW, will look like for the design.

2.5. Market Share & Unit Cost

As a new competitor in the market, it is essential to determine the expected market share that the $MW5$ will have. This strongly influences the feasibility of the program with respect to the profit of the manufacturing company. Considering that the new two regional market competitors, which are Mitsubishi and AVIC, are entering the market and taking respectively 11.8% and 5.3% of the market share, a similar share is expected for the $MW5$. In fact, the new design is aimed to minimise operational costs and improve sustainability, which are factors of great interest for aircraft operators. With this in mind, it is expected that about 10% of the share market will be taken by the $MW5$ design. An amount of 5782 aircraft is forecasted to be delivered in the regional market until 2031 [50], which translates to about 600 $MW5$ deliveries.

As analysed in the Baseline Report [39], the target unit price was set to be of 41 million USD for the 70 to 80 passenger configuration. This was done by considering the willingness to pay extra in unit price in order to have a decrease in operational costs. The analysis resulted in a willingness to pay 9.15% more in unit price for a 10 to 20 % reduction in operational cost. The target unit price was then set by increasing of 9.15% the average unit price of regional aircraft of the same passenger capacity. The target unit price should include the targeted profit rate of the manufacturing company on the $MW5$ program of 20%.

2.6. Requirements Overview

Before getting into the design phase, an overview of the requirements provides a solid design and decision-making guideline. All the requirements, except for the customer requirements, are listed below. The requirements are found through the Requirement Discovery Tree as shown in Figure 2.4, some of the requirements follow from functional breakdown and and functional flow, both of which can be seen in Appendix D. Throughout the project, the stated requirements may be subjected to change and new requirements may be added if required. An overview of the met requirements is given in a compliance matrix at the end of this report in Appendix E.
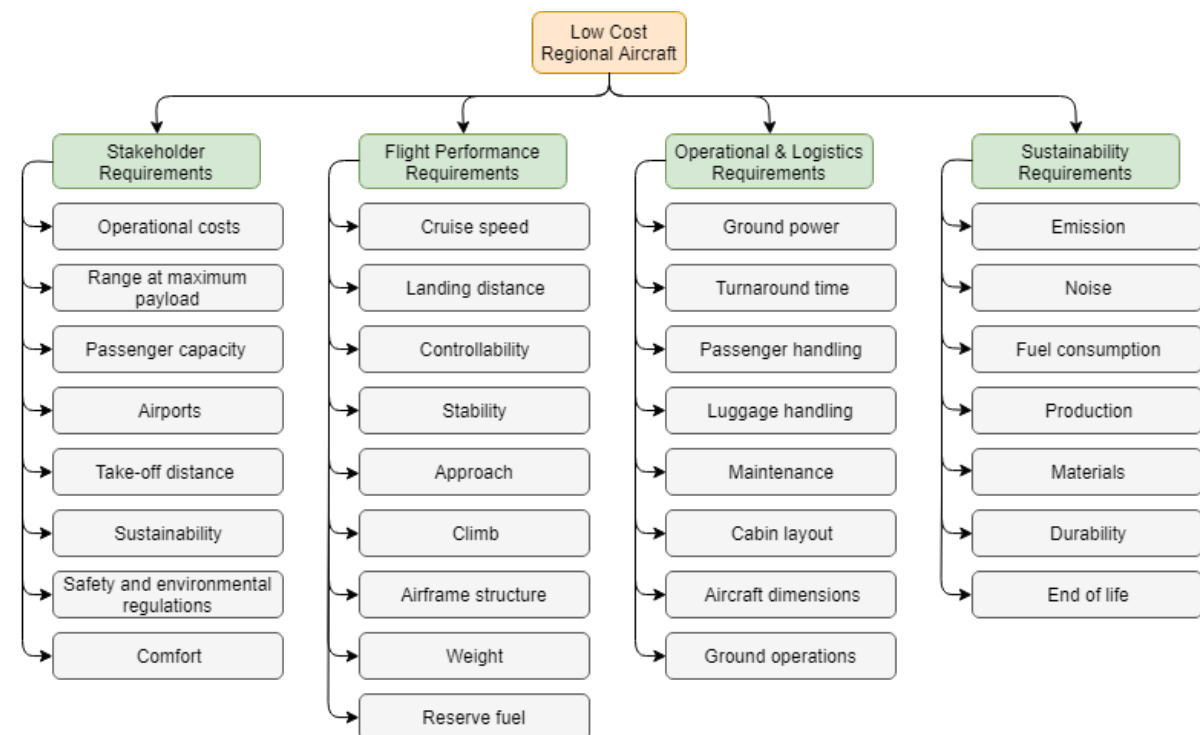
Figure 2.4: *Requirements discovery tree.*

Sys.Perf.1:	The aircraft shall be dynamically stable for the entire range of centre of gravity excursions.
Sys.Perf.2:	The aircraft shall be controllable for the entire range of centre of gravity excursions.
Sys.Perf.3:	The cruise speed of the aircraft shall be in the range of Mach 0.73 to 0.83.

Sys.Perf.5:   The aircraft shall be able to make a steep approach with a flight path gradient of at least -10%.

Sys.Perf.6:   The noise produced by the aircraft shall be less than 264 EPNdB.

Sys.Perf.7:   In landing configuration the steady climb gradient shall not be less than 3.2% at an airspeed of no more than $1.3 V_{\text{stall}}$.

Sys.Perf.8:   The climb gradient during the first take-off segment with one engine inoperative shall be positive.

Sys.Perf.9:   The climb gradient during the second take-off segment with one engine inoperative shall be more than 2.4%.

Sys.Perf.10:   The climb gradient during the final take-off segment with one engine inoperative shall be more than 1.2%.

Sys.Perf.11:   The climb gradient during the en-route segment with one engine inoperative shall be more than 1.1%.

Sys.Perf.12:   The climb gradient during the approach segment with one engine inoperative shall be more than 2.1%.

Sys.Perf.13:   There shall be no uncontrollable ground-looping tendencies in 90° crosswind, up to a wind velocity of 20 kts.

Sys.Perf.14:   The airframe structure shall not fail under ultimate load for a duration of 3 seconds.

Sys.Perf.15:   The number of emergency exits present shall be sufficient to comply with CS-25 regulations.

Sys.Perf.16:   The maximum take-off mass of the aircraft shall be less than 35,000 kg.

Sys.Perf.17:   The operational empty mass of the aircraft shall be less than 20,600 kg.

Sys.Perf.18:   The aircraft shall be able to fly to an alternate airport 100 km away after maximum range flown.

Sys.Perf.19:   The aircraft shall be able to loiter at the alternate for at least 30 minutes.

Sys.Perf.20:   The landing distance on tarmac shall be less than 1500 m.

Sys.O&L.1:   Turnaround time of the aircraft between maximum payload flights shall be less than 30 minutes.

Sys.O&L.2:   The aircraft shall have a lifetime of at least 25 years.

Sys.O&L.3:   The aircraft shall be able to perform three to four daily operations.

Sys.O&L.4:   Lateral ground clearance of the aircraft shall be higher than 5°.

Sys.O&L.5:   The seat pitch shall be equal to 31 in.

Sys.O&L.6:   Maintenance intervals shall be increased due to a safe-life design of components.

Sys.O&L.7:   The aircraft shall not tip over backwards for the entire range of centre of gravity locations during ground loading.

Sys.O&L.8:   The aircraft shall not turn over for any possible loading configuration and turning radius.

Sys.O&L.9:   The aircraft doors shall be compatible with airstairs.

Sys.O$L.10:   All essential aircraft systems shall be operative with ground power only.

Sys.O&L.11:   The wing span shall not exceed 35 m.

Sys.O&L.12:   The total length shall not exceed 35 m.

Sys.Sus.1:   Noise generated by the aircraft shall be less than the Chapter 14 level EPNdB.

Sys.Sus.2:   Fuel consumption per passenger-kilometre shall be less than 120 g.

Sys.Sus.3:   Aircraft structure shall be made of at least 90% recyclable materials.

Sys.Sus.4:   Manufacturing techniques shall be non-toxic.

Sys.Sus.5:   Engine emissions shall comply with current regulations.

Sys.Sus.6:   The fuel burned during operation shall be less than 8900 kg per flight.

Sys.Sus.7:   Employees shall not be subjected to dangerous gases during the production of the aircraft.

3

Configuration & Layout

In this chapter, the reasoning of choosing the final concept is shown along with final internal and external configurations. Firstly, the final six concepts and final trade-off summary table are presented in section Section 3.1. Afterwards, the weight estimations are shown, for both, Class-I and Class-II in section 3.2. Lastly, the external configuration and internal layout are presented in section 3.3 and 3.4 respectively.

3.1. Final Trade-Off

The final trade-off is executed in order to determine the most optimal aircraft design for the set requirements, which will be the final aircraft design. The configuration of the trade-off and the respective legend can be found in Table 3.2. The initial 25 configurations can be seen in appendix G.

3.1.1. Final Six Concepts

In this section, 6 concepts sketches that made it to the final trade-off are presented. Concept number 8 and number 9 are turboprops, concepts 10 and 13 are conventional turbofans, concepts 24 and 25 are hybrids.

| (a) Concept 8. | (b) Concept 9. | (c) Concept 10. |

| (d) Concept 13. | (e) Concept 24. | (f) Concept 25. |
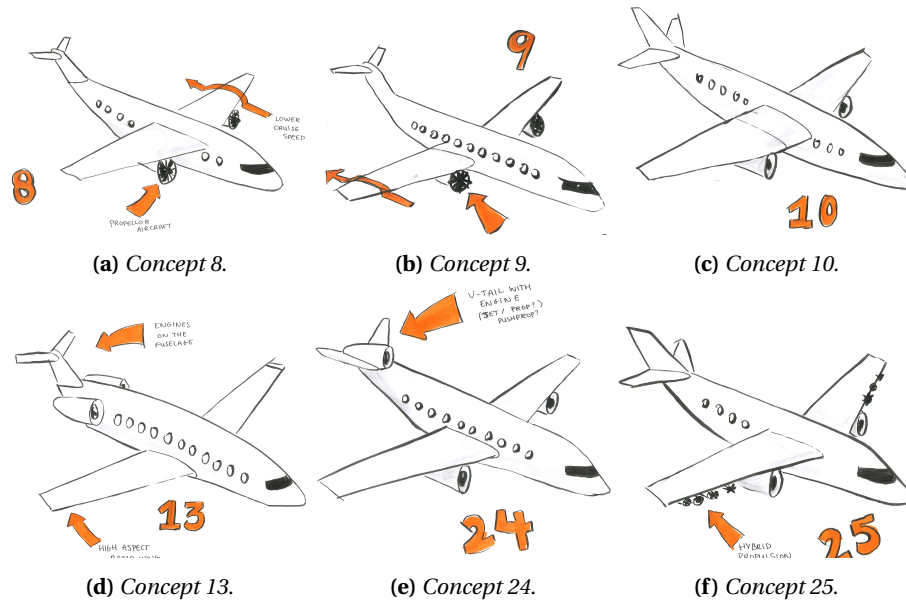
Figure 3.1: *Final six concepts.*

3.1.2. Final Trade-Off Results

The final trade-off is presented in Table 3.2. The width of the six criterion columns corresponds to the relative weights of the criteria. The total trade-off score is calculated by multiplying the weights taken from table 3.1 with the number of plusses or minuses. With double minus being "-2", single minus being "-1" etc.

Table 3.1: *Aircraft configuration trade-off criteria and weights.*

Trade-off criteria	Weight
OEW	0.22
Flight performance	0.21
Manufacturing	0.09
Maintenance	0.19
Ground operations	0.12
Sustainability	0.17

It can be seen from Table 3.2 that the most promising concept is concept 13. With a total score of 0.86, it is clearly better than the other concepts. Design 13 therefore, enters the detailed design phase. Although the other designs did not make it to the detailed design phase, there are some points that are worth considering for the final design. Therefore the other five designs are taken into consideration when going into the detailed design phase.

Table 3.2: *Final trade-off.*

#	OEW	FP	MF	MT	GO	SUS	Total Score
8	+	–	0	0	+	+	0.30
9	+	–	+	0	–	+	0.15
10	0	0	0	+	+	+	0.48
13	0	+	0	+	+	++	0.86
24	0	+	0	––	0	–	−0.34
25	––	0	–	–	0	––	−1.06

Excellent (++)　　Good (+)　　Average (0)　　Undesirable (–)　　Poor (––)

3.2. Class-I & Class-II Weight Estimations

A Class-I weight estimation is performed based on the method as described by Roskam [49]. In this method, a pool of reference aircraft is used which are fairly similar to the new regional aircraft design in size, passenger capacity and design range. From these aircraft, a relation between MTOW and OEW is determined. Then, the fuel weight is determined based on fuel fraction estimations from Roskam [49] and an estimation of fuel consumption during cruise using the Breguet range equations [60], which for jet aircraft is given as

$$\text{Range} = \frac{V}{g \cdot \text{TSFC}} \left(\frac{L}{D} \right) \ln \left(\frac{W_{\text{begin}}}{W_{\text{end}}} \right) \tag{3.1}$$

where V is the cruise speed, TSFC is the thrust-specific fuel consumption in $\text{kg}/(\text{N}\,\text{s})$, L/D is the lift over drag ratio during the cruise, and W_{begin} and W_{end} are the weights at the beginning and the end of the cruise, respectively. With a payload weight of around $6900\,\text{kg}$ based on 76 passengers averaging a weight of $92\,\text{kg}$ including luggage [49], the MTOW can be approximated as

$$\text{MTOW} = \frac{a + W_{\text{payload}}}{1 - \left(b + M_{\text{ff}} + M_{\text{ff}_{\text{trapped}}} \right)} \tag{3.2}$$

where M_{ff} and $M_{\text{ff}_{\text{trapped}}}$ are the fuel fraction and the trapped fuel fraction as a fraction of the MTOW. The variables a and b define the linear relation for the OEW as a function of MTOW based on reference aircraft, where a is the offset value and b the slope. With the results from the Class-I weight estimation, a more detailed weight estimation can be performed. The Class-II weight estimation is based on the Raymer method [75], which consists of 20 equations and 70 input variables such as aspect ratio, MTOW, taper ratio, etc. The output of the Class-II weight estimation are weights of different components (for example, fuselage, vertical stabiliser, horizontal stabiliser, avionics etc.). By adding up all those weights, the operational empty weight is obtained.

The results of the Class-I and Class-II weight estimations are given in Table 3.3 in tonnes.

Table 3.3: *Class-I and Class-II weight estimations in tonnes.*

Concept	MTOW [t]	OEW [t]
Class-I	35.0	20.2
Class-II	-	16.4

3.3. External Configuration

The outside configuration can be seen in Figure 3.2. The aircraft has a low wing configuration, a T-tail and two efficient high-bypass turbofan engines mounted at the rear of the fuselage. The reader can have better insight into the configuration, by looking up the renders and technical drawings in Appendix B.

(a) *Isometric view.*

(b) *Front view.*   **(c)** *Side view.*   **(d)** *Top view.*
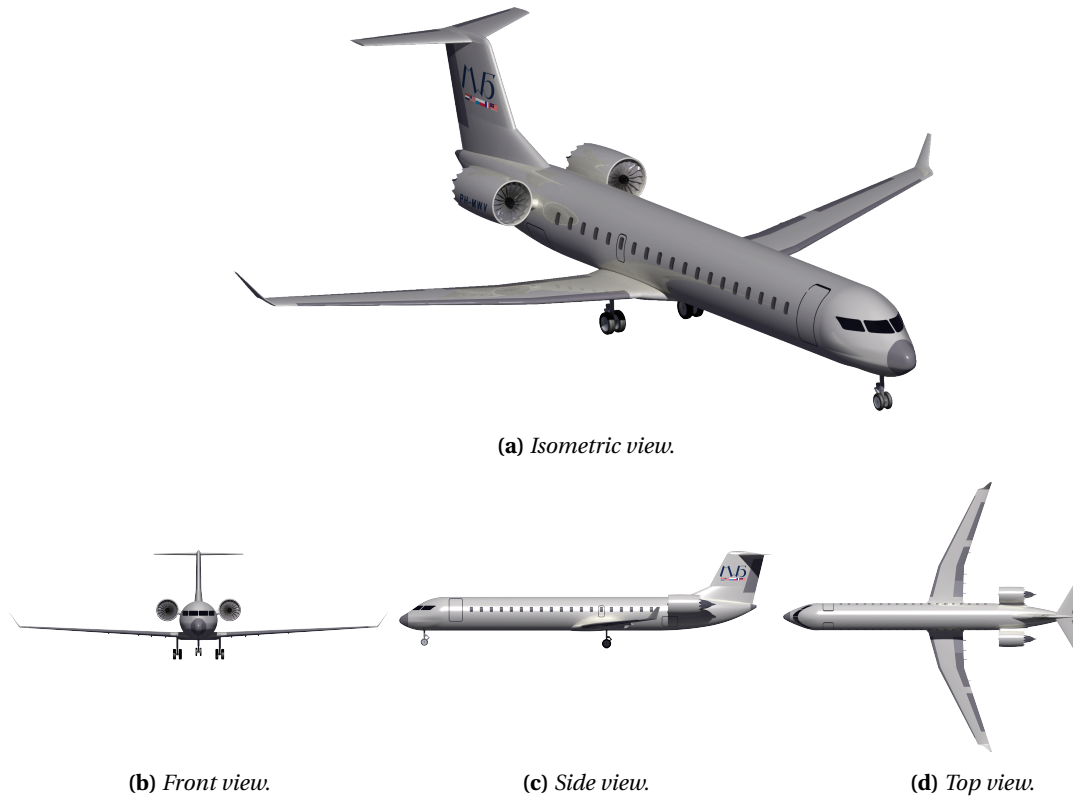
Figure 3.2: *Different views of the MW5 aircraft.*

3.4. Internal Configuration

The cross-section configuration of the fuselage with dimensions can be seen in Figure 3.3. With an inner diameter of 2.5 m, there are 4 seats abreast in 2 + 2 configuration, this is the default arrangement. Different configurations are possible upon request (for example 2 + 1). The different seating configurations are shown in Figure 3.4.

Cargo is stored at the back of the aircraft, with additional overhead luggage located inside the cabin. The total volume of the non-pressurised cargo compartment is 20.3 m³ (0.267 m³ per passenger), which is comparable to reference aircraft [51]. The overhead cargo volume is equal to 5.66 m³, which is ample room for the cabin luggage of the passengers. With standard suitcase dimensions of 55x39x25 cm, 76 suitcases can be fitted in the overhead storage, one for each passenger.

There are three basic options available: economy, economy+ and mixed. The seat pitch in economy+ is increased by 6 in to 37 in (94 cm) seat pitch. The seats in economy+ have also a bigger recline. All the visual differences between different configurations are shown in Figure 3.4 and are all summarised in Table 3.4.
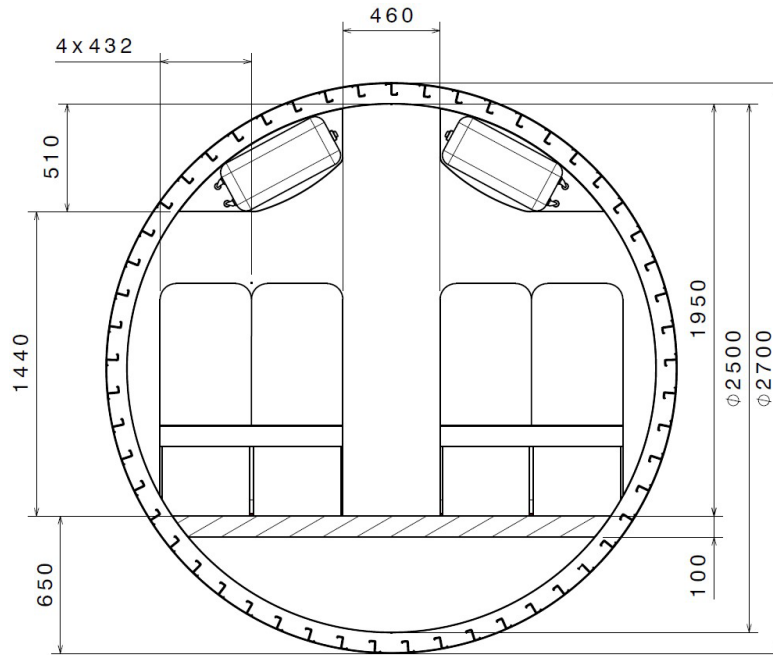
Figure 3.3: *Cabin cross-section, dimenions in mm.*

Table 3.4: *Differences between different configurations.*

Class	Seat pitch [in]	Seat width [in]	Recline [deg]	Rows	Passengers
Economy	31	17	3	19	76
Economy +	37	17	5	16	64
Mixed	31/37	17	3/5	18	72

(a) *Economy.*

(b) *Economy+.*

(c) *Mixed.*
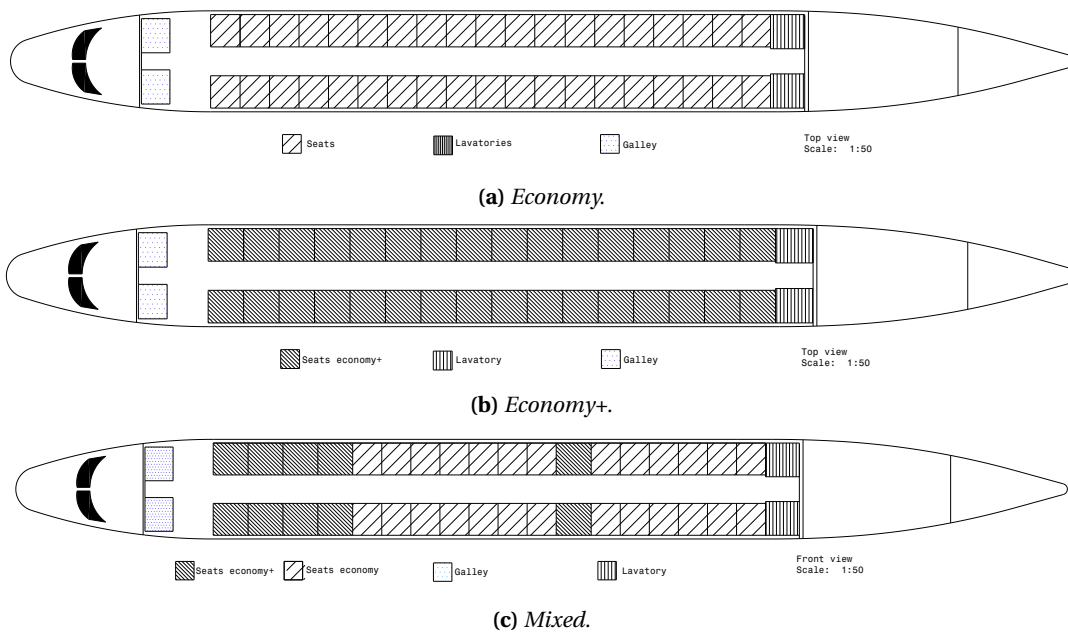
Figure 3.4: *Seating configurations.*

Flight Performance

In this chapter, the flight performance of the design is discussed. Based on flight performance the requirements are met. First, an engine selection will be executed as that is the starting point for flight performance analysis. After that, a detailed description of the flight path will be given and subsequent improvements will be discussed. The final part of this chapter will consist of some typical flight performance characteristics such as a payload-range diagram and turning performance.

4.1. Engine Selection

The flight performance analysis begins with the selection of an engine, as most performance characteristics are based on the available thrust. The first step is to identify the maximum thrust required over the whole flight by analysing the most critical thrust phases. These were identified to be the take-off distance and the second take-off segment. Considering take-off until clearance, the aircraft should be able to take off within a maximum distance of 1500 m. As take-off consists of two phases, this is split up in the airborne and groundroll. For the groundroll, Equation 4.1 [91] was used to determine the minimum required thrust.

$$T_{\text{TO}_{\text{req}}} = \frac{W}{2g_0} \frac{V_{\text{LOF}}^2}{s_{\text{groundroll}_{\text{TO}}}} + D_{\text{TO}} + D_{g_{\text{avg}}} \tag{4.1}$$

where V_{LOF} is the lift-off speed, $s_{\text{groundroll}_{\text{TO}}}$ is the groundroll distance at take-off, D_{TO} is the drag at take-off experienced by the aircraft and $D_{g_{\text{avg}}}$ is the average ground friction drag during take-off. The required thrust for take-off until obstacle clearance was found to be of 84.4 kN, which gives 42.2 kN per engine. However, looking into the balanced field length equation, which will be explained in more detail in Section 4.2, the take-off thrust is found to be 53.5 kN per engine.

Looking into the take-off procedures segments, the aircraft performance at these phases are determined by regulations. These are explained in Subsection 4.3.2. According to CS-25 [3], the aircraft should be able to fly at specific climb gradients G at each of those segments with one engine inoperative (OEI). The equation used to determine the thrust required is shown in Equation 4.2 [57]. The results are shown in Table 4.1.

$$T_{\text{seg}_{\text{req}}} = G_{\text{seg}_{\text{OEI}}} W + D_{\text{seg}} \tag{4.2}$$

Table 4.1: *Climb gradient and required thrust for each take-off segment.*

Phase	G_{OEI} [%]	T_{required} [kN]
First segment	0.0	33.5
Second segment	2.4	42.0
En-route climb	1.1	28.9
Final segment	1.2	31.4

From Table 4.1, the second segment is the most critical. Comparing it with both the take-off until obstacle clearance and the balanced field length, it can be seen that the balanced field length determines the minimum required engine thrust. Therefore, one engine should at least provide a thrust of 53.5 kN at sea level. Based on this, various available engines are identified. A maximum available thrust of 70 kN is set as the upper limit, as otherwise the engine is considered to be overdesigned. The potential engines with their related thrust can be seen in Table 4.4. To perform a proper trade-off, the following criteria and weights are set:

- **Thrust:** as the selected engines provide a higher thrust than required, this criterion is included.
- **TSFC:** thrust specific fuel consumption determines the fuel consumption during the flight.
- **Dry weight:** the lower the weight of an engine the more favourable this criteria is.
- **Flyover noise:** for sustainability, a lower noise is considered to be more optimal, as noise plays an important role around regional airports. Between the various noise types, flyover noise is the most significant to consider at these airports. Nevertheless, if flyover noise is lower, normally also the other types of noise are lower.
- **NO_x emissions:** as CO_2 emissions are directly related with TSFC and thus taken into account with that criteria, NO_x emissions need to be taken into account for sustainability as well. Other emissions types are not considered for the trade-off as much less influential than the two above mentioned.

In order to evaluate the engines, criteria ranges are set for the trade-off in Table 4.2. Values in red are unacceptable, which implies that the engines that have at least one of those are considered not fitting. This is so determined as the aircraft should be comparable or better than competition for these criteria.

Table 4.2: *Engine trade-off ranges for all the criteria.*

	optimal (++)	good (+)	acceptable (0)	unacceptable (−−)
Thrust [kN]	56-59	53.5-56	> 59 and < 70	< 53.5 and > 70
TSFC [mg/(N s)]	< 23.4	23.4-24.6	24.6-25.8	> 25.8
Dry weight [kg]	< 1214	1214-1428	1428-1642	> 1642
Flyover noise [EPNdB]	< 96.1	96.1-97.1	97.1-98.1	> 98.1
NO_x emissions [g]	< 2109	2109-2481	2481-2853	> 2853

The thrust ranges are set as such because having a more than the minimum necessary thrust is advantageous. In fact, for maintainability, it is better to not use full throttle, as expressed in [78].

For all the other criteria, an average value of the criteria of current engines was first identified and then the ranges were created by increasing or decreasing by a certain percentage. For TSFC, 5% was chosen as there is a small variation between different engines. Nevertheless, such percentage strongly decreases the fuel consumption and thus the operational costs. For flyover noise, 1% was chosen for the small variations as well. For dry weight and NO_x emissions, a 15% range change was chosen. The reason is that the difference between the current engine values varies in a greater amount and that the influence below such % change is not that strong.

The weighting of each criterion is defined as shown in Table 4.3. The TSFC, flyover noise and NO_x emissions were considered to be the most influential in terms of operational costs and sustainability.

Table 4.3: *Criteria weights for engine trade-off.*

Thrust	TSFC	Dry weight	Flyover noise	NO_x emissions
0.1	0.3	0.15	0.25	0.2

Now that all the ranges are set and explained, the trade-off can be computed. This is shown in Table 4.4. All the engines with a red value are eliminated as they are considered not fitting. By assigning 0 points for a yellow value, 1 point for a light blue value and 2 points for a green value, it can be seen in Table 4.4 that the Pratt & Whitney PW1215G is the most fitting engine for the aircraft design. An image of the engine can be seen in Figure 4.1.

Table 4.4: *Engine trade-off.*

Model	Thrust [kN]	TSFC [mg/(N s)]	Dry weight [kg]	Flyover noise [EPNdB]	NO$_x$ emissions [g]	Score
BR700-710A2-20 [29]	0 65.61	0 25.5	–– 1891	–– 98.2	0 2784	–
GE CF 34-8C [12]	++ 56.36	+ 24	++ 1088	+ 97	+ 2120	1.25
GE CF34-8E5 [11]	0 59.68	+ 24	++ 1179	+ 97	+ 2223	1.05
Progress D-36-4A [73]	0 63.77	+ 24.2	++ 1130	0 97.2	–– 13662	–
Progress D-436-148 [74]	0 64.43	0 24.6	+ 1400	0 97.4	–– 9546	–
SaM146-1S17 [82]	0 69.21	0 25.2	–– 2260	0 97.8	0 2695	–
PW814GA [31]	0 68.63	+ 23.7	+ 1423	+ 96.5	–– 3168	–
PW1215G [95]	0 66.6	++ 21.5	+ 1360	++ 94	++ 1897	1.65
Tay 611-8C [30]	0 61.61	–– 26.8	0 1538	–– 99.6	0 2562	–

However, as this engine delivers a maximum thrust of 66.6 kN, a proposal will be delivered to Pratt & Whitney to manufacture a $MW5$ customised scaled-down version of the PW1215G. In fact, due to the fact that 66.6 kN of power is 20% higher than required, a scaled-down version could result in a reduction in engine dry weight or a more efficient engine. Because the $MW5$ is expected to deliver at least 600 aircraft, this translates into a 1200 engine order for Pratt & Whitney. This amount is expected to be high enough to make it a viable business for the engine manufacturer. The proposal will be to design an engine with a maximum thrust of 58 kN. For further calculations, the design thrust of 53.5 kN will be taken into account, as it is the minimum required thrust.

Figure 4.1: *An illustration of the PW1215G engine [2].*

4.2. Balanced Field Length

The take-off distance can be divided into two parts: the groundroll distance and the airborne distance. If one of the engines fails during the ground run, the aircraft needs to be able to continue take-off and climb to screen height (10.7 m above the runway) or come to a complete stop on the runway[1].

---

[1] Retrieved from: `http://hatcheraviation.com/uploads/Pages%20from%20PHAK-chap%209.2%20Aircraft%20Performance.pdf` on 12/06/2018

The runway length is based on a possible engine failure at the most critical point, which is at V_1. The decision speed V_1 is chosen in such a way that when an engine failure occurs, the pilot is able to abort the take-off and make a full stop on the runway or continue take-off to screen height with one engine out, resulting in the same distance. This distance is defined as the balanced field length. The required take-off distance is equal to the balanced field length, or 115% of the distance over screen height (10.7 m above the runway) with all engines operative, whichever is greater [81].

In Figure 4.2, the balanced field length and the decision speed are shown graphically. It was found that the balanced field length is 1490 m and that this is the limiting factor. The decision speed V_1 is 70 m/s.
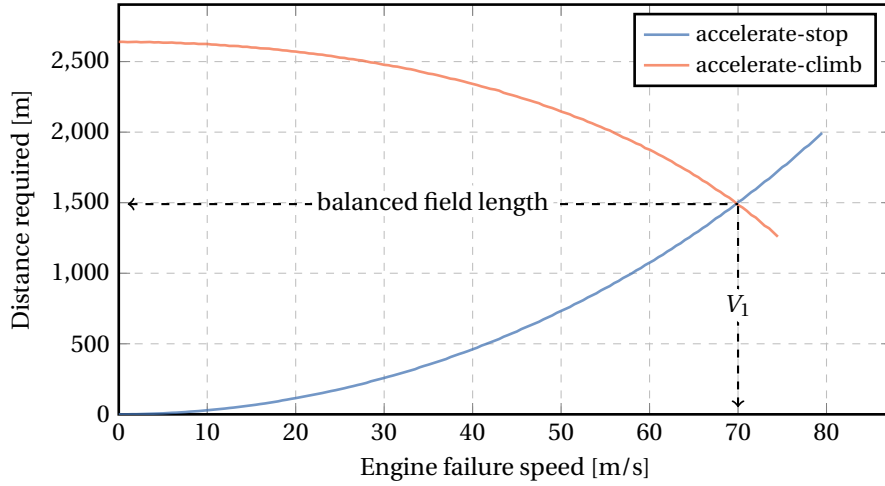
Figure 4.2: *Balanced field length.*

4.3. Flight Path

In this section the complete flight path from take-off to landing is described. The flight starts with the take-off manoeuvre, which is covered in Subsection 4.3.1. After take-off, the different take-off segments and the climb to cruise altitude are described in Subsection 4.3.2 and Subsection 4.3.3, respectively. The calculations for cruise that minimise the fuel burn can be found in Subsection 4.3.4. Finally, the the section concludes with descent and the landing manoeuvre in Subsection 4.3.5, and a short overview of the complete flight path in Subsection 4.3.6.

4.3.1. Take-Off

The take-off starts when the aircraft is at the runway and ends when the aircraft clears the screen height which is set by regulations at 35 ft, or 10.7 m. The take-off consists of two parts: the ground roll and the airborne phase. The calculation of the take-off is based on Anderson [5]. Take-off is done at $1.1V_{\text{stall}}$ as required by CS-25 [3] and is calculated with Equation 4.3. Here, $C_{L_{\text{max}_{\text{TO}}}}$ is the maximum lift coefficient in take-off configuration and is found to be 1.70. The stall speed was found to be 68.2 m/s.

$$V_{\text{stall}} = \sqrt{\frac{\text{MTOW}}{S} \frac{2}{\rho} \frac{1}{C_{L_{\text{max}_{\text{TO}}}}}} \tag{4.3}$$

The acceleration during the ground roll determines how long it takes to reach the take-off speed. Drag and lift can be calculated with Equation 4.4a and Equation 4.4b, where $C_{D_{\text{max}}}$ is calculated with Equation 4.5. $C_{L_{\text{max}_{\text{TO}}}}$ is divided by 1.1 as this gives a safety factor for take-off. With the equations found in Anderson [5, 6], the acceleration equation can be written as in Equation 4.6.

$$L = \frac{1}{2} \frac{C_{L_{\text{max}_{\text{TO}}}}}{1.1^2} \rho_0 V^2 S \quad \text{(a)} \qquad\qquad\qquad D = \frac{1}{2} C_{D_{\text{max}}} \rho_0 V^2 S \quad \text{(b)} \tag{4.4}$$

$$C_{D_{\max}} = C_{D_0} + \frac{C_{L_{\max_{\text{TO}}}}^2}{\pi A e} \tag{4.5}$$

$$a = \frac{g_0}{W}(T - D - \mu_r(W - L)) \tag{4.6}$$

For the airborne phase of the take-off, a circular path is assumed. The radius of this path is calculated with Equation 4.7. The load factor (n) is set to be 1.21 by regulations. The groundroll and airborne phase can be seen in Figure 4.3 and the increase in speed can be found in Figure 4.4.

$$R = \frac{V_{\text{LOF}}^2}{g_0(n-1)} \tag{4.7}$$

The fuel burned during this segment can be calculated using the thrust specific fuel consumption and the thrust applied. Fuel burn per second can be calculated with Equation 4.8. Taking the time it takes to complete the take-off, the total fuel burned can be calculated. The TSFC is given at sea-level and in coming stages, a correction factor should be applied.

$$\dot{m}_{\text{fuel}} = \text{TSFC} \times T \tag{4.8}$$

The fuel burn is calculated to be 62.3 kg. After clearance of the screen height, the following parameters for the aircraft can be found in Table 4.5. Here, it can be seen that it takes approximately 28 s to take-off.
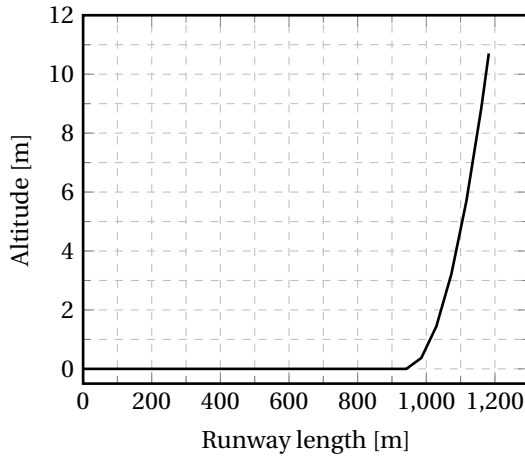
Figure 4.3: *Runway covered to clearance of screen height.*
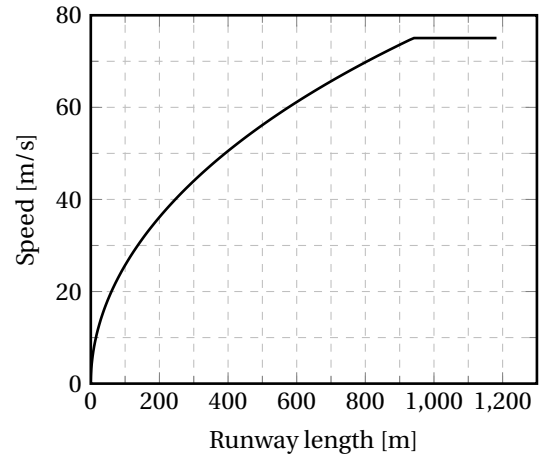
Figure 4.4: *Speed increase during take-off.*

4.3.2. Take-off Segments

The take-off segments begin after the screen height until the beginning of the steady climb. During each of the segments, the aircraft performs specific actions that are required for the correct operational procedure. The segments are subdivided into a first segment, a second segment, en-route climb and final segment.

First & second segment   In the first segment, the landing gear is retracted. According to ESDU [68], the retraction time is approximately 13 s. After completion, the aircraft steepens its flight path to climb to 122 m (400 ft), which is set by regulations [3]. This short climbing phase is the second segment. The speed during this segments increases 1.1 to 1.2 V_{stall} [57].

En-route climb segment   In this phase, the high lift devices (HLDs) are retracted into cruise configuration and the aircraft is accelerated. The limit on the acceleration is imposed by the maximum speed that the HLDs can support while retracting. This speed is 90 m/s for HLDs that are retracted from a range between 18 to 24° [42]. As an acceleration is performed and more thrust is required, the flight path angle for this phase was set at 1° to minimise fuel consumption.

Final segment In the final segment, the aircraft is preparing for the climb to cruise altitude. The speed is increased to the optimal speed to start climbing at the regulated minimum height of 457.2 m (1500 ft), which is the altitude at which the take-off procedure is concluded. The optimal speed at this height to start climbing is 120 m/s.

Depending on the configuration at which the aircraft is flying at every segment, the lift, drag and Oswald factor change accordingly. The wing area does not change due to the used HLDs. These are based on the analysis performed in Section 6.4. Furthermore, the equation to determine the thrust setting at each segment is expressed as Equation 4.9.

Table 4.5: *Parameters after complete take-off.*

	Before take-off	After clearing h_{scr}	After complete take-off
W [N]	296,160	295,543	295,096
s [m]	0	1182.5	6987
h [m]	0	10.73	457.2
t [s]	0	27.4	88.2

$$T = W \sin(\gamma) + D \tag{4.9}$$

Finally, the aircraft configuration for every segment is displayed in Table 4.6 and the displayed flight path in Figure 4.5 and Figure 4.6. An overview of the characteristics can be found in Table 4.5. From this it can be calculated that the total fuel burned up to this stage is approximately 108.4 kg.

Table 4.6: *Aircraft action and configuration at each take-off segment.*

Segment	First	Second	En-route	Final
Action	*Undercarriage retraction*	*Climb to 122 m*	*High lift devices retraction*	*Climb to 457.2 m*
C_L [-]	1.70	1.70	1.70	1.07
C_{D_0} [-]	0.056	0.036	0.036	0.021
e [-]	0.85	0.85	0.85	0.8
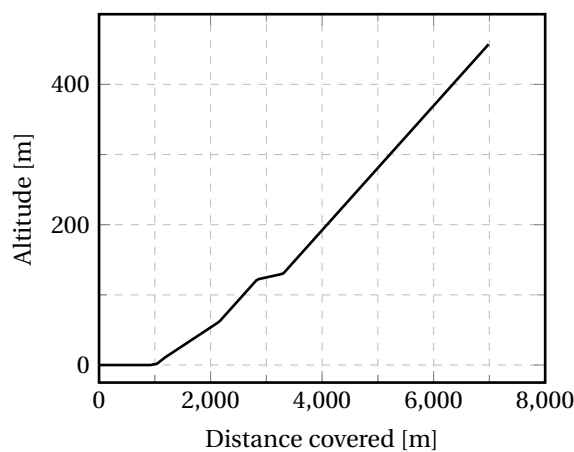
Figure 4.5: *Distance covered up to the climb.*
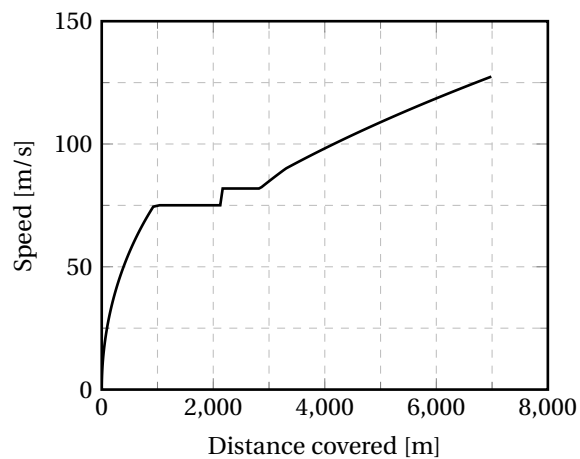
Figure 4.6: *Speed increase during full take-off.*

4.3.3. Climb

After the final take-off segment and the aircraft has climbed to an altitude of 457.2 m (1500 ft) above ground level, the aircraft starts climbing to cruise altitude. For the climb to cruise altitude, it is important to look at the time to climb and the amount of fuel burned.

Time to climb   In general, it is preferred to minimise the time to climb because the aircraft is much more fuel efficient during the cruise. The time to climb can be minimised by climbing at the maximum rate of climb. This is not the most optimum climb regarding fuel consumption, but it is, in fact, a good approximation [5]. The airspeed at which the maximum rate of climb occurs increases with height. Therefore, a portion of the available excess power must be used to accelerate [81]. In order to minimise the time to climb, the rate of climb needs to be maximum at each altitude. The maximum rate of climb was calculated at different altitudes between 457.2 m and 10,000 m altitude with increments of 100 m using Equation 4.10,

$$\text{ROC}\left[1 + \frac{V}{g}\frac{dV}{dh}\right] = \frac{P_a - P_r}{W},\tag{4.10}$$

where the right-hand side is the specific excess power and the expression between square brackets the kinetic energy correction factor. The total time to climb is obtained by adding the increments in time between the different altitude intervals.

$$t = \sum_{i=1}^{n}\left[\frac{\Delta h}{\text{ROC}_i}\right]\tag{4.11}$$

The climb is an unsteady quasi-rectilinear climb: unsteady because the airspeed increases with increasing height, and quasi-rectilinear, because the flight path angle remains more or less constant. During climb, the flight path angle slowly decreases from 3.6° at the beginning of climb to 0.8° at cruise altitude. Because the time required to climb to cruise altitude is approximately 20 minutes, the rate of change of flight path angle is close to zero.

Fuel burned during climb   The fuel burned during climb also needs to be taken into account. The fuel flow at any moment in time depends on the thrust-specific fuel consumption and the thrust setting. The fuel flow can be calculated using Equation 4.8 as mentioned earlier. When fuel is burned the aircraft becomes lighter and the maximum rate of climb that can be achieved increases. The reduction in fuel weight is taken into account when calculating the time to climb to cruise altitude and the fuel burned during the climb.

Limitations on the ROC   The highest rate of climb that can be achieved is limited by ATC procedures which restrict the calibrated airspeed of aircraft under 10,000 ft to 250 kts[2] and the rate of change of cabin pressure. Because the airspeed at which the maximum rate of climb occurs is generally higher than 250 kts, the maximum rate of climb can often not be achieved below 10,000 ft.

The other factor that limits the highest rate of climb is the rate of change of cabin pressure [81]. When the cabin pressure changes too quickly, this can be unpleasant or even painful. In general, ambient pressure changes are not perceived when the time rate of change of pressure is kept within the following limits:

$$-30 < \frac{dp}{dt} < 18\,\text{Pa/s}$$

The lower limit is applicable to climb and the upper limit applies to descent. At a normal cruise altitude of 10,000 m, the cabin pressure[3] (p_c) is usually equal to the atmospheric pressure at a geo-potential altitude of 1800 to 2400 m. The pressure at the highest geo-potential altitude was chosen because this results in the lowest pressure difference between the inside and outside of the fuselage. However, this also results in the largest difference in cabin pressure during climb, resulting in a lower allowable rate of climb than when a geo-potential altitude of 1800 m was chosen for the cabin pressure. The minimum time to lower the cabin pressure from the air pressure at sea-level to the air pressure at cruise altitude can be calculated using:

$$t = \frac{p_0(1 - p_c/p_0)}{dp/dt}\tag{4.12}$$

When the air pressure in the cabin is equivalent to the outside pressure at an altitude of 2400 m, the pressure ratio $p_c/p_0 = 0.75$. This results in a minimum time to climb of 857 s. Consequently, the rate of climb should never exceed 10,000 m / 857 s = 11.7 m/s.

---

[2]Retrieved   from: `https://www.faasafety.gov/files/events/ea/ea03/2012/ea0345029/airspace_made_easy.pdf`   on 26/06/2018

[3]Retrieved from: `http://www.who.int/ith/mode_of_travel/cab/en/` on 11/06/2018

The limitations due to the rate of change of cabin pressure and the airspeed restriction below 10,000 ft were both taken into account when calculating the minimum time to climb. Below 10,000 ft the maximum rate of climb is limited by the airspeed restriction and the rate of change of cabin pressure, and just above 10,000 ft the maximum rate of climb is limited by the rate of change of cabin pressure only.

Maximum ROC By calculating the rate of climb at different altitudes and at different airspeeds, a contour plot with lines of a constant rate of climb can be made. This is shown in Figure 4.7. The maximum rate of climb is the highest at sea-level and decreases with increasing altitude. The altitude at which the maximum rate of climb is zero is defined as the absolute ceiling. This is the highest altitude the aircraft can theoretically reach. A more useful quantity is the service ceiling, conventionally defined as the altitude at which the maximum rate of climb is 0.5 m/s. The service ceiling is a practical upper limit for steady, level flight [5]. It was found that the calculated theoretical ceiling is 15,890 m.

However, these values are determined to be the upper limit as the decrease in engine thrust due to increased airspeed was not taken into account. Therefore, the operational service ceiling is for now set to be 12,500 m and will be elaborated further in Section 4.6.

In Figure 4.8 the rate of climb is given as a function of airspeed at different altitudes. The maximum rate of climb at each altitude is represented by the dashed line. Note that the ROC has not been calculated for airspeeds below stall speed. Besides the rate of climb, the maximum airspeed that can be achieved at each altitude can also be read from the graph. The maximum airspeed at each altitude can be found by looking at the intersection point with the x-axis that corresponds with the highest true airspeed.
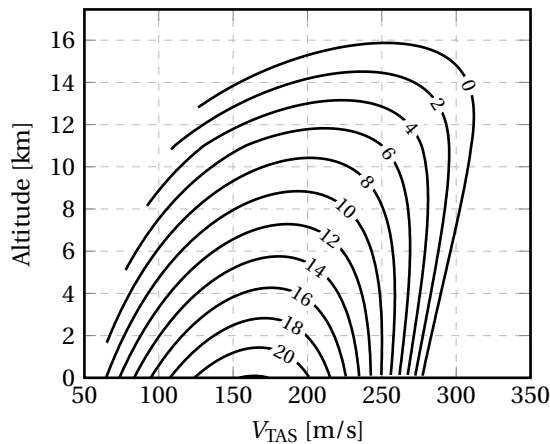
Figure 4.7: *Lines of constant rate of climb.*
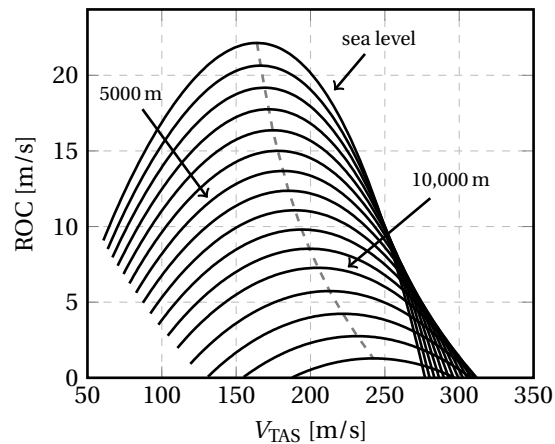
Figure 4.8: *ROC as a function of altitude and true airspeed.*

4.3.4. Cruise

In terms of fuel burn and time the cruise stage the most significant stage. The cruise Mach number is set to 0.78 to be competitive with other regional aircraft and is elaborated in more detail in Section 4.6. Cruise is defined as optimal under the following condition:

$$C_{L_{opt}} = \sqrt{\frac{1}{3} C_{D_0} \pi A e} \tag{4.13}$$

With this the thrust setting can be determined with Equation 4.14a and with the aforementioned Equation 4.8 the fuel burned during the cruise can be calculated. The thrust specific fuel consumption needs to be corrected for the height, as the TSFC is given at sea-level. This is done by multiplying it with Equation 4.14b to the power 0.75. After setting these parameters, the optimal height can be calculated by rewriting the lift equation. This will output the optimal ρ which in turn gives a height to fly at.

$$T = W \frac{C_D}{C_L} \quad \text{(a)} \qquad\qquad\qquad \sigma = \frac{\rho}{\rho_0} \quad \text{(b)} \tag{4.14}$$

In Figure 4.9 and Figure 4.10 the flight path and speed changes can be found respectively. The range is set in such a way that when landing is included the maximum set distance of 2500 km is reached. The parameters

at the end of the cruise stage are shown in Table 4.7. In there it can be seen that the fuel burned during cruise is approximately 3407 kg and that it takes 2.9 hours to reach that distance, which is 2280 km.

Table 4.7: *Parameters after completion of cruise.*

	Beginning of cruise	End of cruise
W [N]	285,122	251,696
s [km]	201.7	2280.0
h [m]	10,252	11,043
t [min]	21.9	172
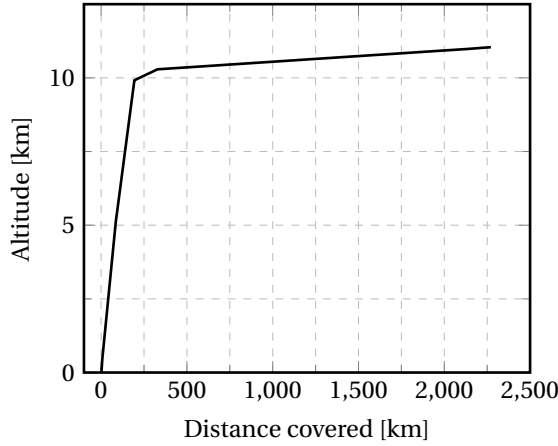
Figure 4.9: *Distance covered up until the end of cruise stage.*
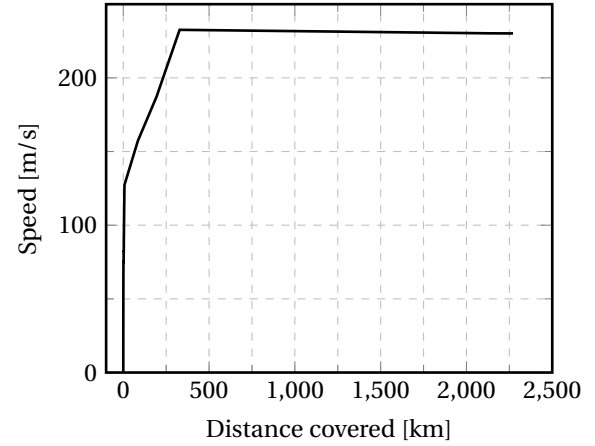
Figure 4.10: *Speed changes up until cruise stage.*

4.3.5. Descent & Landing
The phases that take place after cruise are descent and landing. Besides descent and landing, this subsection also covers limitations on the rate of descent.

Descent   At the end of cruise the aircraft starts to descent, which is done with the thrust levers set to idle thrust. If it is assumed that the idle thrust can be neglected, the minimum angle of descent is constant and can be calculated using

$$\bar{\gamma} = \arctan\left(\frac{C_D}{C_{L_\mathrm{opt}}}\right) \qquad \text{where} \qquad C_{L_\mathrm{opt}} = \sqrt{C_{D_0}\pi A e} \tag{4.15}$$

where the descent angle $\bar{\gamma}$ is independent of the aircraft weight.

Limitations on the ROD   Just as with climb, the rate of descent is limited by the rate of change of cabin pressure. For descent, the rate of change of cabin pressure is not allowed to exceed 18 Pa/s. If the same cabin pressure and cruise altitude are assumed, i.e., $p_c/p_0 = 0.75$, the minimum time to descent is 1428 seconds. Consequently, the rate of descent should never exceed 10,000 m / 1428 s = 7.0 m/s.

It was found that for descent, the airspeed restriction of 250 kts below 10,000 ft does not impose any restrictions on the minimum angle of descent when the thrust levers are set to idle.

Landing   After descent, the landing phase of the flight will be the final phase. The landing is the reverse of the take-off and also consist of two parts; the approach and groundroll phase. The approach speed is determined by $1.3V_\mathrm{stall}$ where V_{stall} is defined as in Equation 4.3. The approach is done at a descent angle $\bar{\gamma}$ of 3°. After the flare height is reached, a circular path is followed, which is calculated as:

$$R = \frac{1.3V_\mathrm{stall}}{\Delta n \cdot g_0} \tag{4.16}$$

In this equation, Δn is set to be 0.10 by statistical data based on jets [91]. After the aircraft reaches the runway a transition phase is incorporated in the path in which the aircraft is rotated to land; this takes approximately 2 seconds. After touchdown, the groundroll is done, in which the deceleration is given by:

$$a_{\mathrm{br}} = \frac{g_0}{W}(D + \mu_{\mathrm{br}}(W - L)) \tag{4.17}$$

The distance covered is calculated by the time it takes to decelerate from landing speed to standstill. The result of the landing phase can be seen in Figure 4.11 and Figure 4.12. It takes approximately 1450 m to come to completely stop, which is lower than the set requirement of 1500 m.
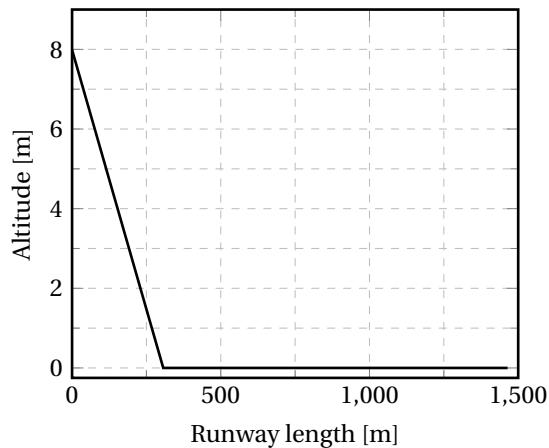
Figure 4.11: *Runway covered from flare height to standstill.*
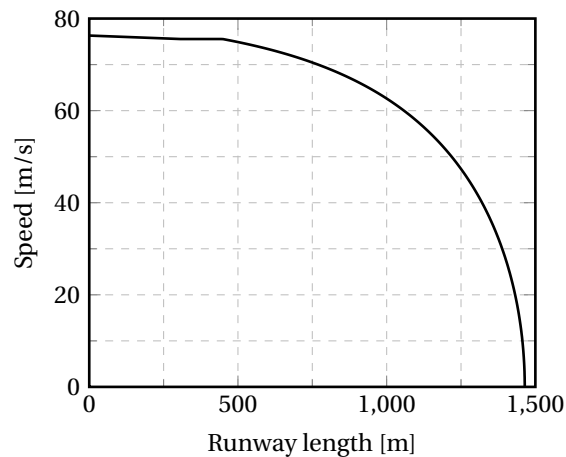
Figure 4.12: *Speed decrease during landing.*

4.3.6. Total Flight Path

Now that all the different phases of the flight path are discussed, all of those can be put together to show the total flight path. The flight path result can be found in Figure 4.13 and Figure 4.14. The characteristics that describe the total path can be found in Table 4.8.

Table 4.8: *Performance overview.*

	After landing
W [N]	248990
Fuel burned [kg]	4808
s [km]	2498
h_{max} [km]	11.0
t [hr]	3.34

4.4. Flight Performance Optimisation

The flight performance optimisation aims at decreasing operational costs as much as possible. This is done by reducing fuel consumption with still a competitive time to travel. Based on [78], certain actions were taken to optimise the performance.

Cruise climb   Cruise climb was already implemented in the main flight path shown in Figure 4.13. This ended up in 21 kg less fuel, which is about a 0.4% decrease in the total fuel. This is a small percentage but it makes sense considering the short range and the fact that a bigger descent would be needed. A small decrease in fuel can lead to enormous savings for the airline as multiple flights per day are executed.

Full runway use   Making use of the full runway can be beneficial in various aspects. Due to the fact that the engine can deliver more thrust than required to take off within 1500 m, a reduced throttle setting leads to less
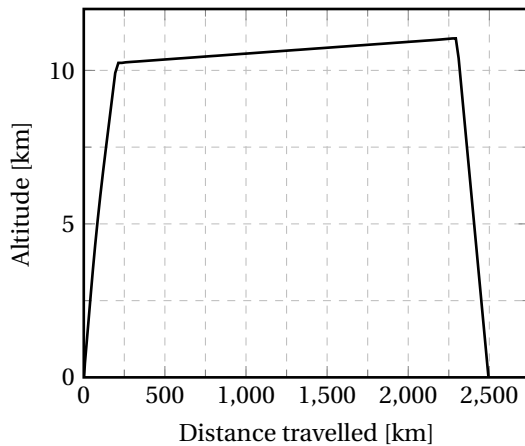
Figure 4.13: *Runway covered to clearance of screen height.*
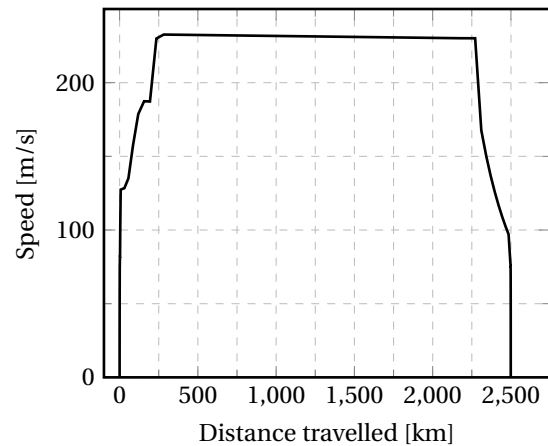
Figure 4.14: *Runway covered to distance of screen height.*

fuel consumed. Additionally, a lower thrust setting is better for the engine because this results in less engine wear, which results in less maintenance. Besides this, a lower thrust setting also results in a decrease in noise both from the airframe as from the engines.

Take-off segments   A more continuous climb during the take-off segments results in less noise at the ground and a faster climb with reduced fuel consumption than the step-wise climb. This leads to 68 kg of less fuel burned.

Steep approach   Finally, it was decided to adapt the aircraft design to a steeper approach. In fact, by improving the high lift devices to create a $C_{L_{max}}$ at landing of 1.97, the aircraft is able to fly slower while approaching. This results in fewer stresses on the landing gear while landing, which makes it possible to increase the approach angle. By increasing it 3 to 4°, the procedure ensures to decrease noise at landing [7]. Furthermore, 1 kg less fuel is consumed.

By considering all these optimisation actions, a much lower noise is produced at take-off and landing procedures and 90 kg of fuel are saved each flight. This value represents a decrease of 1.5% decrease in the total fuel consumption. This is a small saving for one single flight but when considering 1 year of operations it could represent a significant increase in revenues for the aircraft operator.

4.5. Payload-Range

The payload-range diagram of the final aircraft design is shown in Figure 4.15. On the vertical axis the payload is given and on the horizontal axis the still air range, which is the range with zero wind velocity.

With maximum payload, or 76 passengers, the aircraft taking off at its MTOW will be able to fly a distance equal to 2500 km. After this point, the range can be increased further by reducing the number passengers and carrying more fuel. When the maximum fuel capacity is reached, 62 passengers can be transported over a distance of 2945 km. Finally, when the payload weight is reduced to zero and no passengers are present, the aircraft can reach 4175 km.

4.6. Flight Envelope

The flight envelope is provided to summarise the operational limits of the aircraft in terms of true airspeed and altitude. It is first generated by calculating the stall speeds at varying altitudes for the aircraft in clean configuration as well as with full flaps deployed.

The operating service ceiling is set at this stage of the design process to be at 41,000 ft (12500 m), which is identical to the service ceiling of the Bombardier CRJ700[4] and the Embraer E170[5]. Flying higher than this

---

[4]http://www2.bombardier.com/CRJ/en/specifications.jsp?langId=en&crjId=700
[5]https://www.embraercommercialaviation.com/commercial-jets/e170/
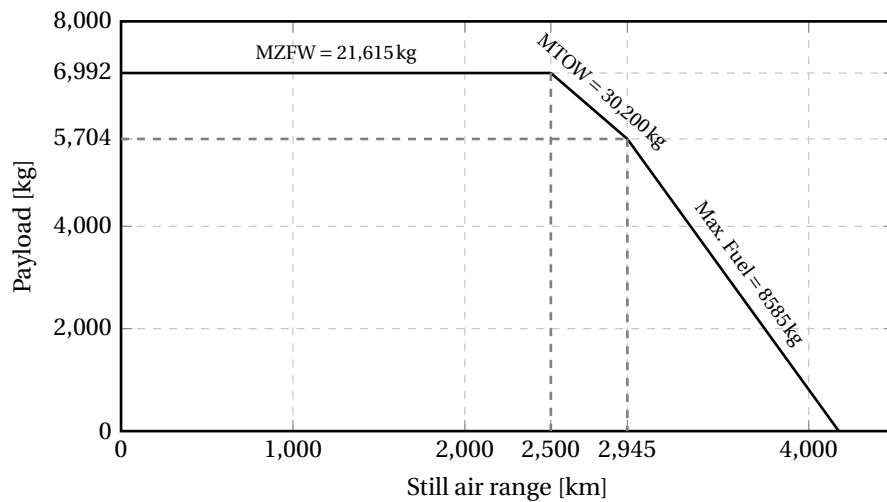
Figure 4.15: *Payload-range diagram.*

altitude is rare with large passenger aircraft as safety critical problems related to propulsion and control will arise from the thinner air density.

Following that, the limit operating speeds are calculated. There are two limits that need to be observed in the operation of the aircraft, which are the maximum operating equivalent airspeed and the maximum operating Mach number. The maximum operating equivalent airspeed should not be exceeded as it may cause structural damage due to aeroelastic effects, whereas the maximum operating Mach number should not be exceeded as shock-waves will form on the wing as the airflow becomes locally supersonic. To be competitive with the CRJ700 and E170, the maximum operating airspeed and Mach number is set to be at 335 m/s KEAS (172 m/s EAS) and 0.78 respectively.

The flight envelope is presented in Figure 4.16 and is calculated for the MTOW of the aircraft. The stall limits of the aircraft will move to the left if the aircraft is loaded lighter than the MTOW. It can be observed that the true airspeed limit shifts from the equivalent airspeed limit to the Mach limit at approximately 8000 m. Also, the true airspeed limit from 11,000 m upwards remains constant as the Mach number does not change due to the constant temperature in the tropopause.
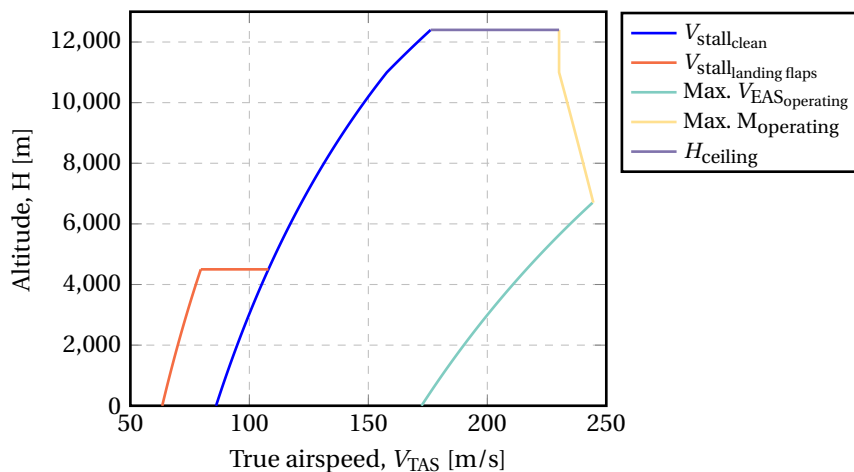
Figure 4.16: *Flight Envelope at MTOW.*

4.7. *V*-*n* **Diagram**

The *V*-*n* diagram is constructed in order to determine the maximum load factors that the aircraft needs to be designed for, as well as to clearly define the operational limits of the aircraft for pilots. The constructed *V*-*n* diagram is contained in Figure 4.17. To construct the *V*-*n* diagram, certification specifications from the

European Aviation Safety Agency (EASA) CS-25 requirements are referenced [3].

From CS 25.337 [3], the maximum positive limit load factor of an aircraft of the weight class of the designed regional aircraft is 2.5 while the negative limit load factor is –1. The left boundary of the manoeuvre limit is determined by the load factor experienced by the aircraft in the maximum and minimum C_L values. The manoeuvre limit for flaps is also included to meet requirement CS 25.345 [3] that states that the flaps need to meet a maximum positive limit load factor of 2. The maximum flap deployment speed, V_F is constrained by its structural strength and meets the requirement of being at least 1.8 times the stall speed at landing configuration. The designed dive speed is the maximum speed the V-n diagram takes into consideration and is driven by CS 25.335(b) [3], which states that it should be at least 1.25 times larger than the designed cruise speed except when the speed is Mach limited.

In addition to manoeuvre loading, the gust loading also needs to be taken into consideration at the cruise and dive speeds as stated by CS 25.335(d) [3]. The change in load factor due to a gust is calculated with

$$\Delta n = 1 + \frac{\rho V C_{L_\alpha} K U}{W/S} \tag{4.18}$$

where U is the gust velocities defined in CS 25.345(a)(5)(i) [3] and K is defined as

$$K = \frac{0.88\mu}{5.3 + \mu}.$$

The parameter μ is given by

$$\mu = \frac{2W/S}{\rho c}.$$

It was found that the load increase due to gusts does not exceed the load factors due to the manoeuvre loading. This is due to the small surface area and the chord length of the wing combined.
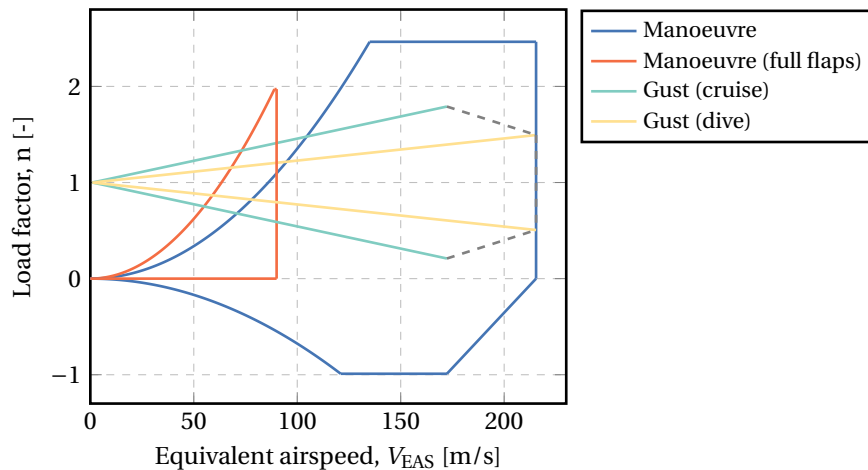
Figure 4.17: *V-n diagram at MTOW.*

4.8. Turning Performance

The turning performance of the aircraft at MTOW is investigated in this section. The holding phase of the flight is found to contain the most demanding turning requirements and hence it was decided to evaluate the turning performance at an altitude of 7000 ft which is the maximum altitude of typical holds directed by ATC [35].

Firstly, the maximum achievable load factors at different flight velocities need to be calculated. The maximum achievable load factor is limited by the available engine thrust and the maximum load factor that the aircraft is certified to manoeuvre at, which is 2.5. The drag increases with increasing load factor and is given by $D_n = D_{n=1}n$. The stall speed also increases with increasing load factor and is given by $V_{\text{stall}_n} = V_{\text{stall}_{n=1}}\sqrt{n}$. This is also calculated for a partially deployed flap setting to achieve a C_L of 1.50 (the maximum C_L attainable from full flap deployment is 1.97). This generates the diagram of available thrust and drags at load factors ranging from 1 to 2.5 in Figure 4.18. From Figure 4.18, the relationship of the maximum achievable load factor versus airspeed can be found and is contained in Figure 4.19.
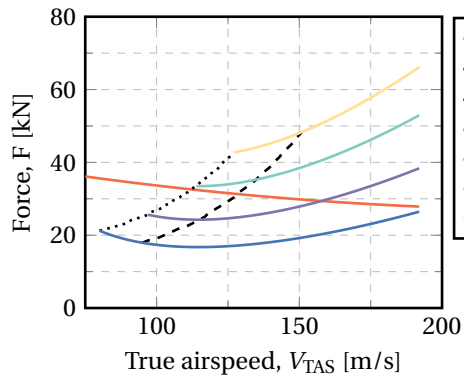
Figure 4.18: *Drag at different load factors and the available thrust.*
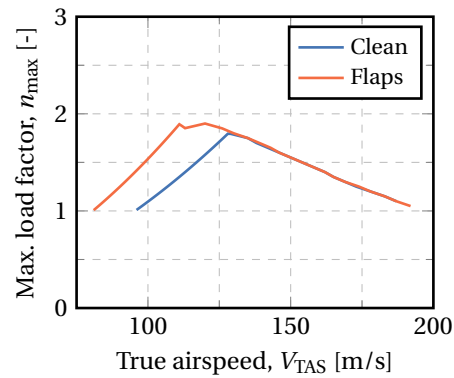
Figure 4.19: *Maximum achievable load factor at MTOW at 7000 ft.*

The turn radius, R is found using the formula

$$R = \frac{V^2}{g\sqrt{n^2 - 1}} \tag{4.19}$$

From the information in Figure 4.19, the turn radius at every airspeed at its corresponding load factor is calculated and is presented in Figure 4.20.

It should be realised however that the condition for minimum turn radius does not necessarily equal give the condition for the minimum time to turn. Therefore, the minimum time to turn is found by the formula

$$T_{2\pi} = \frac{2\pi R}{V} \tag{4.20}$$

The results of the calculations are summarised in Table 4.9. The results demonstrate that at maximum take-off weight, the $MW5$ is capable of meeting standard rate two turns (6 deg/s) at the upper-limit of typical holding altitudes of 7000 ft.
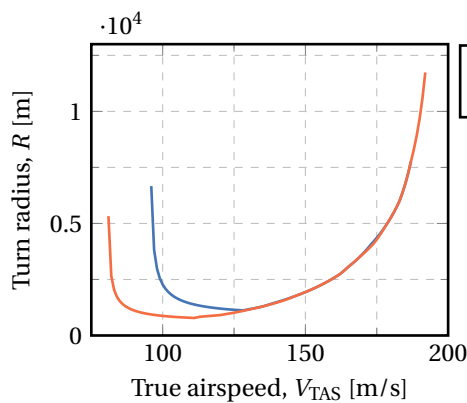
Figure 4.20: *Turn radius at MTOW at an altitude of 7000 ft.*
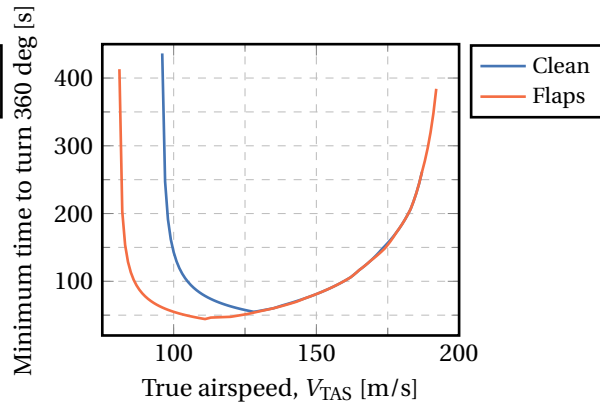
Figure 4.21: *Turn radius at MTOW at an altitude of 7000 ft.*

Table 4.9: *Turn performance parameters calculated at MTOW at 7000 ft.*

	Clean	Partial flaps ($C_L = 1.5$)
Min. turn radius [m]	1202	782
Fastest time to turn 360° [s]	55	44
Max. turn rate [deg/s]	6.5	8.1

4.9. Verification & Validation

In this section, the verification and validation methods of the programs for the flight performance calculations are described. Verification is performed to see whether the calculations are correct. After verification, validation is used to check if the program solves the problem correctly. The verification and validation procedures that were used to verify and validate the programs in this chapter can be found in Appendix A.

4.9.1. Verification

Verification can be divided into two parts: code verification and calculation verification. The purpose of code verification is to make sure that the program does not contain syntax errors or other errors that prevent the program from working correctly. Once the code is free of programming errors, the program should be checked to make sure that the numerical model is correct. This was done on a small scale (unit tests) and on a larger scale (system tests).

Different unit tests were performed to verify the correctness of the individual units of code:

- **International Standard Atmosphere (ISA):** For the calculation of the air temperature, air pressure and air density, the International Standard Atmosphere was used. The calculations of the properties of the ISA were checked by comparing these values to other Standard International Atmosphere tables [6].

- **Take-off and landing:** For the calculation of the required runway length for take-off and landing the results were checked by using data from different textbook examples. The results of the textbook examples were then compared to the numerical results calculated by the program. For take-off, example 6.25 from *Introduction to Flight* by John D. Anderson [6] was used, and for landing example 6.26.

- **Flight:** For climb, cruise and descent the calculations were also verified by using data from textbook examples and comparing the results of these examples with the results as calculated by the different programs. For climb example 6.18 from *Introduction to Flight* by John D. Anderson [6] was used. For cruise example 6.20 was used and for descent the example in section 13.1 from *Elements of airplane performance* by Ger J.J. Ruijgrok was used.

- **Balanced field length:** For the verification of the balanced field length examples 6.25 and 6.26 from *Introduction to Flight* by John D. Anderson [6] were used to verify the numerical results of the program.

After the individual units of code were tested and determined to be functioning properly, the program that models the complete flight from take-off to landing was tested. This was done by o.a. changing some input parameters and checking the influence of these changes on the output of the program. For example, when the thrust-specific fuel consumption was set to zero, the aircraft weight remained constant, and when it was increased, the fuel consumption increased.

4.9.2. Validation

After verification, validation was performed in order to determine that the main program accurately models the complete flight. For the validation of the program that models the complete flight from take-off to landing, the fuel consumption, maximum rate of climb, time to climb, cruise speed, time to descent, and other parameters were compared to different regional aircraft. For the comparison, mainly the Bombardier CRJ700 was used. The reason for this is that the CRJ700 is very similar to the $MW5$ and carries almost the same number of passengers. Besides the comparisons with other regional aircraft, the dimensions and characteristics of these aircraft were used as inputs for the program. The outputs of the program, e.g. fuel consumption, rate of climb, cruise speed, etc., were then compared to the actual values of the comparable aircraft to validate the correctness of the calculations.

4.10. Sensitivity Analysis

Besides verification and validation, a sensitivity analysis was performed to quantify the influence of different parameters on the performance of the aircraft. The four input parameters that were varied are:

- Zero-lift drag coefficient, C_{D_0}
- Effective aspect ratio, A_{eff}
- Wing area, S
- Maximum take-off weight, MTOW

The effects of varying the values of these parameters can be found in Tables 4.10 through 4.13. In these tables, the sensitivity to different output parameters can be found. These output parameters are the take-off length, the maximum rate of climb at sea level, the time to climb to a cruise altitude of 10 km, the fuel burned during the climb, the cruise time and the fuel burned during the cruise.

As can be seen in Table 4.10, the zero-lift drag coefficient has the biggest influence on the rate of climb and the fuel consumption. The higher the zero-lift drag coefficient, the higher the fuel consumption and vice versa. The influence on the time to climb is negligible, because the rate of climb is limited by the maximum rate of change of cabin pressure that is still experienced comfortable by the passengers, and not by the maximum rate of climb that can be achieved. This is the result of the slightly over-designed engines.

Table 4.10: *Sensitivity of performance parameters to the zero-lift drag coefficient ($C_{D_0} = 0.056$).*

%Difference	%$s_{\text{take-off}}$	%ROC_{max}	%t_{climb}	%$(m_{\text{fuel}})_{\text{climb}}$	%t_{cruise}	%$(m_{\text{fuel}})_{\text{cruise}}$
−20	−1.11	14.47	0.00	−7.86	−1.40	−12.23
−10	−1.56	6.67	0.00	−3.67	−0.69	−5.93
+10	0.57	−5.79	0.00	3.31	0.56	5.52
+20	1.14	−10.88	0.00	6.57	0.92	10.65

The effective aspect ratio has a relatively small influence on the take-off distance, rate of climb and time to climb. The influence on the fuel consumption is a bit larger. A higher effective aspect ratio results in a lower fuel consumption, hence lower operational costs per block hour. The effective aspect ratio was increased by adding winglets to the wing tips.

Table 4.11: *Sensitivity of performance parameters to the aspect ratio ($A_{eff} = 10.5$).*

%Difference	%$s_{\text{take-off}}$	%ROC_{max}	%t_{climb}	%$(m_{\text{fuel}})_{\text{climb}}$	%t_{cruise}	%$(m_{\text{fuel}})_{\text{cruise}}$
−20	1.79	−2.96	0.00	5.32	−1.08	8.31
−10	0.79	−1.32	0.00	2.37	−0.50	3.84
+10	−0.63	1.08	0.00	−2.04	0.38	−3.37
+20	−1.16	1.99	0.00	−3.82	0.58	−6.42

As can be seen in Table 4.12, changing the area of the wing has a relatively large impact on the take-off distance and the maximum rate of climb at sea level. Reducing the wing area increases the take-off length, but reduces the fuel consumption and time spent during climb and cruise.

Table 4.12: *Sensitivity of performance parameters to the wing area ($S = 61.10\,\text{m}^2$).*

%Difference	%$s_{\text{take-off}}$	%ROC_{max}	%t_{climb}	%$(m_{\text{fuel}})_{\text{climb}}$	%t_{cruise}	%$(m_{\text{fuel}})_{\text{cruise}}$
−20	18.24	11.80	−1.06	−4.72	−2.65	−4.94
−10	9.06	5.41	−0.34	−2.04	−1.23	−2.32
+10	−8.81	−4.61	−1.05	1.45	0.19	1.29
+20	−17.68	−8.71	−0.81	4.12	0.52	2.85

In Table 4.13 the sensitivity of different parameters to the maximum take-off weight can be found. The maximum take-off weight has the biggest influence on the take-off distance. It can be seen that a weight reduction of 20% results in almost 50% less take-off distance required. This seems like a big difference, but it can be explained. If the aircraft is lighter, it accelerates quicker to the lift-off velocity. Because the lift-off velocity is proportional to the square root of the wing loading, the lift-off velocity is lower for a lower maximum take-off weight. Furthermore, the ground run distance reduces even more due to the lower friction force between the landing gear and the runway.

Table 4.13: *Sensitivity of performance parameters to the maximum take-off weight (MTOW = 30,200 kg).*

%Difference	%$s_{\text{take-off}}$	%ROC_{max}	%t_{climb}	%$(m_{\text{fuel}})_{\text{climb}}$	%t_{cruise}	%$(m_{\text{fuel}})_{\text{cruise}}$
−20	−48.45	30.38	−0.62	−18.82	−0.07	−17.71
−10	−21.00	13.63	−1.02	−9.85	−0.06	−8.86
+10	16.37	−11.36	−1.72	6.80	−1.57	7.23
+20	29.33	−21.00	−2.12	14.44	−2.45	14.81

<div style="text-align: right; font-size: 3em;">5</div>

Aerodynamics

In this chapter, the aerodynamic design of the aircraft will be discussed. First, the wing optimisation will be discussed in Section 5.1, including both the 2D planform as well as the airfoils. Then, both the horizontal tail as well as the vertical tail will be sized in Section 5.2. The results of the planform optimisation are provided in Subsection 5.1.5. Finally, the verification and validation of the models used for the wing planform optimisation is done in Section 5.4.

5.1. Wing Optimisation

In this section, the 3D-wing optimisation will be implemented. This optimisation is based on AVL and Vortex-Lattice theory which will be explained first in Subsection 5.1.1. Then the 2D planform optimisation will be discussed in Subsection 5.1.2, followed by the airfoil optimisation in Subsection 5.1.3.

5.1.1. Vortex Lattice Theory

In order to compute the aerodynamic properties of the wing, AVL[1] is used and thus of Vortex-Lattice Methods (VLM). These methods will be briefly introduced in this section.

VLM is a practical and versatile aerodynamic tool able to reach a high accuracy using relatively simple numerical techniques [59] which makes it therefore very well suited for this project. VLM models the lifting surfaces, such as a wing, as an infinitely thin sheet on which horseshoe vortices are placed, usually in a grid pattern, as shown in Figure 5.2. The pattern used by AVL is shown in Figure 5.1
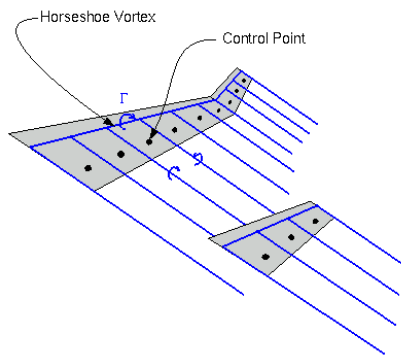
Figure 5.1: *Example of horseshoe vortices on a lifting surface.* **Figure 5.2:** *AVL vortex pattern.*
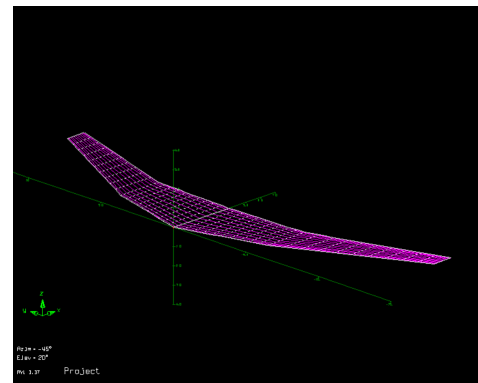
Nonetheless, there are limits to the validity of VLM. AVL is only valid until Mach effects occur, i.e. when a Mach number of 1 is reached locally. At this point the equations of VLM are not valid anymore. Unfortunately, with a cruise Mach number of 0.78, the chances a of local sonic boom is relatively high. On the other hand, methods that can take this into account are complex, hard to use and very time intensive, and thus out of the scope of the design process at this stage. However, there are airfoils that are designed to avoid supersonic effects, even at high Mach numbers: supercritical airfoils. With these airfoils, it is reasonable to assume that no supersonic effects occur during the usual Mach regimes, especially since there are many other aircraft that cruise at higher Mach numbers (0.82-0.85) with these airfoils.

---

[1]H. Youngren, M. Drela, AVL, MIT, for more information see *Program and Code Bibliography* on page 115

[1]S.J. Hulshoff, Non-Linear Lifting-Line Solver, Faculty of Aerospace Engineering, Delft University of Technology, (2007), retrieved on 06/06/2018 from `https://aerodynamics.lr.tudelft.nl/~shulshoff/nlll/doc/manual.html`

Thus, for this analysis, VLM is used, since they yield accurate results using relatively simple numerical techniques. Furthermore, it is assumed that the local Mach number does not reach 1 at any point when using supercritical airfoils.

5.1.2. 2D Wing Planform

In this section the 2D wing planform will be optimised based on Vortex-Lattice theory and AVL. The first step to an optimisation is to define the parameters to be optimized. In order to do so, the planform has to be parametrised. The parametrisation used is given in Figure 5.3. Furthermore, to perform the iteration, a minimum set that defines all other parameters is chosen so to minimize computational time. The equations governing the planform are given by Equation 5.1. The full set of planform parameters that are used is given by Table 5.1. The set of parameters that are chosen to iterate are A, λ_1, λ_2, Λ_1 and Λ_2.
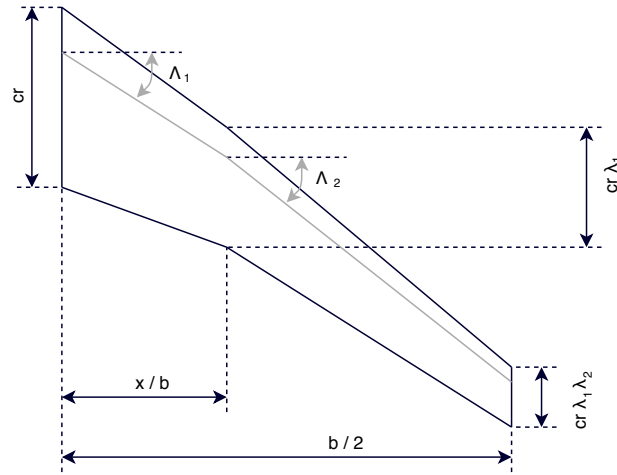
Figure 5.3: *Planform Parameters.*

Table 5.1: *Wing parameters.*

Planform parameters			
ρ	[kg/m]	Air density	Fixed by fixed altitude
a	[m/s]	Speed of sound	Fixed by fixed altitude
M	[-]	Mach number	Set by performance
V	[m/s]	Cruise speed	Set by M and a
S	[m^2]	Surface area	Set by altitude c_l and M
A	[-]	Aspect ratio	Iterated
b	[m]	Span	Set by A and S
λ_1	[-]	Taper ratio root to kink	Iterated
λ_2	[-]	Taper ratio kink to tip	Iterated
Λ_1	[deg]	Sweep angle root to kink	Iterated
Λ_2	[deg]	Sweep angle kink to tip	Iterated
x_k/b	[-]	Kink location	Fixed based on reference aircraft

Now that the input parameters are defined, the next step is to define the output to be minimised. The best indicator of the wing performance is the lift over drag ratio (L/D). Indeed, a maximum value of (L/D) is the best indicator for minimum fuel consumption for a given weight, which is very important for operational cost. However, since the lift is fixed since the aircraft weight is known, this is equivalent to minimising drag. Using Python and AVL, a function that takes the parameters to be optimised as inputs, and the drag from AVL as output is built. This is then minimised and the results are given in Table 5.2.

$$b = \sqrt{S \cdot A} \qquad\qquad c_r = \frac{2 \cdot S}{(1 + \lambda) \cdot b} \qquad\qquad c_{mac} = c_r \cdot (2/3) \cdot \frac{1 + \lambda + \lambda^2}{1 + \lambda} \qquad (5.1)$$

The wing optimisation is based on SciPy's basin hopping algorithm[2]. This algorithm is a powerful all-round optimiser that is adapted to non-convex optimisation, which the drag function is not, and even though it can be powerful when lot's is known about optimisation and the function behaviour, it can also figure out some of the settings itself so is easy to use for beginners in the field of optimisation. Therefore it is well suited for this project. The results of the optimisation are given in Table 5.2.

Table 5.2: *Starting values based on statistics compared to end values after optimisation.*

	A [-]	λ_1 [-]	λ_2 [-]	Λ_1 [deg]	Λ_2 [deg]	D [kN]
Before optimisation	10.0	0.80	0.40	10	25	3.9
After optimisation	10.5	0.68	0.44	12	25	3.2

5.1.3. Airfoil Selection

In this section, the airfoils will be selected. Three airfoils are needed: one at the root, one at the kink and one at the wingtip. At all other locations, the airfoil is constructed by interpolation. As discussed in Subsection 5.1.1, since the cruise Mach number is 0.78, the selection is focused on supercritical airfoils.

Data for 21 different supercritical airfoils has been found, yielding 10,643 different possible combinations of 3 airfoils. Since this is too much to analyse in a realistic amount of time and the analysis can not be sped up by using a gradient-based optimisation method such as for the planform, the airfoils have been divided into two groups. Those with a (t/c) more than 0.10 are candidates for the root and kink airfoil, and those with a (t/c) between 0.06 and 0.10 are candidates for the tip. The airfoils with a (t/c) of 0.04 and less have been excluded from this study, since those are most often used for winglets instead of the wing itself. This method lowers the number of possible combinations from more than 10,000 to a bit less than 400. It is found that the minimum drag was achieved with the Whitcomb airfoil at the root and the kink, and NASA's SC21010 at the wingtip.

Table 5.3: *List of airfoils used.*

High (t/c)	Low (t/c)
NASA SC20012	NASA SC20106
NASA SC20412	NASA SC20406
NASA SC20414	NASA SC20606
NASA SC20518	NASA SC20706
NASA SC20614	NASA SC20110
NASA SC20714	NASA SC20410
Whitcomb	NASA SC20610
	NASA SC20710

However, since the tip airfoil stalls at a lower angle of attack than the root airfoil as shown in Table 5.4, a twist needs to be added to the wing. Indeed, the desired behaviour is for the root to stall first, so that control over the aileron can be kept as long as possible. At sea level and cruise conditions, the difference is of 2.2° and 2.5° respectively. To add a bit of a margin, the tip twist limit has been set at −3.5° in order to avoid tip stall. A more detailed analysis is required in a later stage of the program, since the wing twist changes during the mission due to aerodynamic loading.

Table 5.4: *Angle of attack at maximum c_l for main and tip airfoil in different conditions.*

	Sea level conditions	Cruise conditions
Main airfoil [deg]	5.0	10
Tip airfoil [deg]	2.8	7.5

---

[2]Basin hopping algorithm, SciPy, documentation of this algorithm can be found https://docs.scipy.org/doc/scipy/reference/generated/scipy.optimize.basinhopping.html

5.1.4. 3D Wing Planform

In this section, the 3D geometry of the wing planform is determined in order to increase the stability of the design. The parameters considered in this section are the incidence angle of the wing with respect to the fuselage, the dihedral angle of the wing as well as winglets.

Incidence angle   With the new planform parameters, the optimum wing lift coefficient for cruise is found to be 0.4149. From calculations in AVL it follows that the angle of attack of the wing corresponding to this wing lift coefficient is 0.061°. The wing is installed with an incidence angle of the same amount to ensure that the floor of the fuselage is level during cruise. The fact that the floor of the fuselage is level during cruise makes it easier for flight attendants to push food carts through the aisle.

Dihedral angle   In order to increase the lateral stability of the aircraft, the wings are installed with a dihedral angle of 3°. The dihedral angle of 3° is an initial estimate based on reference aircraft and has to be checked in the eigenmotion analysis.

Wingtip devices   The induced drag component is reduced by installing winglets at the wing tips of the aircraft. Winglets reduce the effect of wingtip vortices by blocking the cross-flow from the lower to the upper side of the wing. Furthermore, lift spoiling effects at the most outboard section of the wing is also limited by blocking the cross-flow. Finally, if installed properly the cross-flow component generates a thrust component at the tip.

The main benefit of using winglets is that the effect is similar to having higher aspect ratio wings, without the drawback of a higher bending moment and hence a heavier wing. A properly designed winglet can yield an effective aspect ratio of about 20% higher than the geometrical aspect ratio of the wing [32]. The effective aspect ratio is the value to be used for the next iteration of the performance calculations.

5.1.5. Wing Performance

Now the wing has been designed, its performance will be analyzed in this section. Two plots will be generated: the lift distribution and the c_{l_α} curve. In order to generate the lift distribution, AVL was used. The resultant plot can be found in Figure 5.4. Next, the c_{l_α} curve has been generated using AVL as well, computing the c_l every three degrees between −9° and 12°, and fitting a parabola through the resulting points. The resulting curve can be found in Figure 5.5.
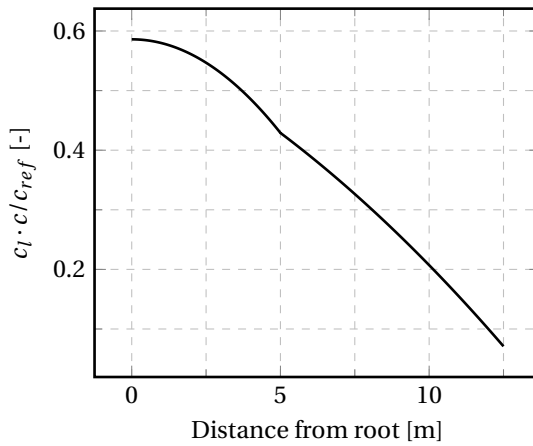
Figure 5.4: *Spanwise lift distribution.*
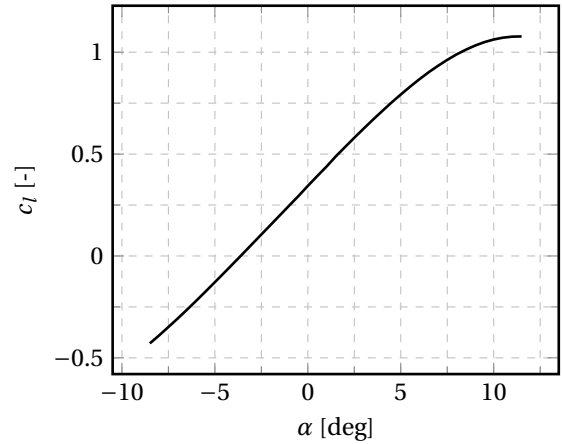
Figure 5.5: c_{l_α} *curve of the clean wing at M = 0.2.*

5.2. Tail Sizing

Now that the geometry of the main wing has been determined, the horizontal and vertical tail surfaces can be sized. Just like for the wing, the surface area, the quarter chord sweep, aspect ratio, taper ratio and airfoil have to be determined for both. First the sizing of the horizontal tail is discussed. Secondly, the sizing of the vertical tail is discussed.

5.2.1. Horizontal Tail

The ratio between the surface of the main wing and the horizontal tail surface (S_h) is determined to be 0.177 in Chapter 6. This ratio results in an horizontal tail surface of $10.1\,\text{m}^2$.
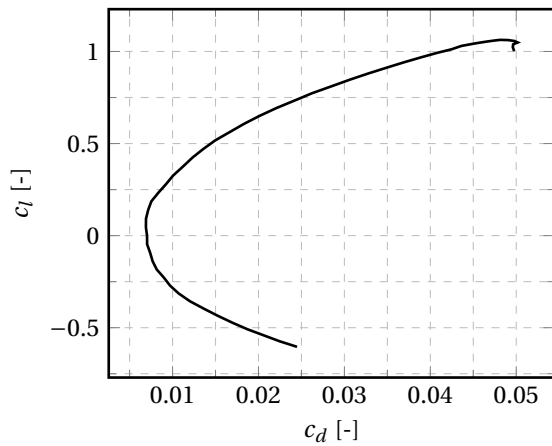
Figure 5.6: *Drag polar of the wing.*
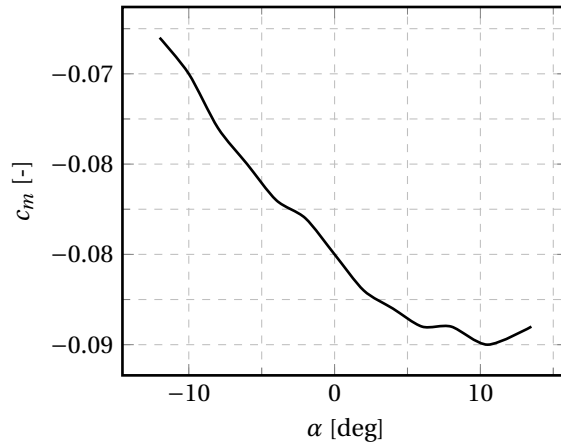
Figure 5.7: c_{m_α} *curve of the clean wing at M = 0.2.*

Taper and aspect ratio In general the aspect ratio and taper ratio of the horizontal tail are selected in such a way that the structural weight of these components is reduced, keeping the aerodynamic performance of the horizontal tail in mind. For the horizontal tail reduction of structural weight is preferred over the reduction of induced drag. From historical data it follows that the aspect ratio of the horizontal tail is between 3 and 5 and that the taper ratio of the horizontal tail is between 0.3 and 0.6 [90]. For the initial sizing of the horizontal tail the average of the aspect ratio and taper ratio ranges are selected, which are 4 and 0.45 respectively.

Quarter chord sweep The last parameter required to determine the planform of the horizontal tail is the sweep of the quarter chord line. Because the horizontal tail is located well above the main wing it is assumed that the velocity ratio between the main wing and the horizontal tail is approximately 1.0. This means that the horizontal tail experiences the same velocity, and hence Mach number, as the main wing. To postpone the drag divergence due to Mach effects, the quarter chord line sweep of the horizontal tail is set the same as the quarter chord line sweep of the main wing.

Airfoil selection Now that the planform of the horizontal tail surface is fully defined, the last element required to fully define the geometry of the horizontal tail surface is the airfoil used at the tip and root chord. Because the horizontal tail has to be able to generate lift in both the upward and downward direction, a symmetrical airfoil is employed on the horizontal tail surface. The drag divergence Mach number for the horizontal tail should be higher than the drag divergence Mach number of the main wing. In order to achieve this, the (t/c) of the horizontal tail surface is about 90% of the (t/c) of the main wing, both at the tip and at the root.

The parameters of the horizontal tail surface are provided in Table 5.5.

Table 5.5: *Horizontal tail geometry.*

Parameter	Value
S_h [m^2]	10.1
$b/2$ [m]	3.18
A_h [-]	4.0
λ_h [-]	0.45
$\Lambda_{0.25h}$ [deg]	25.2
c_{rh} [m]	2.20
c_{th} [m]	0.99
Root airfoil	NACA 0010
Tip airfoil	NACA 0009

Table 5.6: *Vertical tail geometry.*

Parameter	Value
S_v [m^2]	11.85
b_v [m]	3.36
A_v [-]	0.95
λ_v [-]	0.75
$\Lambda_{0.25v}$ [deg]	25.2
c_{rv} [m]	4.04
c_{tv} [m]	3.03
Root airfoil	NACA 0011
Tip airfoil	NACA 0011

5.2.2. Vertical Tail

The ratio between the surface area of the vertical tail and main wing surface area is determined by using a historical average of the tail volume coefficient. The surface area of the vertical tail is calculated by using Equation 5.2. From this equation it follows that an initial estimate of the vertical tail area is $11.85\,\text{m}^2$.

$$\frac{S_v}{S} = \frac{C_v \cdot b}{l_v} = \frac{0.08 \cdot 25.5}{10.5} = 0.194 \tag{5.2}$$

Taper and aspect ratio   The aspect ratio and taper ratio of the vertical tail are sized in a similar fashion as the aspect ratio and taper ratio of the horizontal tail. The ranges for the aspect ratio of the vertical tail for a T-tail configuration are between 0.9 and 1.2, so an initial guess of 0.95 is used for the initial vertical tail design. The taper ratio for T-tail configuration aircraft ranges between 0.6 and 1.0, which results in an average value of 0.8 for the initial estimate of the taper ratio of the vertical tail[90].

Quarter chord sweep   Similar to the horizontal tail design, the quarter chord sweep angle of the vertical tail is set to the same value as the quarter chord sweep of the wing to postpone drag divergence due to Mach number. The vertical tail is not located in the slipstream of any other element, so the velocity, and hence also the Mach number, over the vertical tail is equal to that of the free stream.

Airfoil selection   The vertical tail has to produce a side-force in the direction opposite to the angle of attack, or side-slip in this case, it experiences. This means that the zero lift angle of attack of the airfoil selected for the vertical tail should be zero. The zero lift angle of attack requirement and the direction of side-force production requires a symmetrical airfoil for the vertical tail. As a guideline for the initial airfoil selection for the vertical tail, the (t/c) of the airfoil of the vertical tail is approximately 98% of the (t/c) of the main wing.

The main parameters of the resulting vertical tail geometry are presented in Table 5.6.

5.3. Resulting Wing

The final design of the wing can be visualised in Figure 5.8. The wing and tail, as well as their respective location, are to scale. The dark grey areas are the high-lift devices and the light grey areas are the control surfaces. The design of the control surfaces is discussed in Section 6.3.
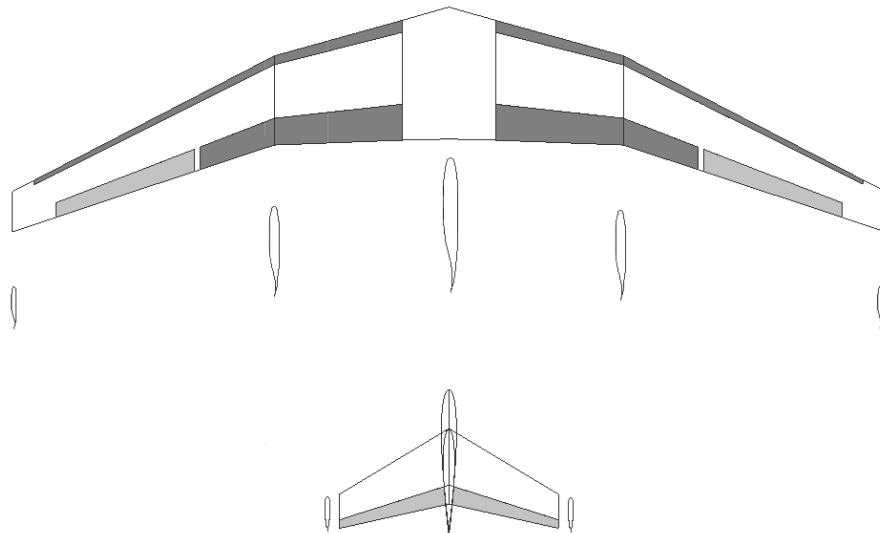
Figure 5.8: *Top view of the final wing planform including the airfoils.*

All the airfoils used are given in Figure 5.9 for the main wing, and in Figure 5.10 for the horizontal and vertical stabilisers.

(a) *Whitcomb, root and kink airfoil.*

(b) *NASA SC21010, tip airfoil.*

Figure 5.9: *Airfoils used for the main wing.*

(a) *NACA 0011, used for the vertical stabiliser.*

(b) *NACA 0010, root airfoil horizontal stabilser.*

(c) *NACA 0009, tip airfoil horizontal stabilser.*

Figure 5.10: *Airfoils used for vertical and horizontal stabiliser.*

The horizontal tail mainly contributes to the longitudinal stability of the aircraft by changing the moment coefficient. The contribution of the horizontal tail to the moment coefficient curve is presented in Figure 5.11. The main destabilising factor on the longitudinal stability is the contribution of the fuselage, which is estimated by using the data available for the fuselage contribution of the Cessna Citation II [61].

The horizontal tail does not only influence the moment coefficient of the aircraft, but also the lift coefficient by producing additional lift if it experiences a positive angle of attack. The contribution of the horizontal tail to the total lift coefficient generated by the aircraft is given in Figure 5.12. The contribution to the lift coefficient of the horizontal tail is notably less significant than the contribution to the moment coefficient due to the large distance between the horizontal tail and the main wing.
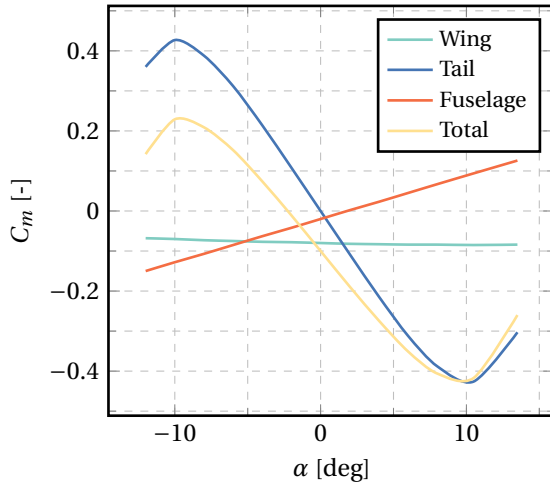
Figure 5.11: *Contribution of various elements to the moment coefficient.*
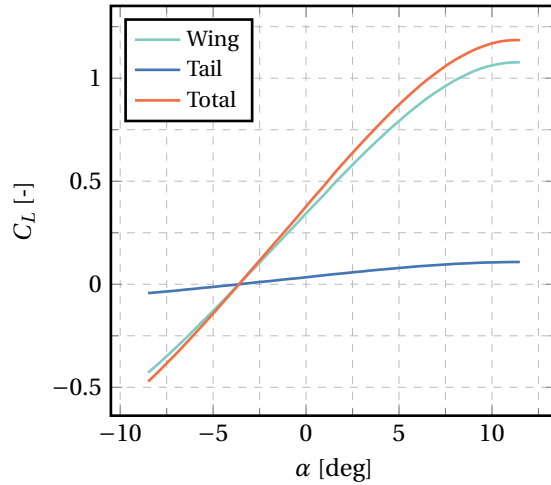
Figure 5.12: *Contribution of the horizontal tail to the lift curve.*

The tail does not only contribute to lift and moment generation, but also to the generation of induced and parasitic drag. The contribution of the tail surfaces, both horizontal and vertical, can be seen in Figure 5.13. The vertical tail does not contribute to the lift production, as it is oriented perpendicular to the wing and horizontal tail, and hence only shifts the lift curve to the right. The contribution of the vertical tail to the drag coefficient in cruise condition is found to be 0.001383. The horizontal tail does produce a changing lift with a changing angle of attack, and hence a changing amount of induced drag. The contribution of the fuselage to the total drag consists of friction drag and pressure drag. The drag contribution of the fuselage is given by the estimation of the viscous drag provided by Raymer [75], as is presented in Equation 5.3. The drag contribution of the fuselage depends on the form factor of the fuselage, which is calculated using Equation 5.4, the fuselage area and the local Reynolds number over the fuselage. The form factor of the fuselage depends on the fuselage length and diameter.

$$C_{D_{\text{fus}}} = FF_{\text{fus}} \frac{S_{wfus}}{S} \frac{0.455}{\left(\log_{10}(\text{Re})\right)^{2.58}\left(1 + 0.114 M^2\right)^{0.65}} \tag{5.3}$$

$$FF_{\text{fus}} = 1 + \frac{60}{\left(\frac{l_f}{d_f}\right)^3} + \frac{\frac{l_f}{d_f}}{400} \tag{5.4}$$
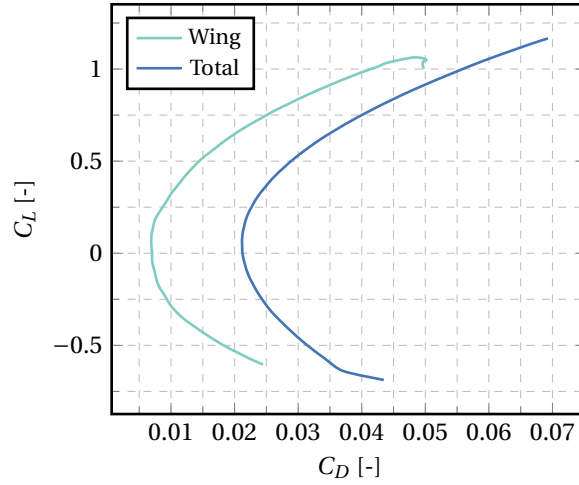
Figure 5.13: *Contribution of the tail and fuselage to the lift drag polar.*

From Figure 5.13 it follows that the zero-lift drag coefficient of the entire design is 0.02128, which is 1.4% higher than the initial estimate of 0.021. The Oswald efficiency factor of the wing planform is estimated using the method presented by Sholz [84]. The method for estimating the Oswald efficiency factor is presented in Equation 5.5. The resulting Oswald efficiency factor is 0.784, which is 2.05% lower than the initial estimate for the Oswald efficiency factor of 0.8.

$$e = \frac{1}{\left(1 + 0.12 M^6\right)\left(1 + \frac{0.142 + f(\lambda)A\left(10\frac{t}{c}\right)^{0.33}}{\cos^2(\Lambda_{0.25c})} + \frac{0.1}{(4+A)^{0.8}}\right)} \tag{5.5}$$

5.4. Verification & Validation

In this section, the verification and validation procedures for the aerodynamic programmes will be discussed. The procedures for verification and validation can be found in Appendix A. First the programmes are verified, that is to say that the calculations are correct and the program gives the desired output for the desired input. Next the program will be validated, to verify the methods themselves.

5.4.1. Verification

The goal of verification is to check whether the code does actually compute what it is built for, and there are no mistakes in the code.

- **AVL**: It was checked that the input to AVL was correct by inspecting the geometry of the wing plotted by AVL based on those inputs, as well as comparing the c_l as predicted by AVL to the c_l as predicted by JavaFoil at the same angle of attack and Mach number, when taking into account some of the 3D effects.
- **Input to XFLR**: The correctness of the input to XFLR is verified by comparing the result of wing and tail planform calculations to the input in XFLR. Furthermore, a visual inspection is performed in XFLR to ensure the correctness of the inputs provided.
- **Code to compute** C_{l_α}: A code was created to compute C_{l_α} automatically from the data points of the C_{l_α} curve from JavaFoil. This was compared to a graphical estimate of the slope of the plot.
- **Code to compute planform parameters**: This code generates a full planform based on the iterated inputs. It was tested by filling in the inputs of a reference aircraft and plotting the resulting planform, checking things such as the wing area from the drawn planform against the output from the code, and inspecting if it did not produce odd things.

5.4.2. Validation

The XFLR and AVL programs are validated by comparing the results to experimental data gathered in a wind tunnel. The results from the wind tunnel experiment, XFLR and AVL computations are presented in Figure 5.14 and Figure 5.15 respectively. Both XFLR and AVL predict a linear increase in lift with increasing angle of attack, which is valid for low angles of attack but becomes invalid as the angle of attack is increased. The difference between the AVL computations and experimental data is below 10% for an angle of attack lower than 13°. The angle of attack below which XFLR yields a reliable result, with less than 10% error, is also below 13°. The usage of XFLR and AVL is validated for angles of attack lower than 13°.
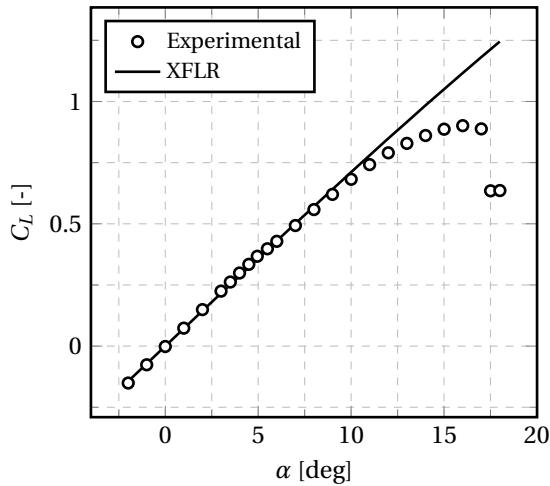
Figure 5.14: *XFLR results versus experimental data.*
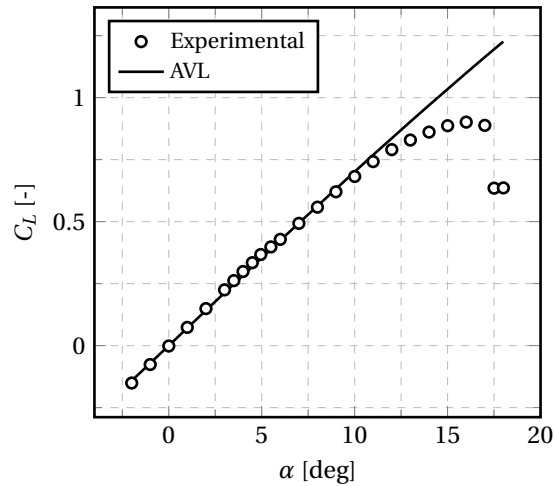
Figure 5.15: *AVL results versus experimental data.*

5.4.3. Sensitivity Analysis

Besides verification and validation, a sensitivity analysis is performed to quantify the influence of different parameters on the performance of the aircraft

Wing optimisation   For the wing optimisation, sensitivity is not relevant. The most important inputs are the boundaries on the iterated parameters, and since the results are in the middle of the rages and not near a limit, different limits should not change the outcomes.

Most of the other inputs were given as outputs by performance, no sensitivity analysis is performed on them.

6

Flight Dynamics

The purpose of this chapter is to analyse and determine the behaviour of the aircraft during flight. First, the tail and control surfaces are sized, followed by determining the aircraft characteristics. Lastly, the eigenmotions of the aircraft are determined and checked for stability.

6.1. Result of Previous Iteration & Sizing

In the previous report, initial sizing of the tail was done based on Class-I weight estimation methods and general aircraft geometry based on reference aircraft. At the time, little detailed information about the aircraft was known, and therefore detailed tail sizing was not possible. In this chapter however, tail sizing is performed once more, using new information from iterations and more accurate estimation methods. The detailed design was based on a combination of Class-II weight estimation and subsystem weight calculations from other engineering departments within the group. Table 6.1 and Table 6.2 display the geometrical data used during the initial and final sizing, the first row being the initial sizing and the second row the detailed sizing. Notable differences between the two are the increase in total length of the fuselage and the aft movement of the main wing. These changes are reflected in Table 6.2, where the extreme c.g. positions for the updated design are further aft than for the initial design.

Table 6.1: *Geometric properties of new design.*

Fuselage Length [m]	Xlemac [m]	MAC [m]	Distance Nose to 1st Row [m]	Distance Nose to Cargo Bay [m]	Seating Configuration	Seat Pitch [cm]
26.93	13.15	2.74	6.24	24	2+2	78.74
28.5	15.55	2.74	5.48	23.5	2+2	78.74

Table 6.2: *c.g. positions based on loading diagram.*

Most Front c.g. [m]	%MAC	Most Aft c.g. [m]	%MAC	c.g. Range [%MAC]
13.85m	0.53	14.60m	0.89	0.35
16.16m	0.20	17.54m	0.74	0.54

6.2. Detailed Sizing

A more detailed weight estimation, as done in a Class-II method, allowed for a more accurate calculation of c.g. of the aircraft. Once again, a loading diagram is constructed and a scissor plot is made. Finally, the c.g. range is fitted in the scissor plot and the tail size determined.

6.2.1. Weight of Subsystems

For sizing of the tail, the aircraft is divided into two groups. The wing group comprises all components that, if the main wing is moved, move along with it. The other group, the fuselage group, is made up of components whose location is independent of the main wing position.

Table 6.3: *Geometric properties of new design.*

Fuselage Group component	Weight [kg]	c.g. position [m]	Wing Group component	Weight [kg]	c.g. location [%MAC]
Fus Structure	3330.3	12.825	Wing Structure	2414.7	70
Empennage	1431.5	27.45	Landing Gear	1197.9	90
Engines	2381	25	Fuel System	600	40
Finishing	500	14.25	De-Icing	244.1	50
APU	100	28	Hydraulics	219.5	90
Eng Contol+Starter	126.9	9.28	Slats	62.8	5
Tail Control	188.45	27.1			
Flight Instruments	137.3	1.425			
Electrical System	860	11.4			
Avionics	87.6	0.85			
Airconditioning	244.1	14.25			
Galleys&Lavatories	800	10.84			
Seats	1287.6	12.89			
Total	11,497.2	16.68	Total	4864.7	70.93

By using the weights of the subsystems of both groups and their corresponding c.g. location from Table 6.3, the location of the main wing w.r.t. the fuselage can be iterated and the optimum determined. The optimum wing location is taken to be where the loading diagram provides the required range of c.g. locations, as required to minimise the total tail area.

6.2.2. Updated Loading Diagram & Scissor Plot

The loading diagram and scissor plot are constructed in the same way as during the Midterm Phase. Previously it was estimated that a minimum tail size of 12.5% of the main wing area was possible. However, more accurate estimates and calculations required the main wing to be placed further aft and, mainly due to the shorter tail arm, a larger tail area is required than expected. From the scissor plot, the minimum required tail area was found to be equal to 17.7% of the main wing area. By looking at the loading diagram, it can be observed that during flight, the c.g. is located relatively far forward. Combining this information with the information provided in the scissor plot, the aircraft stability and control is seen to be mostly limited by the controllability curve. This is common for aircraft with engines at the rear, as passengers shift the c.g. significantly forward.

(a) *Final aircraft loading diagram.*
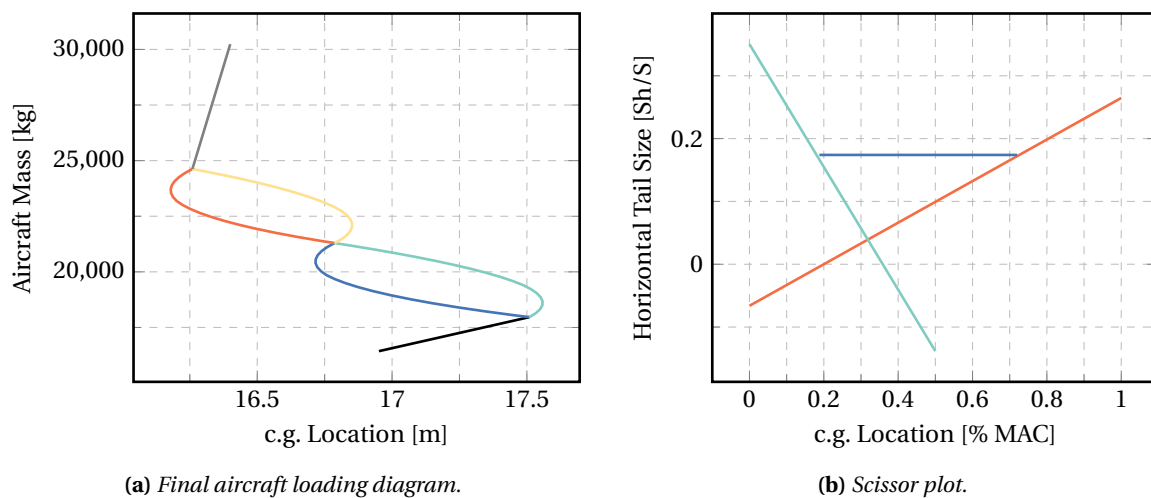
(b) *Scissor plot.*

Figure 6.1: *Final loading diagram & scissor plot of the aircraft.*

6.3. Control Surface Sizing

In this section the ailerons, elevator, rudder and high lift devices are sized. The effectiveness of the elevator and rudder is computed using XFLR5.

6.3.1. Aileron Sizing

The initial sizing of the ailerons is based on historical guidelines on the aileron span over the wing span and the aileron chord length over the total chord length. These guidelines are presented in Figure 6.2 [49]. From the historical guidelines it follows that for an aileron chord over total chord ratio of 0.3 the aileron span over total span is typically between 0.30 and 0.36, of which the average of 0.33 is selected as an initial guess for the aileron span.
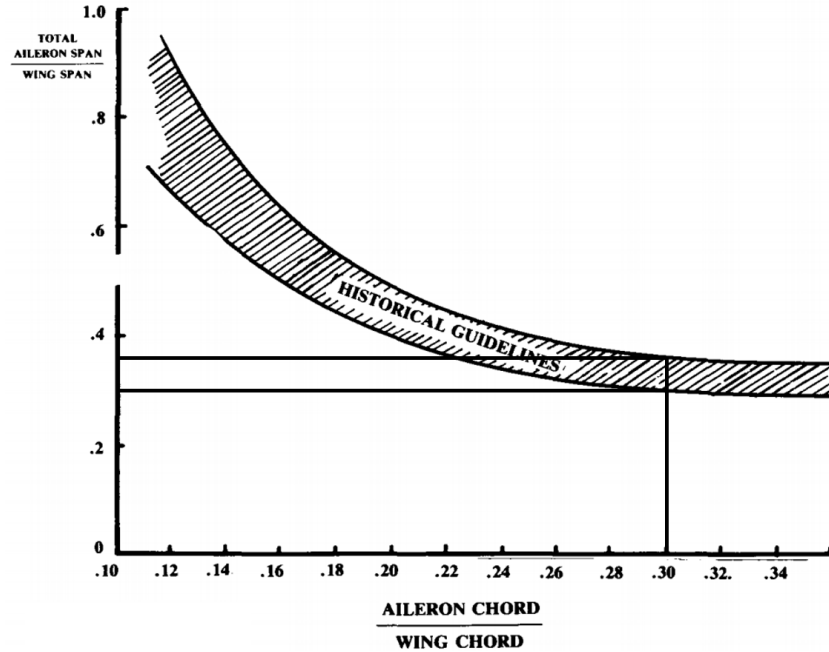
Figure 6.2: *Historical guidelines for initial aileron design.*

Ailerons are typically located from 50% of the span up to 90% of the span. Because only 33% of the wing span is needed for the ailerons, the ailerons are located between 57% and 90% of the wing span. This leaves some space for the placement of mechanisms that drive both the flaps and the ailerons. To reduce the adverse yawing effect caused by a deflection of the aileron on one side of the aircraft, it is decided to implement differential ailerons.

During cruise the outboard ailerons can not be used because of aeroelastic effects on the wing. In order to provide lateral control during cruise part of the flaps can be deflected in opposite direction to function as ailerons: flaperons. The flaperons are located between 16% of the wing span and 28% of the wing span.

6.3.2. Elevator Sizing

In order to generate the required downforce for rotation of the aircraft in take-off, it is necessary to place elevators on the horizontal tail. The elevators are positioned between 10% and 90% of the span of the horizontal tail as an initial estimate. The local chord length of the elevator is assumed to be 25% of the local chord length of the horizontal tail. The horizontal tail lift coefficient as a function of elevator deflection and angle of attack can be seen in Figure 6.3. The data represented in Figure 6.3 is obtained using XFLR5.

From Figure 6.3 it can be concluded that invariant of the angle of attack, the horizontal tail lift coefficient increases linearly with increasing elevator deflection. The horizontal tail lift coefficient can be translated to a moment contribution to the aircraft using Equation 6.1. Because the lift coefficient increases linearly with elevator deflection, the elevator moment contribution also increases linearly with elevator deflection. Using Equation 6.1 it is found that for zero angle of attack the moment change due to a change in elevator deflection ($C_{m_{\delta a}}$) is -0.06879.
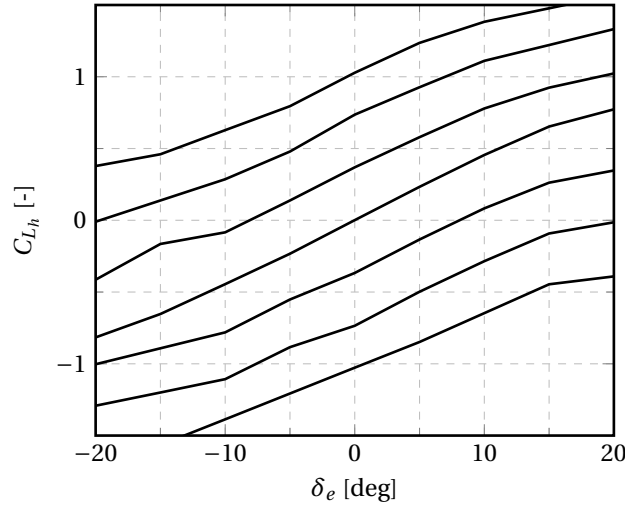
Figure 6.3: *Elevator lift coefficient as function of elevator deflection and angle of attack.*

$$C_{m_h} = -C_{L_h} \frac{l_h S_h}{S} \tag{6.1}$$

6.3.3. Rudder

In order to increase stability when the aircraft experiences a sideslip angle with respect to the free stream velocity a vertical tail is used to generate a yawing moment. The rudder can be used to limit the sideslip angle by increasing the camber of the vertical tail in both directions. The rudder is positioned at the aft 25% of the vertical tail and spans from 10% to 90% of the span of the vertical tail. The side force produced by the vertical as a function of the rudder deflection angle and side force angle can be seen in Figure 6.4. The data represented in Figure 6.3 is obtained using XFLR5.
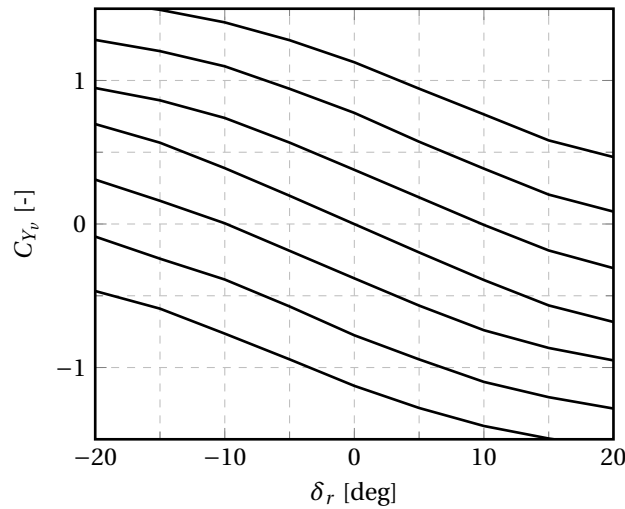
Figure 6.4: *Rudder side force coefficient as function of rudder deflection and angle of sideslip.*

In a similar fashion as the pitch moment contribution of the elevator, the yawing moment due to the side force generated by the vertical tail is determined using Equation 6.2. From Figure 6.4 it can be seen that the amount of side force generated by the vertical tail increases with increasing rudder deflection angle. The negative correlation between the angle of sideslip and side force is explained by the fact that the angle of sideslip is defined positive in the negative y-direction. Using Equation 6.1 it is found that for zero angle of sideslip the yawing moment change due to a change in rudder deflection ($C_{n_{\delta r}}$) is -0.0702.

$$C_{n_v} = -C_{Y_v} \frac{l_v S_v}{S} \tag{6.2}$$

6.4. High Lift Devices

In order to meet the required lift coefficient at take-off and landing, high lift devices have to be deployed on the wing. The two main locations for the positioning of high lift devices are at the leading and trailing edge of the wing.

6.4.1. Leading Edge

In order to maximise the effect of high lift devices on the leading edge, slats are selected that span from 10% of the wing span up to 95% of the wing span. This results in a wing area affected by the slats of 78% of the total wing surface area.

The contribution of the slats on the lift curve can be seen in Figure 6.5. Because the slats do not cause an extension of the total wing area, the slope of the lift curve with slats is the same as the one without flaps. The influence of the presence of slats on the zero lift angle of attack is found to be negligible.

6.4.2. Trailing Edge

Based on the aileron sizing, the remaining wing area which can be affected by the flaps is found to be $33.7\,\mathrm{m}^2$. For the trailing edge high lift devices there are several possibilities with different characteristics. The trailing edge high lift devices considered for the design are:

- Plain and split
- Slotted
- Fowler
- Double slotted
- Triple slotted

Because the different trailing edge high lift devices have a different level of effectiveness, the resulting maximum wing lift coefficient depends on the selected types. The change in maximum wing lift coefficient due to the high lift devices is given by Equation 6.3

$$\Delta C_{L_{\max}} = 0.9 \Delta C_{l_{\max}} \frac{S_{wf}}{S} \cos(\Lambda_{0.7c}) \tag{6.3}$$

Each high lift device type has a different value of $\Delta C_{l_{\max}}$, which also results in a different $\Delta C_{L_{\max}}$ value for each type of high lift device. The resulting flap area values for each type of high lift device are presented in Table 6.4.

Each high lift device requires a different operating mechanism with a different amount of parts, and hence a different mass. The mass, amount of parts and manufacturing costs are determined based on the methods described in Rudolph [80]. The manufacturing cost, in USD, of the high lift devices is calculated using Equation 6.4.

$$\text{Cost} = 1.8881 \times \text{weight} \times (\text{part count})^{0.7} \tag{6.4}$$

Along with the maximum wing lift coefficient and production costs, the mass and the amount of parts for each type of high lift devices are presented in Table 6.4. The part count is used as an indicator for maintenance of the system, as more parts generally implies higher maintenance costs. Due to high manufacturing cost, high maintenance and heavy weight the triple slotted and double slotted flaps are eliminated. As an initial estimate the lightest and cheapest type high lift device is selected, so the simple slotted flap.

The influence of the high lift devices on the maximum lift coefficient in different configurations can be found in Figure 6.5. The black line in Figure 6.5 indicates the lift curve of the wing in clean configuration. As expected the leading edge high lift devices, indicated by the blue line, do not significantly influence the zero lift angle of attack, but only increase the maximum lift coefficient. The flaps on the other hand, indicated with the red line for landing configuration, have a large influence on the shift in zero lift angle of attack and the maximum wing lift coefficient. The green line indicates the contribution of the flaps in take-off configuration, which is lower compared to when the flaps are fully extended.

Table 6.4: *High lift devices characteristics.*

Flap system	Wing lift coefficient	Mass [kg]	Production cost [M USD]	Part count [-]
Plain and split	− 1.77	+ 464	++ 0.58	+ 1715
Slotted	0 1.97	++ 439	++ 0.51	++ 1540
Fowler	0 2.30	0 530	+ 0.68	+ 1800
Double Slotted Fowler	+ 2.59	− 651	−− 1.04	− 2430
Triple Slotted Fowler	+ 2.80	−− 740	−− 1.33	−− 2880
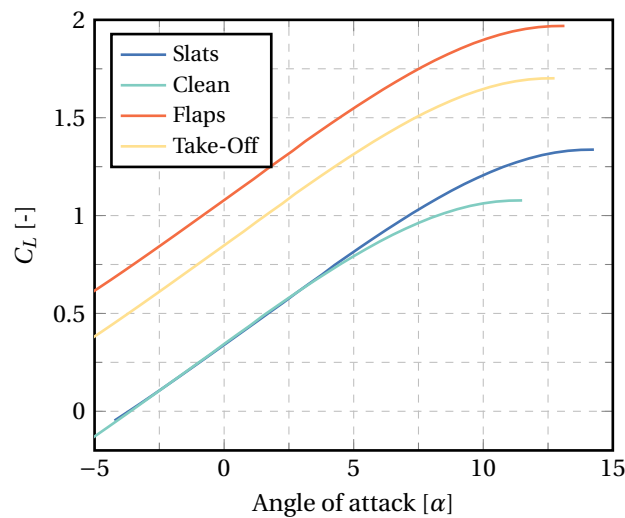
Figure 6.5: *Effect of high lift devices on the lift curve.*

6.5. Aircraft Flight Dynamics Characteristics

The Aerodynamic and Geometrical properties of the aircraft's (control) surfaces all together determine how the aircraft behaves. It is crucial that the aircraft is safe and pleasant to fly, so the geometry of the aircraft has to be designed in such a way that this is guaranteed. Correctly designing the aircraft aerodynamic subsystems ensures the aircraft is both stable and pleasant to fly.

6.5.1. Requirements

CS-25 regulations require the aircraft to be both statically and dynamically stable for almost all possible c.g. locations that can be encountered during aircraft operation, the only exception being that a lightly unstable roll instability is allowed. This information was found and documented in the Baseline Report [39], with corresponding requirements set as following:

Sys.Perf.1:   The aircraft shall be dynamically stable for the entire range of c.g. excursions.

Sys.Perf.2:   The aircraft shall be controllable for the entire range of c.g. excursions.

An aircraft that is dynamically stable is by definition also statically stable, and therefore static stability was not explicitly mentioned in the Performance Requirements.

6.5.2. Assumptions

In order to facilitate the mathematical analysis of the flight dynamics characteristics, several assumptions are made. These assumptions either neglect several phenomena or slightly alter them [61]. All assumptions are validated by analyzing the change in value of the parameters that are involved in each assumption.

Assumption 1: Constant gravity field
   The Earth is not completely round, but rather an ellipsoid. At the poles, the Earth's radius is slightly smaller than it is at the equator. As a result, gravity is stronger at the poles. This difference in gravity is assumed to be negligible. At the equator, gravitational acceleration is equal to around 9.780m/s, and 9.832m/s at the poles. The difference is less than 0.5%, and therefore it can be neglected.

Assumption 2: Forces due to gravity are assumed to be independent of altitude
   Expanding on Assumption 1, it is assumed that gravitational acceleration does not change with varying altitude. In reality, the higher the aircraft flies, the lower the effect of gravity becomes. However, it was calculated that one has to fly at an altitude of around $32km$ in order to reduce the gravity force by 1%. As a result, it is assumed that this difference can be assumed to be negligible.

Assumption 3: Rigid Body
   When the aircraft is changing its attitude, it deforms slightly under the loads required for manoeuvring. It is assumed that the deformation can be neglected and subsequently, the moment of inertia remains constant as well.

Assumption 4: Earth is considered flat and non-rotating
   This assumption removed the Coriolis effect and the centripetal accelerations caused by the rotation of the Earth. However, this assumption is only valid if the time frame in which the aircraft is analysed, is small. For eigenmotion analysis, this time-frame is in the order of minutes and considered small enough.

Assumption 5: The aircraft is symmetric around the length of the fuselage
   By assuming at least one plane of symmetry, calculations simplify because the moments of inertia I_{xy} and I_{yz} are equal to zero. Commercial aircraft are nearly symmetric along the length of the fuselage, the only differences being the passengers on either side, and the aircraft systems running through the fuselage. Since these components are relatively close to the c.g., their effect on the moment of inertia are considered negligible.

6.5.3. Approach & Method
Before the behaviour of the aircraft can be determined, it is required to know what forces act on the aircraft during flight. These forces can then be used to set up the equations of motion. After that it will be analysed what the stability derivatives are. These derivatives state in what way the aircraft reacts to a certain perturbation or change in attitude. The required control derivatives to counter these perturbations are determined after that. Control derivatives will size the required control surfaces and the forces that they generate to manoeuvre the aircraft. This manoeuvring part will round up this chapter.

6.6. Dynamic Stability Analysis
The assumptions made during the previous section are used to construct the equations of motion. Due to the assumptions, the equations of motion are simplified, and analysis can be performed more easily at a minimum loss of accuracy.

6.6.1. Criteria for Stability
To determine whether the eigenmotions are stable or unstable, one must look at the eigenvalues. For stability, the real part of the eigenvalues must be negative [61]. The imaginary part of the eigenvalues only determines the oscillatory part of the eigenmotions, and does not affect stability. The eigenvalues are determined by calculating the discriminant of the matrix, and solving for the eigenvalues by setting the discriminant equal to zero.

6.6.2. Longitudinal & Lateral Stability Derivatives
Longitudinal stability derivatives describe the behaviour of the aircraft regarding the symmetric motion. For this type of motion, in the body-fixed reference frame, the X-Z plane is observed. The linearised equations of motion, in dimensionless form are shown in Equation 6.5

$$\begin{bmatrix} C_{X_u} - 2\mu_c D_c & C_{X_\alpha} & C_{Z_0} & 0 \\ C_{Z_u} & C_{Z_\alpha} + (C_{Z_{\dot\alpha}} - 2\mu_c)D_c & -C_{X_0} & C_{Z_q} + 2\mu_c \\ 0 & 0 & -D_c & 1 \\ C_{m_u} & C_{m_\alpha} + C_{m_{\dot\alpha}} D_c & 0 & C_{m_q} - 2\mu_c K_Y^2 D_c \end{bmatrix} \begin{bmatrix} \hat{u} \\ \alpha \\ \theta \\ \frac{q\bar{c}}{V} \end{bmatrix} = \begin{bmatrix} -C_{X_{\delta e}} \\ -C_{Z_{\delta e}} \\ 0 \\ -C_{m_{\delta e}} \end{bmatrix} \delta_e \qquad (6.5)$$

To determine the stability characteristics, one calculates the discriminant of the left-most matrix and solves for the eigenvalues. These eigenvalues describe the symmetric eigenmotions, the phugoid and the short period. The phugoid is characterised as a lightly damped motion with a long period. The short period on the other hand is highly damped and has, as the name already suggests, a short period.

Lateral stability derivatives describe the behaviour of the aircraft regarding the asymmetric motion. Rolling and yawing motion is part of the asymmetric motion, and described here. The linearised equations of motion, in dimensionless form are shown in Equation 6.6

$$
\begin{bmatrix}
C_{Y_\beta} + (C_{Y_{\dot\beta}} - 2\mu_b)D_b & C_L & C_{Y_p} & C_{Y_r} - 4\mu_b \\
0 & -\frac{1}{2}D_b & 1 & 0 \\
C_{l_\beta} & 0 & C_{l_p} - 4\mu_b K_X^2 D_b & C_{l_r} + 4\mu_b K_{XZ} D_b \\
C_{n_\beta} + C_{n_{\dot\beta}} D_b & 0 & C_{n_p} + 4\mu_b K_{XZ} D_b & C_{n_r} - 4\mu_b K_{Z^2} D_b
\end{bmatrix}
\begin{bmatrix}
\beta \\
\phi \\
\frac{pb}{2V} \\
\frac{rb}{2V}
\end{bmatrix} = 0
\tag{6.6}
$$

Aircraft behaviour is determined in the same way as during the symmetric analysis. Setting the discriminant equal to zero provides the eigenvalues, which when real and negative indicate stable behaviour of the eigenmotions. The two eigenmotions for asymmetric motion are the Dutch Roll and the Spiral. Based on the current aircraft geometry, the stability derivatives were determined with the use of the AVL program. The result of running this program is shown in Table 6.5 up to Table 6.7.

Table 6.5: *Stability derivatives part 1.*

Direction	α		β	
Z force	C_{L_α}	6.458202	C_{L_β}	0
Y force	C_{Y_α}	−0.000068	C_{Y_β}	−0.36011
X moment	C_{l_α}	0.000001	C_{l_β}	−0.12488
Y moment	C_{m_α}	−8.505626	C_{m_β}	0
Z moment	C_{n_α}	0.000014	C_{n_β}	0.162044

Table 6.6: *Stability derivatives part 2.*

	Roll rate		Pitch rate		Yaw rate	
X force	C_{X_p}	0.0	C_{X_q}	0.41411	C_{X_r}	0.0
Y force	C_{Y_p}	−0.01471	C_{Y_q}	−0.00035	C_{Y_r}	0.382926
Z force	C_{L_p}	0.0	C_{L_q}	0.460768	C_{L_r}	0.0
X moment	C_{l_p}	−0.590909	C_{l_q}	0.000005	C_{l_r}	0.195302
Y moment	C_{m_p}	0	C_{m_q}	−1.13905	C_{m_r}	0.0
Z moment	C_{n_p}	−0.003993	C_{n_q}	0.000076	C_{n_r}	−0.18945

Table 6.7: *Stability derivatives part 3.*

	Axial velocity		Sideslip velocity		Normal velocity	
X force	C_{X_u}	−0.07009	C_{X_v}	0	C_{X_w}	0.213944
Y force	C_{Y_u}	−0.000001	C_{Y_v}	−0.36011	C_{Y_w}	−0.000068
Z force	C_{Z_u}	−0.910241	C_{Z_r}	0	C_{Z_w}	−6.483863
X moment	C_{l_u}	0	C_{l_v}	−0.1231	C_{l_w}	0
Y moment	C_{m_u}	−1.127677	C_{m_v}	0	C_{m_w}	−8.495908
Z moment	C_{n_u}	0	C_{n_v}v	0.162953	C_{n_w}	0.000014

6.6.3. Control Surfaces
The purpose of the control surfaces is to generate moments about the aircraft to either balance the aircraft or initiate rotation. For lateral control, moments are generated about the X and Z-axes of the aircraft body,

while for longitudinal control the elevator is deflected to generate a moment about the Y-axis. While control surfaces primarily generate rotation about one axes, they also indirectly influence rotation about other axes, which is often undesired [61].

Table 6.8: *Control derivatives of the aircraft.*

Control derivative	Meaning	Value/Sign
Aileron control derivatives		
$C_{Y_{\delta_a}}$	Effect of aileron deflection on force in Y-direction	0
$C_{l_{\delta_a}}$	Effect of aileron deflection on rolling moment	-
$C_{n_{\delta_a}}$	Effect of aileron deflection on yawing moment	+
Rudder control derivatives		
$C_{Y_{\delta_r}}$	Effect of rudder deflection on force in Y-direction	+
$C_{l_{\delta_r}}$	Effect of rudder deflection on rolling moment	+
$C_{n_{\delta_r}}$	Effect of rudder deflection on yawing moment	-
Elevator control derivatives		
$C_{X_{\delta_e}}$	Effect of elevator deflection on force in X-direction	0
$C_{Z_{\delta_e}}$	Effect of elevator deflection on force in Z-direction	-
$C_{m_{\delta_e}}$	Effect of elevator deflection on aircraft pitching moment	-

Aileron Control Derivatives   Deflection of the ailerons is related to a total of three control derivatives. $C_{Y_{\delta_a}}$ displays the effect of deflecting the ailerons on the side force of the aircraft. While it is non-zero for swept-wing aircraft, it is small enough compared to the other derivatives that it can be omitted.The primary function of the ailerons is to induce a rolling moment and subsequently rolling motion, described by the control derivative $C_{l_{\delta_a}}$. Its value is negative, as a positive (deflection downwards on the right wing) deflection increases the lift on the right wing and decreases that on the left wing. The result is the aircraft starts rolling towards the left, which is considered negative rolling. $C_{n_{\delta_a}}$ related the yawing moment introduced by deflecting the ailerons. For positive aileron deflection, more lift generated on the right wing also means that the drag is locally increased, with the adverse being true on the left wing. Therefore, while the aircraft starts rolling to the left, the locally increased drag introduces a positive yawing moment, counteracting the rolling motion. The value of this control derivative is kept small by making the downward aileron deflection smaller than the upward one. Hereby the change in drag is reduced, and the induced yawing moment lowered subsequently.

Rudder Control Derivatives   Like for the aileron deflection, deflecting the rudder is also related to three control derivatives. The force generated by deflecting the rudder is described by $C_{Y_{\delta_r}}$. If δ_r is positive, the lateral force it generates is also positive. The lateral force on the vertical tailplane will generate a moment around the X-axis of the aircraft, and for positive rudder deflection, this moment is positive and the aircraft starts rolling to the right, this motion is decribed by $C_{l_{\delta_r}}$. The main purpose of the rudder is to introduce a yawing moment, with effectiveness described by $C_{n_{\delta_r}}$. It has a negative sign, so a positive rudder deflection creates a negative yawing moment. $C_{n_{\delta_r}}$ is related to $C_{Y_{\delta_r}}$ by the negative ratio of vertical tail arm and the wingspan.

Elevator Control Derivatives   Once again, deflecting the elevator control surface has effects described by three control derivatives. $C_{X_{\delta_e}}$ relates the deflection of the elevator with a change of force in the X-direction. A non-zero elevator deflection alters the drag of the horizontal tailplane. While the total tailplane drag is not negligible, changes due to elevator deflection are deemed so small, that they can be neglected. The main purpose of the elevator is to alter the lift produced to the desired value required for either stability or manoeuvring, depicted as $C_{Z_{\delta_e}}$. Deflecting the elevator allows for altering the pitching moment of the aircraft, as depicted in the final control derivative $C_{m_{\delta_e}}$.

6.7. Eigenmotion Analysis
All the stability and control derivatives are now collected and used to solve the equations of motion. The desired outcome is to have sufficient stability to pass the CS-25 regulations. The stability derivatives provided

in Table 6.5 up to Table 6.7 are used as inputs in the equations of motion. The stability derivatives that could not be determined at this point are estimated using the available information of the Cessna Citation II [21], this aircraft has a geometry that is relatively close to the one designed here. A graphical representation of the symmetrical and asymmetrical eigenmotions of the aircraft can be found in Figure 6.6 and Figure 6.7 respectively. The eigenvalues related to the eigenmotions for the symmetrical and asymmetrical eigenmotions can be found in Table 6.9.

Table 6.9: *Eigenvalues and corresponding characteristics of the eigenmotions.*

Motion	Eigenvalues	Damping ratio	Period [s]	Half amplitude [s]
Symmetrical	$-0.2937 + 0.5696i$	0.4583	11.031	2.3599
	$-0.0045 + 0.1839i$	0.0242	34.157	155.4851
Asymmetrical	-1.7868	1.0000	-	0.3879
	$-0.0879 + 1.2631i$	0.0694	4.9742	7.8892
	0.0146	1.0000	-	-47.4753

The negative real part for the symmetrical eigenmotions implies that both the short period and phugoid motion are damped. As expected, the short period motion is strongly damped and has a time to half amplitude of less than $2.4s$. The phugoid motion takes significantly longer, approximately $155s$, to reduce the amplitude of the motion to half of the initial amplitude. For the asymmetrical eigenmotions the real part of the eigenvalue is only negative for the aperiodic roll and Dutch roll.
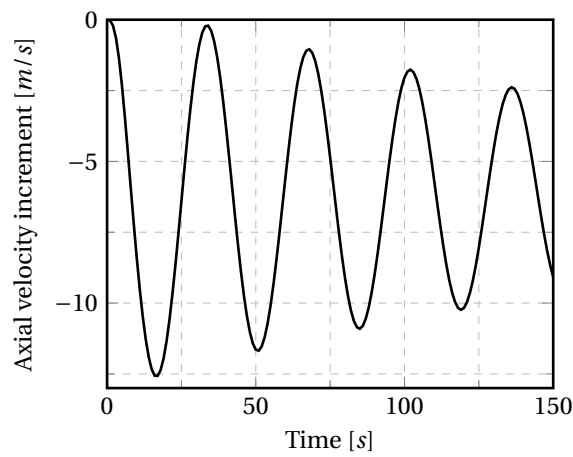
(a) *Velocity change during the symmetrical eigenmotion.*
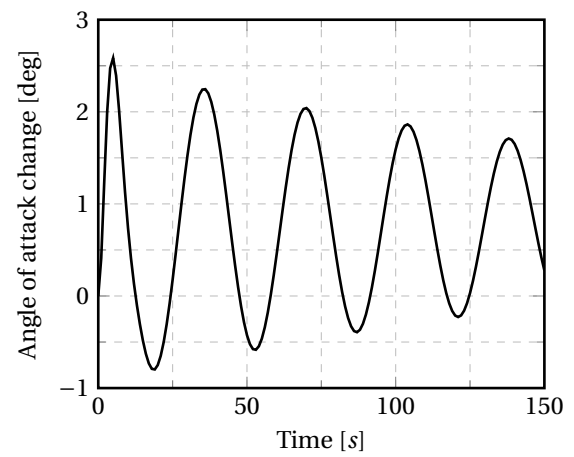
(b) *Angle of attack change during the symmetrical eigenmotion.*
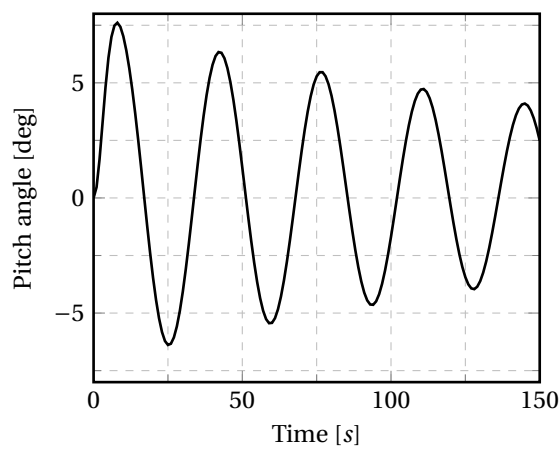
(c) *Pitch angle change during the symmetrical eigenmotion.*
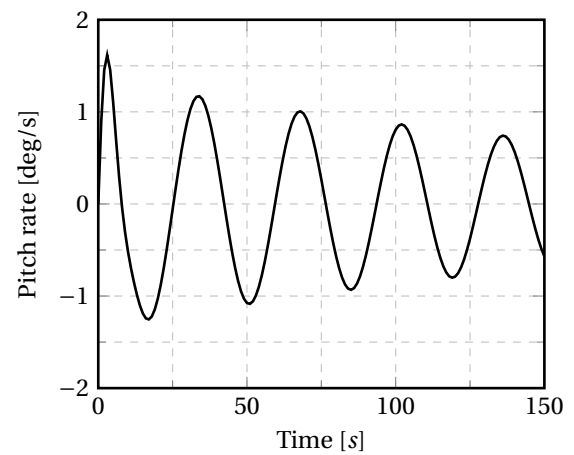
(d) *Pitch rate change during the symmetrical eigenmotion.*

Figure 6.6: *Symmetric eigenmotion.*
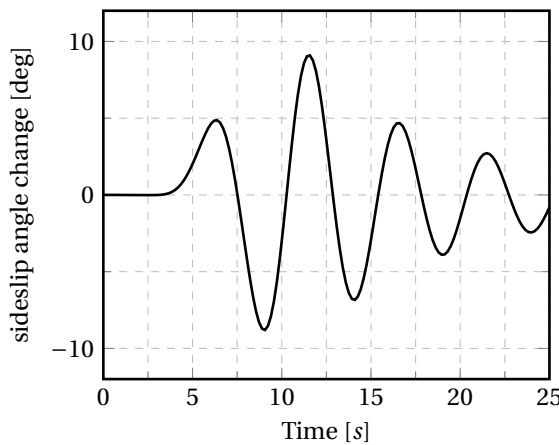
(a) *Angle of sideslip change during the asymmetrical eigenmotion.*
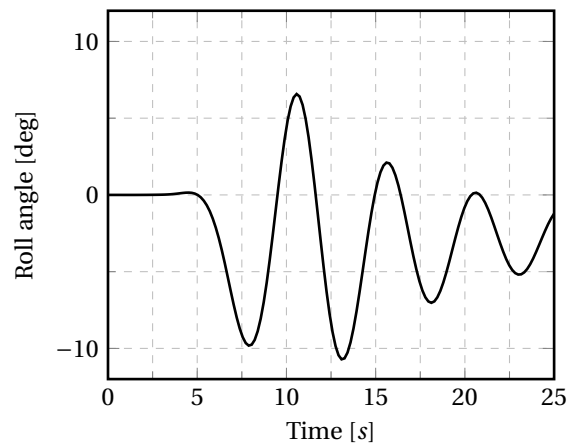
(b) *Roll angle change during the asymmetrical eigenmotion.*
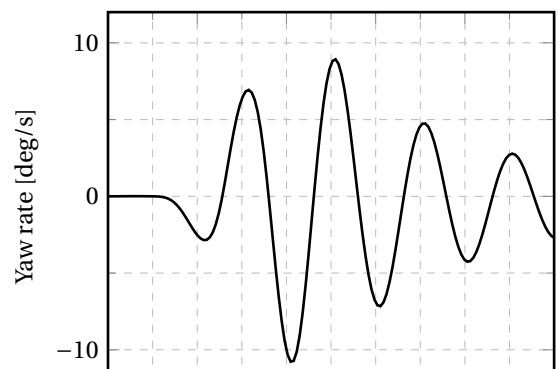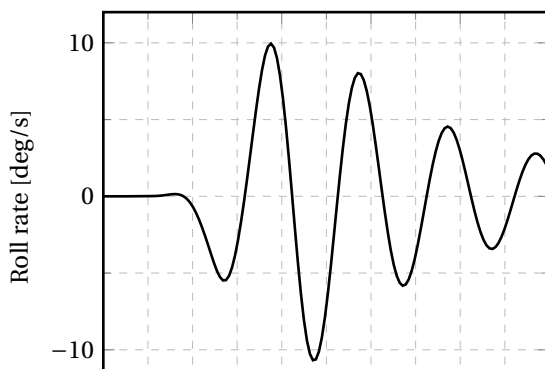
6.8. Static Stability Analysis

The static stability analysis focuses on analysing the ability of the aircraft to recover from disturbances to steady flight. For stability, any small perturbation from an equilibrium position shall be damped and the initial position reestablished. Instability would result in the disturbance increasing in amplitude over time, and continuous flight control input would be necessary to maintain steady flight.

6.8.1. Conditions Required for Equilibrium

During steady flight, the forces acting on the aircraft are in equilibrium. To analyse the forces that are present, some assumptions are to be made first. Firstly, the effect of propulsion is neglected. These forces do not change due to a perturbation, and as such their effects can be neglected. Additionally, the contribution of tail drag is neglected in both the force and the moment equation. Furthermore, drag of the main wing is deemed to cause a negligible moment about the Y-axis, and therefore omitted. The force itself is kept. Lastly, considering the airfoil of the tail is symmetric, it is assumed to have a moment coefficient around its a.c. of zero. With these assumptions, the pitching moment of the aircraft can be stated, and is shown in Equation 6.7.

$$C_m = C_{m_{ac}} + C_{L_w} \frac{x_{c.g.} - x_w}{\bar{c}} - C_{L_h} \frac{S_h l_h}{S \bar{c}} \tag{6.7}$$

6.8.2. Elevator Deflection

It is important to investigate the required deflection of the elevator during critical flight stages. It is desired that deflection is low during cruise to minimise the tail drag, additionally the possible deflection should be sufficient to manoeuvre the aircraft during take-off and landing. As seen in Equation 6.7, the force that has to be provided by the horizontal tailplane varies with c.g. location. Therefore, the critical values of horizontal tailplane force will be for the extreme c.g. locations. These locations size the tailplane. The force of the tailplane is a function of three parameters, angle of attack α, elevator deflection δ_e and trim tab angle δ_t. It is assumed that the tailplane force varies linearly with each variable. Downwash and velocity ratios are neglected, as the aircraft has a T-tail configuration. Splitting up Equation 6.7 into two components, α & δ_e, one can solve for the required elevator deflection [61].

$$\begin{cases} \delta_e = \frac{-1}{C_{m_{\delta_e}}} (C_{m_0} + C_{m_\alpha}(\alpha - \alpha_0)) \\[2mm] C_{m_{\delta_e}} = -C_{L_{h_\delta}} \frac{S_h l_h}{S \bar{c}} \\[2mm] C_{m_\alpha} = C_{L_{w_\alpha}} \frac{x_{c.g.} - x_w}{\bar{c}} - C_{L_{h_\alpha}} \frac{S_h l_h}{S \bar{c}} \end{cases} \tag{6.8}$$

What can be deducted from these equations, is that during flight the elevator deflection depends on airspeed and c.g. location. To obtain a low elevator deflection and thereby low tail drag, it is desired to have these parameters cancel each other out. From the loading diagram it can be observed that the c.g. is located behind the a.c. This combined with a high elevator effectiveness at cruise speed allows for relatively low elevator deflection for trim conditions. For the extreme c.g. locations as described in the loading diagram, and the lift gradients of the airfoils, Equation 6.8 can be evaluated.

Based on the current aerodynamic parameters of the aircraft, combined with the information from the loading diagram, a range of elevator deflection was determined for stability. The elevator deflection ranges from 0.25° at MTOW to 2.9° at most aft c.g. position. Such a large elevator deflection translates to a significant trim drag, however, this c.g. position is only encountered on the ground. During flight it is virtually impossible to achieve this c.g. position. At MLW the required elevator deflection is slightly higher than at MTOW, equalling 0.8° due to slightly more aft c.g..

6.8.3. Lateral Static Stability

Lateral static stability represents the ability of the aircraft to maintain steady flight in the lateral plane. Conditions like sideslip try to put the aircraft of-course and it is desired that its effect on the aircraft heading is as low as possible. The stability derivative that describes this behaviour is C_{n_β}, the effect of sideslip on the yawing moment of the aircraft. Its main contributor is the vertical tail, however large main wing sweep angles influence it significantly too. Splitting C_{n_β} up in these two components (main wing and vertical tail, effects of

the fuselage and horizontal tail are assumed to be negligible), with expressions for each of them from Corke [24], its magnitude can be determined.

$$C_{n_\beta} = C_{n_{\beta_w}} + C_{n_{\beta_{vt}}} \tag{6.9}$$

$$C_{n_{\beta_w}} = C_L^2 \frac{1}{4\pi A} - \frac{\tan\Lambda}{\pi A(A + 4cos\Lambda)}\cos\Lambda - \frac{A}{2} - \frac{A^2}{8\cos\Lambda} + 6\frac{x}{\bar{c}}\frac{\sin\Lambda}{A} \tag{6.10}$$

$$C_{n_{\beta_{vt}}} = V_{vt}C_{L_{\alpha_{vt}}}\left(1 + \frac{d\theta}{d\beta}\right)\frac{q_{vt}}{q} \tag{6.11}$$

Equation 6.11 takes into account the effect of the fuselage on the vertical tail. This type of downwash is difficult to estimate. An empirical relation [36]is used to approximate the relation of sidewash and vertical tail aspect ratio, and this value is taken. For an aspect ratio of 0.95, sidewash ratio is equal to 0.43. Applying all the Aerodynamic parameters known at this point, the value for C_{n_β} is found to be 0.16. Concluding is that, since the value is positive, stability is found. If made more positive in the future, stability is improved but controllability is worsened. Because C_{n_β} is positive, C_{Y_β} must also be positive.

6.8.4. Stick-Fixed vs Stick-Free Conditions
Regulations state that the aircraft shall be stable in all possible configurations. This means that when the pilot is unable to exert forces on the control stick, the aircraft should still remain stable. This is called a stick-free scenario, and differs slightly from the stick-fixed scenario in several ways. During stick free conditions, the elevator is free to move, as opposed to stick-fixed conditions. On the other hand, the moment at the hinge of the elevator is zero for stick-free conditions, while it is non-zero otherwise. The difference in stability between the two scenarios depends on the tailplane airfoil planform. If the lift gradient of the airfoil is positive, an increase in α cause a positive elevator deflection and therefore more lift. As a result, in this case, stick-free stability is better than stick-fixed. The opposite is true for negative lift gradient, and for zero lift gradient there is no change in elevator deflection at all. Because the lift gradient of the aircraft in this case is positive, stick-fixed stability is worse than stick-free and is therefore critical for tailplane sizing.

6.9. Verification & Validation
In this section the Verification and Validation procedures for the programs used in the flight dynamics analysis are discussed. First the programmes are verified, which ensures that the values produced by the code are correct. Next the programs are validated, this checks if the code is actually solving what it should solve.

6.9.1. Verification
The goal of verification is to check the code does actually compute what it is build for, and there are no mistakes in the code. The code used in this chapter was the AVL program made by MIT. Verifying the results was done by manipulating the values entered in the program in such a way, that the correct result was known beforehand and significantly different from the initial result. For example, the tail arm was made negative, which produced unstable symmetric motion, as expected. Other changes that were made include removing the vertical tail and applying forward sweep. All changes in aircraft geometry were drastic in order to get significant changes in program results. All subsequent results produced by the AVL file were correct and therefore the initial results are deemed accurate and thereby verified.

6.9.2. Validation
The program is validated by checking if the results meet the requirements. According to Sys.Perf.1 & Sys.Perf.2 the aircraft has to be dynamically stable for all possible flying scenarios. If these requirements are met, the results are validated. Looking at the eigenvalues of the aircraft in Table 6.9, it can be seen that four out of five eigenvalues have negative real parts. Combined with a non-zero damping ratio, it can be said that dynamic stability is achieved, and the requirements are met. The one eigenvalue that does not have a negative real part is the one that corresponds to the spiral motion. The aircraft is unstable with regards to this eigenmotion, and therefore technically not dynamically stable in all possible flight scenarios. However, CS-25 regulations tolerate an unstable spiral motion as long as the degree of instability is not too severe. In Table 6.9 it can be seen that the time taken to double the amplitude of the spiral motion is more than 47 seconds. This indicates that the pilot has plenty of time to react to this disturbance, and this time to double amplitude is within the bounds set by CS-25 regulations.

Considering all the eigenvalues and corresponding eigenmotions are either dynamically stable or not too unstable according to regulations, the flight dynamics characteristics satisfy the requirements and are therefore valid.

<div style="text-align: right; font-size: 3em;">7</div>

Structures

To make sure the aircraft is able to carry the loads subjected on it during operation, it is vital to have an adequate structure which is able to carry these loads. In this chapter, two main structural elements of the aircraft will be investigated in more detail. First, however, the material for these two structural elements is determined in Section 7.1. Next, the fuselage sizing and wing sizing can be found in Section 7.2 and Section 7.3, respectively. Finally, the results will be verified and validated in Section 7.4 and sensitivity analysis is presented in Section 7.5.

7.1. Material Selection

For the design of an aircraft focused on achieving a reduction of the operational costs of around 12% compared to reference aircraft [39], it is important to choose an appropriate material. The material selection aims at determining a material for the fuselage and wing. This is done using two trade-offs. First, an initial material trade-off will be performed after which a more detailed trade-off will determine the final material. The materials considered can be found in a material database presented in Appendix F. This database is compiled using information from the CES EduPack 2017 [55], as well as several other sources [27, 37, 88, 70, 4]. In case a range of values is given, the average is taken.

7.1.1. First Material Trade-off

The first choice to be made is between metals and composites. Composites materials are becoming more and more common because they have some specific advantages, such as the high fatigue and corrosion resistance and high strength to weight ratio [62]. However, compared to metals, there is less knowledge about manufacturing and maintenance for composites, making them more costly. Also, the recyclability of composites is very low due to their inherent hetrogenic properties [96]. In recent years, there have been some studies on the use of natural fibres and thermoplastic resins in order to improve sustainability and recyclability [70]. Unfortunately, these innovations will not be implemented in primary structures in the foreseeable future because natural fibre composites (NFC) development has to overcome degradation hurdles [13] as well as flammability issues [22]. This leaves metals as the main material choice.

Several material choices can be made with respect to metals. In the aerospace industry, aluminium and titanium alloys are the most frequently used metals [43, 53]. In order for the material to be as light and sustainable as possible (while retaining good manufacturing properties) a lot of research is conducted into the different alloying elements. Recent innovations in alloying aluminium with lithium, magnesium, beryllium and scandium resulted in several promising alloys [88, 44, 72, 37, 92]. Looking at Table F.1, the beryllium alloy can be eliminated due to the high material costs. Also, beryllium is a toxic material, making it hard to manufacture and maintain [55, 88]. Titanium is eliminated due to a combination of high material prices and difficulties in manufacturing [71]. As titanium is a very hard metal, tool wear can drive tooling expenses to an unacceptable level. Aluminium-scandium alloys are also a new development promising a large reduction in weight while maintaining key structural properties [44]. However, since this material is relatively expensive and new (therefore unknown in terms of maintenance), it is also dropped. It might, however, be interesting for the future.

The properties of the remaining materials are compared to determine the results of the initial trade-off. The aluminium lithium alloys have similar strength compared to the regular Al-2xxx and 7xxx series. However, they have a significantly lower density (almost 10%) making them really attractive in terms of weight reduction. Also, the maintainability is similar to the regular alloys, making them suitable as well. The drawbacks

<div style="text-align: center;">56</div>

compared to the regular materials are the high material costs and the difficulties in manufacturing. Compared to aluminium alloys without lithium, alloys containing lithium can contaminate tools. This requires a separate production line and equipment. Also, lithium is slightly toxic, meaning that handling should be carefully considered. However, the good strength characteristics, low density and relatively low increase in material costs outweigh the disadvantages. Therefore, aluminium-lithium alloys are chosen as the main material of the aircraft.

7.1.2. Second Material Trade-off

Now that the first trade-off is finished, the remaining two materials will enter the second trade-off. In this trade-off, the effect of the material choice on the fuel consumption and manufacturing is assessed.

The density of each material is used to give an initial estimate of the weight reduction by that material compared to a reference material, in this case Al2024-T351. Because the analysis mainly focuses on the fuselage and the wing, the weight reduction for these two components is determined in order to calculate a new OEW and MTOW. Using the code from the Flight Performance and Propulsion (FPP) department, this translates into a reduction of fuel which can be used to calculate the amount of money saved after the operational lifetime[1]. The return on investment is subsequently calculated using an operational lifetime of 12.5 years with 4 cycles a day. All the results can be found in Table 7.1.

Table 7.1: *Material weight saving rate of return based on fuel consumption.*

Alloy	ρ [kg/m^3]	OEW [kg]	MTOW [kg]	Fuel used [kg]	Fuel saved OL [kEUR]	Material Cost [EUR]	Extra material cost [kEUR]	RoI Mat [Mth]	Contingency (20%) [Mth]
Al 2024-T351	2750	16416	30190	4791.1	-	1.90	-	-	-
Al-Li 2090-T83	2600	16103	29748	4730.3	538	12.0	163	46	11
Al-Li 8090-T851	2540	15978	29572	4705.6	756	12.4	168	34	8

The different materials also have different manufacturing properties and therefore influence the production costs. The production costs can be as high as 70 to 85% of the purchase price of the aircraft [1]. The machining speed is used as an estimate to evaluate the effect of material choice on production costs. Assigning the average value of 31.5 million EUR [1] to the reference material and calculating the differences, the results in Table 7.2 can be calculated. Since the production costs are based on the weight, a correction for the density between the materials and the reference material is also applied.

Table 7.2: *Change in production cost with respect to the base material.*

Alloy	ρ [kg/m^3]	Machining Speed [m/s]	Extra Machining Cost [M EUR]	Contingency (20%) [MEUR]
Al 2024-T351	2750	67.1	-	-
Al-Li 2090-T83	2600	42.7	15.3	7.8
Al-Li 8090-T851	2540	54.9	4.06	5.9

Looking at this table, it can be concluded that the first material increases the production costs dramatically. The second material changes the production costs by a relatively small amount, making the total production costs slightly higher than the upper bound of 35 million EUR presented in the Baseline Report [1].

Table 7.1 shows that the second material, Al-Li 8090-T851, has a faster ROI compared to the first material. Looking only at the raw material influence, Al-Li 8090-T851 results in a total cost saving of 588,000 EUR over

---

[1]Calculations based on A1 jet fuel for a fuel price of 0.4844 EUR/kg, determined from `http://www.iata.org/publications/economics/fuel-monitor/Pages/index.aspx`, accessed on 12-06-2018

the total operational lifetime. Therefore, looking at the results from both evaluations, Al-Li 8090-T851 is chosen as the material for the aircraft.

7.1.3. Additional Considerations

The material selection has been performed for the wing and fuselage, but additional remarks can be made for other parts of the aircraft. For the landing gear, strong material is required with good casting properties and high strength. Therefore, a steel alloy is most suitable for this purpose. Recycling of control surfaces and stabilisers is not as important as recycling the fuselage or wing, because their weight contribution is significantly lower. Therefore, in order to reduce weight, these components can be made from a composite material such as carbon fibre reinforced polymers. Also, since these components are relatively small, it is sufficient to replace them. In areas where high damage tolerance is required, another material can be chosen as well. The best suited material for this purpose would be a fibre metal laminate, such as GLARE, as it combines the low density of composites with the durability of metals. This material can, for example, be applied at the leading edges of the wing and stabilisers. Finally, some additional considerations need to be made with respect to sustainability and more specifically towards recyclability. The main material for the $MW5$ is 100% recyclable. About 40% is re-used in the same capacity, whereas the rest is down-cycled [55]. The additional materials are less recyclable, but can still be down-cycled. Therefore, the recyclability of the aircraft is very high.

7.2. Fuselage Sizing

In this section, the fuselage sizing will be presented. Firstly, the results and recommendations are given in Subsection 7.2.4, later the sizing method with all the assumptions used is described in Subsection 7.2.3.

7.2.1. Loading Diagrams

In order to calculate the design loads for the fuselage, it is necessary to determine the loads acting on the fuselage. There are several main contributors to these loads, such as the different structural weights and forces acting on the structure. Below, the assumptions and used parameters are stated. Next, the loading diagrams for the fuselage are presented.

Assumptions and Parameters   Several assumptions are made in order to construct the loading diagrams for the fuselage. First, the load case needs to be determined. For this, the in-cruise condition was chosen. Next, the fuselage is assumed to consist of two cantilever beams connected at the centre of gravity. The different structural weights, determined by the Class-II weight estimation method, are assumed to be constant distributed loads. The main and tail lift acting on the structure are assumed to be point loads acting at their respective aerodynamic centres (located at 25% of their respective MAC). The c.g. is assumed to be the average of the c.g. range mentioned in the Stability & Control chapter (6). This c.g. value equals 16.87 m. A summary of the distributed and point loads can be found in Table 7.3 below.

Table 7.3: *Summary of fuselage applied loads.*

Distributed				Point		
Load	**Start [m]**	**End [m]**	**Magnitude [kN/m]**	**Load**	**Location [m]**	**Magnitude [kN]**
Fuselage struc.	0	28.5	3.51	Cargo	23.5	16.77
Passengers	5.48	21.49	4.08	Main lift	16.27	272.81
Fuel weight	15.58	18.34	2.62	Tail lift	27.1	34.12
Wing struc.	15.58	18.34	8.58			
Engines	21.46	24.96	6.67			
Tail struc.	26.86	27.82	1.46			

Loading diagrams   The load distribution for the load case described above can be seen in Figure 7.1 and Figure 7.2. From these graphs, it can be seen that the maximum shear force is equal to 154.23 kN and the maximum bending moment to be 709.92 kN m.

These loads will be multiplied by the maximum load factor in the most critical load case and a safety factor to get the design stresses and forces. The first factor follows from the flight envelope determined in Section 4.6 and equals 2.5. For the fuselage design, a safety factor of 2 is used.
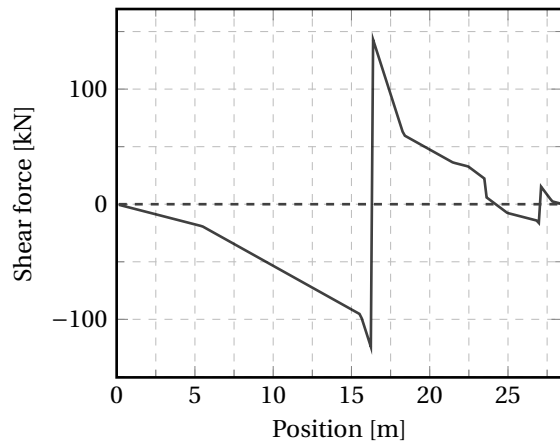
Figure 7.1: *Shear force diagram along the fuselage.*
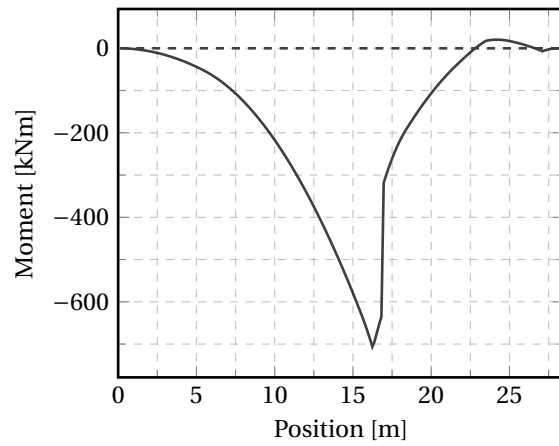
Figure 7.2: *Moment diagram along the fuselage.*

7.2.2. Stringers Trade-off

In this section, different stringers geometries and their properties will be discussed. In Figure 7.3 different extruded stringers geometries are presented whereas in Figure 7.4 different formed stringers geometries are shown. Integrally stiffened panels are not considered for the fuselage since they require complicated machining.
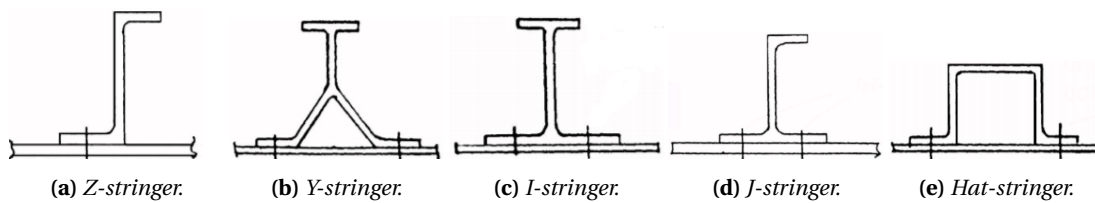
(a) *Z-stringer.*   **(b)** *Y-stringer.*   **(c)** *I-stringer.*   **(d)** *J-stringer.*   **(e)** *Hat-stringer.*

Figure 7.3: *Different extruded stringers geometries [63].*

(a) *Z-stringer.*   **(b)** *Open hat-stringer.*   **(c)** *Closed hat-stringer.*
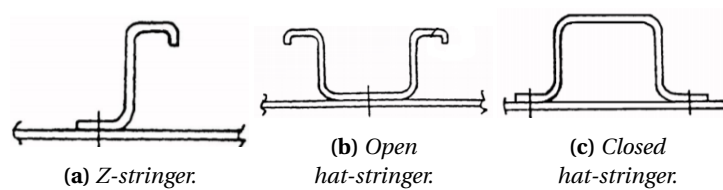
Figure 7.4: *Different formed stringers geometries [63].*

Table 7.4: *Stringer properties.*

Stringer type	Characteristics
Extruded	
Z-stringer	• High structural efficiency • Easy to manufacture
Y-stringer	• Corrosion inspection problem • Highest structural efficiency • Good fail-safe characteristics due to double row of fasteners
I-stringer	• Good structural efficiency • Good fail-safe characteristics due to double row of fasteners
J-stringer	• Good fail-safe characteristics due to double row of fasteners
Hat-stringer	• Corrosion inspection problem • High structural efficiency
Formed	
Z-stringer	• High structural efficiency
Open hat-stringer	• High structural efficiency
Closed hat-stringer	• Corrosion inspection problem

For fuselage application, all closed stringers (extruded Y-stringer, extruded hat-stringer, and formed closed-hat stringer) cannot be used due to (corrosion) inspection issues, which would considerably increase the maintenance of fuselage. J-stringer and I-stringer also eliminated due to added weight of extra rivets and additional maintenance costs. The main disadvantage of extruded stringers is their cost and limitations on the minimum thickness, therefore, formed Z-stringer will be used in the fuselage.

7.2.3. Fuselage Sizing Method
In this section the assumptions and their implications for fuselage sizing are given. Then the fuselage sizing method is discussed.

Assumptions

1. For crippling the Z-stringer is sized for Al7075-T6 due to lack of data for aluminium-lithium alloys.
   Implications: Different stringer geometry might be optimal for aluminium-lithium alloys.
2. For crippling sizing the thickness across the stringer is constant.
   Implication: The geometry of the stringer can further be optimised, for example for weight.
3. The total width of the stringer is the same as the total height of the stringer
   Implication: The geometry of the stringer can further be optimised, for example for weight or area.
4. The skin carries the shear stress
5. The stringers carry normal stress (longitudinal stress)
6. Moments of inertia of stringers about their centroid is significantly smaller than their Steiner term, therefore they are neglected.
   Implications: Slightly lower moments of inertia, which would yield higher tensile stresses per boom. Therefore the structure will be marginally overdesigned
7. For skin buckling, the skin between frames and stringers is considered flat.
   Implications: Higher skin buckling stress would be achieved with a curved plate. Therefore the structure will be overdesigned.
8. For skin buckling, the skin is considered clamped between frames and hinged between stringers.
9. Stringer geometry is the same for all the sections
   Implications: Different stringer types might be optimal for different loading conditions. Therefore there is a possibility to reduce weight by introducing different stringers.
10. Stringers are equally spaced in the fuselage cross-section.
    Implications: For different loading conditions, different sections of the fuselage will need a different

number of stringers. Therefore the amount of stringers will be overestimated as it is estimated for critical conditions.

11. Fuselage cross-section has a constant thickness.
    Implications: The skin thickness will be designed to withstand the critical load case, thus it will be overdesigned for all location other than critical location.
12. The analysis is done only for the cylindrical part of the fuselage.
    Implications: Cone analysis is out of the scope for this report

Most assumptions used in this section are leading to more conservative design, leaving space to further optimise the structure.

Structure idealisation   The structure is idealised with equally spaced booms. Boom area is calculated using Equation 7.1 from Megson [56].

$$B_n = A_{\text{stringer}} + \frac{t_{\text{skin}} \cdot b_{n,n+1}}{6} \cdot \left(2 + \frac{\sigma_{n+1}}{\sigma_n}\right) + \frac{t_{\text{skin}} \cdot b_{n,n-1}}{6} \cdot \left(2 + \frac{\sigma_{n-1}}{\sigma_n}\right) \tag{7.1}$$

Where A_{stringer} is the area of the stringer, t_{skin} is the skin thickness, b is the distance between boom n and boom $n+1$. σ represents the direct stresses in the booms. The number of booms is equal to the number of stringers needed. Once the boom areas and boom locations are known, moments of inertia are calculated using Equation 7.2 [56]. Due to the symmetry of the fuselage, the centroid is in the geometrical centre of the cross-section.

$$I_{xx} = \sum_1^n B_n \cdot x_n^2 \qquad\qquad I_{yy} = \sum_1^n B_n \cdot y_n^2 \qquad\qquad I_{xy} = \sum_1^n B_n \cdot x_n \cdot y_n \tag{7.2}$$

Due to symmetry, the I_{xy} will be zero. All the stresses are calculated to withstand allowable loads. Allowable loads are calculated as follows:

$$\sigma_{max_{\text{all}}} = \frac{\sigma_{\text{tensile}_{\text{yield}}}}{n_{\text{load}} \cdot n_{\text{safety}}} \qquad\qquad \sigma_{min_{\text{all}}} = \frac{\sigma_{\text{compressive}_{\text{yield}}}}{n_{\text{load}} \cdot n_{\text{safety}}} \qquad\qquad \tau_{max_{\text{all}}} = \frac{\tau_{\text{max}}}{n_{\text{load}} \cdot n_{\text{safety}}} \tag{7.3}$$

The skin buckling is calculated to withstand the given loads per section, obtained from Figure 7.1 and Figure 7.2.

Crippling   Compression in the aircraft fuselage can result in local instability failure, further referred to as crippling. The crippling stress for entire geometry is computed by taking weighted average for each segment, see Equation 7.4 [63].

$$\sigma_{cc} = \frac{\sum_1^n (b_n \cdot t_n \cdot F_{ccn})}{\sum_1^n (b_n \cdot t_n)} \tag{7.4}$$

Where b_n is the segment width, t_n is the segment thickness, and F_{ccn} is crippling stress for a segment. Value for F_{ccn} can be found in appropriate graphs in the book of Niu [63].

Bending   Normal stress due to bending is found using Equation 7.5 from Megson [56].

$$\sigma_z = \left(\frac{M_y \cdot I_{xx} - M_x \cdot I_{xy}}{I_{xx} \cdot I_{yy} - I_{xy}^2}\right) \cdot x + \left(\frac{M_x \cdot I_{yy} - M_y \cdot I_{xy}}{I_{xx} \cdot I_{yy} - I_{xy}^2}\right) \cdot y \tag{7.5}$$

Where M_y and M_x are bending moments in y and x-direction, respectively. x and y are the distances between booms and x and y-axis, respectively.

Shear   Shear flow due to shear force is calculated using the Equation 7.6 [56].

$$q_s = -\left(\frac{S_x \cdot I_{xx} - S_y \cdot I_{xy}}{I_{xx} \cdot I_{yy} - I_{xy}^2}\right) \sum_1^n (B_n \cdot x_n) - \left(\frac{S_y \cdot I_{yy} - S_x \cdot I_{xy}}{I_{xx} \cdot I_{yy} - I_{xy}^2}\right) \sum_1^n (B_n \cdot y_n) + q_{s,0} \tag{7.6}$$

Where S_x and S_y are shear forces in x- and y-direction. Since the shear forces are assumed to be symmetric, the resultant shear force will act through the centre of geometry which is also the shear centre. Therefore the shear of the closed section $q_{s,0}$ is zero. To obtain the shear stress, the shear flow needs to be divided by the skin thickness.

Torsion   Shear stress due to torsion is calculated using Equation 7.7 [56].

$$\tau_{torsion} = \frac{T}{2 \cdot A_{en} \cdot t_{skin}} \tag{7.7}$$

Where T is the torque applied, and A_{en} is the enclosed area.

Radial stress   Radial stress is calculated as follows [63]:

$$\sigma_{r_{max}} = \frac{p_i \cdot r_i^2 - p_o \cdot r_o^2}{r_0^2 - r_i^2} + r_i^2 \cdot r_o^2 \frac{p_o - p_i}{r_o^2(r_o^2 - r_i^2)} \tag{7.8}$$

Where p_o and p_i are outside and inner pressure respectively, r_o and r_i are the outer and inner radii. However due to the fact that skin thickness is more than thousand times smaller than the radius of the fuselage, the radial stress will be insignificant for stress calculation, therefore it is neglected.

Axial stress   The axial stress due to pressure is calculated using Equation 7.9 [63].

$$\sigma_a = \frac{p_i \cdot r}{2 \cdot t_{skin}} \tag{7.9}$$

where r is the fuselage radius.

Circumferential stress   Circumferential stress, also known as hoop stress is calculated in Equation 7.10 [63]:

$$\sigma_{hoop} = \frac{p_i \cdot r}{t_{skin}} \tag{7.10}$$

Skin buckling   Skin buckling is used to size the frame pitch. Firstly the effective stringer width is calculated using Equation 7.11 [63].

$$b_{eff} = \sqrt{\frac{K_e \cdot E}{F_{st}}} \cdot t_{skin} \tag{7.11}$$

where K_e is a compression buckling constant, E is the elastic modulus of the material and F_{st} is the stringer allowable stress. Then the stringer pitch is calculated taking into account the effective width of the stringer. Skin buckling under in-plane compression is calculated from Equation 7.12 [63] and skin buckling under in-plane shear is calculated using Equation 7.13.

$$F_{c,cr} = K_c \cdot \eta_c \cdot E \cdot \left(\frac{t_{skin}}{b_{stringer}}\right)^2 \tag{7.12} \qquad\qquad F_{s,cr} = K_s \cdot \eta_s \cdot E \cdot \left(\frac{t_{skin}}{b_{stringer}}\right)^2 \tag{7.13}$$

Where K_c and K_s are constants for flat plate buckling. η_c and η_s are plasticity reductions factors for in-plane compression and in-plane shear, respectively. $b_{stringer}$ is the stringer pitch. K_c and K_s are based on the ratio of stringer pitch to frame pitch and the boundary conditions. The appropriate graphs can be found in the book of Niu [63].

Von Mises criterion   The von Mises criterion for multi-axial loading is also implemented. Equation 7.14 shows the formula used [64].

$$\sigma_y > \sqrt{\frac{(\sigma_x - \sigma_y)^2 + (\sigma_x - \sigma_z)^2 + (\sigma_y - \sigma_z)^2 + 6 \cdot (\tau_{xy}^2 + \tau_{yz}^2 + \tau_{zx}^2)}{2}} \tag{7.14}$$

7.2.4. Results and Recommendations
The results for the critical cross-section can be found in Table 7.5. The cross-section was optimised for weight.

Table 7.5: *Results for critical cross-section.*

X_{crit} [m]	σ_{max} [MPa]	σ_{min} [MPa]	τ_{max} [MPa]	t_{skin} [mm]	$n_{stringers}$ [-]	$b_{stringer}$ [cm]	n_{frames} [-]	b_{frame} [cm]
16.27	162.92	−129.28	132.62	1.5	53	16	14	108.2

One can see that 53 stringers are needed with a stringer pitch of 16 cm. From crippling calculation, the optimal geometry for formed Z-stringer is found to be 54 mm by 54 mm (symmetric about its web) with 0.9 mm thickness. It cripples at maximum allowable compressive stress. The skin thickness is equal to 1.5 mm. The frame pitch is 108.8 cm with 14 frames. However, for passenger comfort, there will be 20 frames to assure each window seat has a window. The visualisation of the cylindrical part of the fuselage can be seen in Figure 7.5.
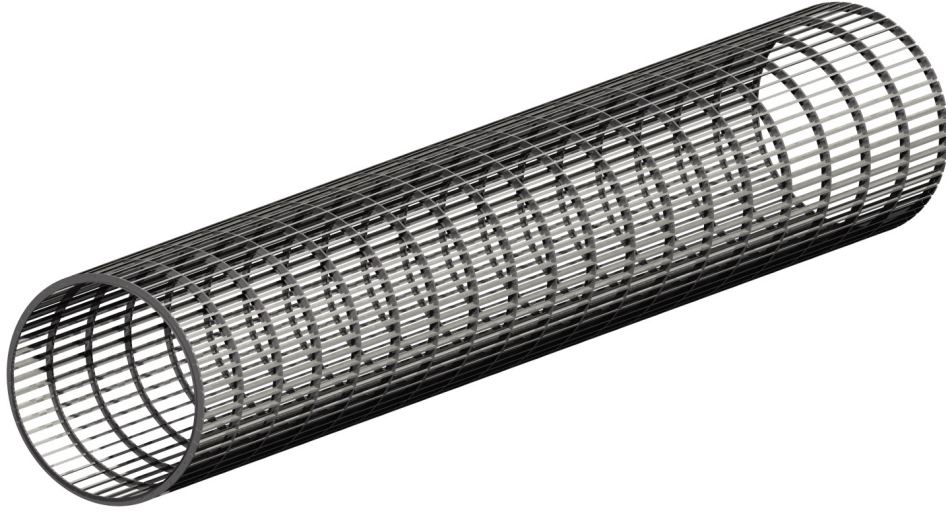
Figure 7.5: *Visualisation of the fuselage structure.*

In Figure 7.6 the optimised number of stringers of the cylindrical section is given. One can see that the for the critical cross-section 53 stringers are needed, whereas for the least loaded cross-section 26 stringers are needed. In Figure 7.7 the allowable stresses for aluminium-lithium 8090 are given (continuous lines), and the actual stresses experienced by the stringers (dashed lines). The dashed lines do not go beyond their allowable counterpart. It means that the structure can withstand loads from Figure 7.1 and Figure 7.2, and not fail. An ideal situation would be if the dashed lines coincide with continuous lines. This would mean that properties of the material and structure are used to the fullest.
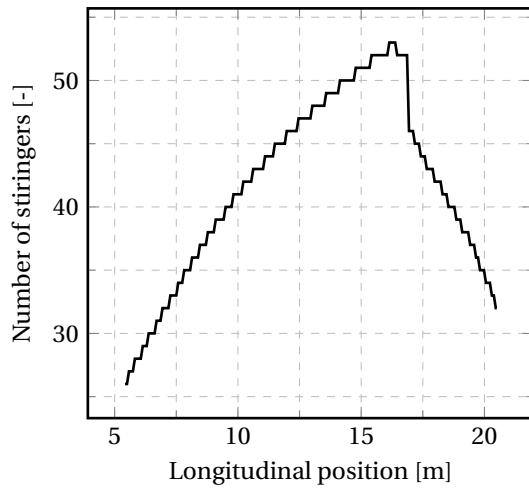
Figure 7.6: *Number of stringers versus longitudinal position* ($t_{skin} = 1.5$ mm).
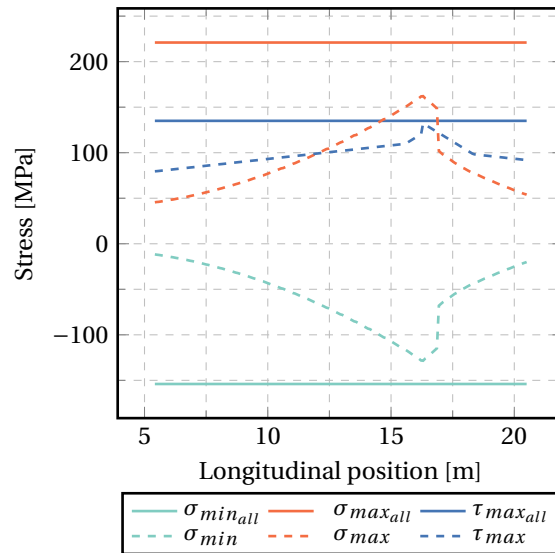
Figure 7.7: *Stresses experienced by stringers across fuselage* ($t_{skin} = 1.5$ mm).

In Figure 7.8 the normal, shear and von Mises stress distribution are present for skin thickness of 1.5 mm and 53 stringers (stresses are expressed in MPa). In Figure 7.8a one can see that critical loads are in top and bottom of the fuselage (due to longitudinal bending). With the top being in tension and the bottom being in

compression. In Figure 7.8b the critical location is on the sides of the fuselage, this is precisely the longitudinal location of the lift force. The last figure shows the distribution of the Von Mises stresses for multi-axial loading. It can be seen that the normal stress has a major contribution.

(a) *Normal stress.*   **(b)** *Shear stress.*   **(c)** *Von Mises stress.*
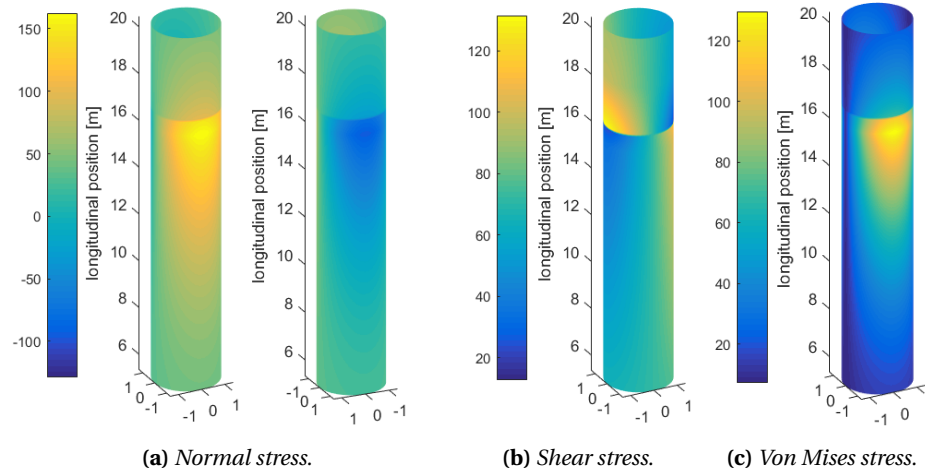
Figure 7.8: *Stress distributions ($n_{stringer}$ = 53, t_{skin} = 1.5 mm).*

As one can see in Figure 7.8 the structure is overdesigned and is thus too heavy. An ideal situation would be when all the failure modes occur at the design loads. Therefore, there are still opportunities for enhancement:

- As mentioned previously for less loaded sections at the front of the fuselage or at the back, fewer stringers are needed. Further research into optimising the structure is recommended. One way to optimise the structure is to reduce the number of stringers where possible. Hence reducing the weight of the structure. However, cutting the stringer will result in stress concentrations. There need to be some other structural element at that point to reduce it and carry the load from the missing stringer.

- A variable skin thickness can also reduce the weight, hence optimise the structure. One needs to remember, however, that there is a limitation to minimum skin thickness, mostly due to the need of fastening the stringers and other structural elements.

- Different stringer geometries have different specific properties. For example, in the section primarily loaded in torsion, closed stringer are superior to open stringers. Therefore, fewer stringers would be needed.

Other methods of structure optimisation can also be considered. The most efficient practice would be to combine all different methods. This would result in having variable skin thickness, variable number of stringers and different stringers geometry for differently loaded sections. However, such calculations are out of the scope for this project.

7.3. Wing Sizing

For the initial wing sizing, the layout of the main load carrying structure, namely the wing box, is determined. It is assumed the wing will only be subjected to vertical loads (i.e. lift, fuel weight, structure weight), resulting in shear forces, bending moments and torsion. The wing box is designed such that it can carry these loads at any flight scenario as presented in the flight envelope (presented in Section 4.6).

Although in reality the entire wing structure will contribute to its stiffness, initially it is assumed that only the wing box will carry the loads. This assumption is a conservative one and during later stages of the design it is possible to optimise the structural weight by determining the added stiffness of a leading and trailing edge structure. This section is structured such that loading diagrams for the wing will be presented first, after which a detailed explanation will follow on the wing box design process. In this design process the wing box is initially arbitrarily assumed to be a 1 mm thick box with a left spar at 15% chord length and the right spar at 60% [40]. This sizing is because the leading and trailing edge are reserved for slats, flaps, control surfaces and other systems. The initial wing box is updated during the design iterations based on the calculated stresses. The local effects of taper on stresses are not taken into account for this initial sizing.

7.3.1. Loading Diagrams

When determining the loading diagrams the sweep is assumed to be constant over the span, using the highest sweep for the calculations this results in a conservative design at the root where in reality the sweep is lower and thus the torsional loads will be lower. In Figure 7.9 the wing loading is given as a function of the span wise distance from the root. This is based on a method proposed by Schrenk [83], where the lift distribution is an average of the elliptical distribution and a distribution based on actual the wing geometry.
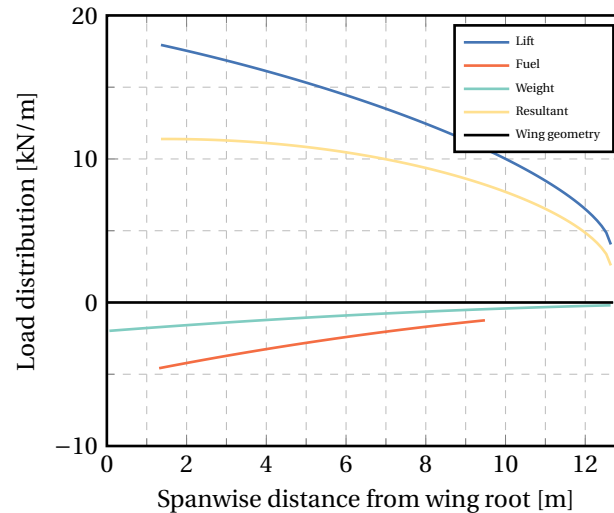
Figure 7.9: *Wing loading.*

7.3.2. Design for Bending

Starting from a structure with two spars, a top and bottom skin with thickness of 1 mm it is possible to calculate the normal stresses at all wing box locations using classical beam theory where the normal stress at any location for the maximum bending loads in the structure is calculated using Equation 7.5. Taking into account a safety factor of 1.5 [34] a new value for the thickness at each location can be determined based on the yield stress of the used material as found in Section 7.1. Then for the updated thicknesses an iteration can be performed for which the stress can be calculated again for the updated structure. Performing several iterations results in a wing box design as illustrated in Figure 7.10.
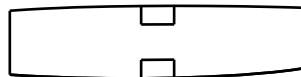
Figure 7.10: *Wingbox geometry.*

From Figure 7.10 it is clear that an optimal design for bending is reached when the thickness is increased at the location that is furthest from the neutral axis. Given this theoretical design it is possible to define a stiffener area and determine the number of stiffeners in combination with a skin thickness which results in acceptable normal stresses (i.e. below yield stress). This results in an initial layout which can be determined for the entire wing box based on local wing geometry and wing loading.

7.3.3. Stresses Due to Shear and Torsion

With the given design that is able to withstand the bending loads, the structure can be idealised to determine the shear stresses as a result of the shear forces and torsion. The structural idealisation is done as explained in Subsection 7.2.3. To determine shear stresses, first, the shear centre location will be determined. Since only vertical shear forces are taken into consideration only the location on the x-axis is relevant. The shear centre of the wing box is found by making a cut at the left spar, solving for all the open section shear flows and determining the constant shear flow from closing the cut. In Figure 7.11, a visual representation is given of the wing box at the root with the cut. Solving for the constant shear flow is done using Equation 7.15 [56] from the fact that there will be no twist when the shear force acts through the shear centre. Then the shear centre

location is found using moment equivalence.
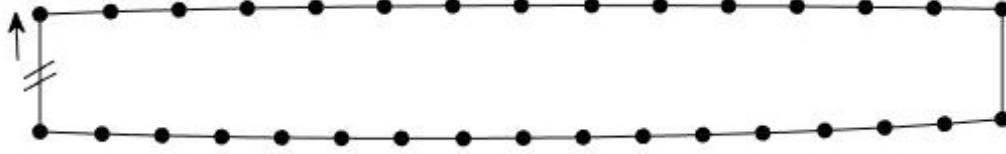
Figure 7.11: *Idealised wing box.*

$$q_{s,0} = -\frac{\oint (q_b/Gt)\,ds}{\oint ds/Gt} \tag{7.15}$$

When the shear centre has been found as a function of the span, the lift force can be moved to the shear centre and an additional torque (which will be the local lift force multiplied by the local distance to the shear centre) can be added to accommodate the move. Shear flows in between booms can then be determined for the whole cross-section at all spanwise locations. Shear flows in the idealised structure are calculated using Equation 7.6. For the torque the shear flow will be determined using Equation 7.7. Shear flows can then be translated to shear stresses using the local thickness as seen in Equation 7.16. From these calculations the design can be updated to make sure shear stresses do not exceed the maximum allowable shear stresses given by the material selection as given in Section 7.1. Performing several iterations the cross-section of the wing at the root is illustrated in Figure 7.12.

$$\tau = \frac{q}{t} \tag{7.16}$$
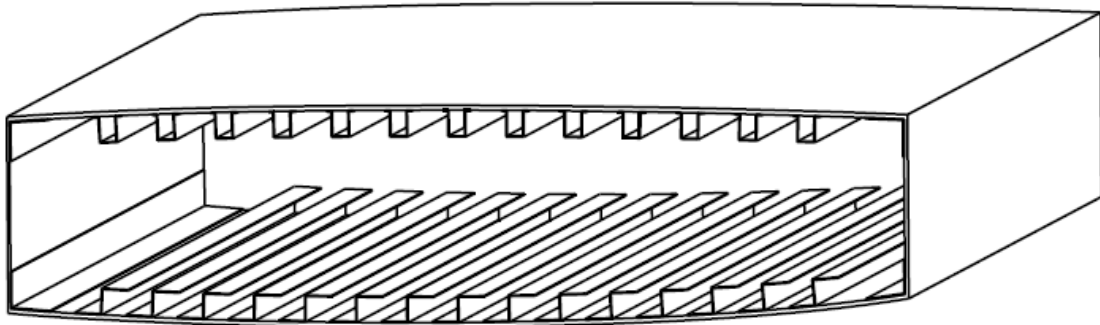
Figure 7.12: *Wing box geometry at the root.*

For the stiffener selection, reference aircraft have been studied since local skin buckling and stiffener crippling is not taken into account for this initial sizing. As these values greatly influence the stiffener type selection it was decided to base that on reference aircraft. Therefore hat-stiffeners are used at the top skin and

Z-stiffeners at the bottom skin as that is found to be very common in reference aircraft. The stiffener dimensions are based on what is needed to deal with the applied loads (i.e. keep the normal stresses below yield stresses), they can be found in Figure 7.13. The top and bottom skin thickness at the root is determined to be 9 mm and the front and aft spar are designed to be 5 mm and 7 mm respectively. The aft spar is slightly thicker due to the increased shear stresses. These occur there because of stresses due to shear and stresses due to torsion act in the same direction at the aft spar, while they are counteracting at the front spar.

(a) *Z-stiffener.*   **(b)** *L-stiffener.*   **(c)** *hat-stiffener.*
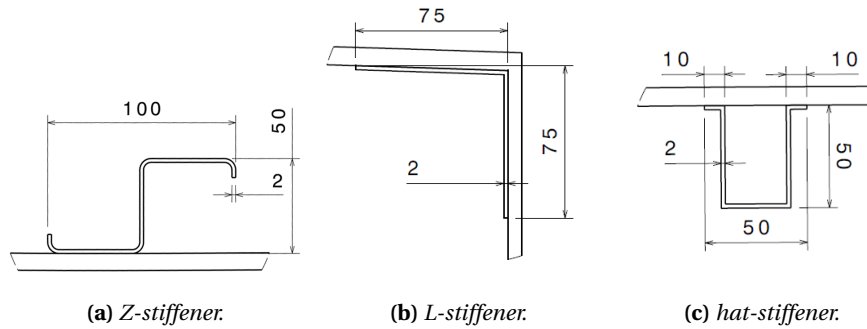
Figure 7.13: *Wing box stiffener geometry.*

7.3.4. Sweep

The sweep creates an additional torque applied to the structure. The shear stresses caused by this torque will be determined using the principle of superposition. The shear stress will be a function of the enclosed area of the wing box and local thickness as seen in Equation 7.7. Aside from the additional torsional loads there will also be local increases in stress at the root. At the leading edge, the stresses will increase due to the shear-lag effect [63]. To relieve these stresses additional material needs to be added at the trailing edge. This problem is not solvable using beam theory and is therefore reserved for a later stage in the design.

7.3.5. Rib Spacing

The top skin of the wing will be under significant compression loads during the flight. This means it is susceptible to buckling and ribs will be placed over the entire span to account for this. The rib spacing is determined by assuming the stiffeners carry all normal stresses and they are pinned at the locations of the rib. The loads on the stiffener are determined using the local stress and area of the stiffeners. These loads should be smaller than the Euler buckling load as given by Equation 7.17 given a certain length and for the stiffener moment of inertia I_{xx} and Young's modulus E. The equation can be rewritten and solved for the length L which will be the rib spacing and for the root location this can be calculated to 0.465 m, given a stiffener I_{xx} of 1.04×10^{-7} m^4 and local load per stiffener of 120 kN.

$$P_{\text{crit}} = \frac{\pi^2 E I}{L^2} \tag{7.17}$$

7.3.6. Von Mises Stress

When looking at a structure subjected to normal and shear stresses in different directions, yielding stress of a ductile material (which is being used in the design) can be approximated using the von Mises yield criterion [64]. In Subsection 7.2.3, Equation 7.14 is given from which the equivalent Von Mises stress is calculated. This stress should be smaller than the material yield stress for every situation and location. Again this criterion can be used to update the wing box design at any location.

7.4. Verification & Validation

In this section the verification and validation methods are discussed specific to the structural design of the $MW5$ aircraft. In Appendix A an extensive but less specific overview is given of the applied verification and validation procedures.

7.4.1. Verification

This subsection contains the verification for the structures chapter. More insight into verification and validation procedures can be gained by reading Appendix A. First, material selection is treated followed by the loading diagrams. Next, the fuselage and wing sizing are discussed.

Material selection   A MATLAB program was written for the calculations used during the second material trade-off. In order to verify the outcome of this program, hand calculations are performed to make sure the outcomes are correct. The methods used are based on linear comparisons between material properties, but there is no reference as to the validity of this approach.

Loading diagrams   Several steps are taken in order to verify the code used to generate the loading diagrams. First, the code was debugged to make sure there were no syntax errors. After this, the results are verified by comparing them to hand calculations as well as an online interpreter[2]. These calculations match and therefore the code can be considered verified.

Fuselage sizing   The MATLAB code is verified by different means. As coding progressed debugging is done on a regular basis. Once all the coding is done, the boom locations, areas and moments of inertia of the whole idealised cross-section are tested against example 22.1 from Megson [56]. Then the shear stress and normal stress are tested against example 22.2 from Megson [56]. For both, the MATLAB results are the same as the results in the book. Therefore, those functions in the code are verified. The crippling stress function is tested against example 1, page 441 [63], here the results are within a reasonable margin. The discrepancy occurred due to the necessity of line approximation in MATLAB code. Skin buckling and stresses due to pressurisation are verified by testing different inputs, limits and later comparing them to manual calculations. Skin buckling is within the margin due to another line approximation. Stresses due to pressurisation are the same, when calculated in MATLAB and when calculated by hand. Therefore, the code is verified.

Wing sizing   For the verification of the wing sizing calculations the MATLAB code used is verified in several ways throughout the whole process. For the loading diagrams manual calculations were done to verify that the total wing loading equals the aircraft's weight with load factors added. Also several manual calculations are performed to approximate the torsion and shear loads at fixed locations and see if the results are close the values given by the MATLAB program. For bending loads manual calculations were performed on a highly simplified wing box, approximated as a square box with a boom at each corner. In this way also shear flow calculations have been verified. Furthermore, the MATLAB program which calculates shear flow from boom locations and sizes is applied to examples from Megson [56] to verify its outputs. With matching results in all above examples the code is considered verified.

7.4.2. Validation

This section contains the validation of the loading diagrams, fuselage and wing sizing respectively.

Loading diagrams   Several aspects of the results can be used to prove the validity of the program. For example, it is known that free ends of a structure do not carry loads. Since this is also reflected in the outcome of the program, the program is considered to be validated.

Fuselage   To validate the results of fuselage sizing building a prototype is recommended. First, a scaled model should be built and tested, when small-scale model passes all the tests and experiments, the actual size model should be built and tested (only the fuselage). Once the second model passes all the tests, the assembly can be made and tested.

Wing sizing   For validation of the design it is recommended to build the wing box structure and then apply the in flight loads to it. Stresses at several locations can then be measured using strain gauges and the calculations can be validated. This should be done during a later stage of the design process.

---

[2]SkyCiv Cloud Engineering Software, `https://platform.skyciv.com/login`, first accessed on 07-06-2018

7.5. Sensitivity Analysis

In this section sensitivity analysis will be presented. First the analysis will be performed for the fuselage and thereafter the same will be done for the wing.

7.5.1. Sensitivity of the Material Selection

Sensitivity for a 20% increase of the fuel price is shown in Table 7.1. The column shows the effect on the return on investment in months. A contingency of 20% decrease in machining speeds has been implemented in the second evaluation. The influence on the extra machining costs can be found in Table 7.2. This value is in millions of Euros.

7.5.2. Fuselage Sensitivity Analysis

The primary focus for the fuselage sizing is weight, so using fewer stringers is better for weight optimisation. Since the dominant inputs are loads, the different load cases will be checked. In Table 7.6 the sensitivity for different loads is presented. The skin thickness is kept constant at 1.5 mm. One needs to bear in mind that one boom is equal to the one stringer and skin around the stringer. One surprising thing is the lower number of stringers at higher load. This is due to the fact that booms, located at the line of action of the shear force, are not carrying any shear flow. Therefore at 20% extra load there are only 54 booms that actually carry shear flow and 2 ineffective booms. This issue arises from the initial positioning of the booms, with the first boom being at the top of the fuselage. One can also see that the normal and shear stresses are proportional to the load, but still below the allowable design loads, which is an expected result. Since skin thickness was held constant, shear stress carried by structure was the closest to the allowable design loads. The cross-section with the largest number of stringers needs to be expanded from 0.2 m from the baseline load case to almost 1 m in the +30% load case.

7.5.3. Wing Sensitivity Analysis

For the sensitivity analysis of the wing it was determined what the change in loads would do the structure of the wing. Mainly, how much extra or less material is needed when the loads increase or decrease. Since at the root, normal stress due to the applied moment is the critical design factor it is determined how much extra or less area away from the neutral axis is needed when the loads are changed. This increase in area is directly related to weight. From Equation 7.5 it can be seen that when the stresses should remain below the yield stress and the bending loads (given as M_y) are increased the increase in moment of inertia necessary can be calculated. Moments of inertia are most efficiently increased by adding material at the locations furthest away from the neutral axis. The results from this analysis are given in Table 7.7.

Table 7.6: *Sensitivity analysis for fuselage loads.*

Diff [%]	σ_{max} [MPa]	σ_{min} [MPa]	τ_{max} [MPa]	t_{skin} [mm]	$n_{stringers}$ [-]
+30%	196	−162.00	134.95	1.5	55
+20%	169.23	−135.36	134.93	1.5	56
+10%	174.87	−141.01	126.46	1.5	54
Base	162.92	−129.28	132.62	1.5	53
−10%	147.3	−113.07	123.88	1.5	52
−20%	136.34	−102.67	118.44	1.5	51
−30%	118.65	−84.96	108.2	1.5	49

Table 7.7: *Sensitivity analysis wing.*

Bending moment change	Change in area
+30%	+28%
+20%	+18%
+10%	+9%
0%	0%
−10%	−9%
−20%	−18%
−30%	−28%

8

Production Plan

In this chapter, the production of the aircraft will be set up. First manufacturing techniques for several metal parts of the aircraft will be discussed in Section 8.1, with a focus on the wing. Then a manufacturing process will be selected for a typical composite part, the ailerons in Section 8.2. Finally the manufacturing sequence of all components of the aircraft will be shown in Section 8.3.

8.1. Manufacturing Processes for Metal Components

In this section, manufacturing processes for the metal components of the aircraft will be studied. In this stage of the project, the focus will be on the wing, since it includes most of the representative parts are present in the other manufacturing divisions. First the manufacturing properties of the main metal used will be studied, then manufacturing processes for the stiffeners as well as the ribs are discussed.

8.1.1. Manufacturing properties of Al-Li 8090

In this section the manufacturing properties of the main metal used, Al-Li 8090 will be studied in order to be able to select proper manufacturing processes for all different metal parts.

Table 8.1: *Processing properties of Al-Li 8090 [25].*

Process type	Suitability	Typical processes
Casting	Suitable	Sand-casting, die-casting
Cold forming	Acceptable	Bending, stretching
Press-forming	Suitable	Rubber forming
Hot forming	Excellent	Extrusion
Weldability	Excellent	Point welding, line welding

Five types of manufacturing processes are discussed. In casting, a molten metal is poured into a mold which contains a hollow cavity of the desired shape, then it is cooled down and separated of the mold. This process allows for complex shapes. In the next process, forming, permanent deformation is introduced by grain dislocation by applying external forces. This process can also be done at high temperatures to lower the forces required, however, this disrupts the treatment of the alloy. The welding process joins parts by melting their surface and press them together while cooling down. The suitability of Al-Li 8090 to each of these methods is given in Table 8.1.

Table 8.2: *Different separating processes for sheet metal.*

	Laser	Water jet	Machining	Sheet metal cutting	Punching
Equipment cost	−− expensive	−− expensive	−− expensive	+ medium	+ medium
Mold cost	+ low	+ low	+ low	++ none	− medium
Quality	++ high	+ medium	+ medium	− low	+ medium
Complexity	+ 2D, high	+ 2D, high	++ 3D, high	−− 2D, low	+ medium

Besides the manufacturing processes themselves, pre-processes and post-processes are needed, such as separating processes and joining methods. For now, only pre-processing methods will be discussed. Four different post-processing methods are compared in Table 8.2. Labour cost as well as raw material cost were left out of the trade-off since they were similar for all methods. No trade-off can be made yet, since the relative weight of each criteria is part dependent.

8.1.2. Manufacturing Process of Stringers

In this section the manufacturing processes for stringers will be studied more in detail. There are two types of stringers present in the wing box: Z-stringers and hat-stringers. There are a few main factors to take into account for producing stringers.

Batch size   About 53 stringers are needed per aircraft for the fuselage alone, so the production process must be able to handle relatively large batch sizes.

Shape: The parts are simple: thin-walled beams without taper, with a continuous cross-section. The tolerances are average (in the order of ± 0.1 mm).

Adaptability   Even though many stringers are needed, there will be some variation. For instance, the Z stringers from the fuselage are going to have different dimensions as those from the wing. A manufacturing technique that can be easily adapted for the different beams with low additional tooling cost is preferred.

Production cost   The last factor taken into account is the production cost per unit, this includes labour, tooling cost and the raw material cost, which may differ per process due to the form it is in or the amount of waste.

There are a few different methods that are able to achieve this shape: extrusion, deep-drawing, superplastic deformation and bending, they are evaluated below based on J. Sinke [85].

Extrusion   This technique is able to produce large batch sizes, and is well adapted for constant cross-section beams. However, it becomes expensive quickly when lots of different cross-sections are needed, even if they have the same shape but different sizes. Therefore, it is not sufficiently adaptable.

Deep drawing   Deep drawing is a much used process since it allows a large number of different products. However this process has a really high equipment cost and is therefore only suitable for really large batch sizes, therefore not well adapted for this case.

Superplastic deformation   This type of permanent deformation only occurs in very specific conditions, leading to only grain boundary sliding without changing the shape of the grains. This is therefore a very expensive and time-consuming process. This process is eliminated due to complexity and cost.

Bending   This is one of the most common and simple processes for simple prismatic elements. The equipment cost is relatively low since the equipment used are more or less universal machines. The cost for different sizes of the same cross section is negligible, since the same die can be used when the angle remains the same.

From this, it can be concluded that bending is the best process to produce the stringers, since the material cost is low and is well adapted for many different sizes and shapes.

8.1.3. Manufacturing Processes of Ribs

Next, the ribs will be analysed. The ribs have not been designed in detail yet, however, it can be safely assumed that the ribs are metal, thin-walled and usually with many holes for equipment and weight saving. Usually the borders of the holes are bent out-of-plane for stiffness.

Batch size   Since each rib has a different size, thus only 600 of each rib need to be produced over the course of 15 years,therefore the batch sizes are relatively small.

Shape   The ribs are more complex compared to stringers, because they are curved and with many holes. The tolerances are average (in the order of ± 0.1 mm).

Adaptability   Since each rib of the wing has a different size, a manufacturing technique that can be easily adapted for the different beams with low additional tooling cost is preferred.

Production cost   The last factor taken into account is production cost per unit. This includes labour, tooling cost and the raw material cost, which may differ per process due to the form it is in or the amount of waste.

The following methods can be used to achieve the desired shape: rubber forming, milling and casting. These will be compared based on [85]

Milling   Milling allows for a high amount of complexity, even in 3D. The right shape for each rib is directly achievable without any pre-processing, and the mold or programming cost is low. However milling ribs requires quite some handling since it will have to be clamped twice, and thus must be outlined very accurately the second time. Therefore this process is both expensive in equipment, and in labour. Furthermore, it creates a lot of waste.

Casting   There are two main types of casting processes, reusable and non reusable mold casting. Due to the high cost of the mold, reusable mold casting is only well adapted for series larger that 1000 units. In the perishable mold category, sand casting can be immediately eliminated due to the too high minimal product thickness (3 mm for aluminium). This leaves investment casting, this process has low to moderate mould cost, however, it has high labour cost.

Rubber forming   Rubber forming is a press forming process involving two tools: a rigid tool and a soft tool. The rigid tool is shaped for the particular geometry of the piece. The soft tool is a universal rubber tool that forces the sheet in or over the rigid tool by pressure. About 50% of parts in the aerospace industry are made using rubber forming due to the low tooling cost and simplicity of the process. However the long cycle time, in the order of a few minutes, could be a disadvantage

To conclude, since on average 40 sets of ribs need to be produced a year, the simplicity and low costs of the rubber forming process outweigh the long cycle cost. Therefore rubber forming is chosen to produce the ribs.

8.2. Manufacturing Processes for Composite Components

In this section, manufacturing processes for composite parts will be analysed. Focus will be on the ailerons, but the methods and techniques discussed here can be easily extrapolated to other high-lift devices and control surfaces such as the elevator or the rudder. First, general manufacturing techniques for carbon fibre reinforced polymers will be discussed, then the production process for the ailerons will be described in detail.

8.2.1. Manufacturing Techniques for Carbon Fibre Reinforced Polymers

The first step to select the right manufacturing technique is to study the strengths and weaknesses of different processes for Carbon Fibre Reinforced Polymers (CFRP). Six different methods will be compared: pulltrusion, filament winding, hand-layup, infusion, prepreg lay-up, and tape-laying. A comparison based on 5 different criteria can be found in Table 8.3

Table 8.3: *Manufacturing processes for long fibre carbon reinforced polymers.*

	Batch size	Labour cost	Machining cost	Material cost	Finish
Pulltrusion	larger	+ low	−− pulltrusion machine	++ lower	−−
Filament winding	larger	+ low	− mold and filament winder	++ lower	−
Hand lay-up	small	− high	+ mold and vacuum pump	0 lower	−
Infusion	medium	− high	+ mold and vacuum pump	0 medium	+ smooth
Prepreg	small	−− very high	+ mold and vacuum pump	− high	+ smooth
Tape-laying	small	+ low	−− mold, pump and machine	− high	+ smooth

The first technique is pulltrusion. This is a process that is a bit similar to extrusion. First the fibres are wind on spools, than the are impregnated with resin and then pulled trough a hot die, curing the product and

fixing its shape. The product now needs to be cut in pieces. This produces constant cross-section beams, with continuous fibres[1].

Filament winding is a technique that is mainly used to manufacture both open and closed cylinder-like structures such as pressure vessels. This process involves winding filaments impregnated in a bath with resin under tension over a rotating mold, laying down fibres in the desired pattern or angle. The resulting product can then be cured in a vacuum-bag, at room temperature or in a autoclave or oven.

Next, hand lay-up is the simplest technique for CFRP, involving laying pieces of woven of braided carbon-fibre fabric on a mold. After each layer, the resin is brushed on manually in order to impregnate the fibres, before being put in a vacuum-bag and cured, either at room temperature, in an oven or in an autoclave. The production rate is usually slow, since it involved large amounts of hand-labour, however the equipment investment required is minimal so is well adapted for small batch sizes.

For infusion, like hand lay-up, pieces of woven or braided carbonfibre fabric are laid dry a mold. Then a vacuum mold is build around it, and the space between the bag and mold is emptied of air. Once all the air has been removed from the bag, liquid epoxy resin is introduced to the bag through a pipe which then infuses through the fibres. After the product is fully infused, the supply of resin is cut off (using a pipe clamp) and the resin is left to cure, still under vacuum pressure at room temperature. Sometimes a post-cure is needed in an oven or autoclave to change the resin properties, such as to increase the glass transition temperature.

Prepegs are fabrics of carbon fibres that are pre-impregnated with resin. These fabrics are sticky on one side, and are carefully stuck on a mold, checking that there are no bubbles or airgaps between layers. This method allows for a higher fibre-to-resin concentration compared to previous methods, yielding usually lighter structures. However, the rolls of prepregs are very expensive and the technique is very labour intensive.

8.2.2. Manufacturing Process for Ailerons
The selection process for the aileron is representative for most of the control surfaces and high-lift devices, and will be discussed in thos section

Batch size   For each aircraft, there are four different parts for the ailerons, two on each side. It is expected to sell 600 aircraft over the course of 15 years, therefore the batch sizes will be quite small. It is therefore probably not interesting to invest in expensive machinery.

Surface finish   As for all aerodynamic components, surface finish is an important criteria, especially at the leading edge, which is also the best location for a mold line. However, since the leading edge of the aileron is not exposed, the possibility of flashlines is not really an issue.

Shape   The cross-section of the ailerons is not constant, they are treated as a tapered beam. No double curvature is present.

First, the pulltrusion process is eliminated since it is impossible to make tapered beams using this process. Next, tape laying is eliminated for being too expensive. Furthermore, filament winding is not well adapted to the desired shape. For more complex shapes, the filament speed and angle control becomes too complex to predict accurately, and leads to a decrease in quality.

The three procedures that are left are hand-layup, infusion and prepregs. Prepregs are by far more expensive, due to raw materials and labour costs, while scoring similarly on all other criteria. Therefore this process is eliminated. Between hand lay-up and infusion, infusion is slightly more expensive due to the fact that more consumables are needed. However this process is faster, and better suited for our batch size and allows for a more consistent product. Therefore, the ailerons will be made using infusion.

8.3. Manufacturing Sequence
After producing all the parts, it is time to assemble the aircraft. In order to achieve this, it is important to decide on the manufacturing sequence. The preliminary manufacturing sequence is presented in Figure 8.1. In this figure, one can see that the aircraft is composed of four main components from least complex to assemble, the engines, to the tail, the fuselage, and finally the most complex, the wings. It is desired to have equally sized work packages in order to limit waiting times and the risk for delays.

First, the engines are really simple to manufacture, since they will be delivered assembled, including the nacelles.

---

[1]The Pulltrusion Process, bedford reinforced plastics, retrieved from `https://bedfordreinforced.com/the-pultrusion-process/` accessed on 22-06-18

Next the tail is more complex, since it involves moving parts. From the figure, it is clear that there are many steps that can be performed in parallel. Furthermore, the steps of the horizontal tail and vertical tail are similar, so the work packages that will be performed at the same time will all be of the same size. Therefore, the tail is an element that can be paralised well.

The next element in order of complexity is the fuselage. The fuselage can be subdivided in four main components from rear to front: the cone, the tube, the flight deck and the randome. Contrary to the tail, these elements are not as well balanced, since they are not as similar.

Finally the most complex part, the wing. The wing is composed of many subsystems itself. The work packages are difficult to balance. Building one wingbox, including making all the ribs, stringers and including the fuel tanks more time consuming than making the ailerons. In a next stage the wing has to be investigated into further detail in order to limit waiting times and delays as much as possible.
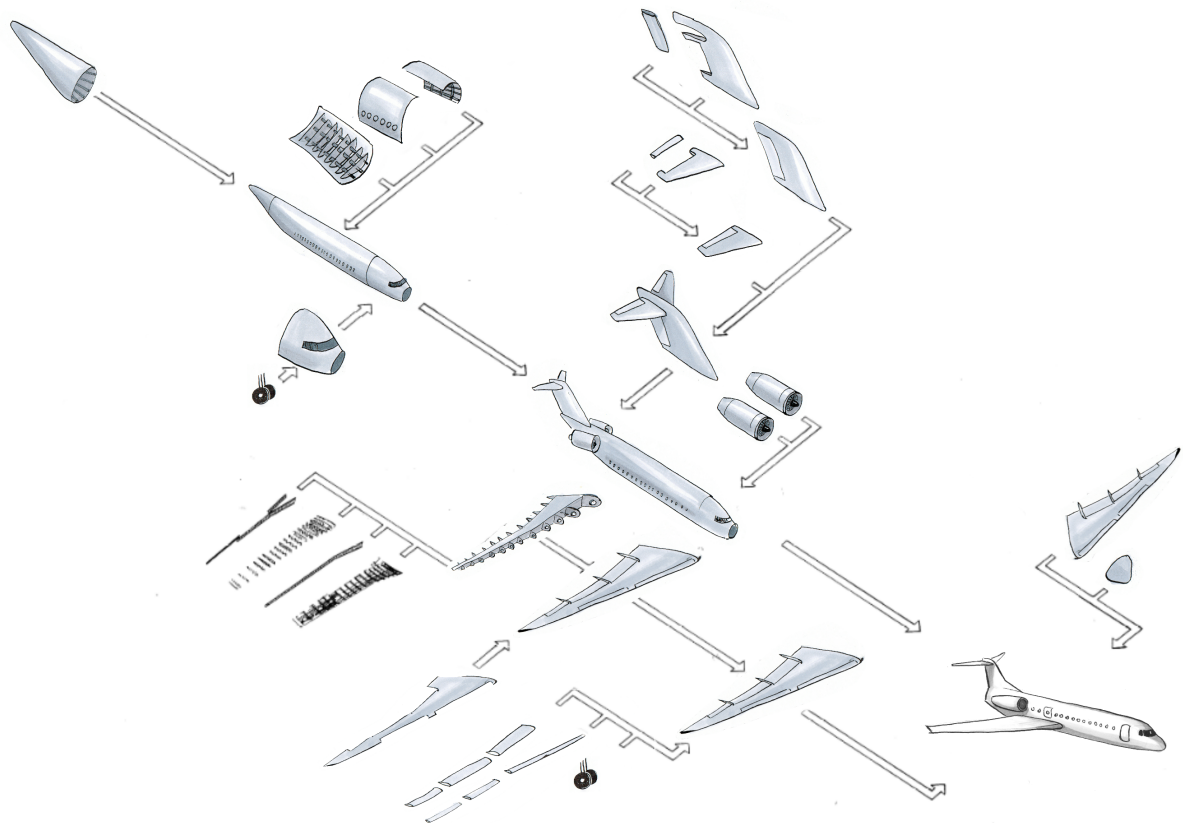
Figure 8.1: *Manufacturing sequence.*

9

Operations & Logistics

The operations and logistics (O&L) of the aircraft can be mainly subdivided into flight operations, ground operations and logistics and maintenance scheduling and logistics. The flight operations are described in the Flight Performance chapter, which is Chapter 4. The other two major components will be analysed in this chapter. In Section 9.1 the ground O&L will be analysed in detail and in Section 9.2 the maintenance scheduling and logistics will be studied.

9.1. Ground Operations & Logistics

The ground operations and logistics are analysed and evaluated through the turnaround time (TAT). The TAT is determined by the time spent on the ground to perform all necessary aircraft operations. These operational activities include the completion of a cycle, such as passengers disembarking, and the preparation of the new cycle, such as refuelling. A shorter TAT means a shorter flight cycle, which translates to a decrease in total operational costs per cycle and less non-revenue-making time. Therefore, it is essential to reduce the TAT as much as possible. This is done by selecting time-efficient operation methodologies and equipment, as well as perform as many operational actions at the same time as possible.

Firstly, The TAT is analysed and the outcome is displayed by using a Program Evaluation and Review Technique (PERT) model. This model is essential to determine the most time-consuming path, which is called the critical path. By knowing this operational path, an evaluation of the critical steps can be made such that the TAT and delays can be further minimised. After the most optimal ground operations and logistics in terms of costs and time are identified, a Gantt chart of all the turnaround operations is shown. This contains a detailed plan of action of the ground operations.

9.1.1. PERT Model

The PERT model is used to determine the critical path in the ground operations. The resulting model after the performed operational analysis can be found in Figure 9.1. The circled numbers are the main operational actions during turnaround and each line path represents an action line path. Each path is performed independently from each other, but it does not imply that all the paths can be performed at the same time. The actions that the circled numbers are related to are shown in Table 9.1. Furthermore, the earliest start (ES), the latest start (LS), the earliest completion (EC), the latest completion (LC) and the slack of each action are shown in Table 9.1. These are also displayed in the PERT model in the four spaced boxes.

Critical path   The most critical path follows the action succession 1-2-7-10-11-12 and it takes 27.5 minutes when no delays are present. This can be seen in Figure 9.1 by following the thick-circled actions. Important to consider is the fact that the EC of actions 4 and 7 are at the same time, which means that they both represent the critical path. Depending on which action finishes first, the latest completed action becomes part of the critical path. A total slack time of 9 minutes was found for maximum delays [38].

Operation actions time estimation   The time that each action of the ground operations takes is based on the analysis performed by Gok [38]. On the other hand, some actions have different completion time depending on which equipment is used and in which method the action is performed. For these operations, further analysis is performed to determine the most optimal option in terms of time and costs. These operations are identified to be embarking and luggage loading and unloading. Some remarks are also made about fuelling and the use of an electric push-back.

Table 9.1: *Activities in the PERT model [38].*

	Activity	Time [min]	ES	EC	LS	LC	Slack
1	Chocks on	1	0	0	1	1	0
2	Passenger disembarking	3.5	1	4.5	1	5.5	1
3	Routine maintenance checks	10	4.5	14.5	5.5	15.5	0
4	Fuelling	6	4.5	10.5	5.5	13.5	2
5	Luggage unloading	2.75	1	3.75	3	6	2.25
6	Luggage loading	3.75	3.75	7.5	6	9.75	0
7	Cleaning and water service	6	4.5	10.5	5.5	13.5	2
8	Catering unloading	1	4.5	5.5	5.5	7.5	1
9	Catering loading	1	5.5	6.5	7.5	9.5	1
10	Passenger embarking	11	10.5	21.5	13.5	29.5	5
11	Flight OPS and procedures	5	21.5	26.5	29.5	34.5	0
12	Chocks off	1	26.5	27.5	34.5	36.5	1
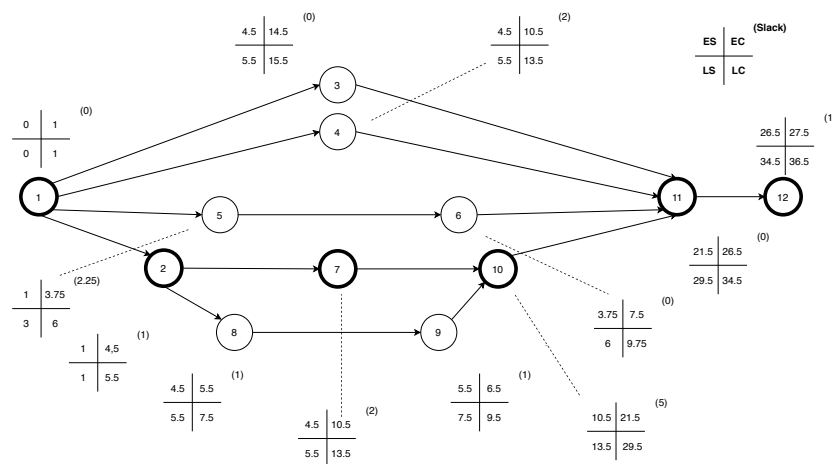
Figure 9.1: *PERT model for ground operations.*

9.1.2. Embarking

Embarking is considered to be one of the most time-consuming actions when the aircraft is on the ground. Therefore, different types of boarding are considered in order to determine the optimal one in terms of time. In addition, the presence of hand luggage in the cabin has an impact on the boarding time. Two other aspects of the boarding procedures that are considered are the aircraft chair type and the platform type to get in and out of the aircraft. The different options are shown in Figure 9.2.
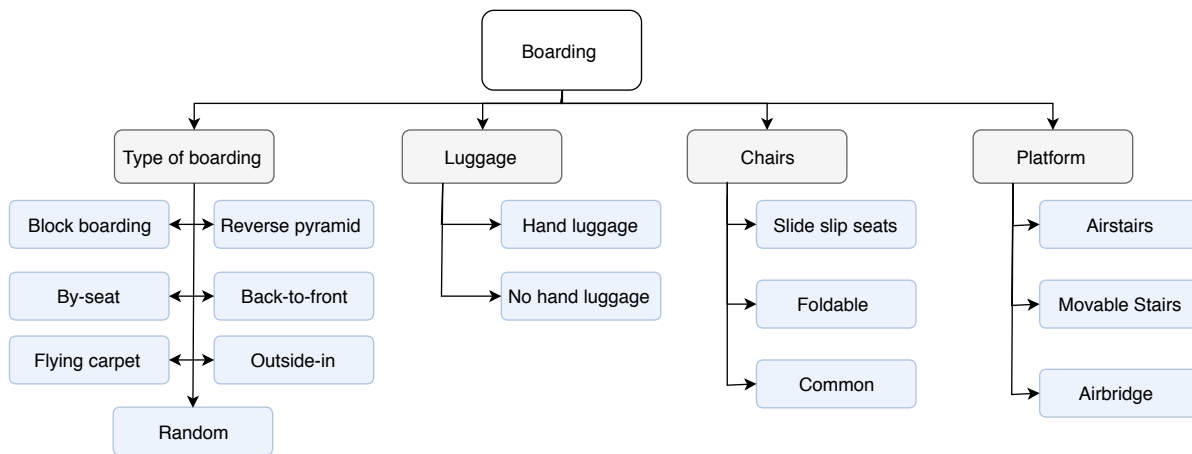
Figure 9.2: *Different options for boarding.*

The type of boarding depends heavily on the loading platform, which will be discussed first. The type of chairs present in the plane will be discussed after that, followed by the presence of hand luggage. Finally the different types of boarding will discussed and an advisement for the aircraft operator will be given.

Platform   For the embarkment and disembarkment of the passengers, three types of loading platforms can be used: airbridges, movable stairs and airstairs. The decision on which one to use depends on the aircraft operator, but an analysis is performed to identify the optimal platform to minimise operational costs and decrease TAT.

Airbridges are the most convenient loading platforms considering passenger comfort. Walking to the plane or a bus service is not necessary and head count is not needed. However, in terms of operational costs, airbridges are the most expensive and take the longest time to connect to the aircraft. Besides that, airbridges can cause damage to the aircraft which decreases the maintenance intervals. Also the airbridge might not even be capable of connecting to a low aircraft. Because regional airports do not necessarily have bridges, this option is not used.

Movable stairs are available at most regional airports. They are cheaper in use than airbridges, but are not faster in terms of connecting and have the same risk of causing damage. Delays may occur if stairs are not present or used for other aircraft.

Airstairs are built-in stairs in the door of the aircraft. Positioning them does not take much time and due to the short height of the plane they can be easily implemented on the door of the plane. Airstairs have the disadvantage that they add weight to the plane. However, because of their small size this would only be an extra weight of 65 kg [20]. The stairs increases 0.06% of the Direct Operating Cost (8 USD per trip) but are still much cheaper than the movable stairs or airbridges, which commonly cost about 20 and 110 USD respectively [20]. On the other hand, depending on where the aircraft is parked, people would need to walk to the aircraft or use a bus service, which could cost time and money. Considering though that the airstairs need only 30 seconds to get ready to be used and to put them back, they need a decrease of 3 minutes in the TAT, which is about 10% less than the total TAT. Due to the lower cost and shorter turnaround time, airstairs are selected.

Chairs   The three types of chairs are shown in Figure 9.3. Side slip seats are only available for a 3 chairs seating configuration, which means that they are not applicable on the $MW5$. Furthermore, foldable chairs could be advantageous for a 2 seat configuration but the advantages are not that big that it makes sense to implement them. Therefore, conventional seats are advised to be the best seating option.

Luggage   Having passengers without any hand-luggage in the cabin could drastically decrease the embarking time to 3.5 minutes [19]. Although this seems optimal, the solution is not favoured for the sake of passenger comfort. Also, the time to load the luggage as cargo would strongly increase. Therefore, an aircraft without luggage in the cabin is not an option that is explored.

Boarding Types   The type of boarding has the most impact on the time to board. All the different methodologies are discussed and subsequently analysed to identify the optimal boarding type. Boarding types are

(a) *Side slip seat.*

(c) *Conventional seat.*

(b) *Foldable chair type.*
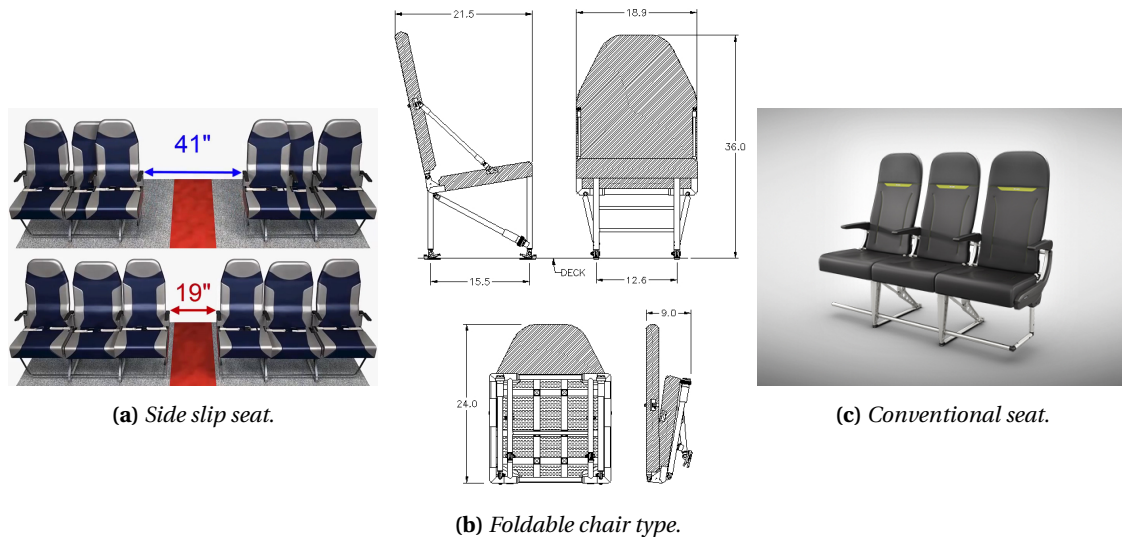
Figure 9.3: *Different types of seats.*

decided by the aircraft operators but an analysis with recommending purpose is performed. All these methods were studied by Van den Briel [41] and the times to embark were adapted to 76 passengers. The resulting embarking time per type can be seen in Table 9.2. The values in the table are without considering the type of platform used.

- **Back-to-front:** all the seats are filled from the back to the front, but there is no difference made between window or aisle seats.
- **Outside-in:** with this method the passengers are boarding in columns, meaning first all the window seats are filled and after that all the aisle seats.
- **Block boarding:** this is basically the same method as the outside-in method, but it is subdivided into zones, where the zones are ordered back to front.
- **By-seat:** this method calls each passenger per seat. For larger aircraft, this is a time consuming and unfeasible strategy.
- **Flying carpet:** this is a new method in which the passengers stand on a numbered carpet according to their seat number; after this, the back located seats are allowed to enter first.
- **Random:** this boarding method does not have a particular order in which the passengers can embark the aircraft.
- **Reverse pyramid:** this method is the combination of outside-in and back to front boarding.

Table 9.2: *Embarking time of 76 passengers for each boarding methodology [41].*

Method	Time [min]
Back-to-front	15
Outside-in	9
Block	11
By-seat	5
Flying carpet	5
Random	11
Reverse pyramid	9

Back-to-front boarding is not advised as it is the slowest. Even though they are quick embarking types, reverse pyramid and by-seat are also not advised as they are complex methods. This leads to high delay susceptibility, which would potentially make the embarking procedure longer than other simpler methods. The flying carpet has been studied to be potentially the fastest embarking methodology, but this would only be advantageous if an airbridge would be used, which was discussed to be generally not available at the targeted airports. For this reason, only block, random and outside-in are the embarking types that are considered most optimal.

For the PERT model analysis, the random embarking methodology was taken as it is the most commonly used, and it was calculated to take about 11 minutes to embark 76 passengers. If an outside-in embarking method would be used, 2 minutes could be potentially saved from the total turnaround time. The downside of this method is that people travelling together might board at different times, which may be not the preferred solution.

Regarding disembarking, 2 seconds per passenger are needed for the procedure [38]. For this reason, 2.5 minutes are needed to disembark all the passengers if no issue occurs. In case that it goes slower, 3 seconds per passenger are taken into account.

9.1.3. Cargo Loading & Unloading

Cargo loading and unloading is an operational activity that may be part of the critical path, depending on how much luggage needs to be handled and how fast these are done. The currently available methods are:

- No conveyors;
- Classic belt loader;
- Ramp snake;
- Power stow;
- Sliding carpet.

Considering regional airports, ramp snakes and sliding carpets are predominantly not available. The "no conveyor" solution is not advised, unless it is the only possibility, as it is not favourable for workers. Lastly, the classic belt loader and the power stow are left. These are both usually available in regional airports and can be utilised depending on the preference of the operator. The normal belt loader is able to load one bag every 10 seconds, while the power stow one every 7 seconds [89]. Considering that the power stow is easily and quickly put in place, the time advantage of the power stow is significant. For this reason, the power stow is advised and used for the TAT analysis. Assuming that normally 25% of the passengers bring checked luggage for short regional flights, about 20 luggage pieces need to be loaded and unloaded each cycle. This results in 2.5 minutes to load and 1.5 minutes to unload, as 5 seconds per luggage piece are needed for the latter.

9.1.4. Fuelling

For fuelling during the ground operations several assumptions are made. As most regional airports have different facilities to fuel an aircraft, a worst-case scenario was made. It is assumed that on regional airports, tank trucks which are capable of refuelling at a rate of 1100 l/min are present. An estimate of 5000 kg of fuel is needed, which is approximately 6350 l; it then takes 5.8 minutes to fill the tanks. Because the valve needs to be attached and detached, the fuelling time is rounded up to 6 minutes. At bigger airports, fuel trucks or even build-in fuel stations are capable of fuelling at a much higher rate. This will also mean that the fuel time will be much lower for those cases. Finally, fuelling is crucial when considering the critical path. In fact, passengers are not allowed to embark or disembark while this procedure is done, due to safety reasons. If fuelling takes many minutes, it may become part of the critical path and increase the total TAT. For this reason, the faster the refuelling rate the better it is.

9.1.5. Electric Push-back

An electric push-back was selected to be mounted on the aircraft. This system will increase the aircraft weight of 100 kg, which will translate to about an additional 15 USD/trip . By adding around 5 USD/trip due to depreciation and maintenance, the total costs to use the electric push-back system is still cheaper than using the aircraft equipment, which normally amounts to 172 USD/trip [20]. Furthermore, the system is not susceptible to delays. In terms of TAT, the electric push-back saves about 2 minutes compared to the conventional method [20].

9.1.6. Gantt Chart

The detailed action plan of all the ground operations are shown in the Gantt chart displayed in Figure 9.4. The Gantt chart also gives the overview at what order the actions should be performed.

As normally regional aircraft take 30 minutes for their TAT [38], the $MW5$ is 2.5 minutes faster with the selected O&L. This represents an 8.33% decrease. Furthermore, 2 minutes are saved for push-back, which is another 6% decrease with respect to other aircraft.
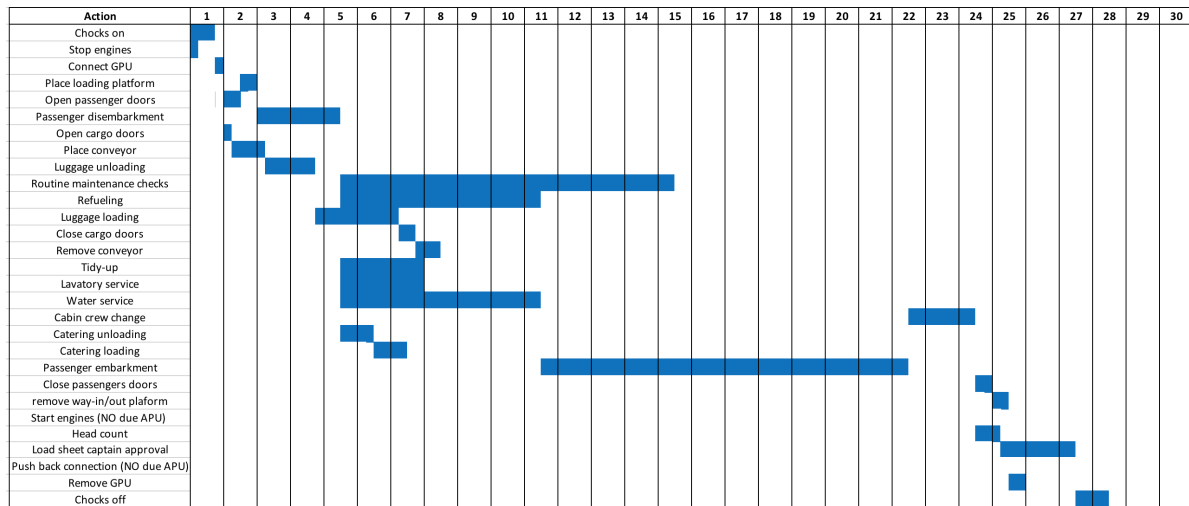
Figure 9.4: *Gantt chart for the ground operations.*

9.2. Maintenance

The final main element of the operations and logistics of the design is maintenance scheduling and logistics. Maintenance strategies and scheduling will be elaborated upon in this section.

9.2.1. Maintenance Definitions

Two types of maintenance have to be conducted by the airliner or operator of the aircraft: scheduled and unscheduled maintenance. Scheduled maintenance consists of:

- En-route servicing
- Terminating pre-flight checks
- Service checks
- Maintenance checks (A, B, C, D)

Besides scheduled maintenance, there is also unscheduled maintenance which is defined in the ATA-100 specification as:

> *Those maintenance checks and inspections on the aircraft, its systems and units which are dictated by special or unusual conditions which are not related to the time limits specified. Includes inspections and checks such as hard landing, overweight landing, bird strike, turbulent air, lightning strike, slush ingestion, radioactive contamination, maintenance checks prior to engine-out ferry, etc.*

In order to reduce the maintenance cost, and hence the operational cost for the airline, the maintenance has to be performed as easily as possible. This is done by guaranteeing easy access to parts or subsystems which are prone to maintenance. In terms of downtime of the aircraft scheduled maintenance is always preferred over unscheduled maintenance.

The chosen logistical strategy is to regularly operate the aircraft at regional airports that have minimal technical support, only enabling routine checks, and to land at airports with appropriate maintenance facilities when other types of checks and maintenance are required. The operator is advised to combine this strategy with a commercial flight, such that the generated revenue is increased.

9.2.2. Maintenance Strategies

The three types maintenance that can be considered for airlines are corrective, preventive and predictive maintenance.

Corrective maintenance   Fixing or replacing components either when they have failed or when they are found to be failing. There are no interventions until a failure has occurred. The advantage of corrective maintenance is that the component lifetime is extended to the maximum potential. However, it also has some severe implications on safety and grouping of maintenance because 100% of the maintenance which has to be performed is unscheduled.

Preventive maintenance   Replacing or repairing components or systems before failure occurs. The advantage of preventive maintenance is that failures of critical systems and consequential damage as a result of failure of critical systems is reduced. The downside of preventive maintenance is that it is hard to determine the optimal moment for replacement of the part. Preventive replacement means that the full useful life of the part is not used, which increases the maintenance cost. Furthermore, early replacement may push a component back to the infant failure regime.

Predictive maintenance   Replacing or repairing components or systems based on determination of in-service equipment condition. Predictive maintenance allows for convenient scheduling and planning of maintenance and limits unexpected equipment failures. The drawback of predictive maintenance is that it requires dedicated monitoring systems and not all systems can be monitored.

9.2.3. Maintenance Planning
The scheduled maintenance is divided in different elements. The guidelines for the scheduled maintenance can be seen in Table 9.3. The initial estimates of the amount of flight hours between the checks are rather conservative to detect any flaws in the initial design, but the maintenance interval can be increased if the design turns out to be reliable. The description of the tasks in Table 9.3 are meant to provide a general idea of what is included in what check and is not conclusive. The C check can also be dephased in multiple checks if this is desired by the operator. The maintenance checks mentioned in Table 9.3, besides the pre-flight and after flight checks, need to be performed at airports which are provided with appropriate facilities.

Table 9.3: *Maintenance scheduling guidelines.*

Check	Interval	Description	Required man hours
Pre-flight	Before every flight	Visual inspection of the aircraft at the airport	0.5
A	Every 400 flight hours	Visual inspection of the structural elements of the aircraft, test electronic systems, test hydraulic actuators	50
B	Every 1200 flight hours	A check, including detailed check of components and systems	160
C	Every 2400 flight hours	A and B check, including inspection of the engine inlet and door seals	5000
D	Every 24,000 flight hours	A, B and C check, including complete overhaul of the aircraft	50,000

9.2.4. Accessibility
Because the fuselage is situated 1.4 m above the ground it is easily accessible from the ground for maintenance checks of the lower part of the fuselage. The low wing configuration also allows for easy accessibility for the wings from the ground without requiring any maintenance platforms.

Maintenance platforms are only required to provide accessibility to the upper side of the fuselage, the tail and the engines. The low required amount of maintenance platforms means that most of the maintenance activities can also be performed at workshops with limited facilities.

Aircraft Systems

In this chapter, the different systems in the aircraft will be described. First, the resource allocation will be discussed in Section 10.1, consisting of the mass budget and the power budget. Thereafter, in Section 10.2, the initial sizing of the landing gear covered and in Section 10.3 a description of the Auxiliary Power Unit is given. The hardware and software diagram, data handling block diagram and electrical block diagram can be found in Section 10.4, Section 10.5 and Section 10.6, respectively. The communication flow diagram is given in Section 10.7. Next, the hydraulic system description, fuel system description can be found in Section 10.9 and Section 10.10, respectively. Finally, the chapter concludes with a section about the safety characteristics of the aircraft.

10.1. Resource Allocation

In this section, the mass budget and power budget will be introduced. Since this is still preliminary design phase there is contingency factor of 10% included in the budget allocation. First, mass budget is be presented in Subsection 10.1.1. Next, the power allocation is shown in Subsection 10.1.2.

10.1.1. Mass budget

For mass budget, the results from Class-II weight estimation are used. The contingency factor of 10% to account for future growth or shrinkage will give the maximum and minimum values for the final weight of particular subsystem. The results are presented in Table 10.1.

Table 10.1: *Mass budget.*

Subsystem	Mass [kg]	Mass, max. [kg]	Mass, min. [kg]
Wing	2414	2655	2172
Fuselage	3330	3663	2997
Empennage	1431	1574	1287
Landing gear	1197	1316	1077
Installed engines	2381	2619	2142
Systems	5160	5675	4644
Others	500	550	450
Total	$16,413$	$18,054$	$14,771$

10.1.2. Power budget

In Table 10.2 one can see the power budget. The reference for power budget is the McDonnell Douglas DC-10 [79]. However, some values need to be adjusted since the DC-10 is large aircraft produced 30 years ago. The passenger cabin lighting and galleys are scaled down for 76 passengers (from 380 passengers DC-10 has). The avionics are multiplied with a factor 2, hydraulics, flight control and electrical power are multiplied with a factor 1.5 to take into account the fact that more and more subsystems rely on electronics. The total power needed is 81,172 W, comparing it to 80,000 W CRJ700 can generate, the first estimation comes relatively close [18].

Table 10.2: *Power budget.*

Component	Power [W]	Power, max. [W]	Power, min. [W]
Exterior lighting	3850	4235	3465
Flight compartment lighting	2765	3041	2488
Galley	16,357	17,992	14,721
Windshield heating	6000	6600	5400
Avionics	14,800	16,280	13,320
Air conditioning	1600	1760	1440
Fuel	6500	7150	5850
Hydraulics	13,200	14,520	11,880
Flight control	4000	4400	3600
Electrical power (converted to DC)	11,850	13,035	10,665
Miscellaneous	250	275	225
Total	81,172	89,289	73,054

10.2. Landing Gear

This section covers the initial sizing of the landing gear and some design considerations with respect to the location of each of the wheels. First, the size of the wheels is determined as well as their location on the aircraft.

10.2.1. Wheel Sizing

In conceptual design the sizing of the landing gear wheels can be mostly based on statistical data. The method used is based on Raymer [75]. For the most-aft c.g. position the nose-wheels will typically carry most of the static load [75], which is 30.2 t. With four main wheels this will be 8 t per main wheel, from FAR 25 [34] a 7% margin should be added to the maximum load. Now equation Equation 10.1 [75] is used to determine the main wheels diameter and width. Coefficients A and B follow from statistical data and W represents the maximum static load.

$$\text{diameter/width} = A_{D/W} \times W^{B_{D/W}} \tag{10.1}$$

From Equation 10.1 it is found that the main wheels' diameters are approximately 0.79 m and their width is around 0.25 m. The nose gear carries a maximum of 15% of the weight [75]. For the nose gear a dynamic load from breaking also needs to be taken into account. The dynamic breaking load can be calculated using Equation 10.2 [75]. The maximum static load is represented by W, H is the aircraft c.g. height with respect to the ground which is as a first approximation assumed to be in the midpoint of the fuselage and B is the distance between the main and nose-wheels. To determine the values for H and B the location and height of the main landing gear need to be determined. These will be determined in the next subsection. Using those results and by calculating the maximum load on the nose-wheel, a nose-wheel diameter of 0.6 m with 0.14 m width is found to be required. This is 80% of the main wheel parameters which seems a reasonable first estimation for nose-wheel sizing [75]. For the selection of tires a tire book from the manufacturer can be requested. Then, the smallest tires that are able to carry the maximum loads are selected.

$$\text{dynamic load} = \frac{10 \times H \times W}{g \times B} \tag{10.2}$$

10.2.2. Landing Gear Location

When looking at Figure 10.1, a tip back angle is defined which is the maximum aircraft nose up attitude when the tail touches the ground. This angle should be anywhere in between 15% and 25-30% for most aft and most forward c.g. positions respectively. The most aft c.g. angle constraint is to make sure the aircraft will not tip back during operation while the most forward c.g. constraint angle is to make sure it is not to difficult to lift up the nose during take-off. From the tip back angle constraints and the known c.g. locations the location for the main landing gear can be constructed. A visual representation of this can be seen in Figure 10.1. The c.g. position during operation will be between 16.26 m to 16.95 m from the nose and during ground handling the c.g. can shift to a most aft position which is 17.54 m from the nose. The landing gear should be placed

such that during operation the most aft c.g. tip back angle is minimally 15° and the most forward c.g. tip back angle is maximally 30°. During ground handling (passenger embarking and cargo loading) the c.g. should stay in front of the landing gear so it does not tip back. The location of the nose-wheel can than be determined by assuming the nose-wheel carries less than 15% of the weight with the c.g. in the most forward position and more than 5% for the most aft position (this is important during operation for good nose-wheel traction). We then find the main gear is located 17.85 m from the nose of the aircraft and the nose-wheels are located at 2 m. The nose wheel then carries in between 6% to 10% of the aircraft weight during operation.
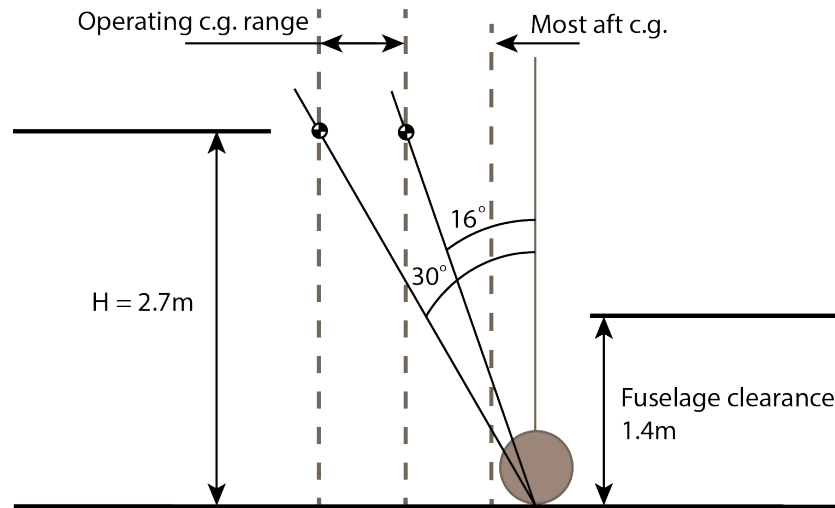
Figure 10.1: *Main landing gear location based on tip back.*

For determining the wheelbase the overturn angle is the main constraining factor. In Figure 10.2 [75] a visualisation is given of how to find the overturn angle. This angle should not exceed 63° [75], from which the static ground line can be calculated to be 1.38 m. Then the angle between the c.g., the nose-wheel and the main wheel can be calculated. This is found to be 4.5° giving a minimal wheel base of 2.82 m, meaning the wheel track is slightly wider than the fuselage diameter. For this reason the main wheels will be attached to the wing, aft of the wing box. The retracting system, struts, brakes and more will be designed in a later stage of the development. Based on the main wheel height and location it can be found that the lateral ground clearance is 7.4° which is more than the required 5° [34].
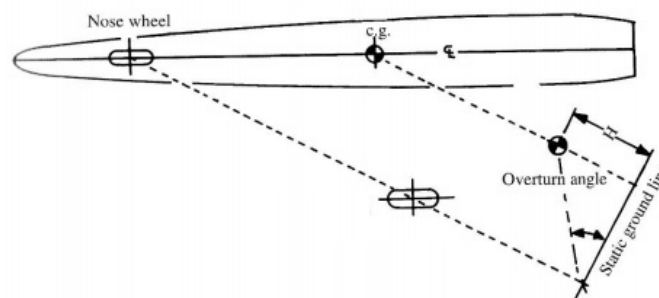
Figure 10.2: *Main landing gear location based on overturn angle.*

10.2.3. Electric Push-back
To minimise airport facility usage and, thus, reduce the turnaround time the WheelTug technology will be used. The WheelTug technology uses an electrical motor, installed in the main landing gear wheel, which allows for an independent push-back to the gate and back. The main drawback of the WheelTug is its added weight since a more powerful APU might be needed as well the motor weight itself. This adds up to roughly 100kg heavier OEW which corresponds to 15 USD/trip cost [20]. Another aspect one needs to think about is the small maintenance and the depreciation, which was estimated to cost around 5 USD/trip [20]. The main

advantage, however, is reduced total ground time, since no ground tug nor ground crew will be needed. An estimated 2 to 7 minutes [23] per flight can be saved using wheel tug, this translates to roughly 172 USD/trip saving [20].

10.3. Auxiliary Power Unit

The Auxiliary Power Unit (APU) is used to provide the aircraft with ground power for systems such as air conditioning, cabin lighting, cockpit avionics. This makes the aircraft independent of any ground power when no GPU is available. Also, the APU is used to start the engines on the ground, and in emergency situations can provide power for essential systems like hydraulics and cabin pressurisation. Because the APU is basically a jet engine, it requires an inlet as well as an outlet and due to high maintenance requirements it should be easily accessible. Often, the APU is located in the tail just below the vertical stabiliser and for the $MW5$ design this will be no different. When selecting an appropriate APU, power requirements need to be taken into account. For the specific $MW5$ regional jet design, another important factor is its weight and fuel consumption, which both impact the operating cost of the aircraft by impacting fuel consumption. As mentioned in Section 10.2 the $MW5$ design will be able to push back using an electric motor within the landing gear. This system draws power from the APU so for APU selection the added power requirement needs to be taken into account, though it is not possible at this moment to quantify this requirement.

10.4. Hardware and Software Diagrams

The hardware and software block diagram describes the relation between the various components of the system. The diagram has been divided into five hardware components, with names as displayed at the top of each block. Each hardware component is then subdivided into a greater number of smaller components, each called software blocks. The smallest components within each group are those that make up the software block and are required for it to perform as desired.
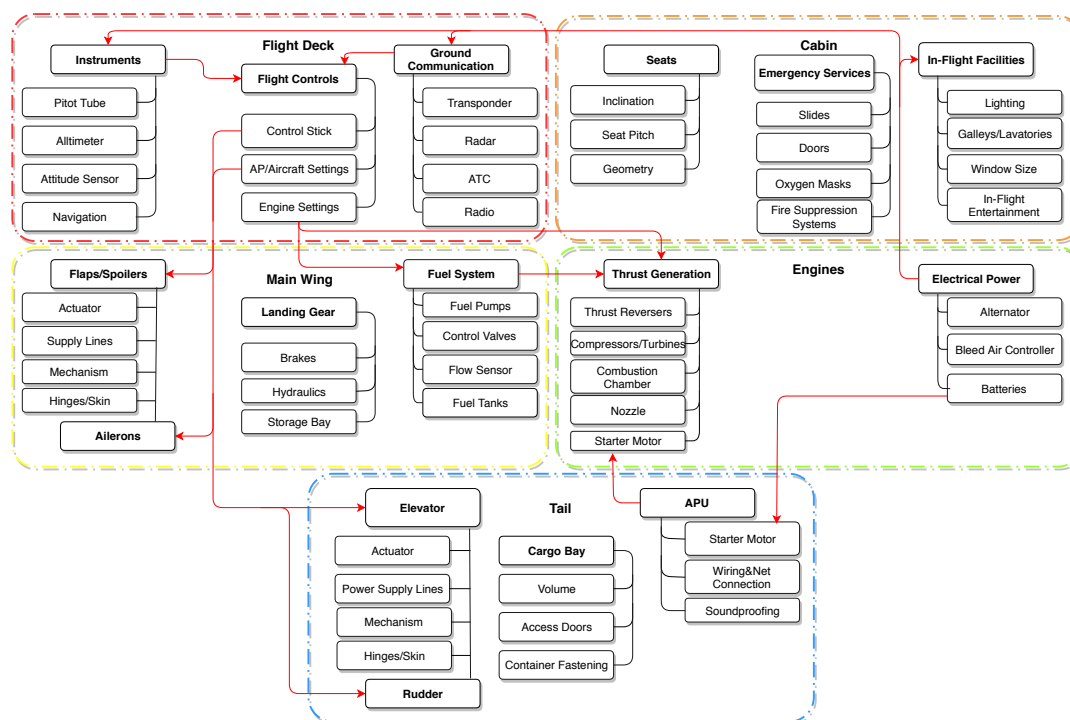
Figure 10.3: *Hardware and software block diagram.*

In Figure 10.3 observe that the five hardware components are marked with variously coloured dotted lines, with the name of the block shown at the top. The software blocks are shown within the dotted block, with their names shown in bold. Components of the software block are collected vertically, with names shown in regular font. Relations between individual hardware or software blocks are shown by means of red arrow

lines.

10.5. Data Handling Block Diagram

The data handling system of the aircraft consists of a lot of components, of which the primary flight computer is the most important one. The primary flight computer processes the data gathered by different sensors and subsystems and sends it to other components [8]. The data flows in the aircraft are shown in Figure 10.4.

Besides the primary flight computer, other important components are:

Flight Controls: The flight controls can be divided into primary flight controls and secondary flight controls. The primary flight controls are used to control the aircraft in pitch, roll and yaw, and are absolutely necessary to control the aircraft during flight. The secondary flight controls are primarily used to improve the flight characteristics during certain flight phases and manoeuvres [54]. The aircraft uses an electrical fly-by-wire control system, because this is lighter than a conventional manual flight control system. Input from the primary flight computer goes to the control column to provide the pilots with feedback. A stick shaker is also fitted into the control column, which shakes the control column when the aircraft is about to stall.

Air Data Inertial Reference Unit: The Air Data Inertial Reference Units (ADIRUs) are one of the key components as they collect air data and provide position and altitude information [8]. Normally the data of ADIRU 1 is used, and the data of ADIRU 2 is used to verify that the data provided by ADIRU 1 is correct.

Flight Management System: The flight management system uses the data of the air data inertial reference unit, the flight controls, the autopilot settings and weather data to determine the current position. It also calculates the optimum course and vertical flight path to follow to minimise fuel consumption. [58]

Electronic Flight Instrument Systems: The electronic flight instruments systems consists of a primary flight display (PFD), a multi-function display (MFD) and the engine indicators and crew alerting system (EICAS) display, which is shared by the captain and the co-pilot.

Flight Control Surface Actuators: The inputs on the flight controls and autopilot settings are processed by the primary flight computer and send to the control surface actuators, which are subsequently used to move the control surfaces.

The data flows between the other components can also be found in Figure 10.4.

10.6. Electrical Block Diagram

To get a better understanding of the functions and layout of the electrical components of the Aircraft, the Electrical Block Diagram is constructed. It shows all the major systems that are either driven by electrical power or provide it to other components. It is used to gain a better understanding of how the electrics work, and allows tracing of any electrical problems, should they arise. The Electrical Block Diagram (EBD) is provided in Figure 10.5.

The EBD is divided into a total of three segments, components that provide, demand or store electrical power. In each segment the relevant components that fall into that category are identified. Lastly, components that require input or output from other components within the EBD were connected by black arrows lines.

Power Provision: These components are the ones responsible for generating the electrical power to be used by the other systems. When the aircraft is parked, the main source of power is often ground power. Many airports prefer the use of ground power over the APU in order to reduce the noise and pollution produced. For this reason, the APU is only used when ground power is unavailable, to start the main engines or during an emergency in flight.

Power Storage: The Power Storage department contains the components that hold the materials that are converted into electrical energy by the Power Provision department. Electrical energy is either stored directly in the main battery or indirectly in the form of jet fuel. The battery provides the power necessary to start the APU, which in turn is used to start the main engines. The jet fuel is an indirect source of electrical power, as it is first combusted, after which electrical power is generated.
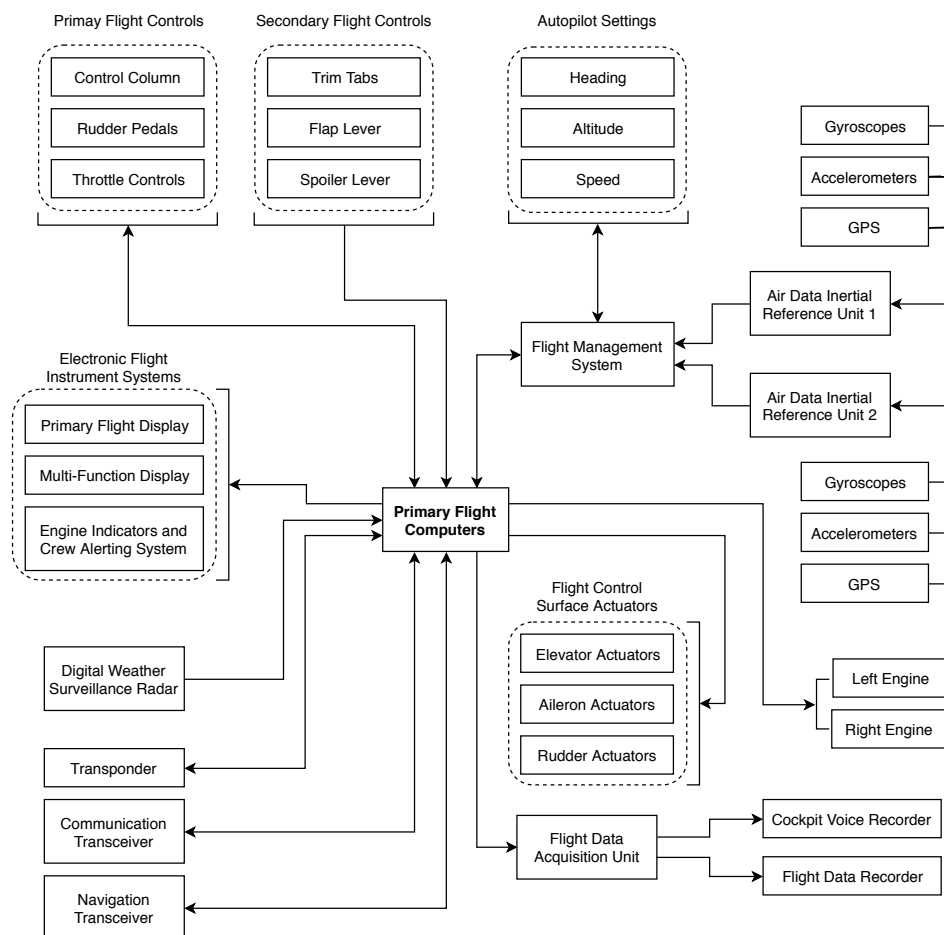
Figure 10.4: *Data handling block diagram.*

Power Demand: Shown here are the main aircraft components that require electrical power. The functions of these components range from monitoring the aircraft status, to provide passenger comfort or to guarantee the safety of the people on board.

Power Conversion: This block represents the components that convert the power into the voltage/current required by the components in the Power Demand department. The engine provides $115V/230V$ Alternating current (AC), to be converted into $28V$ and for some components into direct current (DC) as well.

The arrows connecting the components speak for themselves. In the Power Storage department, the fuel tanks supply fuel to the main engines, and the batteries provide electricity to start the APU. The Power Provision department then recharges the batteries through means of an alternator. On the ground, power is supplied by either the APU or the airport supply, depending on which is available. In the air, the engines are the main source of power. Only in an emergency, during which the engines are unable to supply power for whatever reason, will the APU or the Ram Air Turbine take over and supply power to critical systems. The supplied power is then converted into the desired type and voltage of the components in the Power Demand department.

10.7. Communication Flow Diagram

In order to get a better understanding of how the communication takes place, the communication flow diagram was created, which is given in Figure 10.6. The centre of the communication is the captain. Together with the co-pilot, he is responsible for the major communication flows to the external parties, such as the air traffic control and the flight attendants. He is also responsible for providing the right inputs to the aircraft control surfaces.
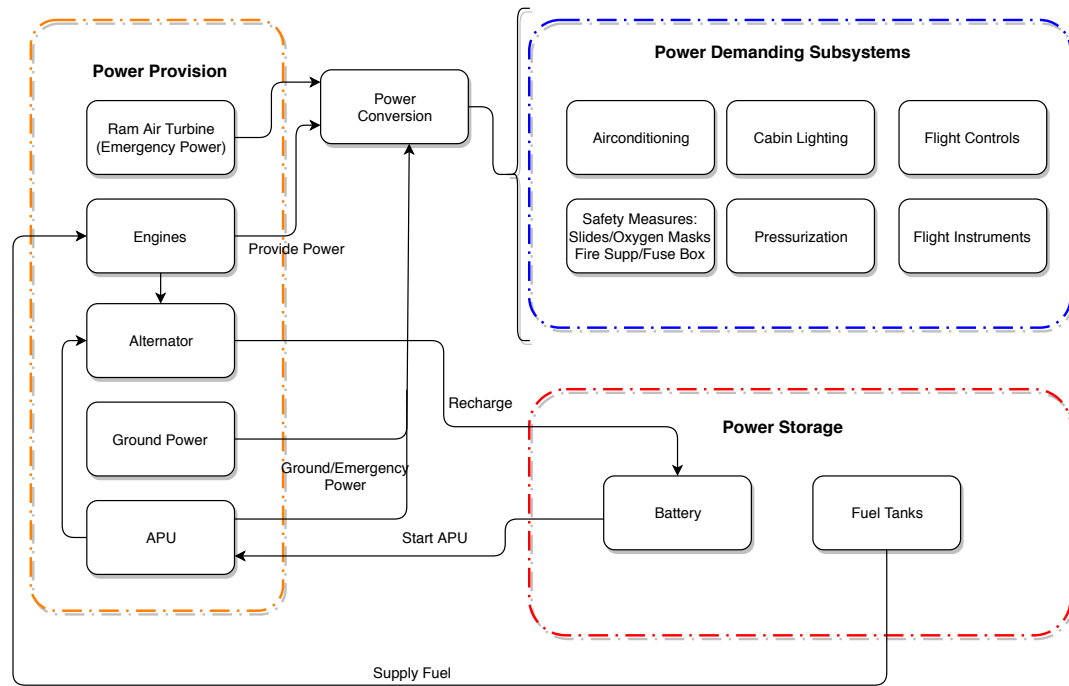
Figure 10.5: *Electrical block diagram.*
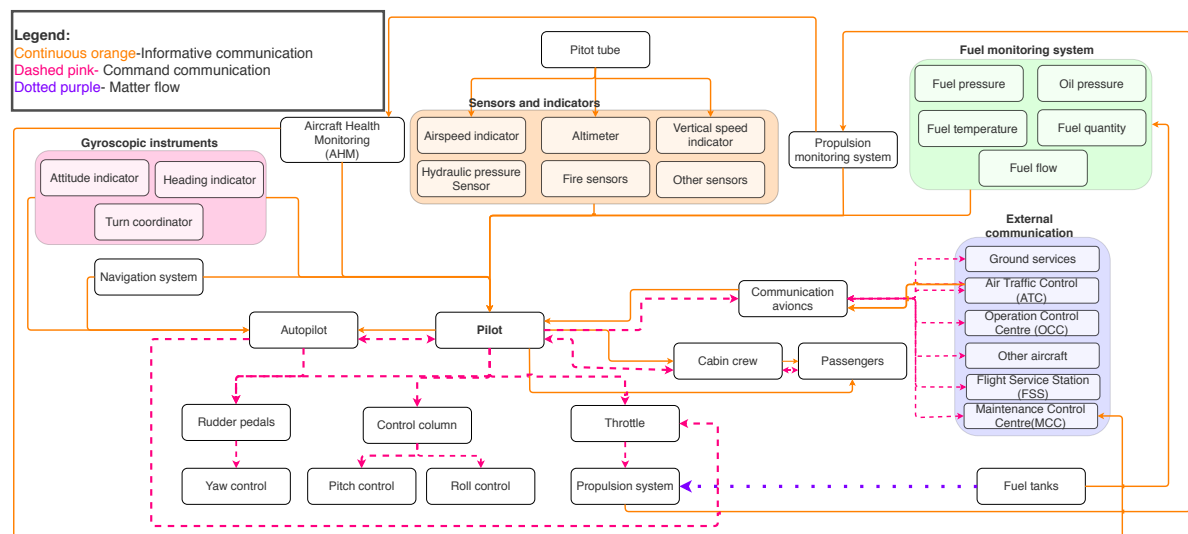
Figure 10.6: *Communication flow diagram.*

10.8. Safety & Reliability Characteristics

This section addresses the safety and reliability characteristics of the aircraft. Subsection 10.8.1 addresses the safety-critical systems contained in the aircraft while Subsection 10.8.2 addresses the redundancy philosophy applied to the safety-critical systems.

10.8.1. Safety-Critical Systems

Safety-critical systems in the aircraft are systems whose failure or malfunction may result in death or serious injury, loss or severe damage to property/equipment, or environmental harm [1]. A preliminary list of the safety-critical systems are contained in this section.

---

[1] Retrieved from: `http://iansommerville.com/software-engineering-book/web/critical-systems/` on 18/06/2018

Engines   An engine failure occurs if one of the engines suddenly stops producing thrust due to a malfunction other than fuel exhaustion. An engine failure during one of the critical phases, such as take-off or landing, can endanger the continuation of the flight significantly.

Hydraulic system   Because the hydraulic system is an important safety-critical system, the aircraft has separate and redundant systems to power the control surfaces, flaps, landing gear, brakes and spoilers.Each of the two engines is equipped with a hydraulic pump and there is also an electric power hydraulic pump as a back-up in case of a double-engine failure.

Fuel system   The fuel system includes the fuel tanks to store the fuel and the pumps to feed the engine from the tanks to the engine. The failure of the fuel pumps that send fuel to the engines will result in the loss fuel delivered to the engines as gravity feed isn't possible because they are mounted higher than the fuel tanks. Also, fuel pumps are also required to prevent large fuel imbalances in the wing that will make it difficult to control the aircraft.

Avionics   The avionics provide crucial information such as the altitude and airspeed to the pilot and flight computer. The failure of systems related to the avionic system would result in the aircraft being unsafe to fly, especially in poor visibility conditions.

Flight control system   The flight control system is crucial for translating the pilot inputs to deflections on the control surface. The fight computers between the pilot inputs and control surface deflections need to protect the aircraft against manoeuvres that would bring it out of the flight envelope and expose the airframe to large stresses.

Fire suppression system   There are areas on the aircraft that are exposed to the combination of high temperatures and combustible materials such as the engines and landing gear bays. Areas identified to have a high risk of catching fire will need to be equipped with fire suppression systems to contain the fire and preventing it to spreading to other areas of the aircraft.

10.8.2. Redundancy Philosophy
For safety-critical systems it is important that back-up systems are present. The redundancy philosophy applied on the relevant safety-critical systems mentioned in Subsection 10.8.1 is explained here.

Engines   There are two engines on the aircraft for redundancy. The aircraft is designed to be able to maintain level flight in the event of a single engine failure. To provide redundancy in the remote case of a double engine failure, a ram air turbine will need to be incorporated in the power subsystem to continue providing electricity to power flight critical systems.

Hydraulic systems   The redundancy philosophy applied for the hydraulic system is to have triple redundant hydraulic systems. The goal of this is to eliminate single points of failure that could cripple the hydraulic system.

Fuel system   There will be multiple fuel pumps in the fuel system of the aircraft to ensure redundancy. Additionally, there will be independent fuel lines from the tanks to the engine to prevent a blockage in one tank to causing the entire fuel system to fail.

Avionics   The entire avionic system from the pitot tubes to the displays will be redundant with independent instruments for the pilot and co-pilot.

Flight control systems   Given its importance to control the aircraft, the fly-by-wire control system and flight computers will require many layers of duplication to ensure redundancy from failures from faulty or damaged components. An extra form of redundancy will be achieved by allowing the flight computers to use alternate or direct control laws when the avionics provide faulty data. There will also be a mechanical backup via the elevator and rudder trim controls to give the pilots some pitch and lateral control in the very remote event

of a complete failure of the flight control system or while resetting the flight control computers after a loss of electrical power.

10.9. Hydraulic System

The hydraulic system is one of the most critical systems of the aircraft: If a total failure occurs, all control over the aircraft is lost. It is therefore a system that requires redundancy for all critical elements. This is the reason why there are up to three separate hydraulic systems in commercial aircraft. Should pressure be lost at a certain hydraulic actuator, prohibiting it from functioning properly, it is possible to close off one system to that actuator and let the other system take over. The hydraulic system is in other words designed to be fail-safe, minimising the chance of losing control of the aircraft. Hydraulic lines of different systems should be far apart from each other, such that when a section of the aircraft gets structurally damaged, it is less likely that both hydraulic systems are damaged at once.
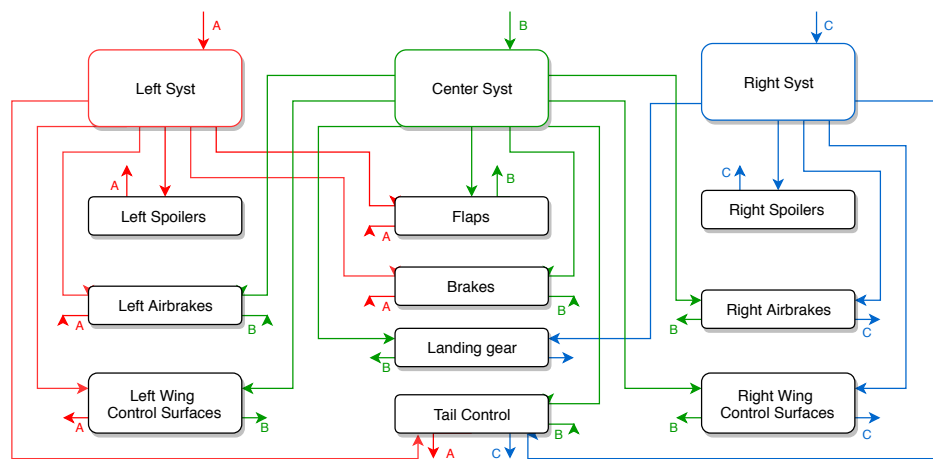
Figure 10.7: *Hydraulic system layout.*

Figure 10.7 displays the schematic layout of the hydraulic system as of now. Components like flaps, brakes, landing gear and tail control systems have been given redundancy by being operated by two hydraulic systems. This is done because these components are seen as critical components, for which failure of one of these results in significantly reduced aircraft performance or the aircraft even being unable to fly at all. Redundancy for the components on the main wing, excluding HLDs, is provided in a slightly different way. Instead of having each component powered by multiple hydraulic systems, each component is split into two parts, with each part powered by a different hydraulic system. The components for which this is done are the spoilers, airbrakes and ailerons. Should any of these components fail on one side of the wing, the component on the other side is unaffected and will still be functioning properly. The result is a loss in performance of that subsystem, but safe flight remains possible.

10.10. Fuel System

The fuel system is composed of the fuel tanks and all the electronics and other components that connect the tanks with the other related subsystems. The tanks should provide enough capacity for the required maximum fuel, taking trapped fuel into account. The type of tanks that are selected for the aircraft design are integral tanks, as these should be big enough to perform internal inspections and reparations, the tank should not be subdivided into too many parts because the tanks close to the wing tips may end up being too small. Furthermore, more tanks may result in higher maintenance costs. Additionally, more wing tanks have a positive effect on the controllability of the aircraft. Because a swept wing is used, the longitudinal centre of gravity location can be altered by controlling the fuel flow between the tip and root tanks. Also, emptying the tanks at the wingtips first gives better roll control, whereas some bending relief is established by emptying the tanks close to the fuselage first. Taking this behaviour into account, it was selected to have a total of 5 main tanks, of which 2 are situated on each wing and 1 in the fuselage between the two wings. There are also two smaller tanks located at the wingtip of each wing, these are for the reserve fuel and the surge tank. This last tank is used to account for volume changes in the fuel, as well as aid in fuel jettison if necessary. The total fuel tank

size in the wings is 5.37 m^3, within the fuselage another tank of 10 m in length below the floor is needed to have a fuel tank size of 10.7 m^3. The fuel tank requirement was determined in [39] and is based on reference aircraft data. This tank gives a maximum fuel weight of 8.5 t which is more than sufficient for a typical flight and actually allows the $MW5$ design to fly quite some extra kilometres when reducing the number of passengers as can be seen in the payload range diagram Section 4.5.

The fuel system layout is shown in Figure 10.8. The red line in this figure is the wing of one of the reference aircraft, the Fokker 90[2]. The dark green outline represents fuel tanks. Light green lines are crossfeed lines, brown ones go to the engines/APU and the light blue piping is used for fuel jettison. Note: the fuel system layout is assumed to be symmetrical with respect to the longitudinal axis and therefore only half is shown.
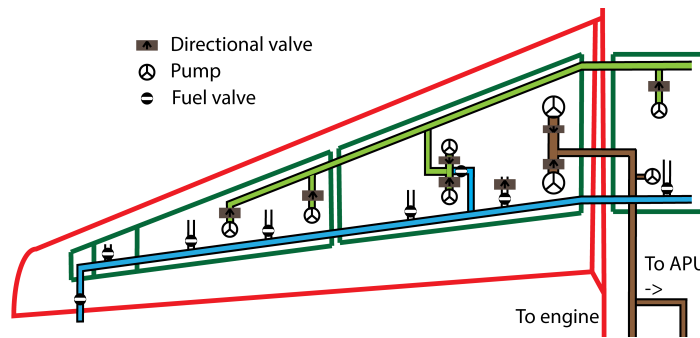
Figure 10.8: *Fuel system.*

Financial Analysis

The financial analysis comprehends all the analysis that are money-related. The first one to be discussed is the program costs, from which the aircraft unit price can be determined. As a result of this price determination, the return on investment (RoI) of the manufacturing company with its related break-even point (BEP) is computed. The same analysis is performed from the point of view of the clients, which are the aircraft operators. This is done subsequently of the operating costs. Finally, the cost breakdown structure (CBS), reliability and availability are tackled.

11.1. Program Costs

The program cost is the sum of the costs that the whole program comprehends. These are subdivided into development and production costs. The program cost is essential to determine the aircraft unit price and, consequently, the RoI and BEP for the manufacturer.

11.1.1. Development Cost

The development cost are made during the first phase of the design of a new aircraft. Its calculation is based on chapter 3 of Roskam [48]. It consists of 6 different parameters:

- Airframe Engineering & Development Cost (AE & DC)
- Development Support & Testing Cost (DS & TC)
- Flight Test Airplanes Cost (FTAC)
- Flight Test Operations Cost (FTOC)
- Research and Development Profit (RDP)
- Cost to finance the Research, Development, Test and Evaluation (RDTE) phases

The total development costs for the entire program are projected to be 1 billion USD. The division between the parameters can be found in Figure 11.1. The share of development cost per aircraft is calculated by dividing the total development cost of the manufactured aircraft, which is estimated to be 600 in 15 years. This gives a development cost per aircraft of 1.6 million USD.
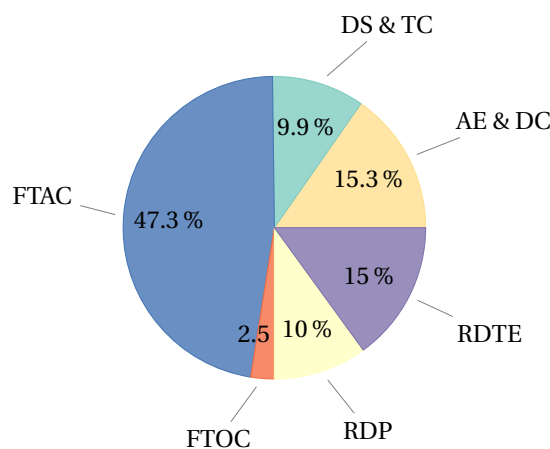
Figure 11.1: *Research, development, test and evaluation cost.*

11.1.2. Production Cost

The production cost comprehends all the costs that are related to the production of all 600 aircraft from the production program. These are subdivided into [48]:

- Airframe Engineering & Design Cost
- Airplane Production Cost
- Production Flight Test Operations Cost
- Cost of financing the manufacturing program

The total production cost for the entire program is projected to be 18.4 billion USD. The production cost per aircraft is calculated by dividing the total production cost over the manufactured aircraft. This gives a production cost per aircraft of 30.4 million USD.

11.1.3. Aircraft Unit Price

Now that all the main cost components are known, the entire program cost can be calculated. Adding up the costs results in a total of 19.4 billion USD, which becomes 32.3 million USD per aircraft. In order to get the aircraft unit price, a profit rate of 20% is added to the costs. Therefore, the unit price is found to be 38.6 million USD, which is 6% below the 41 million USD target. The profit rate was chosen as such due to the break-even point analysis, which is better explained in Subsection 11.4.1. The unit price of direct competitor aircraft can be seen in Table 11.1.

Table 11.1: *Unit price of current large regional aircraft [87, 45, 52, 15].*

Company	Model	Engine type	Unit Price [Million USD]	seating capacity
AVIC	XIAN MA700	turboprop	25	68-86
ATR	72-600	turboprop	26	68-78
AVIC	COMAC ARJ21	turbofan	32	78-105
Bombardier	Q400	turboprop	32.2	82-90
Sukhoi	Superjet 100	turbofan	35.4	87-108
Group 22	$MW5$	turbofan	38.6	64-76
Bombardier	CRJ700	turbofan	41	66-78
Embraer	E170/E175	turbofan	41.5	70-88
Mitsubishi	MRJ70	turbofan	46.3	69-80

The three turboprop aircraft are the ones with the lowest unit price. An exception is seen for the AVIC COMAC ARJ21, which has a price that is comparable to turboprop powered aircraft even if it has turbofan engines.

Furthermore, by looking at Table 11.1, the $MW5$ unit price is about middle priced compared to the competitors. The unit price then results to be 9% more than the average of all the direct competitors and 1.4% less if compared with turbofan mounted aircraft only. These results make the $MW5$ attractive to airline operators as the unit price is about median between competitors. Furthermore, the aircraft is designed to have lower operational costs than comparable aircraft, making it additionally attractive. The operational costs are analysed and displayed in Section 11.2.

11.2. Operating Cost

Since the aim of the project is to design a low-cost regional aircraft, the direct operating costs (DOC) as well as the indirect operating costs (IOC) are an important aspect of the design. In this section, the DOC and IOC of the design are estimated based on methods from Roskam [48] and Jenkinson [51]. Jenkinson provides a calculation of maintenance costs that is based on more recent data, which is the reason this method is chosen for those estimations.

11.2.1. Direct Operating Costs

As it can be seen in Table 11.2, the DOC is subdivided into flying, maintenance, depreciation, landing and navigation fees and finally finance costs. In Table 11.2 fuel consumption, engine maintenance and landing fees have an extra column, this is were the main reduction in DOC in comparison with competitors is obtained. When looking at the average fuel consumption, there is a decrease of 10-15% with respect to similar aircraft (0.047 kg/(seat nmi) compared to, as an example, 0.056 kg/(seat nmi) for the Embraer E-190 [69]),

which is partly due to the aircraft being lighter (Section 3.2) than competitors but also due to a more efficient engine as found in Section 4.1. Furthermore, the maintenance cost of the engine will be significantly lower than the ones that are currently operated. This is the case as the chosen geared turbofans have 1500 less airfoils than current turbofans, which results in a predicted 40% decrease in maintenance costs [93]. As for the landing fees, they are mostly directly related to the maximum landing weight of the aircraft which is significantly lower for the $MW5$ design in comparison to competitors [16]. The effect of fuel burn efficiency, engine maintenance and landing fees on the total DOC is a reduction of 8-11% with respect to current competitive aircraft. The values of cost reductions are given in percentages because the actual numbers are significantly airline dependent. For example, fuel price and maintenance cost largely depend on the amount of operations that an airline performs. The values given in Table 11.2 are typical values but those will be different depending on the operator.

Table 11.2: *Direct operating costs overview.*

DOC component	DOC element	Cost $MW5$ [USD/block hour]	
Flying	Crew Fuel Insurance	$ 255 $ 1267 (492.3 Gallons) $ 56	−10% to −15%
Maintenance	Airframe Engine	$ 410 $ 51	
Depreciation	Airfame Engines Avionics	$ 234 $ 196 $ 52	−40%
Landing & navigation fees	Landing fees Navigation fees Registery taxes	$ 155 (based on $7.75/1000lbs) $ 0 $ 6	−15% to −30%
Finance	Finance	$ 185	
Total		$ 2875	−8% to −11%

11.2.2. Indirect Operating Cost

As for the indirect operating cost (IOC) an estimation can be made based on Roskam [48], where it is approximated to be around 55% of the DOC. Since the IOC can be approximated as a fraction of DOC and is not influenced directly but only indirectly by design choices (by reducing DOC) it is not further elaborated on.

11.3. Return on Investment

Return on Investment gives the projected benefit to an investor for his investment. A high RoI means that for every invested dollar a high return is expected. RoI is used to compare different investments with one another. The RoI analysis is made separately for each investment that is considered. For aircraft industry these are majorly from the manufacturer point of view and the operator point of view.

11.3.1. Manufacturer RoI

The RoI for the manufacturer company is strongly dependent on the costs of the whole aircraft program. In fact, the manufacturer needs to sell enough aircraft in order to make a profit out of the high investment. A negative RoI translates into company losses, which would determine the failure of the program. For this reason, it is essential to determine the expected aircraft sold and select a right profit rate out of the investment. As 600 aircraft are expected to be sold as stated in Section 2.5, 3.7 billion USD of revenues are expected with a profit rate of 20% on the investment. This results in a RoI of 1.19, which is a revenue of 19% of the total investment.

11.3.2. Operator RoI

The operator point of view is also significant for the manufacturing company as the operator is the client, whose aim is to themselves make profit. An estimation of an aircraft operator RoI can be calculated using the methodology proposed in Roskam [48].

The equation to calculate the airline RoI is:

$$\text{RoI} = \frac{(\text{REV} - \text{DOC} - \text{IOC})V_{\text{bl}}}{(\text{AEP})(1 - tx_{\text{inv}})}(1 - tx_{\text{rev}})U_{\text{ann}_{\text{bl}}} \tag{11.1}$$

In this equation REV is given as the revenue in USD per kilometre. Considering a ticket price of 250 EUR per passenger, this is found to be 7.60 EUR per kilometre. The DOC and IOC are the (in)direct operating costs as calculated earlier. These resulted in 3.92 EUR and 2.15 EUR per kilometre accordingly. V_{bl} is the block speed in km/h and is calculated at 629.2 km/h. The AEP is the Aircraft Estimated Price as calculated in Subsection 11.1.3. The tx_{inv} is the investment tax credit rate, which is estimated at 0.10 in United States. The tx_{rev} is the revenue tax rate (0.20 in the United States) [48]. The $U_{\text{ann}_{\text{bl}}}$ is the annual block hours flown by the aircraft, which is calculated to be 4350.8 hours per year.

The RoI for the operator is found to be 1.122, or an earning of 12.2% of the investment.

11.4. Break-Even Point

The break-even point gives the the point at which the total revenues are equal to the cost. At that point, there is nor loss nor profit but the whole investment is repaid. The break-even point gives an indication on how long it takes before a company/investor starts making a profit. The BEP is calculated both from the manufacturer and operator perspective.

11.4.1. Manufacturer

The BEP for the manufacturing company is strongly related to the profit percentage at which each plane is sold. The profit was decided to be 20% the program costs. The reason to chose this rate is explained by the fact that the BEP is wanted to be reached after 45% of the aircraft batch is sold. The manufacturing company wants to keep the risk of not having a positive RoI as low as possible. The 45% is estimated to be a value that is for sure expected to be sold. The break even point is then reached once 270 planes have been sold. Considering the production of 40 planes a year, this is reached after 6.75 years.

11.4.2. Operator

The BEP for the operators is calculated with equation Equation 11.2:

$$\text{BEP} = \frac{\text{AEP}}{(\text{REV} - \text{DOC} - \text{IOC})U_{\text{ann}_{\text{bl}}}V_{\text{bl}}} \tag{11.2}$$

The outcome expresses a BEP after 9.25 years of the beginning of the aircraft operation. This would leave 5 to 10 years of revenues, if considering a 15 to 20 aircraft lifetime.

11.5. Cost Breakdown Structure

The cost elements of the program activities to be taken after the finalisation of this report is contained in the CBS. The CBS is contained in Figure 11.2. The costs of the entire program is divided into three parts. They are the development costs, manufacturing costs and the costs to provide support and services.

11.5.1. Development Costs

The development cost includes the cost of designing the aircraft and ensuring the viability of the program. The main contributors to the development costs are:

- **Management**: The management needs to be paid competitively in order to gain top talent to run the program.
- **Strategy**: Money needs to be spent on marketing to bring awareness to the strengths of the aircraft to potential operators of the aircraft with the goal of convincing them to buy our aircraft. Consultants are hired to give a better view of the market and to provide insights and recommendation that the management can act upon.

- **Engineering**: This includes the cost to design the aircraft and necessary tooling to produce it. The cost to design the aircraft is the cost to hire engineers, build computing capabilities and carry-out testing.
- **Certification**: This is the cost to get the aircraft certified by airworthiness bodies.
- **Office Expenses**: The costs for providing an office for all employees to work in.
- **Financing**: These costs needs to be paid to the bank that is financing the program.

11.5.2. Manufacturing Costs

The manufacturing cost includes the cost of the factory, manpower, equipment and logistics.

- **Factory**: The factory is to be constructed on a piece of land which either has to be bought or leased. The factory has to be maintained and the overhead costs need to be paid for.
- **Manpower**: These workers involved in the production are paid salaries and require insurance for accidents happening on the work floor.
- **Equipment**: For the assembly of the aircraft it is also necessary to have the right tooling, jigs and assembly platform. Quality control requires additional tools, which increase the total equipment cost.
- **Logistics**: Parts have to be stored after batch production in a warehouse, which has to maintain the right atmospheric conditions and takes up space. When required for usage the parts have to be moved from the warehouse to the corresponding production platform.
- **Procurement**: The main items that have to be procured from external parties are materials, engines, avionics and interior items such as seats.

11.5.3. Support & Services Costs

The support and services cost includes the cost of activities to support the aircraft for use in commercial operations.

- **Modifications**: Throughout the operating life of the aircraft, modifications may have to be done to rectify problems or be requested by the operator to improve performance using new technology.
- **Technical Support**: Technical support includes costs for helping operators troubleshoot technical problems that the aircraft is facing as well as providing analytical data and recommendations for aircraft health monitoring service.
- **Part Availability**: The availability of spare parts within a reasonable time is necessary so that the aircraft can operate smoothly in all geographical regions. This means that there are costs for the storage of these parts and the transportation of the parts to the affected operator.
- **Training**: Moreover, the training of flight crews to operate the aircraft incurs additional costs to provide the relevant facilities such as classrooms and simulators as well as instructors to train the pilots.
- **Flight Operations**: This is the cost to provide the service for consulting airlines on optimal flight operations to help operators to fully utilise the cost-saving abilities of the regional aircraft.

11.6. Reliability & Availability

The reliability and availability of the aircraft is an important factor to consider when designing the aircraft for low operational cost. It is difficult to come up with a verifiable number on the reliability and availability of the aircraft at this stage of the design as the detailed subsystems are not well known yet. Therefore, the numbers provided for the expected reliability in Subsection 11.6.1 should be seen as targets to be achieved in the design of the aircraft. For this stage of the design, a preliminary overview of the safety critical systems and their accompanying applied redundancy philosophy are contained in Subsection 10.8.1 and Subsection 10.8.2.

11.6.1. Reliability

One of the most important reliability parameters for aircraft is the dispatch reliability: the percentage of flights that depart within a specified time window of the scheduled departure time. This time window is usually set to 30 minutes, which is short enough that flight schedules are not affected too much and long enough to have time to fix small mechanical problems, assuming spare parts and maintenance personnel are on hand. When the aircraft does not depart within these 30 minutes, the aircraft does not depart "in time" and is considered delayed.[1]

---

[1]Retrieved from: `http://www.aviationpros.com/article/10388070/measuring-reliability-and-availability` on 07/06/2018
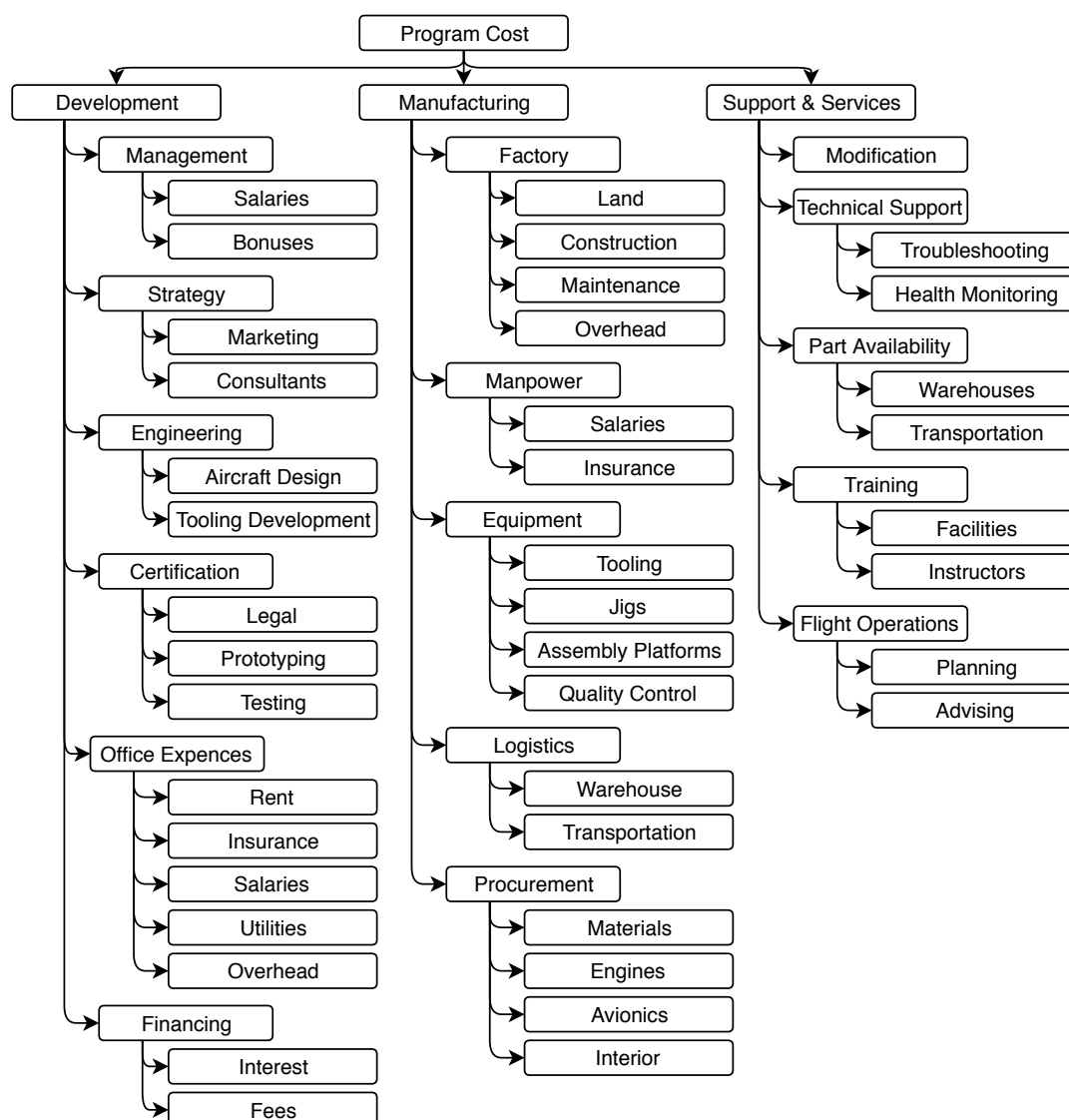
Figure 11.2: *Cost breakdown structure of the program.*

Of all delayed flights, external factors and non-aircraft issues can be excluded. This results in the maintenance dispatch reliability, which only includes delays and cancellations due to unplanned maintenance. External factors that are not dependent on the aircraft used are then not taken into account. The maintenance dispatch reliability strongly depends on cancellations due to controllable reasons and delays due to unplanned maintenance.

In Table 11.3, only the percentage of cancelled flight operations are given per aircraft type for controllable and uncontrollable reasons. Controllable reasons mainly include unplanned maintenance, whereas uncontrollable reasons include external factors and non-aircraft issues, such as severe weather, air traffic control congestion, lack of catering or crew, security, etc. Cancellations due to unplanned maintenance are controllable, because they can be avoided to a certain extent by regularly performing maintenance checks.

Of the 2.6% of the flights with regional jets that were cancelled, 31% was caused by controllable reasons. This means that approximately 0.8% all flights with regional jets are cancelled due to unplanned maintenance, because unplanned maintenance is the largest contribution to cancellations due to controllable reasons.

However, for the maintenance dispatch reliability not only cancellations but also delays have to be taken into account. In Table 11.4 the number of delays and cancellations for different aircraft types can be found. The

Table 11.3: *Flight cancellations due to cause [26].*

A/C type	Cancelled %	Cancellations due to cause %		
		Controllable	Uncontrollable	Diversion
Turboprop	2.9	33.5	66.5	2.1
Regional jet	2.6	31.0	69.0	1.9
Narrow-body	1.0	41.8	58.2	3.3
Wide-body	1.0	57.2	42.8	1.6

data in the table was found by looking at delays and cancellations of 1.95 million scheduled flights.[2]

Table 11.4: *Flight cancellations and delays due to different causes.*

	Turbo-prop aircraft [%]	Small regional jets [%]	Large regional jets [%]	Narrow-body aircraft [%]	Wide-body aircraft [%]
Returned to gate	0.9	0.9	0.9	0.9	1.5
Cancelled due to flight crews	0.7	0.1	0.5	< 0.1	< 0.1
Cancelled due to maintenance	2.1	0.4	0.8	0.1	0.3
Delayed due to maintenance	3.0	4.1	3.8	3.6	5.6
Percent of all flights	8.3	37.1	17.4	33.1	4.2

From the table it can be seen that for small regional jets 4.5 percent of all flights were cancelled or delayed due to maintenance. For large regional jets, 4.6 percent of all flights were cancelled or delayed due to maintenance. For the maintenance dispatch reliability, this results in a reliability of 95.5 percent for small regional jets and a reliability of 95.4 percent for large regional jets. This means that large regional jets are almost as reliable as small regional jets when looking at the maintenance dispatch reliability.

Small regional jets often carry less than 70 passengers, whereas large regional jets typically carry 70 to 100 passengers. Because the $MW5$ can carry 76 passengers, it is a large regional jet and the maintenance dispatch reliability is therefore targeted to be at least equal to the average maintenance dispatch reliability of large regional jets, which is 95.4 percent.

11.6.2. Availability
For the design of the aircraft, the operational availability can be further split into two parts: the operational availability A_o and the inherent availability A_i.

Operational availability is a measurement of the percentage of time the aircraft is available for flight. It takes scheduled and unscheduled maintenance into account, as well as logistic delays. The operational availability depends on the Mean Time Between Maintenance Actions (MTBMA), the Mean Maintenance Time (MMT) and the Mean Logistic Delay Time (MLDT). The operational availability is given in Equation 11.3 and can be improved by increasing the time between maintenance actions, when allowed by regulations, and by reducing the maintenance time and logistic delays.

$$A_o = \frac{\text{MTBMA}}{\text{MTBMA} + \text{MMT} + \text{MLDT}} \quad (11.3)$$

The components of the low-cost regional aircraft that are maintenance intensive i.e. the engines and high-lift devices should have characteristics such as being easily accessible and removable which allows for the MMT to be reduced. This contributes to reducing the direct operational cost of the aircraft.

The inherent availability is a performance parameter that depends on the Mean Time Between Failures (MTBF) and the Mean Time To Repair (MTTR). The formula for the inherent availability is given in Equation 11.4 and can be used as a first estimation, because internal transport and logistic delays are ignored.

$$A_i = \frac{\text{MTBF}}{\text{MTBF} + \text{MTTR}} \quad (11.4)$$

---

[2]Retrieved from: `http://www.worldtek.com/wp-content/uploads/2015/09/Measurement-of-Dispatch-Reliability-Tulinda-Larsen-Sept` pdf on 07-06-2018

The inherent availability is improved over existing aircraft through reducing the MTTR by leveraging the aircraft health monitoring systems proposed in Section 9.2. This allows the operator to better predict when failures are going to occur and pre-allocate resources to address the failures more quickly, thus reducing the MTTR.

<div style="text-align: right; font-size: 3em;">12</div>

Sustainable Development

Commuter air traffic is increasing with 5% per year and is therefore a fast growing sector, where airlines are growing rapidly and air traffic is becoming more affordable. To reduce the environmental influence of growing air traffic, the air traffic sector has to become more sustainable. Sustainable design is a crucial aspect to ensure the future of air traffic. First a definition of sustainable development is provided in Section 12.1. Secondly, the design choices that influence the sustainability of the design are provided in Section 12.2. Finally, the airframe noise is determined and compared to reference aircraft in Section 12.4.

12.1. Definition

In order to implement sustainable development it is first necessary to define sustainable development. The aim of sustainable development is to meet the needs of the current generation, without compromising the ability of future generations to meet their needs [94]. The chosen definition of sustainable development is the definition as is provided in the Oxford Dictionary[1]:

> *"Development that is conducted with the aim to keep the depletion of natural resources and the environmental impact as low as possible."*
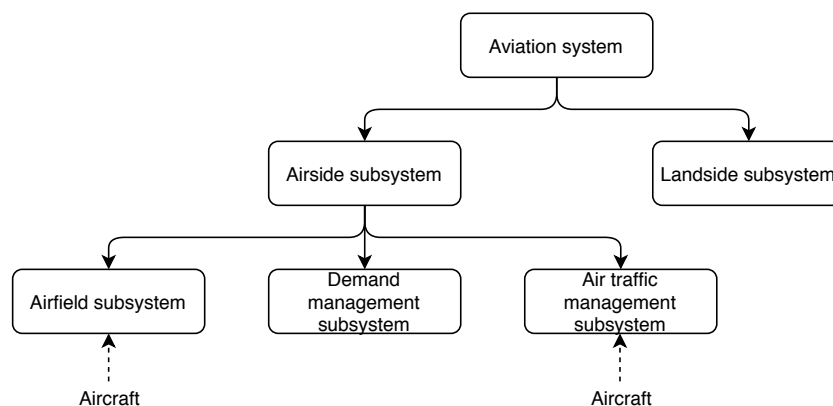
Figure 12.1: *Subsystems in the aviation system.*

Figure 12.1 shows the distinction between the subsystems of the aviation which can or can not be influenced by the aircraft design. Not every aspect of the aviation system can be influenced by implementing new technologies in the aircraft design. However, measures increasing the level of sustainability of the airfield subsystem and the air traffic management subsystem can be implemented. The airfield subsystem can be divided in three different elements: structural, aerodynamic and propulsion.

12.2. Airfield Subsystem

The sustainability airfield subsystem, which is the aircraft, can be influenced by different design aspects. The main aspects focused on during the design phase are the structural design, aerodynamic design and propulsion design.

---

[1] Retrieved from: `https://en.oxforddictionaries.com/definition/sustainable_development` accessed on 18-6-2018

12.2.1. Structural Sustainability

The structural element of sustainability can be further subdivided into separate elements. The main structural elements influencing the sustainability of the aircraft are structural weight and possible end of life solutions of the aircraft.

Structural weight   The structural weight of the aircraft is determined by the loads experienced by the aircraft during operations as well as the selected materials. Because the loads that the aircraft has to be able to withstand are set by the flight envelope and regulations, the only parameter to influence the structural weight of the aircraft is the material selection. The influence of the maximum take-off weight, and hence the operational empty weight, is presented earlier in Table 4.13.

The four main different types of materials considered for aircraft design are metal alloys, fibre reinforced composites, metal matrix composites and fibre metal laminates. Each of the material types has its own range of specific strength, determining the structural weight. In terms of structural weight it is beneficial to select the material with the highest possible specific strength.

End of life solutions   The possible end of life solutions depend on the selected materials, but the general goal is to recycle the materials as much as possible. The materials considered for recyclability are the same materials as mentioned for the structural weight, but metal matrix composites are discarded due to the low technology readiness level.

Recycling metal alloys can be done quite easily by melting the parts that are to be recycled. A metal aircraft can be recycled up to 85% by mass, which is quite attractive in terms of sustainability. Unlike for fibre reinforced composites, the recycled metal alloys are allowed to be reused for critical structural parts.

There are significant challenges in recycling fibre reinforced composites. It is by legislation not allowed to reuse fibre reinforced composite parts for critical structural elements. The most promising, but at this day rather uncertain, method of recycling the resin of fibre reinforced composites is pyrolysis which is the thermal decomposition of the material. However, development of this process is insufficient to consider it as an end of life solution for the design on an industrial scale. A second possible recycling method for fibre reinforced composites is burning the resin and only retrieving the remaining fibres. The fibres can then be used in a different process, such as injection moulding.

According to Boom [17] it is possible to extract up to 98% of the original metal alloy with its original composition, which is a relative high yield of recycled metal alloy. The first step is to separate the metal alloy from the glass fibres making use of thermal delamination. After the metal alloy has been separated from the glass fibres, the metal alloy can be remelted and refined.

12.2.2. Aerodynamic Sustainability

The thrust is directly related to the fuel consumption of the aircraft. In order to minimise the fuel consumption, and hence lower the greenhouse gas emission of the engines, the drag during cruise has to be minimised as well. The drag generated by the wing consists of viscous drag and induced drag, of which the latter one is most prominent during cruise.

The induced drag of the wing planform during cruise is computed using AVL for different aspect ratios, sweep angles and taper ratios for the kink and the wing tip. A basinhopping optimisation method has been used to determine the planform geometry for which the induced drag is minimised. This planform geometry reduces the fuel consumption during cruise, which is the largest part of the flight operation.

12.2.3. Propulsion Sustainability

The most promising current development in propulsion to reduce emissions and noise is the development of the geared turbofan engine. Because the fan and the compressor are linked through a gearbox, both the fan and compressor blades can operate at different rotational velocity which allows for a higher engine efficiency. The higher engine efficiency translates into a better fuel efficiency and a lower noise production, as is presented in Chapter 4.

12.3. Air Traffic Management Subsystem

Several strategies to increase the efficiency of the air traffic management subsystem are provided in [77]. The criteria used for operational mitigation assessment are environmental impact, ease of implementation and

system wide impact. During the different flight phases there are strategies that can be implemented to reduce the environmental influence of the aircraft.

Some of the strategies discussed in [77] already are discussed in Chapter 4, resulting in a total fuel saving of 37 kg per mission, which results in a CO_2 emission reduction of 116.5 kg per operation.

12.4. Aircraft Noise

The aircraft noise can be split up in engine noise and airframe noise. The engine noise has already been discussed in the engine selection, hence only the airframe noise is covered here. The airframe noise is determined by using the Aircraft Noise Prediction Program (ANoPP) developed by NASA. The results of the ANoPP for the design are plotted against the results of comparable aircraft in Figure 12.2. The main parameters influencing the airframe noise are:

- Wing area
- Wing span
- Flap area

- Flap span
- Approach speed
- Landing gear dimensions

The landing gear geometry for the reference aircraft is, within the scope of this project, nearly impossible to obtain, so the same landing gear geometry is used for all aircraft in the ANoPP. The results from the ANoPP show that the airframe noise produced by the design is lower than the airframe noise produced by comparable aircraft.
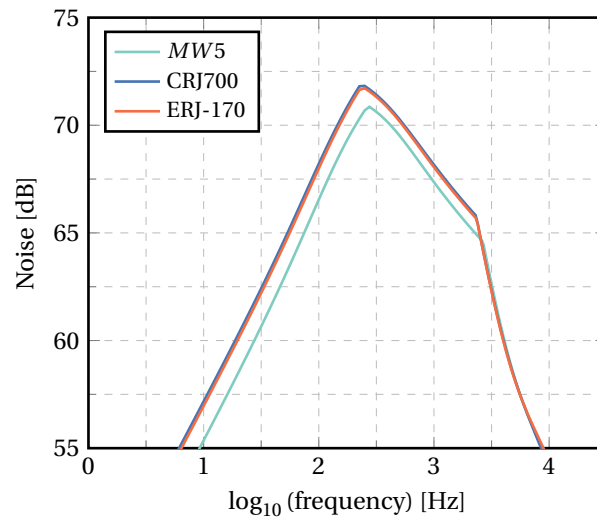
Figure 12.2: *Results of the aircraft noise prediction program.*

13

Technical Risk Assessment

This chapter contains the technical risk assessment of the low-cost regional aircraft under design. Section 13.1 presents the risks the aircraft is exposed to in the operational aspect while in Section 13.2 the developmental risks that may threaten the viability of aircraft program are elaborated. The risks in this chapter are evaluated using the scales of their severities and likelihoods established in Table 13.1. Mitigation strategies are proposed for risks that are assessed to be unacceptable.

Table 13.1: *Scale to measure the severity and likelihood of technical risks.*

Category	Direction of increasing impact $\longrightarrow$			
Severity	Negligible	Marginal	Critical	Catastrophic
Likelihood	Remote	Unlikely	Reasonably Possible	Probable

13.1. Operational Risks

The operational risks are the risks that the aircraft is exposed to over its operational lifetime. Notable risks relevant to the design choice of the regional aircraft are listed in Subsection 13.1.1. Mitigation steps to abate unacceptable risks to be taken in the design are proposed in Subsection 13.1.2.

13.1.1. Risk Identification & Assessment

OP-PR-1: Foreign object debris (FOD) ingestion   Ingestion of foreign object debris (FOD) such as birds and stones poses a threat to the turbofan engines on the aircraft as it may damage the fan blades or enter the core of the engine. The probability of birds entering the engine is low as commercial airports take extensive measures to keep birds away from flight paths. As for the ingestion of debris when the aircraft is on the ground, the likelihood of this is already reduced as the engines are located on the fuselage with a good amount of ground clearance. Hence, FOD ingestion is unlikely with a marginal consequence on aircraft performance.

OP-PR-2: Engine fire   The three essentials for fire are all present at the engines, i.e. fuel, ignition source, and oxygen. Therefore, the likelihood level of an uncontrolled engine fire is set as reasonably possible. In the chosen design concept with fuselage mounted engines, the consequence of an engine fire has the potential to be catastrophic as it can spread to the cabin and empennage.

OP-CS-1: Hydraulic system failure   The total failure of the hydraulic system is catastrophic in severity as it will result in the loss of flight controls but it is unlikely. Also, a special consideration to take into account for the fuselage mounted engines at the rear of the aircraft is that an uncontained engine failure, even though unlikely might result in shrapnel damaging the hydraulic pipes located in its vicinity.

OP-GO-1: Damage from ground operations   Rough handling by the ground crew or collision of ground equipment with the aircraft can cause damage that degrades its performance or creates the need for unscheduled maintenance. Hence, the severity of this event is marginal. Due to the configuration of the final design, the wings and fuselage are close to the ground which make them vulnerable to collision from other fixed and mobile objects which increases the likelihood of this to reasonably possible.

13.1.2. Risk Mitigation

OP-PR-2: Engine fire   To reduce the severity and protect the aircraft from fire the principle of separation, isolation, and control needs to be adopted. Separation and isolation can be achieved with passive systems such as fire-retardant materials and the utilisation of firewalls and reduced the probability of an uncontrolled engine fire. Control is achieved through active air and fuel shut off valves and fire-extinguishing systems.

OP-CS-1: Hydraulic system failure   Due to the severity of this risk event, multiple mitigation actions must be taken such as ensuring redundancy in the entire system and the elimination of single point of failures to reduce the likelihood to remote.

OP-GO-1: Damage from ground operations   To abate this risk, built-in flood lights could be incorporated into the design of the aircraft to assist in ground operations at night. Cameras can also be installed at the tail to allow the pilot to have a better view of the aircraft's surroundings. These mitigation strategies should bring the likelihood down, the event can then be considered unlikely.

13.2. Developmental Risks

The developmental risks that have the potential to threaten the ability of this project to meet the requirements outlined in Section 2.6. The purpose of the analysis of the developmental risks is to identify and assess them in the aircraft development program in order to implement mitigation procedures early on so that the severities of the risks can be reduced and corrections can be made before the design is frozen.

13.2.1. Risk Identification & Assessment

DEV-PR-1: Engine maturity   The selected engine - the PW1215G is a high-bypass turbofan that is a part of the PW1000G family by Pratt & Whitney which incorporates the latest developments in geared turbofan technology. The PW1000G family made its entry into service in 2016 but has however experienced some teething issues that have critical consequences which have caused affected aircraft to be grounded. [1] As the designed low-cost regional aircraft is targeted for an entry into service (EIS) target of 5 years, it is expected that these issues will be resolved well before then as many stakeholders are affected. Hence this developmental risk is deemed unlikely.

DEV-PR-2: Engine integration   The PW1215G has a fan diameter of 1.46 meters and is significantly wider than the General Electric CF34-8C engine used on the Bombardier CRJ700 which has a fan diameter of 1.17 meters[2]. Fuselage-engine integration issues such as aerodynamic interference and flutter could have a critical impact on the program if fixes can not be found, requiring a change to an engine of a smaller diameter. Nevertheless, this is deemed unlikely as there already exist business jets with similar configurations that have engines almost as wide as their fuselages such as the Gulfstream G550.

DEV-AR-1: Shock-waves on wing   The design of the wing utilise supercritical airfoils in order to delay the onset of shock-waves on the wing when flying in the transonic region. CFD was not performed for the wing design due to a lack of time, expertise, and equipment such as computing clusters and hence an assumption was made that compressible effects can be ignored for supercritical airfoils in the transonic region. Nevertheless, there is a risk that the assumption may not be valid and that there are shocks on the wing at the target cruise Mach number. This is accessed to be unlikely as similar regional aircraft such as the CRJ700 and E170 already operate at the designed Mach regimes. The occurrence of shocks would still be critical as it would require the development of new airfoils or at worst a redesign of the wing.

DEV-ST-1: Structural weight change   The structural design of the wings and fuselage make use of many simplifying assumptions at this early stage of the design. The likelihood of a structural weight change is reasonably possible as the structure is overdesigned to some extent for safety and lacks the finer analysis of the smaller details such as cutaways and access hatches. Therefore, it would be possible to see weight changes further down the program. This would have critical implications on the overall design of the regional aircraft as the other subsystems will be affected as well.

---

[1]https://www.wsj.com/articles/airbus-delivers-a320neo-to-lufthansa-1453306044
[2]https://www.geaviation.com/sites/default/files/datasheet-CF34-8C.pdf

DEV-ST-2: Production cost overrun   The materials mix in the $MW5$ includes modern materials namely the Aluminium-Lithium alloy Al-Li 8090-T851 for the wing and fuselage and carbon fibre reinforced polymer (CFRP) for the control surfaces and stabilisers. This carries the risk of ballooning production costs as special considerations must be made such as specialised and separate tooling for AL-Li 8090-T851 to prevent lithium contamination of other parts and increased complexity of quality control for CFRP. This risk is reasonably possible with a marginal impact on the program.

13.2.2. Risk Mitigation

DEV-PR-1: Engine maturity   The program should take into consideration the possibility to use the other engines included in the trade-off in Section 4.1. This will reduce the likelihood of the program to be severely affected by the unavailability of an engine due to technical problems to remote.

DEV-PR-2: Engine integration   Computational fluid dynamics (CFD) and analysis with advanced structural models should be performed in the detailed design in order to identify any possible integration issues early on so that more resources can be invested to address them without causing major program delays. This mitigation step should reduce the severity of this risk to marginal.

DEV-AR-1: Shock-waves on wing   Expertise and computing resources for CFD analysis should be acquired as soon as the detailed design phase begins, in order to validate the wing design or discover any potential problems early on in the project to reduce the severity of this risk to marginal.

DEV-ST-1: Structural weight change   To reduce the severity and likelihood of this risk, finite element modelling with detailed part designs need to be executed. The structures department should also make predictions on which directions the weight change of the different parts will be in and communicate them with the other departments so that necessary preparations can be made.

DEV-ST-2: Production cost overrun   Communication channels should be opened with experts on aircraft production and suppliers for the material and tooling to gain a better understanding of the challenges with producing an aircraft with Aluminium-Lithium and CFRP. This understanding needs to be translated into better estimates of the production costs involved and implementable steps to reduce costs where possible. Lean thinking should also be applied to reduce waste and cost and result in the severity level to be negligible.

13.3. Risk Maps

The risks before and applying the proposed risk mitigation strategies in Subsection 13.1.2 and Subsection 13.2.2 are included in the pre and post-mitigation risk maps in Table 13.2 and Table 13.3 categorised with their likelihoods and severities. The risks in the risk maps can be identified based on their assigned identifiers.

Table 13.2: *Pre-mitigation risk map.*

	Negligible	Marginal	Critical	Catastrophic
Probable				
Reasonably Possible		OP-GO-1, DEV-ST-2	DEV-ST-1	OP-PR-2
Unlikely		OP-PR-1	DEV-PR-1, DEV-PR-2, DEV-AR-1	OP-CS-1
Remote				

Table 13.3: *Post-mitigation risk map.*

	Negligible	Marginal	Critical	Catastrophic
Probable				
Reasonably Possible	DEV-ST-2			
Unlikely		OP-GO-1, DEV-PR-2, DEV-AR-1, DEV-ST-1	OP-PR-2	
Remote		OP-PR-1	DEV-PR-1	OP-CS-1

<div align="right"># 14</div>

Project Design and Development Logic

While the current design phase focuses on the design of the aircraft up to the subsystem level, not all required parts of the aircraft can be designed within the current time-frame. Therefore, it is required to analyse the total work that is left after this phase is completed. Doing so ensures a broad and complete overview of work still to be done, with no subjects left behind or overlooked. First, the different future activities will be discussed, after which the post DSE Gantt chart is presented

14.1. Future Outlook

Figure 14.1 displays the activities to be performed after the current design phase is completed. It ranges from designing the technical aspects of the aircraft into greater detail, to monitoring customer satisfaction.

A total of three further phases are identified, detailed design, development and operational lifetime of the aircraft. The first phase indicates the final part of the detailed design, during which the smallest details of the aircraft are worked out and designed. After that, the aircraft is to be tested before it is allowed entry for commercial use. Lastly, after certification is achieved, the final phase begins and describes the relation between manufacturer and customer during the operational life of the aircraft. This phase is ended when the aircraft is taken out of service and end-of-life procedures are executed.

14.2. Project D&D Gantt Chart

To bring some perspective to the future design phases, a Gantt chart was constructed to give an indication on how much time each work package is estimated to take.

In order to get an overview of the time required for the development of the design after the DSE, it is useful to create a post-DSE Gantt chart. While assigning the time budgets, the time to market of five years has been taken into account. The continuation of the detailed design phase will take up approximately 1.5 years. After this phase is concluded, the development phase of the project starts. This phase includes the production of prototypes, the testing of these prototypes and the type certification for the aircraft. As soon as the aircraft is certified, the aircraft can be commercially produced as it enters the third phase: the operational lifetime. Figure 14.2 shows the post-DSE Gantt chart. In this figure, the appropriate times and dates are shown. Note that the Operational lifetime is only a few blocks long. This is only used as an indication and should continue on for the entire project lifetime. After an aircraft completes its operational lifetime it enters the end-of-life phase.
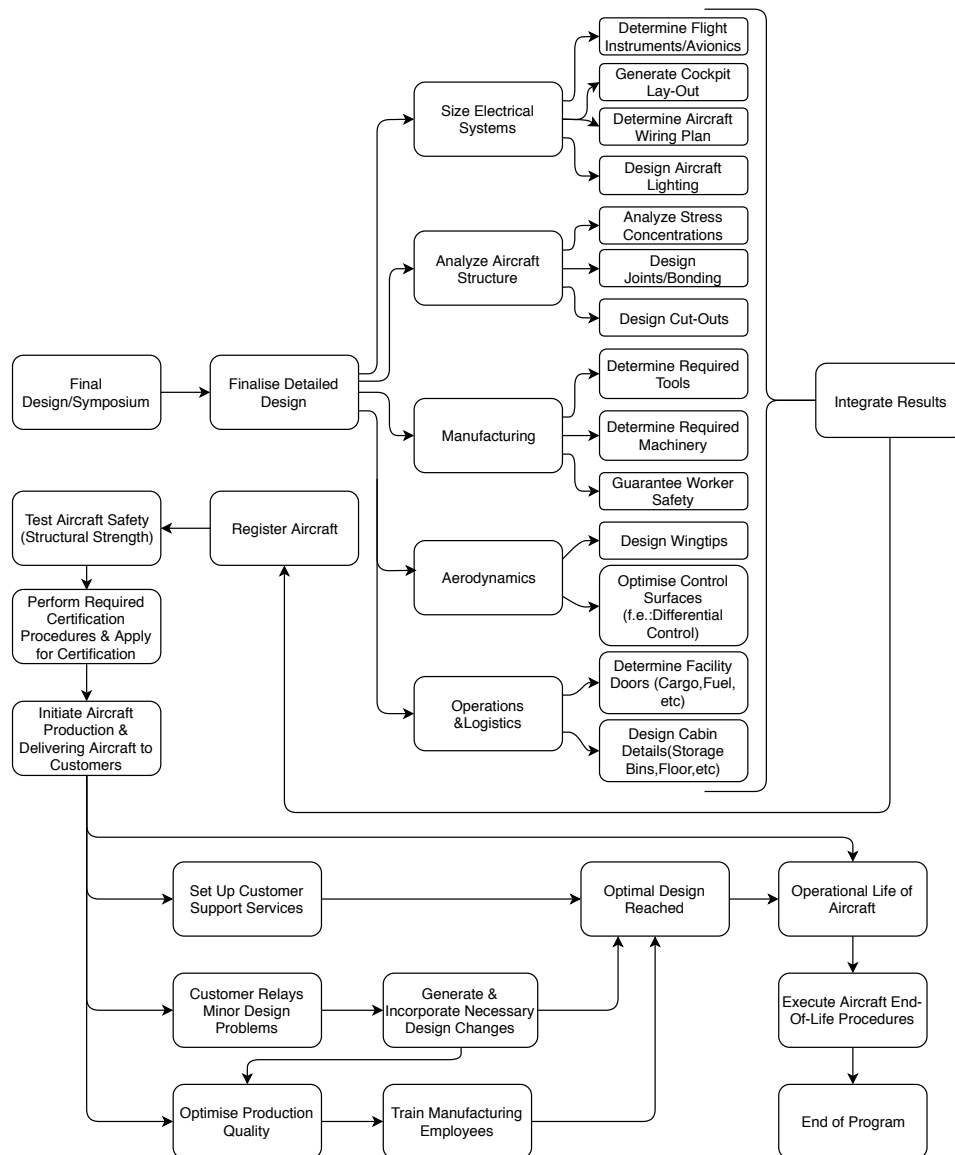
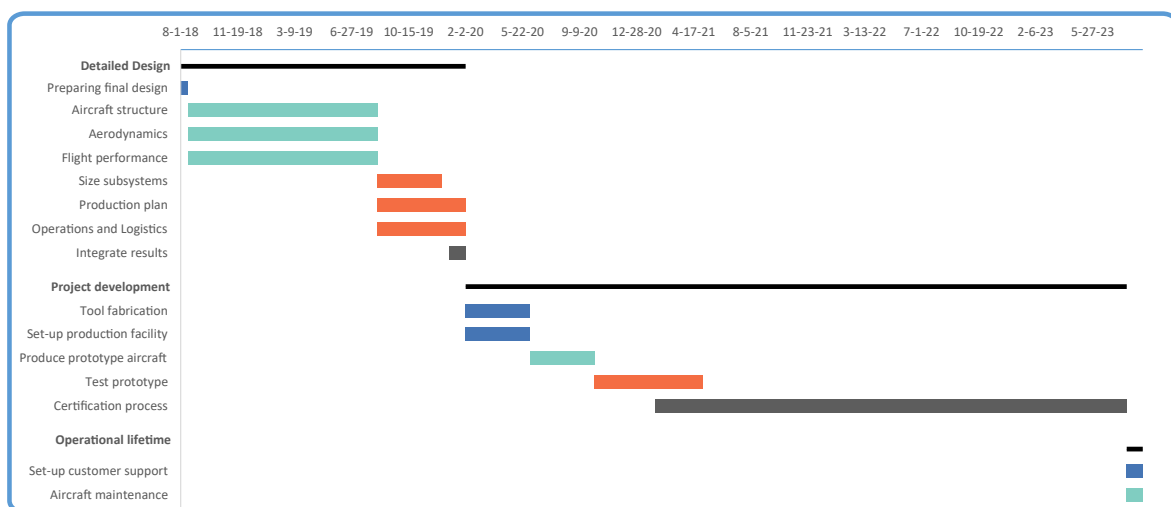**Figure 14.1:** *Project design and development logic.*

Figure 14.2: *Project D&D Gantt chart.*

<div align="right">

15

</div>

Conclusion & Recommendations

As a result of ever increasing air traffic, more flights and more airports are required. This opens the market gap for many new designs. An especially profitable gap is in the regional market. As last clean-sheet design of a regional aircraft was made more than 20 years ago, there is a serious need for a new contemporary, lightweight and efficient aircraft. The goal of this report is to successfully design such an aircraft as specified in the mission need statement below.

> *Transport 50 to 75 passengers with the lowest possible operational costs over a distance of* 1500 *to* 2500 km *with an aircraft from regional airports with* 1500 m *tarmac runway maximum.*

The project was split up into two major parts. The first phase focused on the aircraft design such as flight performance and stability and control. The second part focused on the financial aspects of aircraft exploitation. The first part focused on optimising the aircraft performance, with the main driver being cost to quality ratio, whereas the second part focused on assessing the investment. In this chapter, the final conclusions and recommendations are presented.

Conclusions

Conclusions for both both major parts of the report as explained above are present in this section. The conclusions are categorised to their relevant design department.

Structures For both the wing and the fuselage, critical load cases have been determined and designed for. The whole process of designing has been reported and calculations have been performed for one critical location. For the wing this location is at the root and for the fuselage it is at the location of the wing where the lift acts. The main goal of the project is keeping the MW5 operating cost as low as possible. For the structural design this mostly means keeping the structural weight to a minimum. The critical location for the fuselage is at 16.27 m from the nose of the aircraft(location where the wing lift acts). For that cross-section 53 stringers, 14 frames and skin thickness of 1.5 mm are required to sustain the loads. For the wing, the number of stringers needed at the root is 32 with a local rib pitch of 0.465 m. The goal of lowest weight was obtained by designing a structure that would just withstand the maximum load. By iterating the design, meaning adding and removing material where possible or necessary, the design can be optimised further. The methods of designing the wing and fuselage for critical load conditions can be used to determine an optimal design for the rest of the wing and fuselage as well.

Aerodynamics The wing planform and airfoil selection has been performed with the aim to reduce the induced drag during cruise as much as possible. The resulting lift over drag ratio of the clean wing during cruise is 34.4, but this is excluding the drag caused by the fuselage and tail sections. The optimised wing has an area of $61.1 \, \text{m}^2$ and a total taper ratio of 0.31. The lateral stability of the aircraft is increased by applying a dihedral angle of 3°. The resulting wing can achieve a maximum lift coefficient in clean configuration of 1.07 at an angle of attack of 11.5°.

The horizontal and vertical tail are designed to provide the aircraft with sufficient longitudinal and lateral stability. The computed horizontal tail surface of $10.1 \, \text{m}^2$ is sufficient to ensure both the stability and controllability of the aircraft for each possible centre of gravity location. The vertical tail area of $11.8 \, \text{m}^2$

Flight performance   Firstly, the engine selection was performed based on the thrust required over the entire flight mission, its fuel efficiency, dry weight and environmental impact. Based on these criteria, a scaled-down version of the PW1215G, which belongs to the most advanced geared turbofan family in production as of 2018, was chosen to power the aircraft.

Secondly, the balanced field length was calculated to be 1490 m which fulfils the customer's take-off requirements of 1500 m. Following that, the relevant flight phases were investigated in order to propose operation optimisation strategies to reduce the fuel burn of each flight mission, and hence directly lower its operational cost. The requirement to fly a distance of 2500 km at maximum payload was then verified through the construction of the payload-range diagram. With zero payload, the aircraft is able to travel a distance of 4175 km.

Moreover, the flight envelope and V-n diagram were made to determine the aircraft's operational limits and the structural strength the airframe has to be designed to withstand. To be competitive with comparable regional aircraft such as the Bombardier CRJ700 and Embraer E170, the maximum operating Mach number and service ceiling were set to be 0.78 and 41,000 ft respectively. The V-n diagram determined that the aircraft needs to be designed to handle a maximum and minimum load factor of 2.5 & -1.

The turn performance was investigated to determine the aircraft's maximum achievable turn rate at a critical condition of 7000 ft at MTOW, which is the upper limit of typical hold altitudes. It was determined that the $MW5$ is capable of meeting the most demanding standard turns i.e. the rate 2 turns.

Stability and control   Regulations require the aircraft to be dynamically stable in all expected aircraft conditions and configurations. Based on the expected seating arrangement, subsystem placement and weights, a suitable wing placement and tail size was determined to meet these requirements. As of now, controllability is the most limiting condition, while a large stability margin is guaranteed during flight. Based on the geometry and specifications of the $MW5$ design, a detailed analysis of the aircraft's flight behaviour was performed. This analysis resulted in the five eigenmotions that occur in flight. The conclusion that can be drawn from this analysis is that the aircraft is stable in four of these motions, and the only unstable eigenmotion is stable enough to allow plenty of time for the pilot to react, which is the driving factor to pass aircraft regulations for this eigenmotion.

Finance   The finance chapter discussed all the analyses that are money-related. Firstly, an estimation of the program cost was calculated to be 19.4 billion USD. From these costs, the unit price of the $MW5$ was set as 38.6 million USD, such that a RoI of 19% was obtained for the manufacturing company. This could be achieved by wanting a BEP of not later than 50% of aircraft sold. In fact, the BEP is now found as 45% of the aircraft sold, which is at 270 sold planes. From the operating cost analysis it followed that a reduction of 8% to 11% in operating cost is obtained. Based on that, RoI and BEP could be determined from the perspective of an $MW5$ operator. These were found to be 12.2% and 9.25 years respectively. In order to have a better overview of the financial side of the program, a cost-breakdown analysis was performed. Finally, reliability and availability were tackled. These are crucial to strengthen the interest of investors. In fact, the more the $MW5$ aircraft are expected to be reliable and available, the more revenues an aircraft operator makes.

Recommendations

Further research into the proposed low-cost regional aircraft, $MW5$, is required in order to achieve even lower operational costs. In this section, the recommendations per department are elaborated.

Structures   Now that the preliminary sizing for the wing and fuselage is done, for the next phase in the design it is recommended to continue the design iterations and optimise the design for each specific section of the aircraft. For the wing this means determining the design along the entire cross-section and for the fuselage the next step would be to even further optimise for weight, which can be achieved by introducing stringer discontinuity, variable skin thickness and different stringer's sizes, geometries and placements. Furthermore, it must be noted that the current design only deals with static loads. Once the design has been optimised it is important to look further into the effect of dynamic loading to make sure the aircraft can withstand all possible loading scenario's. The landing gear structure needs to be designed and especially the connection of the landing gear to the wing needs to be designed for relatively high dynamic loads. In the end phase of the design several experimental tests should be performed as validation before the aircraft is able to start test

flights. At that moment loads can be applied to a prototype aircraft structure and strain gauges can be used to read out stresses at all relevant locations.

Aerodynamics   In a next phase of the project, it is recommended to look into CFD in order to test the assumption that no shock-waves are present, and in order to have more accurate results. Also, it is interesting to look into methods to delay transonic effects such as wing fences. Once the correct CFD models are available, it is also recommended to look into the design of wingtip devices. Wingtip devices can further decrease the induced drag during cruise, which saves fuel and hence increases the sustainability of the aircraft and reduces operational costs. The sizing of the vertical tail is based on a statistical method, but a more extensive investigation to the dimensions of the vertical tail has to be performed in the next design phase.

Flight performance   The flight performance can be improved with further and more detailed analysis. Firstly, there should be a deeper look into the take-off and landing phases. More accurate data on tires, engine accelerating performance, take-off operations, reverse thrusters, optimal power and breaking capabilities should be gathered. Secondly, more research can be done into optimal climbs and descents, as also established by regulatory operations. Other flight operations need to be studied in more detail, if they are possible and how they should be dealt with specifically, for example cruise climb. Furthermore, an in depth analysis can be performed regarding noise minimisation. This also should be done by keeping in mind operative regulations. Regarding engine thrust, its effective power varies with altitude and mach number. A detailed performance of the selected engines could be requested to the manufacturing company in order to get more accurate results. This could strongly improve the flight performance analysis. Finally, a flight path analysis with a specific route including a diversion to an alternate airport would give a better understanding of a real-life scenario and the resulting aircraft performance.

Stability and control   While this requirement for the aircraft to be fully stable and controllable for the entire range of c.g. positions is met, improvements can still be made. From the loading diagram it can be observed that the most aft c.g. position occurs on the ground, and while the aircraft is in the air, the c.g. position is significantly more forward. If the position of the aircraft components can be adjusted in such a way, that the c.g. range becomes more centred, the overall stability and control performance of the aircraft can be improved. Aircraft control and manoeuvrability can be further improved by a more detailed analysis of the control surfaces design. Deploying control surfaces often produces forces and moments around undesired axes, which is to be minimised. A possible approach in minimising this is analysing the effect of differential control surface deployment in more detail.

Finance   The financial analysis is based on the results of the current preliminary aircraft design. With the increase of accuracy in further design phases, more reliable values can be found for finance. More analysis can be done to determine the program cost more accurately and consequently the unit cost. More detailed cost descriptions should be found for the various aircraft manufacturing parts. Regarding operating cost, numbers can differ a lot between operators. Therefore it is important to work together with an airline to determine the operating cost specific to their case.

Bibliography

[1] Group 22. *Baseline Report*. Tech. rep. Delft University of Technology, Faculty Aerospace Engineering, May 2018.

[2] MTU Aeroengines. *PW1000G*. URL: `http : / / www . mtu . de / engines / commercial - aircraft - engines/narrowbody-and-regional-jets/pw1000g/`. 2018.

[3] European Aviation Safety Agency. *Certification Specifications for Large Aeroplanes, CS-25*. Cologne, Germany, 2007.

[4] R. Alderliesten. *Fatigue and Fracture of Fibre Metal Laminates, Solid Mechanics and Its Applications*. Springer International Publishing AG, 2017.

[5] John D. Anderson. *Aircraft Performance and Design*. Singapore: McGraw-Hill, 1999.

[6] John D. Anderson. *Introduction to Flight*. 7th. New York, USA: McGraw-Hill, 2012.

[7] Nicolas E. Antoine and Ilan M. Kroo. *Aircraft Optimization for Minimal Environmental Impact*. reader Vol. 41 No. 4. American Institute of Aeronautics and Astronautics, 2004.

[8] J.D. Aplin. "Flight Computer for the Boeing 777". In: *Microprocessors and Microsystems* 20.8 (Apr. 1997), pp. 473–478.

[9] ATR. *Connecting the future, Turboprop Market Forecast 2016-2035*. Tech. rep. ATR, 2015.

[10] Centre for Aviation. *USD1 trillion for airport construction globally - but it's not enough*. Tech. rep. CAPA, 2017.

[11] GE Aviation. *CF34-3 turbofan propulsion engine*. URL: `https : / / www . geaviation . com / sites / default/files/datasheet-CF34-8E.pdf`. 2018.

[12] GE Aviation. *CF34-8C turbofan propulsion system*. URL: `https : / / www . geaviation . com / sites / default/files/datasheet-CF34-8C.pdf`. 2018.

[13] P. Balakrishnan et al. *Natural Fibre Composites and their Applications in Aerospace Engineering*. Vol. 23. 6. 2010, pp. 871–893.

[14] BCA. *Market Forecast BCA 2017-2036*. Tech. rep. Bombardier, 2016.

[15] Bombardier. *Commercial Aircraft Prices*. 2018.

[16] Bombardier. *CRJ Series*. Montreal, Canada, 2015.

[17] R. Boom. *Recycling of aluminum from fibre metal laminates*. Tech. rep. 2012.

[18] A. Boone. *CRJ700 Aircraft Systems Study Guide*. Boone and Rile publishing, 2000.

[19] Menkes van den Briel. *Airplane Boarding*. tech report. 2010.

[20] F.G. Carrasco and Scholz Dieter. *Promising aircraft modifications for low handling costs*. 2008.

[21] Cessna. *Citation II*.

[22] S. Chapple et al. "Flammability of Natural Fiber-reinforced Composites and Strategies for Fire Retardancy: A Review". In: *Chemical Engineering and Processing* 51 (2012), pp. 53–68.

[23] WheelTug Company. *WheelTug technology*. 2017.

[24] T.C. Corke. *Design of Aircraft*. 4th. University of Notre Dame: Pentice Hall, 2003.

[25] Granta Design. *CES EduPack*. comprehensive database of materials and process information. 2017.

[26] Dr. Tulinda Larsen. *The Connected Aircraft: Improving Dispatch Reliability*. Sept. 2015.

[27] T. Dursu et al. "Recent developments in advanced aircraft aluminium alloys". In: *Materials and Design* 56 (2014), pp. 862–871.

[28] E. Mooij, E., Papp, Z.„ van der Wal,W. *Simulation, Verification and Validation:Lecture Notes*. internal publication. Feb. 2018.

[29] EASA. *EASA type certificate data sheet E.018*. URL: `https://www.easa.europa.eu/sites/default/files/dfu/EASA%20TCDS%20E%20018%20issue%2012.pdf`. 2018.

[30] EASA. *EASA type certificate data sheet E.063*. URL: `https://www.easa.europa.eu/sites/default/files/dfu/EASA-TCDS-E.063_Rolls--Royce_Deutschland_Tay_Series_engines-04-18062013.pdf`. 2013.

[31]   EASA. *EASA type certificate data sheet IM.E.096*. URL: `https://www.easa.europa.eu/sites/default/files/dfu/EASA%20TCDS%20IM%20E96_PW814GA-PW815GA_01.pdf`. 2017.

[32]   K.E. Eickmann. *Committee on assessment of aircraft winglets for large aircraft fuel efficiency*. The national academies press, 2007.

[33]   Embraer. *Market Outlook Embraer 2017-2036*. Tech. rep. Embraer, 2016.

[34]   FAR. *Airworthiness Standards: Transport Category Airplanes*. Tech. rep. Feb. 1965.

[35]   Antonio Filippone. *Advanced Aircraft Flight Performance*. Cambridge University Press, 2012.

[36]   Lewis R. Fisher and Herman S. Fletcher. *EFFECT OF LAG OF SIDEWASH ON THE VERTICAL-TAIL CONTRIBUTION TO OSCILLATORY DAMPING IN YAW OF AIRPLANE MODELS*. Langley Field, VA, 1955.

[37]   C. Giummarra et al. "NEW ALUMINUM LITHIUM ALLOYS FOR AEROSPACE APPLICATIONS". In: *Proceedings of the Light Metals Technology Conference* (2007).

[38]   Y.S. Gok. *Scheduling of aircraft turnaround operations using mathematical modelling: Turkish low-cost airline as a case study*. reader. Coventry University, 2014.

[39]   Group 22. *Baseline Report*. Tech. rep. Delft University of Technology, Faculty Aerospace Engineering, May 2018.

[40]   Group 22. *Midterm Report*. Tech. rep. Delft University of Technology, Faculty Aerospace Engineering, June 2018.

[41]   S. Hartjes. *Operations Control and Flight Planning*. internal publication. 2018.

[42]   Lance Sherry Houda Kerkoub Kourdali. *A comparison of two takeoff and climb out flap retraction standard operating procedures*. Tech. rep. URL: `https://ieeexplore.ieee.org/document/7486344/authors`. Delft, Netherlands: Delft University of Technology, 2016.

[43]   I. Inagaki et al. "Application and Features of Titanium for the Aerospace Industry". In: *NIPPON STEEL & SUMITOMO METAL TECHNICAL REPORT* 106 (2014).

[44]   Aleris International Inc. *AEROSPACE ALUMINUM AA5028 AlMgSc*. Tech. rep. 2015.

[45]   Korea Aerospace Research Insitutey. *MRJ(Mitsubishi Regional Jet)의 현황과 개발과정*. URL: `https://www.kari.re.kr/download/viewer/1471022116937/index.html`. 2016.

[46]   S. Jackson. *Systems engineering for commercial aircraft*. Ashgate, 1997.

[47]   Ebad Jahangir. *Aviation and Sustainable Development: Trends and Issues*. Tech. rep. ICAO, 2009.

[48]   Roskam Jan. *Part 8: Cost estimation, Design development, manufacturing and operating*. Ed. by DARcorporation. Basingstoke, UK, 1999.

[49]   Roskam Jan. *Part I: Preliminary Sizing of Airplanes*. Ed. by DARcorporation. Basingstoke, UK, 1999.

[50]   Ray Jaworowski. *Long-Term Growth Projected for Regional Aircraft Market*. Tech. rep. Forecast International, 2017.

[51]   Lloyd R. Jenkinson. *Civil jet aircraft design*. 1st ed. Great Britain: Arnold, 1999.

[52]   David Kaminski-Morrow. *IndiGo tentatively signs for 50 ATRs*. 2017.

[53]   S. Krishna et al. "A Comparative Study of Aluminium Alloy and Titanium Alloy". In: *International Journal on Recent Technologies in Mechanical and Electrical Engineering (IJRMEE)* 2.8 (2015), pp. 85–88.

[54]   Wolfgang Langewiesche. *Stick and Rudder: An Explanation of the Art of Flying*. 1st ed. New York, NY: McGraw-Hill Professional, 1990.

[55]   Granta Design Limited. *CES EduPack 2017, version 17.1.0*. accessed via TU Delft subscription. 2017.

[56]   T.H.G Megson. *Aircraft Structures for engineering students*. Fourth edition. Great Britain: Elsevier Aerospace Series, 2008.

[57]   J. Melkert. *Aerospace design and systems engineering elements slides, Design of the fuselage*. Internal publication. Delft, Zuid-Holland, 2018.

[58]   Sam Miller. "Contribution of Flight Systems to Performance-Based Navigation". In: *AERO Magazine*. Seattle, Washington: Boeing Commercial Airplanes, 2009, pp. 21–28.

[59]   L. R. Miranda, R. D. Elliot, and W. M. Baker. *A generalized vortex lattice method for subsonic and supersonic flow applications*. Contractor Report 2865. Lockheed-California Co for N. A.S.A., 1997.

[60]   MIT lecture outlines. *Unified lecture #2: The Breguet Range Equation*. online. Oct. 2008.

[61]   J.A. Mulder. *Flight Dynamics*. TU Delft, 2013.

[62]   N.V. Nayak et al. "Composite Materials in Aerospace Applications". In: *International Journal of Scientific and Research Publications* 4.9 (2014).

[63]   M.C.Y Niu. *Airframe stress analysis and sizing*. 2nd ed. Granada Hills, CA: Conmilit Press, 1999.

[64]   NPTEL Mech. Eng. lecture outlines. *Plasticity*. online. Oct. 2004.

[65]   Marius G. Oprea. *THE EFFECTS OF GLOBAL ECONOMIC CRISIS ON THE AIR TRANSPORT OF PASSENGERS IN EUROPE AND IN ROMANIA*. Journal. GeoJournal of Tourism and Geosites, 2010.

[66]   International Civil Aviation Organization. *Global Air Transport Outlook To 2032 And Trends To 2042*. Tech. rep. ICAO, 2017.

[67]   International Civil Aviation Organization. *World Aviation and the World Economy*. report. 2012.

[68]   A.N. Page. *ESDU 87018*. Tech. rep. there are many authors but only the chairman is written. 1987.

[69]   Y. Park. "Fuel burn rates of commercial passenger aircraft: variations by seat configuration and stage distance". In: *Journal of Transport Geography* 41 (2014), pp. 137–147.

[70]   K.L. Pickering et al. "A review of recent developments in natural fibre composites and their mechanical performance". In: *Composites: Part A* 83 (2016), pp. 98–112.

[71]   A. Pramanik. "Problems and solutions in machining of titanium alloys". In: *The International Journal of Advanced Manufacturing Technology* 70.5-8 (2014), pp. 919–928.

[72]   N. Prasad et al. "Mechanical behaviour of aluminium–lithium alloys". In: *Sadhana* 28 (2003), pp. 209–246.

[73]   Ivchenko Progress. *D36, Series A Turbofan*. URL: `http://ivchenko-progress.com/?portfolio=d-36-4&lang=en`. 2018.

[74]   Ivchenko Progress. *D-436-148 Bypass Turbofan Aero Engine*. URL: `http://ivchenko-progress.com/?portfolio=d-36-4&lang=en`. 2018.

[75]   Daniel P. Raymer. *Aircraft design: A conceptual approach*. 3th. Reston, Virginia: AIAA education series, 1999.

[76]   Nikkei Asian Review. *Mitsubishi Aircraft loses order for 40 regional jets*. Tech. rep. Nikkei, 2018.

[77]   T. G. Reynolds et al. *EVALUATION OF POTENTIAL NEAR-TERM OPERATIONAL CHANGES TO MITIGATE ENVIRONMENTAL IMPACTS OF AVIATION*. Tech. rep. 2010.

[78]   T.G. et al. Reynolds. *Evaluation of potential near-term operational changes to mitigate environmental impacts of aviation*. Tech. rep. 2010.

[79]   J. Roskam. *Airplane Design Part IV:Layout of landing gear and systems*. DARcorporation, 2000.

[80]   P. K. C. Rudolph. *High-Lift Systems on Commercial Subsonic Airliners*. NASA, 1996.

[81]   Ger J.J. Ruijgrok. *Elements of Airplane Performance*. 2nd ed. Delft: Delft Academic Press (VSSD), 2009.

[82]   Safran. *SaM146: performance and adaptability*. URL: `https://www.safran-aircraft-engines.com/commercial-engines/regional-jets/sam146/sam146-1s17`. 2018.

[83]   Schrenk. "A simple approximation method for determining spanwise lift distribution". In: *NACA Technical Memorandum 948* (1940).

[84]   D. Sholz. *Estimating the Oswald factor from basic aircraft geometrical parameters*. Hamburg, Germany, 2012.

[85]   Jos Sinke. *Production of Aerospace Systems*. reader AE3211-II. internal publication. TU Delft, 2010.

[86]   Matthew Miller Siva Govindasamy. *Exclusive: China-made regional jet set for delivery, but no U.S. certification*. Tech. rep. REUTERS, 2015.

[87]   Richard Smith. *Mitsubishi's jet set for push into Middle East*. 2016.

[88]   W. Speer et al. "Applications of an aluminum–beryllium composite for structural aerospace components". In: *Journal of Air Transport Management* 8 (2004), pp. 895–902.

[89]   Power Stow. *Time measurement for loading with Power Stow Rollertrack*. 2011.

[90] E. G. Tulapurkara. *Airplane design(Aerodynamic)*. Dept. of Aerospace Engg., Indian Institute of Technology, Madras.

[91] M. Voskuijl. *Flight & Orbital Mechanics slides, Airfield Performance*. internal publication. Delft, Zuid-Holland, 2018.

[92] R.J.H. Wanhill. "Status and prospects for aluminium-lithium alloys in aircraft structures". In: *Fatigue* 16.1 (1994).

[93] Graham Warwick. *Civil engines: Pratt & Whitney gears up for the future with GTF*. 2007.

[94] WCED. *Our Common Future; report of the UN commission on Sustainable Development*. Tech. rep. 1987.

[95] Pratt & Whitney. *Pure Power PW1200G Engine*. URL: `https://www.pw.utc.com/Content/Press_Kits/pdf/ce_pw1200g_pCard.pdf`. 2018.

[96] Y. Yang et al. "Recycling of composite materials". In: *Chemical Engineering and Processing* 51 (2012), pp. 53–68.

Program and Code Bibliography

In order to be able to design an aircraft, not only methodologies and techniques as described in books or articles are used, computers and numerical tools were used as well. However, just like design methods, it is important to build on others and not invent everything yourself, while giving credit where it is due. Therefore, this section is dedicated to reference all external programs and libraries used in the design.

All code written by the team, as well as some of the open source libraries used can be found on GitHub, `https://github.com/paulienuij/DSE_group22_Low-Cost-Regional-Aircraft`.

Main Development Tools
The following programs and have been used by the entire team in order to develop the code

- **MATLAB:** version R2018a was used, student licences provided by the TU Delft.

- **Python:** use is made of Anaconda 3, a scientific Python distribution that comes with Python 3.6 and most commonly used scientific packages. In this project, especially SciPy and NumPy are used.

Aerodynamic Toolbox
The following external programs and libraries and programs have been used by the aerodynamics team. Special thanks to our coach Yi Zhang, and his colleague Yu Zhang of the aerodynamic department that helped us find AVL and discover PARSEC and sent us some examples that were good starting point to understand how to use them.

- **AVL:** AVL is a program for the aerodynamic and flight-dynamic analysis of rigid aircraft of arbitrary configuration using vortex-lattice theory. It is an open sourced project created by MIT, and can be found on `http://web.mit.edu/drela/Public/web/avl/`
  A good guide to start with AVL written by Kinga Budziak of Hamburg University of Applied sciences can be found on `http://www.fzt.haw-hamburg.de/pers/Scholz/arbeiten/TextBudziak.pdf`

- **Parsec-airfoils:** This Python library generates and plots the contour of an airfoil using the PARSEC parameterization, it was created Dimitrios Kiousis. It is open source and free to use for non commercial purposes and can be found on `https://github.com/dqsis/parsec-airfoils`

A
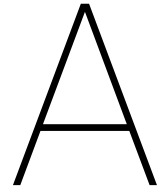
V&V Procedures

During a design process, verification and validation of used methods, code and results is vital to make sure that the process produces the correct results. In this chapter, the verification and validation procedures used during this design process will be explained. In Section A.2 the verification aspects will be discussed whereas Section A.3 will focus on the validation aspects. First, in Section A.1 a short introduction to V&V methods will be given.

A.1. Introduction

Verification and validation are used to monitor the design process and make sure all computations provide the desired results. It is also a useful tool for other users to assess the quality of a method. Lately, V&V procedures get more and more recognition.

Verification answers the question: *Are you solving it right?*. It mainly deals with mathematical issues and proves that a model is solved correctly. It checks whether a product, a service or a systems meets a set of design requirements. Validation answers the question: *Are you solving the right thing?* and deals with entire process. It provides evidence that the correct model for the physical process is solved. The simulation of a physical process can be visualised in Figure A.1. This figure also shows the V&V steps and where they impact the simulation process.
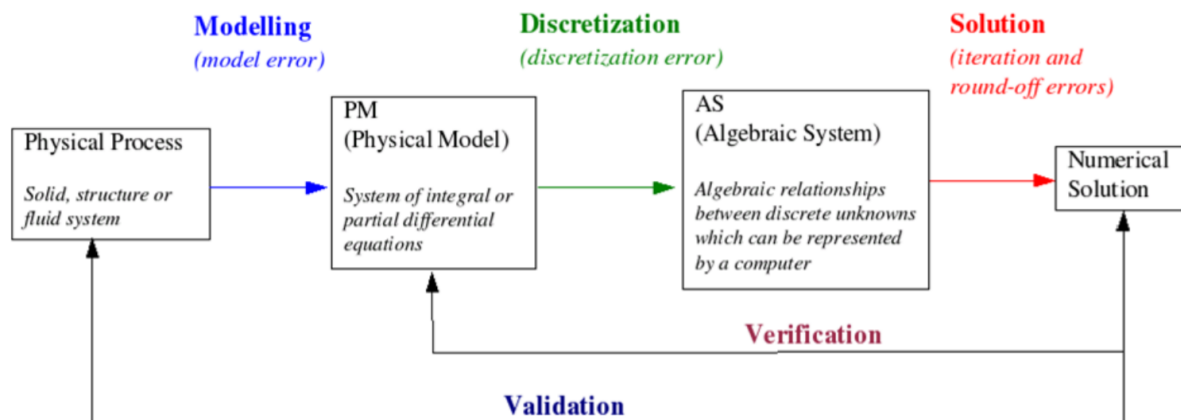
Figure A.1: *Verification and validation model [28].*

A.2. Verification Methods

Verification can be performed by running tests, analysis, demonstration or examination (inspection) [46]. Below all methods are described.

Test   A test type of verification which requires instrumentation, for example, wind tunnel test or flight test. Testing is essential in the certification process. Testing assures that every aircraft element performs the function it was intended to perform, performs it to the expected level of performance and does not perform functions it was not intended to perform [46]. Since there is no instrumentation available, this verification method

will not be used.

Analysis   An analysis is any kind of mathematical, computational or logical task performed to verify a requirement that cannot be verified in any other manner or other verification methods are too expensive. Analysis can be also used in conjunction with testing to extend the envelope of the test results. For example, computer simulation can be used to predict aircraft behaviour in regimes beyond flight data points. Analysis verification includes simulation, in-service data and similarity and system safety assessment [46].

Demonstration   Demonstrations are similar to tests, but contrary to test, do not require instrumentation. However, since there will be no real-life model present, Demonstration method will not be used.

Examination   Examinations are easiest types of verification, they are simply a visual confirmation that a requirement has been met, for example, hardware inspection to check if the required hardware component is installed in the aircraft [46]. This method might be used to verify some of the requirements using the technical drawings.

For the code verification, the analysis method is chosen. Below the verification procedures for codes are described.

Debugging   First step in code verification is debugging. In order to ensure a code works, all the syntax errors due to typos, missing semicolons or others syntax errors have to be identified and fixed. Once all the syntax errors are gone, the code should compile and run, however, it still might not give the correct results.

Unit tests   Next step in verification procedures is unit tests. The code is divided into smaller functions (chunks) and run each function separately. To ensure the chunks are working correctly different input values are tested or different limitations such as boundary conditions, to check whether different output values are obtained. Then the hand calculations for each function are performed. Finally the program outputs are tested against hand calculation outputs.

System test   Once all the functions are verified, they are, again, connected into one code for the system test. The whole system is tested for different input values, to check if different output values are produced, but also to check if all the units interact with each other in desired manner.

A.3. Validation

Validation is testing program outputs against the real values obtained through experiment or measurements. If the model predicts the experimental outcomes within the predetermined accuracy requirements, the model is considered validated for its intended use [28]. If the model is not matching the real-life data, one has to re-consider assumptions used. Once the program gives anticipated results, the discrepancies need to be discussed and explained. If the outputs cannot predict the real-life data the program cannot be validated, otherwise, the program is validated.

Since for this report no real-life data is attainable for the aircraft nor the experiment can be conducted, the group decided to validate the outcome parameters against statistical data obtained from different aircraft. For example, plot MTOW and OEW for similar aircraft, and the designed aircraft thus see if designed aircraft fits in the regression line well. If it does, it can be said that the MTOW and OEW combination was validated.

B

Renders and Technical Drawings
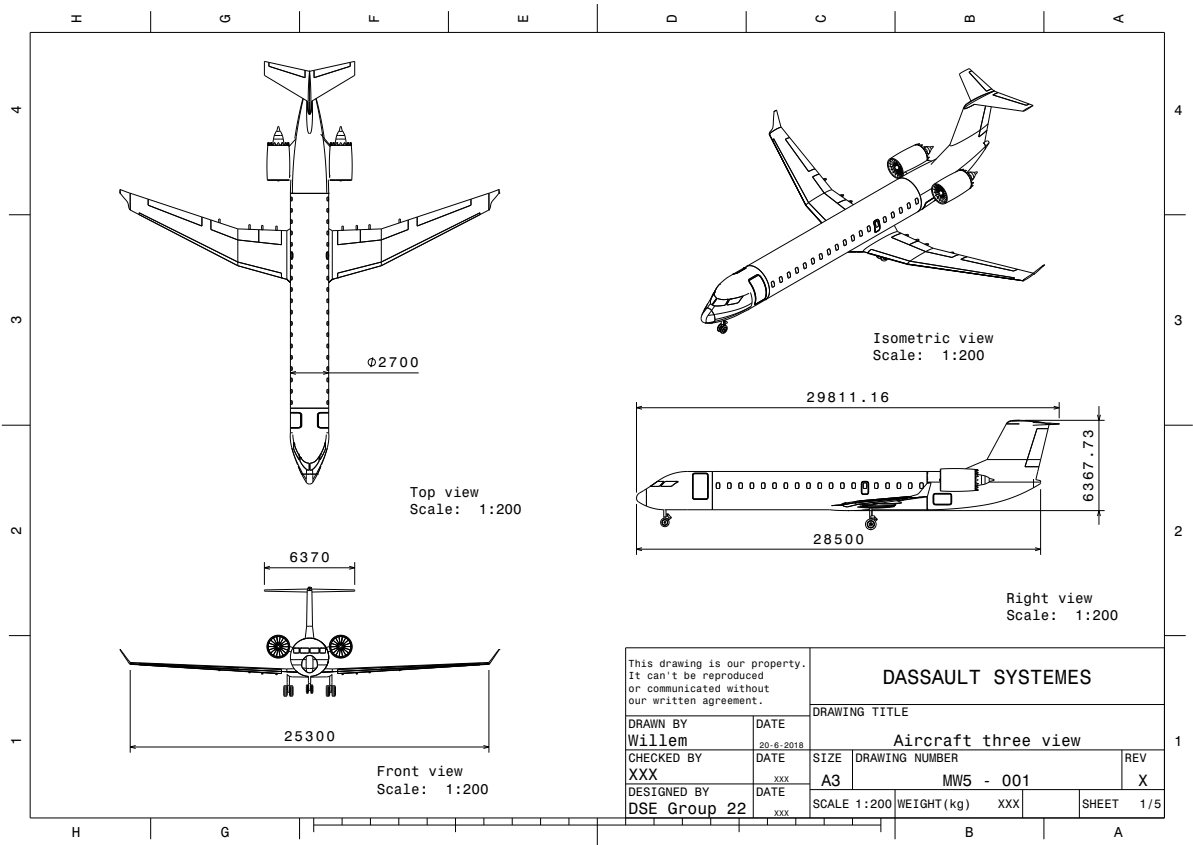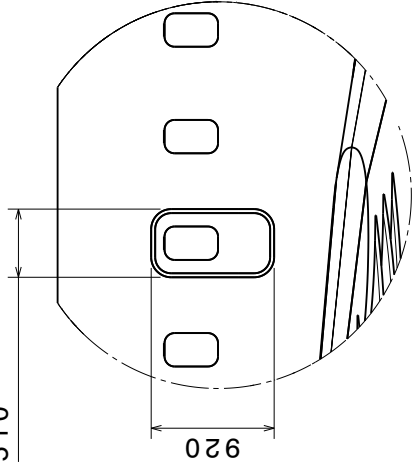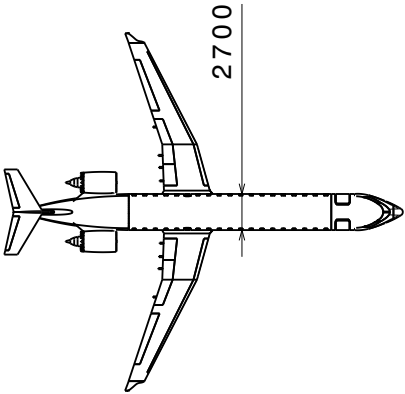
Φ2700

Top view
Scale: 1:200

Isometric view
Scale: 1:200

29811.16

6367.73

28500

Right view
Scale: 1:200

6370

25300

Front view
Scale: 1:200

DASSAULT SYSTEMES

DRAWING TITLE

DRAWN BY
Willem
DATE
20-6-2018

Aircraft three view

CHECKED BY
XXX
DATE
xxx
SIZE
A3
DRAWING NUMBER
MW5 - 001
REV
X

DESIGNED BY
DSE Group 22
DATE
xxx
SCALE 1:200
WEIGHT(kg)   XXX
SHEET   1/5

Detail A
Scale: 1:50

250
400
1100
1850

Rear view
Scale: 1:400

4357.49
6370
25300
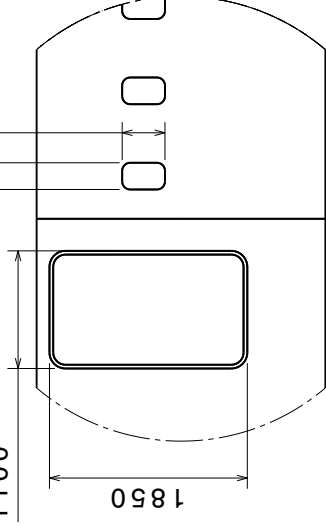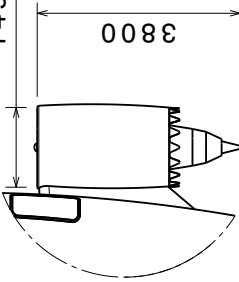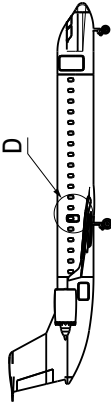
Right view
Scale: 1:400

28500
29811.16
A

Top view
Scale: 1:400

2700
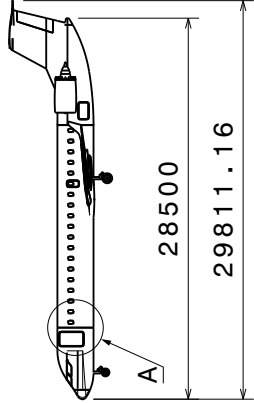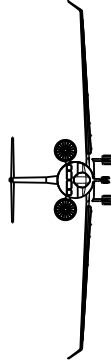
Front view
Scale: 1:400

Bottom view
Scale: 1:400
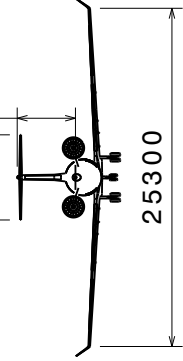
16525
2000
3000
C

Detail D
Scale: 1:40

510
920

Left view
Scale: 1:400

D

Detail C
Scale: 1:100

1491.6
3800

DASSAULT SYSTEMES

DRAWING TITLE

Detailed three view

DRAWN BY	DATE	
Willem	20-6-2018	
CHECKED BY	DATE	SIZE
XXX	xxx	A3
DESIGNED BY	DATE	
DSE Group 22	xxx	

DRAWING NUMBER

MW5 - 002

SCALE 1:200 WEIGHT(kg) XXX

SCALE 1:200

REV

X

SHEET 2/5

C
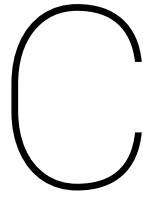
Aircraft Data

Parameter	Value	Unit
Wing geometry		
b_{wing}	25.3	m
λ_{tot}	0.32	–
λ_{inner}	0.8	–
λ_{outer}	0.4	–
$\Lambda_{\text{inner}_{0.25}}$	12	deg
$\Lambda_{\text{outer}_{0.25}}$	35	deg
S_{wing}	61.1	m^2
A_{wing}	10.5	–
Ω_{wing}	0.24	deg/m
Γ_{wing}	3	deg
S_{wf}	33.7	m^2
Airfoil@root	Whitcomb	–
Airfoil@kink	Whitcomb	–
Airforl@tip	SC 20110	–
Horizontal tail geometry		
S_h	10.1	m^2
$b/2$	3.18	m
A_h	4.0	–
λ_h	0.45	–
$\Lambda_{0.25h}$	25.2	–
c_{rh}	2.20	m
c_{th}	0.99	m
Airfoil@root	NACA 0010	–
Airfoil@tip	NACA 0009	–
Vertical tail geometry		
S_v	11.85	m^2
b_v	3.36	m
A_v	0.95	–
λ_v	0.75	–
$\Lambda_{0.25v}$	25.2	deg
c_{rv}	4.04	m
c_{tv}	3.03	m
Airfoil@root	NACA 0011	–
Airfoil@tip	NACA 0011	–
Roll rate derivatives		
C_{L_p}	0	–
C_{Y_p}	-0.02	–
$\vdots$	$\vdots$	$\vdots$

Parameter	Value	Unit
$\vdots$	$\vdots$	$\vdots$
C_{l_p}	-0.59	–
C_{m_p}	0	–
C_{n_p}	0	–
C_{X_p}	0	–
C_{Z_p}	0	–
Pitch rate derivatives		
C_{L_q}	0.46	–
C_{Y_q}	0	–
C_{l_q}	0	–
C_{m_q}	-1.14	–
C_{n_q}	0	–
C_{X_q}	0.41	–
C_{Z_q}	-0.46	–
Yaw rate derivatives		
C_{L_r}	0	–
C_{Y_r}	0.38	–
C_{l_r}	0.2	–
C_{m_r}	0	–
C_{n_r}	-0.19	–
C_{X_r}	0	–
C_{Z_r}	0	-
α derivatives		
C_{L_α}	6.46	–
C_{Y_α}	0	–
C_{l_α}	0	–
C_{m_α}	-8.51	–
C_{n_α}	0	–
β derivatives		
C_{L_β}	0	–
C_{Y_β}	-0.36	–
C_{l_β}	-0.12	–
C_{m_β}	0	–
C_{n_β}	0.16	–
Axial velocity derivatives		
C_{X_u}	-0.07	–
C_{Y_u}	0	–

Parameter	Value	Unit
$\vdots$	$\vdots$	$\vdots$
C_{Z_u}	-0.91	–
C_{l_u}	0	–
C_{m_u}	-1.12	–
C_{n_u}	0	–
Sideslip velocity derivatives		
C_{X_v}	0	–
C_{Y_v}	-0.36	–
C_{Z_v}	0	–
C_{l_v}	-0.12	–
C_{m_v}	0	–
C_{n_v}	0.16	–
Normal velocity derivatives		
C_{X_w}	0.21	–
C_{Y_w}	0	–
C_{Z_w}	-6.48	–
C_{l_w}	0	–
C_{m_w}	-8.5	–
C_{n_w}	0	–
Short period		
λ_{SP}	-0.29 + 0.57i	–
ζ_{SP}	0.46	–
T_{SP}	11.031	s
$T_{\frac{1}{2} SP}$	2.36	s
Phugoid		
$\lambda_{Phugoid}$	-0.01 + 0.18i	–
$\zeta_{Phugoid}$	0.02	–
$T_{Phugoid}$	34.16	s
$T_{\frac{1}{2} Phugoid}$	155.49	s
Aperiodic roll		
λ_{AR}	-1.79	–
ζ_{AR}	1.0	–
T_{AR}	1	s
$T_{\frac{1}{2} AR}$	0.39	s
Dutch roll		
λ_{DR}	-0.00 + 1.26i	–
ζ_{DR}	0.07	–
T_{DR}	4.97	s
$T_{\frac{1}{2} DR}$	7.89	s
Spiral		
λ_{Spiral}	0.01	–
ζ_{Spiral}	1.	–
$T_{\frac{1}{2} Spiral}$	-47.4753	s
Fuselage geometry		
$L_{fuselage}$	28.5	m
$d_{fuselage}$	2.7	m
$L_{nosecone}$	5.35	m
$L_{tailcone}$	8.0	m
$L_{cylindrical}$	15.15	m

Parameter	Value	Unit
$\vdots$	$\vdots$	$\vdots$
$h_{nose\text{-}LG}$	1.19	m
$h_{main\text{-}LG}$	1.40	m
$N_{stringers}$	53	–
N_{frames}	18	–
$b_{stringers}$	16	cm
b_{frames}	78.8	cm
t_{skin}	1.5	mm
Wing box root geometry		
$N_{stringers_{bottom}}$	17	–
$N_{stringers_{top}}$	15	–
$t_{front\text{-}spar}$	5	mm
$t_{rear\text{-}spar}$	7	mm
t_{top}	9	mm
t_{bottom}	9	mm
b_{ribs}	46.5	cm
Flight performance		
$s_{take\text{-}off}$	1500	m
MTOW	30200	kg
T_{req}	53.5	kN
$W_{engine_{dry}}$	1360	kg
$Noise_{fly\text{-}over}$	94	EPNdb
$NO_{x_{emission}}$	1987	g
$d_{engine_{fan}}$	1.42	m
l_{engine}	1500	m
BPR	9:1	–
$V_{stall_{take\text{-}off}}$	68.2	m/s
$V_{stall_{landing}}$	58.1	m/s
$C_{L_{max_{take\text{-}off}}}$	1.7	–
$C_{L_{max_{landing}}}$	1.9	–
$C_{l_{max_{cruise}}}$	1.07	–
h_{screen}	10.7	m
$dC_{D_{0_{Landing\ gear}}}$	0.02	–
$dC_{D_{0_{flaps}}}$	0.015	–
$e_{take\text{-}off}$	0.85	–
$e_{landing}$	0.85	–
e	0.8	–
C_{D_0}	0.056	–
M_{cruise}	0.78	–
g_0	9.80655	m/s^2
μ_r	0.06	–
service ceiling	1250	m
μ_{br}	0.65	–
$s_{landing}$	1450	m
Fuel burn at max. PL	4808	kg
$T_{flight@2500km}$	3.34	h
R@maxPL	2500	km
N_{pax}	76	–
n_{ult}	2.5	–
Min. turn radius @ 7000 ft	1202	m
Max. turn rate @ 7000 ft	6.5	deg/s
ROC_{max}	11.7	m/s
$ROC_{max_{MTOW_{SL}}}$	22	m/s

D
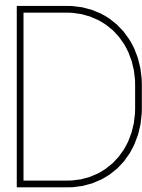
Functional Analysis

D.1. Functional Flow Diagram

Functional Flow Diagram (FFD) represents the functions that the aircraft needs to perform as well as the activities, for example maintenance, that need to be carried out in order to ensure the proper functioning of the aircraft. To properly investigate the function of the aircraft one needs to use the matrix D.1[46]. One needs to keep in mind all combinations are meaningful, for example,

$$
\begin{bmatrix} \text{Perform} \\ \text{pre-flight} \\ \text{operations} \\ \\ \text{Perform} \\ \text{Take-off} \\ \text{operations} \\ \\ \text{Perform} \\ \text{flight} \\ \text{operations} \\ \\ \text{Perform} \\ \text{post-landing} \\ \text{operations} \end{bmatrix} \times \begin{bmatrix} \text{Perform} \\ \text{passenger \& cargo} \\ \text{operations} \\ \\ \text{Perform} \\ \text{Freighter} \\ \text{operations} \\ \\ \text{Perform} \\ \text{non-revenue} \\ \text{operations} \end{bmatrix} \times \begin{bmatrix} \text{Perform} \\ \text{normal} \\ \text{operations} \\ \\ \text{Perform} \\ \text{abnormal} \\ \text{operations} \\ \\ \text{Perform} \\ \text{emergency} \\ \text{operations} \end{bmatrix} \tag{D.1}
$$

With the first matrix being operational phase functions, second being mission functions and last one being situations functions. The functional flow diagram is presented in Figures D.1 through D.3. It was worked out for operational phase functions with passenger and cargo operations under normal conditions as this is most popular profile for the passenger typical aircraft. However, one needs to remember that some other, perhaps critical, function can be present in other configuration. The functional flow diagram is worked out up to 3rd level of detail. Further levels of detail are possible but not necessary at this stage of the design.

Figure D.1: *Top level.*

Figure D.2: *Functional flow first level.*

D.2. Functional Breakdown

Functional breakdown diagram (FBD) represents all the functions that the aircraft needs to perform. The functional breakdown does not indicate at what time the functions need to performed or in what sequence. It is presented in Figure D.4. The breakdown is performed up to 4th level of detail. Further levels of detail are possible but not necessary at this stage of the design.
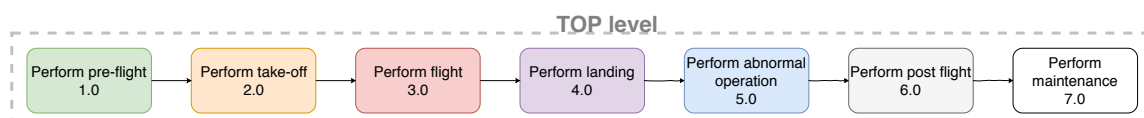
Figure D.3: *Third level of functional flow diagram.*
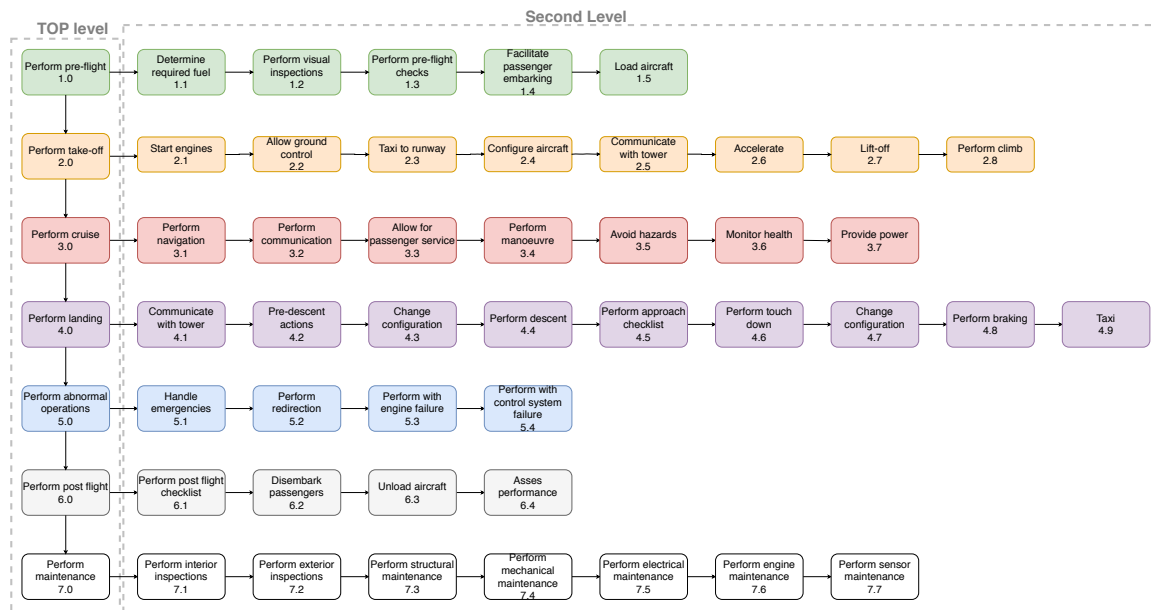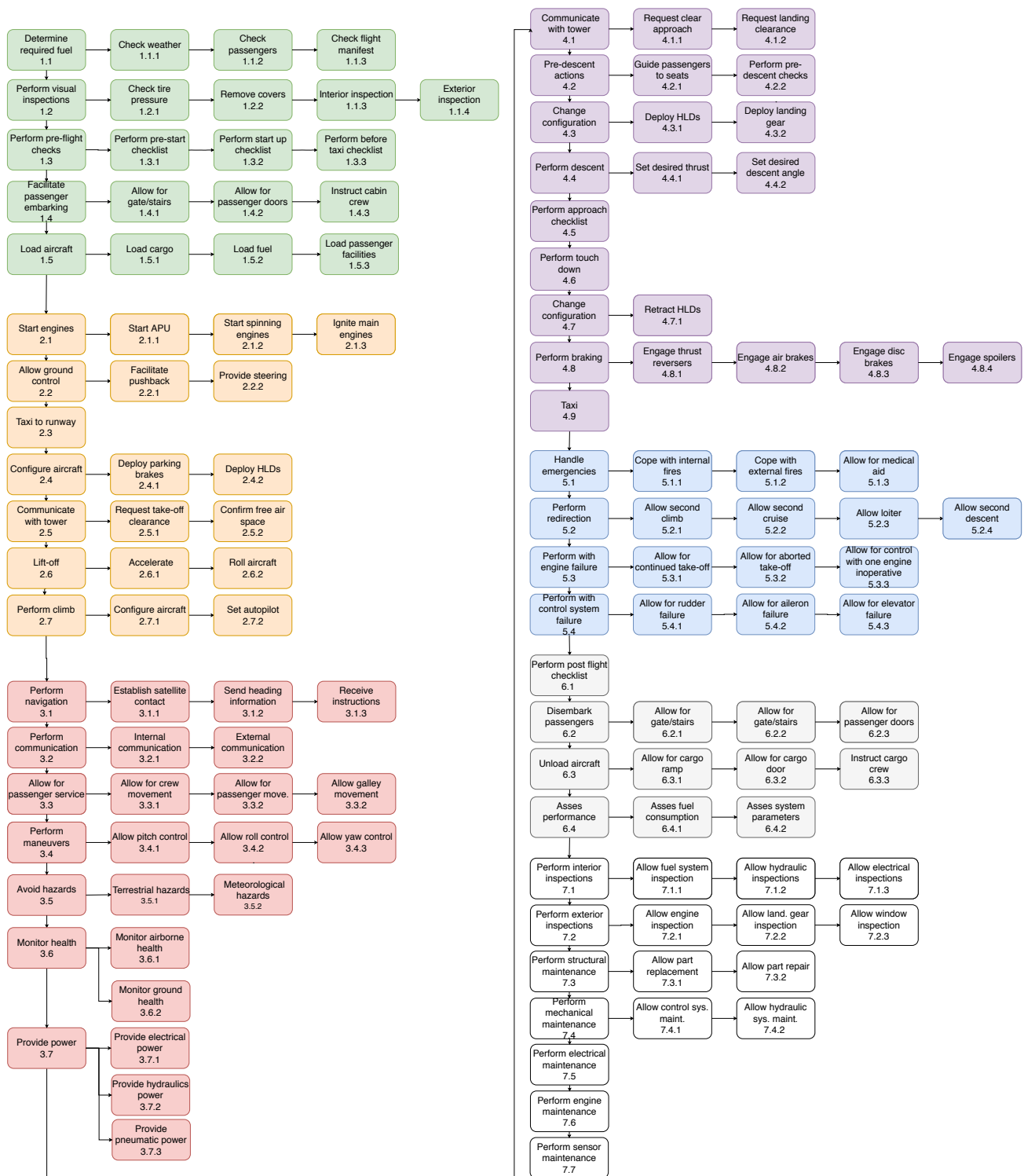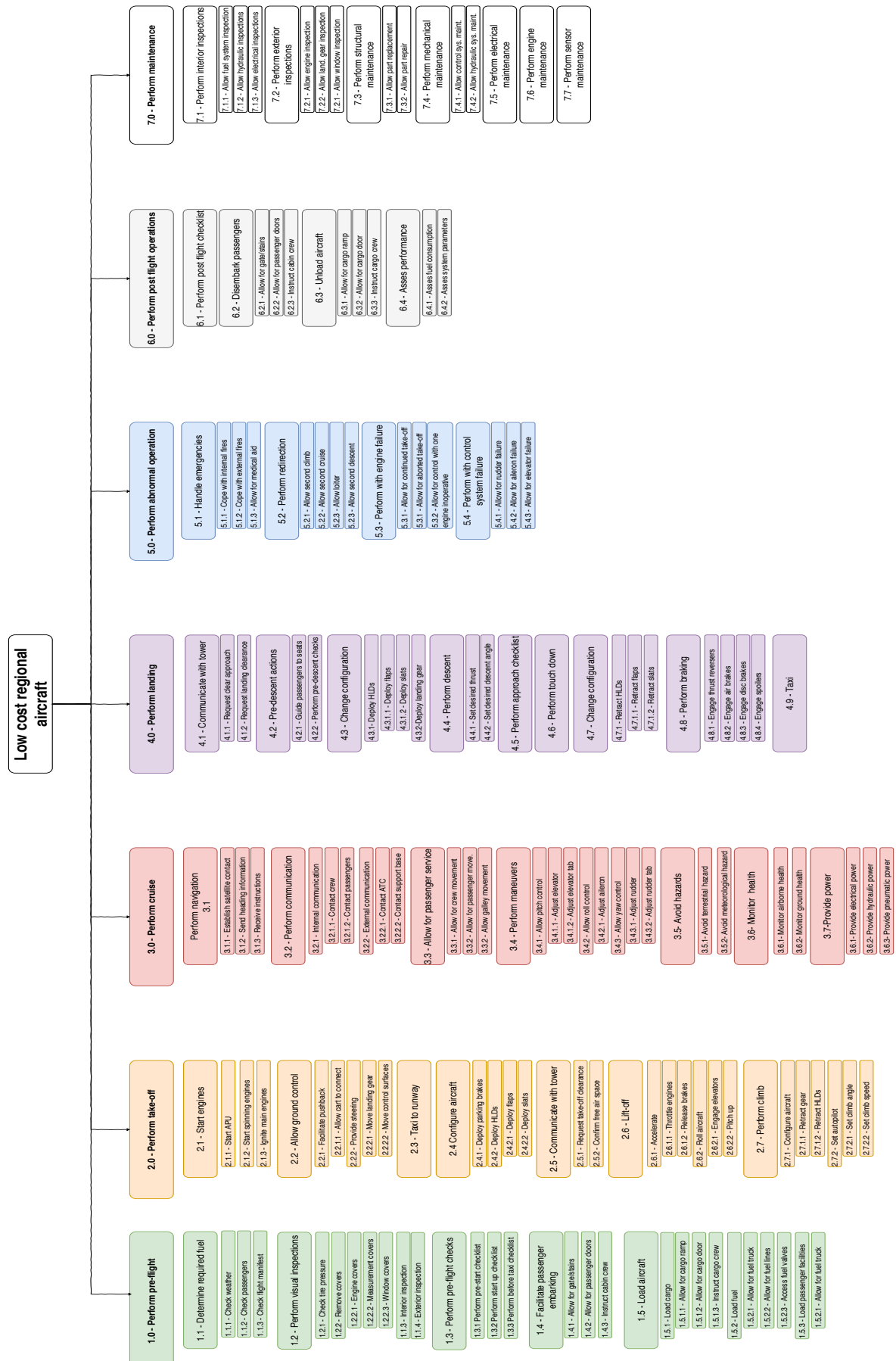
Figure D.4: *Functional breakdown.*

E
Compliance Matrix

The compliance matrix in Table E.1 contains the both the top-level requirements developed in consultation with the customer and the system requirements developed in order to ensure the safe operation of the aircraft, and the status of these requirements along with information on where they have been addressed in the body of the report.

Table E.1: *Compliance matrix.*

Req. ID	Requirement	Status	Reference	Remarks
Cus.1	The operational costs shall be lower compared to competitive aircraft.	Verified	Subsection 11.2.1	6-8% lower Direct operational cost
Cus.2	The range at maximum payload shall be more than 1500 km but less than 2500 km.	Verified	Subsection 4.3.6	
Cus.3	The number of passengers shall be between 50-75 in an economy class setting.	Deleted		Replaced by Cus. 9 (76 passengers in all economy)
Cus.4	The aircraft shall be able to operate from regional airports.	Verified	Chapter 9	
Cus.5	The take-off distance on tarmac shall be less than 1200 m.	Deleted		Replaced by Cus.8
Cus.6	The aircraft design, operation, production and aircraft recycling shall be optimised for sustainability.	Verified	Section 12.2	Materials selection, engine selection and aerodynamic calculations aimed at reducing weight and fuel consumption
Cus.7	The aircraft shall comply with latest safety and environmental regulations.	Deferred		Can only been confirmed after the aircraft has been certified.
Cus. 8	The take-off distance on tarmac shall be less than 1500 m.	Verified	Subsection 4.3.1	After changing the runway length to 1500 m, the team was able to comply with the requirement. The BFL is now 1490 m.
Cus.9	The number of passengers shall be between 50-76 in an economy class setting.	Verified		76 passengers in all economy seating.
Sys.Perf.1	The aircraft shall be dynamically stable for the entire range of centre of gravity excursions.	Verified	Chapter 6	

Sys.Perf.2	The aircraft shall be controllable for the entire range of centre of gravity excursions.	Verified	Chapter 6	
Sys.Perf.3	The cruise speed of the aircraft shall be in the range of 0.73 M-0.83 M.	Verified	Subsection 4.3.4	The maximum cruise Mach number is 0.78
Sys.Perf.4	The landing distance on tarmac shall be less than 1200 m.	Deleted		
Sys.Perf.5	The aircraft shall be able to make a steep approach with a flight path gradient of at least -10%.	Deferred		
Sys.Perf.6	The noise produced by the aircraft shall be less than 264 EPNdB.	Verified	Section 12.4	Airframe noise lower than reference aircraft and new engine technology
Sys.Perf.7	In landing configuration the steady climb gradient shall not be less than 3.2% at an airspeed of no more than $1.3 V_{stall}$.	Verified	Subsection 4.3.5	
Sys.Perf.8	The climb gradient during the first take-off segment with one engine inoperative shall be positive.	Verified	Subsection 4.3.2	
Sys.Perf.9	The climb gradient during the second take-off segment with one engine inoperative shall be more than 2.4%.	Verified	Subsection 4.3.2	
Sys.Perf.10	The climb gradient during the final take-off segment with one engine inoperative shall be more than 1.2%.	Verified	Subsection 4.3.2	
Sys.Perf.11	The climb gradient during the enroute segment with one engine inoperative shall be more than 1.1%.	Verified	Subsection 4.3.2	
Sys.Perf.12	The climb gradient during the approach segment with one engine inoperative shall be more than 2.1%.	Verified	Subsection 4.3.2	
Sys.Perf.13	There shall be no uncontrollable ground-looping tendencies in 90°crosswind, up to a wind velocity of 20 kts.	Deferred		Not in the scope of this design stage
Sys.Perf.14	The airframe structure shall not fail under ultimate load for a duration of 3 seconds.	Deferred		To be verified after the aircraft is built

Sys.Perf.15	The amount of emergency exits present shall be sufficient to comply with CS-25 regulations.	Verified	Chapter 9	No idea what section this is described in
Sys.Perf.16	The maximum take-off mass of the aircraft shall be less than 35,000 kg.	Deffered		To be verified after the aircraft is built
Sys.Perf.17	The operational empty mass of the aircraft shall be less than 20,600 kg.	Deffered		To be verified after the aircraft is built
Sys.Perf.18	The aircraft shall be able to fly to an alternate airport 100 km away after maximum range flown.	Verified	Subsection 4.3.6	
Sys.Perf.19	The aircraft shall be able to loiter at the alternate for 30 minutes.	Verified	Subsection 4.3.6	
Sys.Perf.20	The landing distance on tarmac shall be less than 1200 m.	Deleted		Deleted due to the removal of Cus.3
Sys.Perf.21	The landing distance on tarmac shall be less than 1500 m.	Verified	Subsection 4.3.5	
Sys.O&L.1:	Turnaround time of the aircraft between maximum payload flights shall be less than 30 minutes.	Verified	Chapter 9	Gantt Chart
Sys.O&L.2	The aircraft shall have a lifetime of at least 25 years.	Deferred		No fatigue analysis performed on the main structural elements of the aircraft
Sys.O&L.3	The aircraft shall be able to perform three to four daily operations.	Verified	Chapter 11	When only long range flights are performed (2500km) the aircraft is able to perform 3 daily operations, when the range is shorter 4 is also possible
Sys.O&L.4	Lateral ground clearance of the aircraft shall be more than 5 degrees.	Verified	Section 10.2	
Sys.O&L.5	The seat pitch shall be equal to 31 inches.	Verified	Section 3.4	Verified
Sys.O&L.6	Maintenance intervals shall be increased due to safe-life design of components.	Deferred		No fatigue analysis performed on the structure
Sys.O&L.7	The aircraft shall not tip over backwards for the entire range of center of gravity locations during ground loading.	Verified	Section 10.2	
Sys.O&L.8	The aircraft shall not turn over for any possible loading configuration and turning radius.	Verified	Section 10.2	Based on the main gear track requirement
Sys.O&L.9	The aircraft doors shall be compatible with airstairs.	Verified	Chapter 9	

Sys.O$L.10	All essential aircraft systems shall be operative with ground power only.	Deferred		
Sys.O&L.11	The wing span shall not exceed 35 m.	Verified	Subsection 5.1.2	b = 25.3
Sys.O&L.12	The total length shall not exceed 35 m.	Verified	Appendix B	length = 29.2m
Sys.Sus.1	Noise generated by the aircraft shall be less than the Chapter 14 level EPNdB.	Deferred		To be determined by actual flight testing
Sys.Sus.2	CO_2 emission per pax.km shall be less than 120 g.	Verified	Subsection 4.3.6	Almost 94.5 g per pax.km
Sys.Sus.3	Aircraft structure shall be made of at least 90% recyclable materials.	Verified	Section 7.1	
Sys.Sus.4	Manufacturing techniques shall be non-toxic.	Deferred		Carbon-fibre lay-up is toxic. However, it is expected that the environmental impacts can be reduced in the future.
Sys.Sus.5	Engine emissions shall comply with current regulations.	Verified	Section 4.1	All regulations met
Sys.Sus.6	The fuel burned during operation shall be less than 8900 kg per flight.	Verified	Subsection 4.3.6	4800 kg of fuel burned for a range of 2500 km
Sys.Sus.7	Employees shall not be subjected to dangerous gases during aircraft production.	Deffered		Possible harmful dust (composites) and skin issues (Al-Li alloys)

Material Database

Table F.1: *Material database.*

Class	Material	E [GPa]	G [GPa]	σ_{ult} [MPa]	σ_y [Mpa]	ν [%]	Shape factor [-]	ρ [kg/m^3]	FVC/ lay-up [%]/[-]	Recyclable [Y/N]	Down cycle [Y/N]	Bio- degradable [Y/N]	Price [EUR/kg]
M	Al 2024-T351	72	28.7	428	324	0.33	24	2750	-	Y (43%)	Y	N	1.9
	Al 7075-T6	73	26	507	445	0.33	16	2800	-	Y (40.5%)	Y	N	3.5
	Al 7175-T66	72	27.5	562	490	0.33	15	2800	-	Y (40.5%)	Y	N	3.5
	Al-Li 2090-T83	78	30.5	531	483	0.35	18	2600	-	Y (42%)	Y	N	12
	Al-Li 8090-T851	82	30	500	440	0.3	18	2540	-	Y (42%)	Y	N	12.4
	AlMgSc 5028-H116	74	-	400	325	-	-	2670	-	Y (42%)*	Y	N	42.41
	AlBeMet 162	200	97	338	283	0.17	40	2104	-	N (10%)	Y	N	361.5
	Ti 6Al-4V ann	110	42	924	869	0.34	13	4429	-	Y/N (23%)	Y	N	19.5
C	GLARE 3 LT	56.2	-	666	260	-	-	-	3/2	-	-	-	-
	GLARE 4 LT	48.7	-	562	225	-	-	-	3/2	-	-	-	-
NF	Ramie	86	15.2	669	486	0.35	1	1500	-	N (9%)	Y	Y	1.79
	Jute	33	18	597	550	0.35	1	1600	-	N (9%)	Y	Y	0.83
SF	Carbon HM	380	170	2400	2000	0.1	1	1820	-	N (5%)	Y	N	40
	Carbon HS	235	105	4650	3850	0.1	1	1820	-	N (5%)	Y	N	26
	E-Glass	73	33	2000	1830	0.22	1	2500	-	N (0.1%)	Y	N	2.19
	T-Glass	72	29.5	32	32	0.23	1	2500	-	Y/N (25%)	Y	N	11.90
TSR	Polyester	0.30	0.1	15	12	0.44	3.9	1100	-	N	Y	N	3.60
	Epoxy	2.4	54	67	54	0.4	5.2	1250	-	N	Y	N	2.30
TPR	PEEK	3.85	1.4	95	87	0.4	4.9	1310	-	Y	Y	N	88.8
	PEI	3	1	95	77	0.39	4.6	1270	-	Y	Y	N	15.8

G

Straw-man Concepts and –Groups

Table G.1: *Concepts groups and features.*

#	Description	Concepts	Features	#	Description	Concepts	Features
1	Blended wing body	1, 2	Different engine amount and place	6	Elliptical	9, 22, 23	Different engine #, tails and wings
2	Canard	3 ,4, 5	Different wings, engines	7	Prandtl	17, 18	Different fuselage designs
3	Double fuselage	6	Conventional tail	8	Strutted wing	19, 20	Different wing location and engine type
4	Flying wing	7	Integrated engines	9	Tandem wing	21, 22	Different fuselage, engines and place
5	Conventional	8, 10-16	Different wing place, engine & tail	10	Hybrid designs	24, 25	Different tails, engine # and place

(a) *Concept 1.*   **(b)** *Concept 2.*   **(c)** *Concept 3.*   **(d)** *Concept 4.*   **(e)** *Concept 5.*

(f) *Concept 6.*   **(g)** *Concept 7.*   **(h)** *Concept 8.*   **(i)** *Concept 9.*   **(j)** *Concept 10.*

(k) *Concept 11.*   **(l)** *Concept 12.*   **(m)** *Concept 13.*   **(n)** *Concept 14.*   **(o)** *Concept 15.*

(p) *Concept 16.*   **(q)** *Concept 17.*   **(r)** *Concept 18.*   **(s)** *Concept 19.*   **(t)** *Concept 20.*

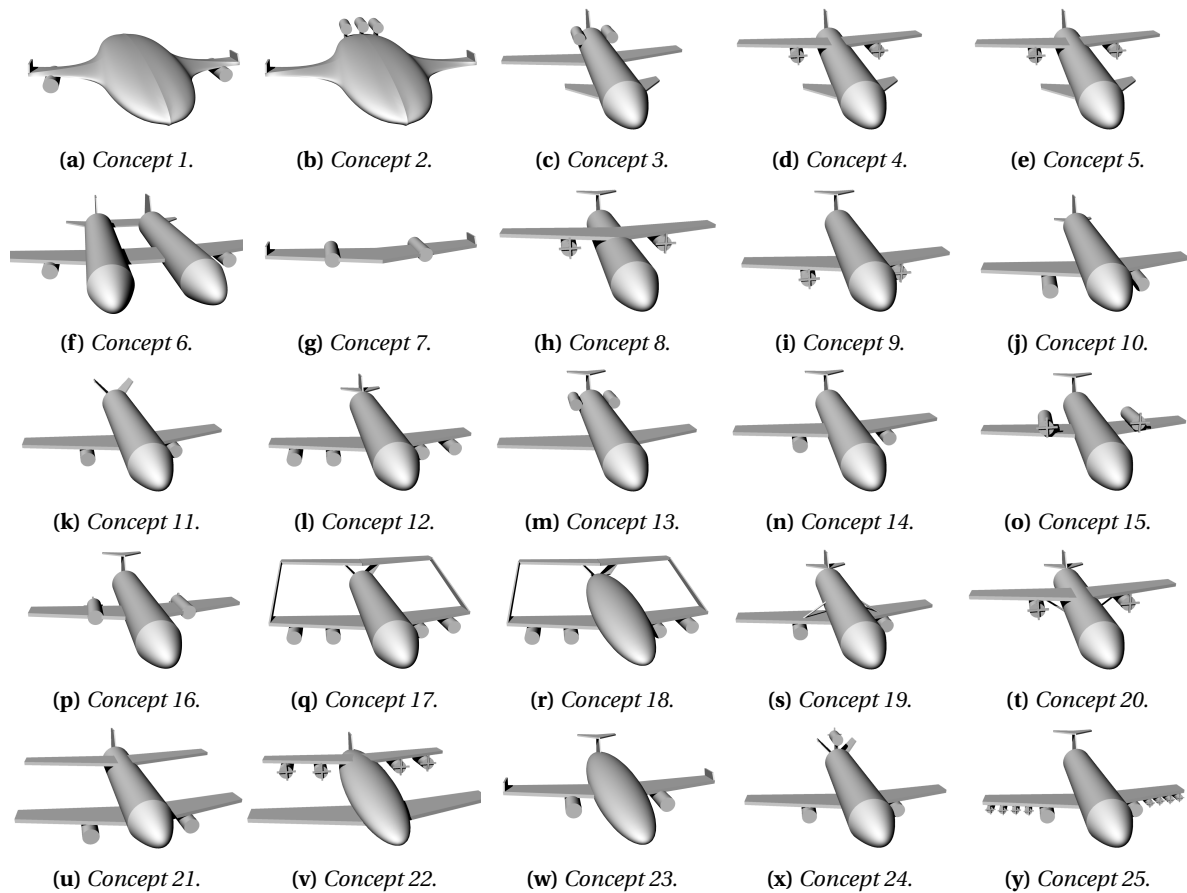**(u)** *Concept 21.*   **(v)** *Concept 22.*   **(w)** *Concept 23.*   **(x)** *Concept 24.*   **(y)** *Concept 25.*

Figure G.1: *Straw-man sketches.*